Elucidation of the molecular mechanism responsible for control of functional properties of myoglobin through the heme electronic structure and heme environment

Ryu Nishimura

Doctoral Program in Chemistry

Submitted to the Graduate School of

Pure and Applied Science

in Partial Fulfillment of the Requirements

for the Degree of Doctor Philosophy in

Science

at the

University of Tsukuba

Contens

Chapter 1

General introduction

Hemoprotein

Hemoproteins have one or more hemes , usually an iron protoporphyrin IX complex (Figure 1-1), in their active sites. They exhibit a variety of biological functions such as oxygen (O_2) storage or transport (myoglobin (Mb) [1,2] or hemoglobin(Hb) [3,4]), electron transfer (cytochromes, etc.) [5,6], oxidase enzymes (peroxidase, etc.) [7], gas sensor (CooA [8], Fix L [9], etc.), NO metabolism [10], and so on. These functional properties of the proteins are evolved and regulated through the heme electronic structure and the heme environment furnished by nearby amino acid residues.

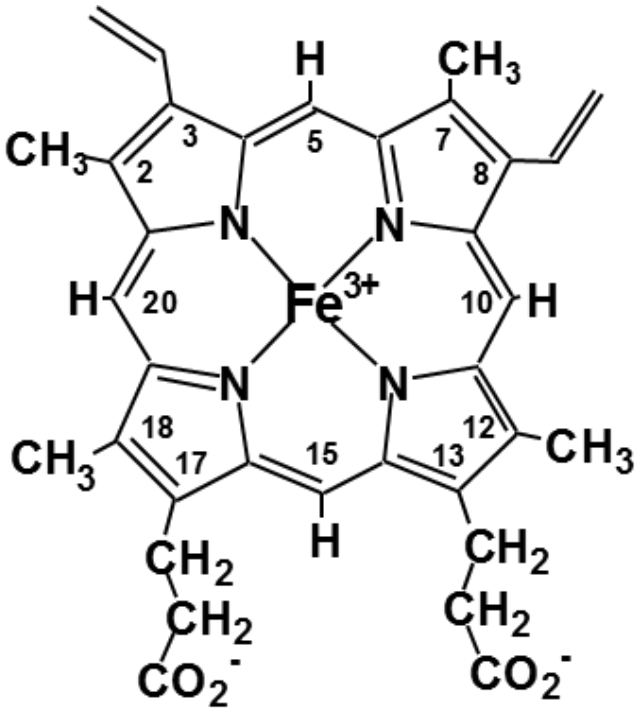

Figure 1-1. Molecular structure and numbering system of heme (protoheme).

Spectroscopic properties of hemoprotein

Hemoproteins have a lot of spectroscopic properties due to a heme moiety. For example, UV-vis spectroscopy [11], Nuclear Magnetic Resonance(NMR) [12], Resonance Raman spectroscopy [13], Mössbauer spectroscopy [14], and so on. Absorption spectrum arisen from π-π* transition of the heme is shifted by a change of external ligand in protein, which reflects electronic state of the heme. NMR is also used to characterize not only the heme electronic structure but also structure determination of hemoproteins. Especially in the presence of unpaired electron at heme iron, nuclei in close proximity of the heme are strongly affected by huge magnetic moment of the unpaired electron and exhibit paramagnetic shifts and paramagnetic relaxations in their NMR spectra [15]. Additionally, their chemical shift reflects the electronic structure of the heme and the environment of the active site. Resonance Raman spectroscopy has been applied widely to hemoproteins [16]. It is known that the visible Resonance Raman spectrum in the high wavenumber region (1200 –1700cm^{-1}) reflects the oxidation state, coordination number, and the spin state of the heme iron [17,18]. Furthermore, Resonance Raman spectroscopy shows not only the direct interactions between the heme and its axial ligand, but also the heme environment furnished by nearby amino acid residues. In particular, the CO stretching frequency has long been used as a probe of structure and bonding in transition metal carbonyl complexes, including CO adducts of the hemeproteins [19]. The CO stretching frequency reflects the heme environment furnished by nearby amino acid residues through the resonance between the two canonical forms of the Fe^{2+}−CO fragment, represented by the valence bond formalism (Scheme 1-1) [20].

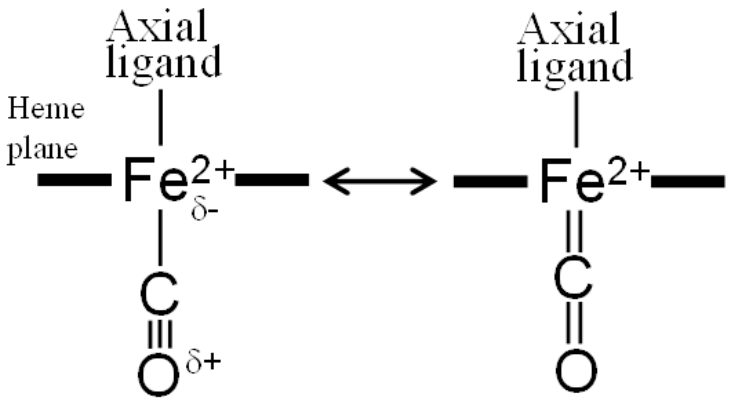

Scheme 1-1. Resonance between the two canonical forms of the Fe-CO fragment, represented by the valence bond formalism[20].

Myoglobin

Mb, an O_2 storage protein found in muscle tissues, is probably the most studied protein, because it has simple structure and function. Structure of Mb determined by X-ray crystallography is illustrated in Figure 1-2 [21,22]. Mb has eight α-helices (labeled A-H form N tenminal of the polypeptide chain), which form hydrophobic space called “heme pocket”, and a single heme (Figure 1-1) is accommodated in the space. The heme iron is coordinated to the protein through a histidine residue, the 8th residue in the F helix (His F8 or His93), as fifth ligand of the heme iron. O_2 binds reversibly to ferrous heme Fe atom as 6th ligand in Mb, and the O_2 binding properties of the protein have been shown to be obtained through subtle tuning of the intrinsic heme Fe reactivity, in addition to the heme environment furnished by nearby amino acid residues.

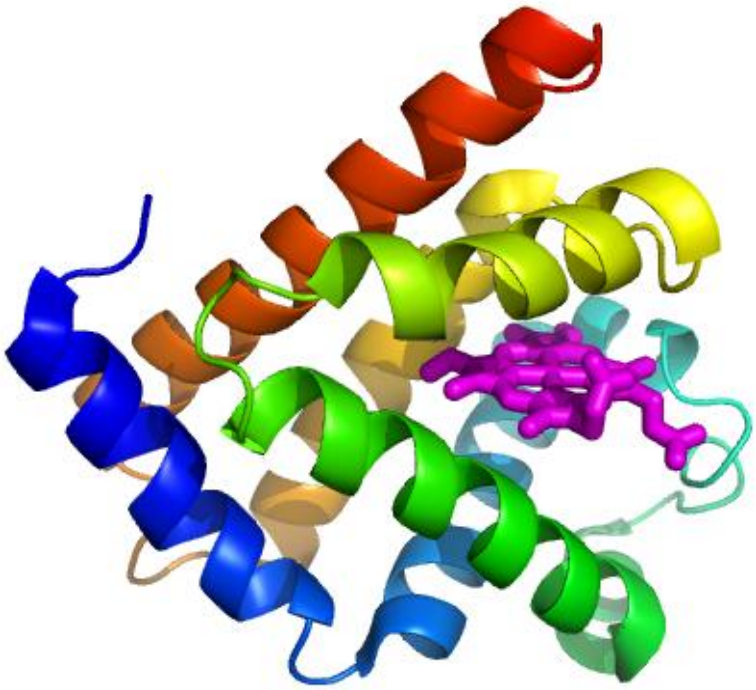

Figure 1-2. X-ray structure of Mb (PDB:1A6M).

Function of myoglobin

Function of Mb is described by scheme 1-2. Scheme 1-2A is the deoxy form of Mb(deoxy Mb). O_2 binds reversibly to heme Fe atom in Mb, the binding of O_2 to the heme Fe is stabilized by the hydrogen bonding between the Fe(II)-bound O_2 and His64(His64 H-bonding) (Scheme 1B) [23,24]. An $Fe^{3+}-O_2^-$-like species has been expected for the $Fe^{2+}-O_2$ bond (Scheme 1C) [25,26]. This process is oxygenation of Mb. However, oxygenated Mb is easily oxidized to metMb, which cannot bind O_2 (Scheme 1D and 1E) [27]. MetMb loses the ability of binding O_2. This process is known as "autoxidation". Understanding of the Mb function demands elucidation of the mechanisms responsible for control of both the O_2 affinity and autoxidation.

O_2 affinity of Mb is described in a form of the so-called oxygen equilibrium curve (OEC) (OEC is the plots of the degree of oxygenation, i.e., % of O_2-bound Mb, vs. partial pressure of O_2 (Figure 1-3)). OEC of Mb can be perfectly described by a hyperbolic curve according to Langmuir's absorption isotherm.

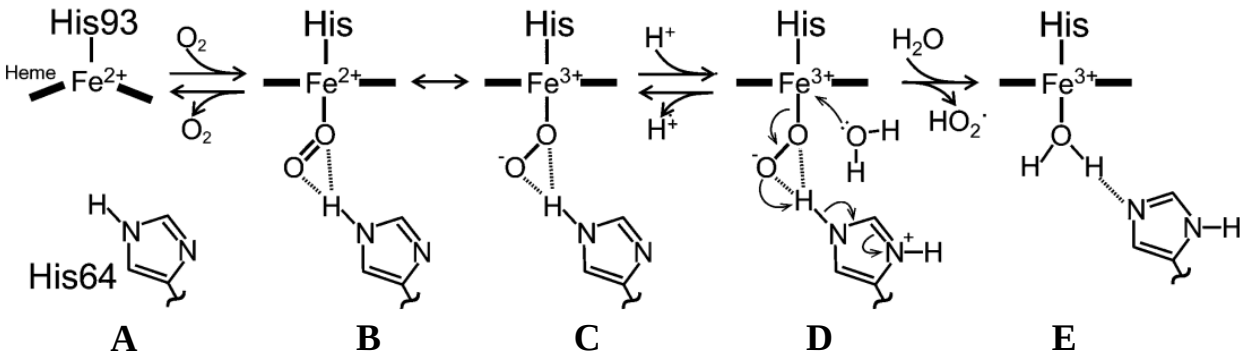

Scheme 1-2. Function of Mb. A: deoxyMb. B: The binding of O_2 to heme Fe atom is stabilized by the hydrogen bonding between the Fe^{2+} -bound O_2 and His64 C: Proposed state of binding O_2 to heme Fe D: Intermediate state of auoxidation E: MetMb

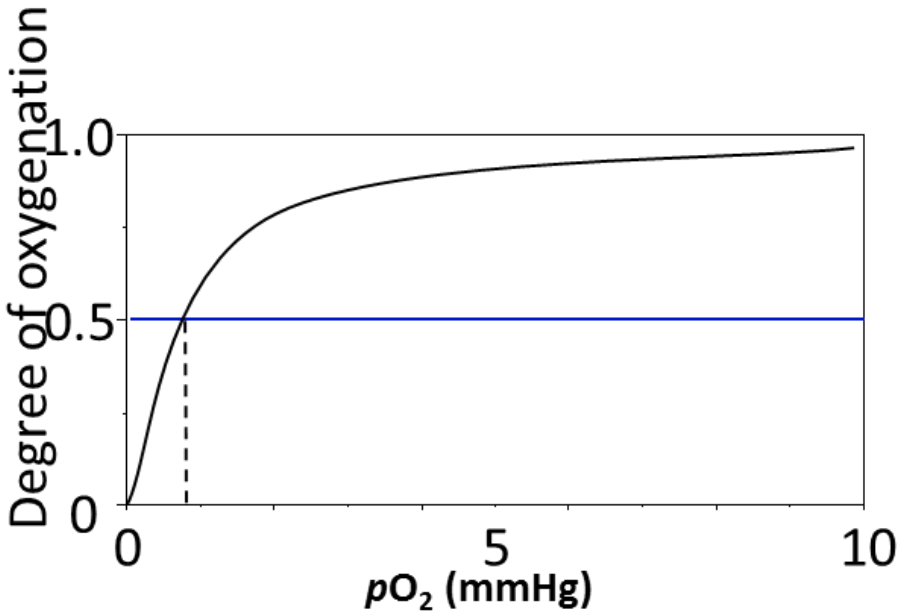

Figure 1-3. OEC of Mb

O_2 versus CO discrimination in oxygen binding hemoprotein.

Two types of Mb or Hb have been reported to exhibit the *M* values, the ratio between the equilibrium constants for CO and O_2 binding (K(CO)/K(O_2)) [28], less than unity. One is Hbs derived from parasitic nematode *Pseudoterranova decipiens* [29] and *Ascaris suum* [29], and trematode *Paramphistomum epiclitum* [30], *Gastrothylax crumenifer* [31], and *Explanatum explanatum* [31]. The other is Mb reconstituted with an iron-porphycene complex [32]. Monomeric *Paramphistomum epiclitum* Hb (*Pe*Hb) has been subjected to systematic mutation studies in order to elucidate molecular mechanisms responsible for control of its ligand binding properties [30]. *Pe*Hb possesses two Tyr residues at the B10 and E7 positions (B10 represents the 10th residue in the B helix and so forth), and exhibits the *M* value of 0.19 [30]. *Pe*Hb exhibited unusually small the rate constant for O_2 dissociton ($k_{off}(O_2)$) value, i.e., 0.07 s^{-1}[33]. The remarkably small $k_{off}(O_2)$ value of *Pe*Hb has been proposed to be due to the stabilization of Fe(II)-bound O_2 through hydrogen bonding with the two Tyr residues at the B10 and E7 positions, in addition to other nearby residues [31]. On the other hand, its relatively large the rate constant for O_2 association ($k_{on}(O_2)$) and the rate constant for CO association (k_{on}(CO)) values are likely to be inherited from a protein folding motif characteristic of O_2 binding hemoproteins, so-called the globin fold, with low kinetic barrier for the ligand entry [33], because these values are thought to be primarily determined by the heme pocket polarity and the accessibility of exogenous ligand to the heme pocket [30]. In addition, the rate constant for CO dissociton (k_{off}(CO)) value of *Pe*Hb reflects the intrinsically large stability of Fe(II)-bound CO in O_2 binding hemoprotein. Thus the preferential binding of O_2 over CO in *Pe*Hb was achieved through remarkably high O_2 affinity due to considerable reduction of the $k_{off}(O_2)$ value. In a similar way, the preferential binding of O_2 over CO in Mb reconstituted with an iron-porphycene complex was achieved through marked reduction of the $k_{off}(O_2)$ value [34].

Regulation of Mb function by amino acid residues around the heme

In order to elucidate roles of amino acid residues in the mechanistic relationship between the O_2 affinity and autoxidation of Mb, Site-directed mutagenesis studies have been studied. Olson and his associates [2,35] have investigated a great variety of artificial mutants. For example, the H64L mutant, in which His64 is replaced by Leu in order to remove the His64 H-bonding, exhibits low O_2 affinity and large autoxidation rate [36]. The removal of the His64 H-bonding decreases the stability of the O_2 bound state. On the other hand, the L29F mutant, where Leu29 is replaced by Phe, exhibits high O_2 affinity and small autoxidation rate [36,37]. The Fe-bound O_2 in the L29F mutant is stabilized by not only the His64 H-bonding, but also unique electrostatic interaction with the introduced Phe29. Hence, there is relationship between the stability of O_2 bound state in Mb and the O_2 affinity of the protein, i.e., Mb possessing lower (higher) O_2 affinity exhibits a larger (smaller) autoxidation rate.

There is an extensive hydrogen bond network among Leu89, Ser92, His93, and heme in the heme active site of Mb such that $N_\delta H$ hydrogen of His93 is hydrogen boded to the carbonyl O atom of Leu89 and O_γ of Ser92, and the $O_\gamma H$ of Ser92 to the carboxylate group of the heme-12-propinate (Figure 1-4) [38,39]. By removing hydrogen bonding interactions between Ser92 and His93 and a heme propionate, hydrophobicity of the heme pocket increases [40]. Then redox potential of the heme increasese. This hydrogen bond is also likely to fix the position of the His93 imidazole ring.

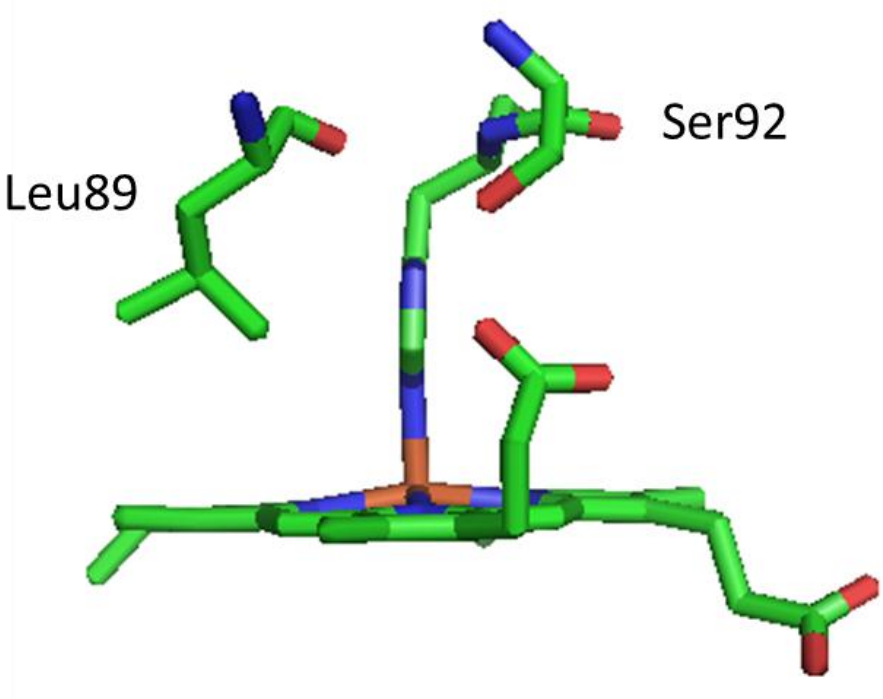

Figure 1-4. Hygrogen bond between $N_\delta H$ hydrogen of His93 is hydrogen boded to the carbonyl O atom of Leu89 and O_γ of Ser92.(PDB:2BLI)

Electronic control of ligand-binding properties of myoglobin

Sono et al. [41] demonstrated that substitution(s) of electron-withdrawing formyl group(s) in heme side chain(s) results in increasing CO affinity. However, the relationship between the heme electronic structure and Fe reactivity has remained to be clarified. Because it is difficult to change the heme electronic structure large enough to allow quantitative characterization of the structure-function relationship of Mb.

Recently, Shibata *et al*. [42] found novel regulation of the Mb functions through electron density of heme Fe atom (ρ_{Fe}). They utilized chemically modified heme cofactors possessing a heme Fe atom with a variety of electron densities (Fig. 1-5). To greatly alter ρ_{Fe}, they substituted strongly electron-withdrawing trifluoromethyl(CF_3) group(s), as peripheral sidechain(s) of the heme cofactor, to prepare 13,17-bis(2-carboxylatoethyl)-3,8-diethyl-2,12,18-trimethyl-7-trifluoromethylporphyrinatoiron(III)(7-PF) [43], 17-bis(2-and 3,17-bis(2-carboxylatoethyl)-3,7-diethyl-12,18-trimethyl-2,8-ditrifluoromethylporphyrinatoiron (III)(2,8-DPF)[42]. In addition, mesoheme(Meso) and 3,8-dimethyldeuteroporphyrinatoiron(III) (3,8-DMD)[44,45] were used as counterparts of 7-PF and 2,8-DPF, respectively. Because there is no covalent bond between heme and His93, the heme can be removed from the heme poket by using organic solvent at an acidic pH (Fig. 1-6) [46]. Obtained apoMb can be reacted with a chemically-modified heme to prepare reconstituted protein. This reaction is called "reconstitution". Using this method, reconstituted Mbs with a variety of chemically modified heme cofactors were prepared to elucidate the effects of a change in the ρ_{Fe} value on the O_2 affinity and autoxidation reaction rate of the proteins. Pairwise comparison between proteins reconstituted with Meso and 7-PF, and between proteins reconstituted with 3,8-DMD and 2,8-DPF, provides the structural and functional consequences of the substitution of one and two CF_3 groups, respectively. The ρ_{Fe} value was manifested in the pK_a one through its effect on the H^+ affinity of the Fe^{3+}-bound OH^-(Figure 1-7). They demonstrated that Mb possessing a smaller (larger) ρ_{Fe} value exhibits lower (higher) O_2 affinity and a smaller (larger) k_{ox} value [47].

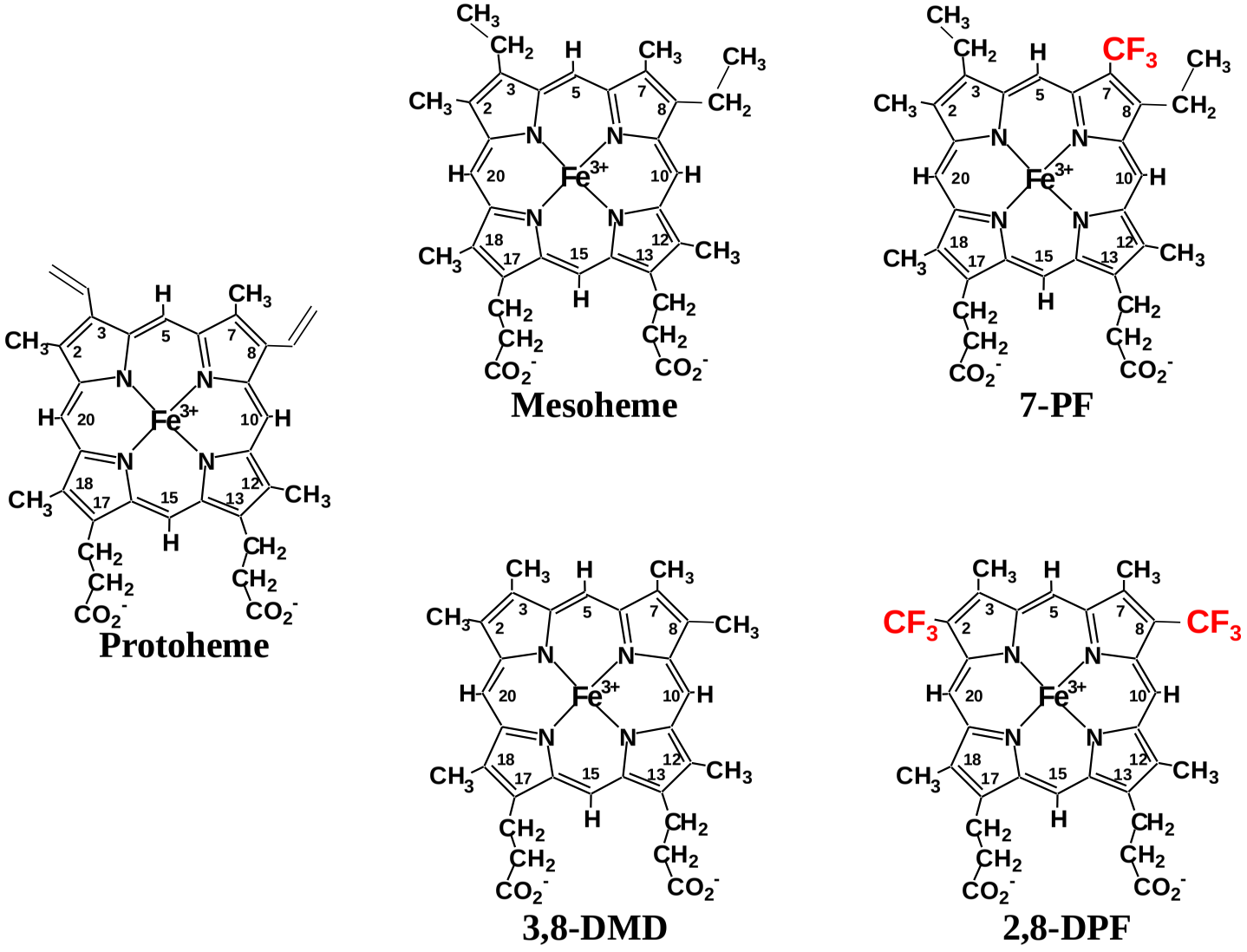

Figure 1-5. Molecular structures of ring-fluorinated hemes used in this study.

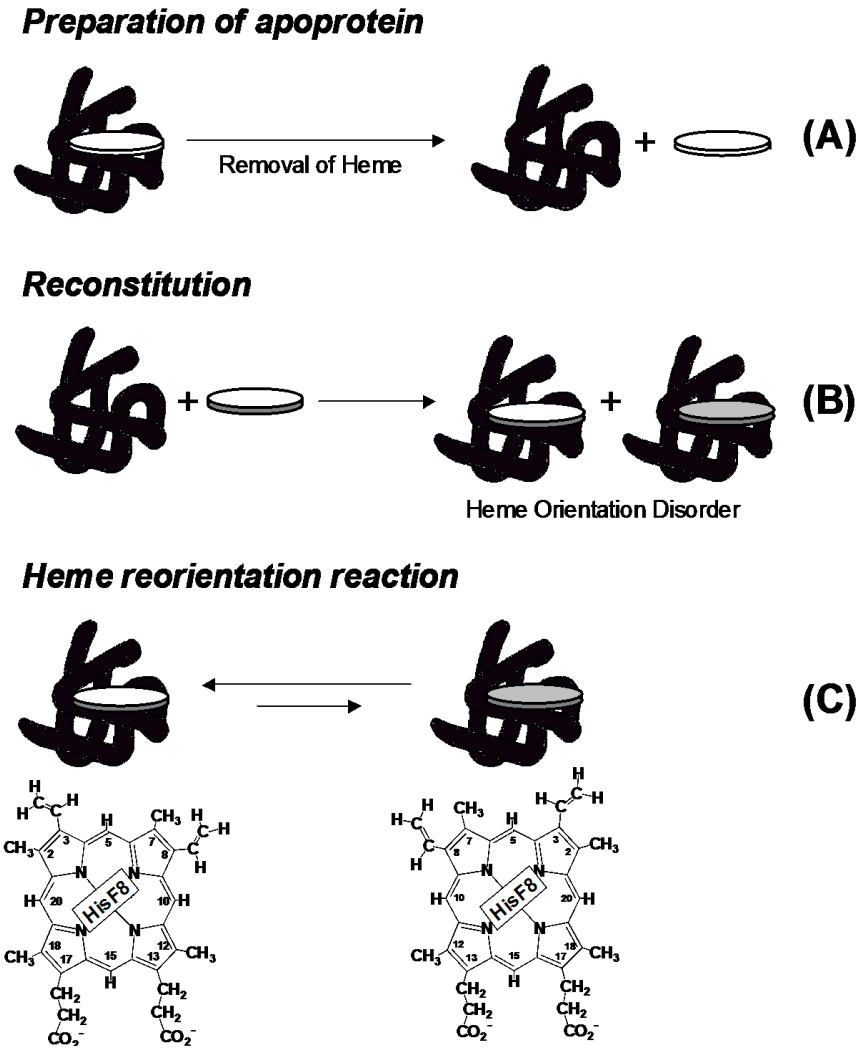

Figure 1-6. Preparation of (A)apoprotein, (B)reconstitution and (C)heme reorientation reaction.

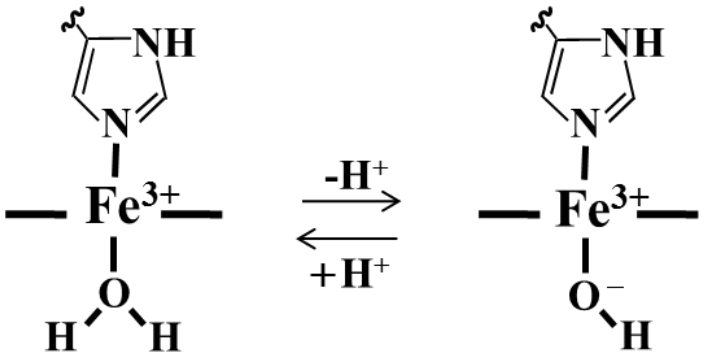

Figure 1-7. Acid-Alkaline Transition in metMb

The purpose of this study

In this dissertation, the molecular mechanism responsible for control of functional properties of myoglobin through the heme electronic structure and heme environment is discussed.

In chapter 2, quantitative evaluation method of electron density of the heme Fe atom (ρ_{Fe}) in the proteins is described. I found that the stretching frequency of Fe-bound CO(ν_{CO}) increases with decreasing the ρ_{Fe} value.

In chapter 3, the O_2 and CO binding properties of the H64L mutant of myoglobin are described. I found that the O_2 and CO affinities of Mb lacking the His64 H-bonding can be controlled solely by the ρ_{Fe} value.
A novel relationship between the regulation of the Mb function through the heme environment furnished by the His64 H-bonding and that effect of intrinsic heme Fe reactivity through the ρ_{Fe} value is revealed.

In chapter 4, the O_2 versus CO ligand binding preference of the L29F mutant is controlled through altering the ρ_{Fe} value. I demonstrated the ratio between the equilibrium constants for CO and O_2 binding of Mb can be regulated over a range of $\sim 10^5$ through combined use of the chemical modification of heme cofactors and the replacements of amino acid residues in the distal heme pocket.

In chapter 5, the effect of a change in the ρ_{Fe} value on the electronic nature of the His93 imidazole in deoxy Mb is discussed. I found that the bond between the heme Fe atom and His93 becomes stronger with increasing number of CF_3 substitutions because of an increase in acidity of the His93N_δH hydrogen bonded to the carbonyl O atom of Leu89.

In chapter 6, the conclusions of the study are summarized.

References

[1] Antonini, E.; Brunori, M. In *Hemoglobins and Myoglobins and their Reactions with Ligands*; North Holland Publishing: Amsterdam, **1971**.

[2] Springer, B. A.; Sligar, S. G.; Olson, J. S.; Phillips, G. N., Jr. *Chem. Rev*., **1994**, 94, 699-714.

[3] Perutz, M. F. *Nature*, **1970**, 228, 726-734

[4] Lukin, J. A.; Kontaxis, G.; Simplaceanu, V.; Yuan, Y.; Bax, A.; Ho, C. Proc. *Natl. Acad. Sci.* , **2003,** 100, 517-520.

[5] Scott, R. A.; Mauk, A. G. University Science Books, Sausalito, **1996**

[6] Yamamoto, Y.; Terui, N.; Tachiiri, N.; Minakawa, K.; Matsuo, H.; Kameda, T.; Hasegawa, J.; Sambongi, Y.; Uchiyama, S.; Kobayashi, Y.; Igarashi, Y. *J. Am. Chem. Soc.*, **2002**, 124, 11574-11575.

[7] Sono, M.; Roach, M. P.; Coulter, E. D.; Dawson, J. H. *Chem. Rev.* , **1996**, 96, 2841-2887

[8] Aono, S. *Dalton Trans.*, **2008**, 3137-3146.

[9] David, M.; Daveran, M.-L.; Batut, J.; Dedieu, A.; Domergue, O.; Ghai, J.; Hertig, C.; Boistard, P.; Kahn, D. *Cell*, **1988**, 54, 671-683.

[10] Stuehr, D. J. *Biochim. Biophys. Acta*, **1999**, 1411, 217-230.

[11] Hanania G.I.; Yeghiayan A.; Cameron B.F. *Biochem J.*, **1966,** 98(1), 189-192.

[12] Yamamoto Y. *Annu. Rep. NMR Spectro.*, **1998**, 36, 1-77.

[13] Hu S.; Smith K. M.; Spiro T. G. *J. Am. Chem. Soc.*, **1996**, 118, 12638-12646.

[14] Rang, G.; Asakura, T.; Yonetani, T. *Biochim. Biophys. Acta*, **1970**, 214, 381-388.

[15] La Mar, G. N.; Satterlee, J. D.; de Ropp, J. S. In *The Porphyrin Handbook*, (Kadish, K., Smith, K. M., and Guilard, R., eds.), Academic Press, New York, **2000**, pp 185-298.

[16] Spiro T. G.; Zgierski, M. Z.; Kozlowski, P. W. *Coord. Chem. Rev.*, **2001**, 923, 219-221.

[17] Spiro T. G.; Burke J. M. *J. Am. Chem. Soc.*, **1976**, 98, 5482-5489.

[18] Kitagawa T.; Kyogoku Y.; Iizuka T.; Saito M.I. *J. Am. Chem. Soc.*, **1976**, 98, 5169-5173.

[19] Li T.S.; Quillin M.L.; Phillips G.N.; Olson J.S. *Biochemistry*, **1994**, 33, 1433–1446.

[20] Alben J. O.; Caughey, W. S. *Biochemistry*, **1968**, 7, 175-183.

[21] Perutz M. F.; Rossmann M. G.; Cullis A. F.; Muirhead H.; Will G.; North A. C. *Nature*, **1960**, 185, 416-422.

[22] Kendrew J. C.; Dickerson R.E.; Strandberg B. E.; Hart R.G.; Davies D. R.; Phillips D. C.; Shore V. C. *Nature*, **1960**, 185, 422-427.

[23] Phillips, S. E. V.; Schoenborn, B. P. *Nature*, **1981**, 292, 81-82.

[24] Lukin, J. A.; Simplaceanu, V.; Zou, M.; Ho, N. T.; Ho, C. *Proc. Natl. Acad. Sci. U.S.A.*, **2000**, 97, 10354-10358.

[25] Pauling, L. *Nature*, **1964**, 203, 182-183.

[26] Maxwell, J. C.; Volpe, J. A.; Barlow, C. H.; Caughey, W. S. *Biochem. Biophys. Res. Commun.*, **1974**, 58, 166-171.

[27] George, L.; Stratmann, C. J. *Biochem. J.*, **1954**, 57, 568-573.

[28] Springer, B. A.; Egeberg, K. D.; Sligar, S. G.; Rohlfs, R. J.; Mathews, A. J.; Olson, J. S. *J. Biol. Chem.*, **1989**, 264, 3057-3060.

[29] Gibson, Q. H.; Regan, R.; Olson, J. S.; Carver, T. E.; Dixon, B.; Pohajdak, B.; Sharma, P. K.; Vinogradov, S. N. *J. Biol. Chem.*, **1983**, 268, 16993-16998.

[30] Pesce, A.; Dewide, S.; Kinger, L.; Milani, M.; Ascenzi, P.; Marden, M. C.; Van Hauwaert, M.; Vanfleteren, J.; Moens, L.; Bolognesi, M. *J. Mol. Biol.*, **2001**, 309, 153-1164.

[31] Kinger, L.; Rashid, A. K.; Griffon, N.; Haque, M.; Moens, L.; Gibson, Q. H.; Poyart, C.; Marden, M. C. *Biophys. J.*, **1998**, 75, 990-998.

[32] La Mar, G. N.; Budd, D. L.; Visco, D. B.; Smith, K. M.; Langry, L. C. Proc. *Natl. Acad. Sci. U. S. A.*, **1978**, 75, 5755-5759.

[33] Birukou, I.; Schweers, R. L.; Olson, J. S. *J. Biol. Chem.*, **2010**, 285, 8840-8854.

[34] Matsuo, T.; Dejima, H.; Hirota, S.; Murata, D.; Sato, H.; Ikegami, T.; Hori, H.; Hisaeda, Y.; Hayashi, T. *J. Am. Chem. Soc.*, **2004**, 126, 16007-16017.

[35] Olson, J. S.; Phillips, G. N., Jr. *J. Biol. Inorg. Chem.*, **1997**, 2, 544−552.

[36] Brantly, R. E.; Smerdon, S. J.; Wilkinson, A. J.; Singleton, E. W.; Olson J. S. *J. Biol. Inorg. Chem.*, **1993**, 268, 6995-7010.

[37] Carver, T. E.; Brantly, R. E. Jr.; Singleton, E. W.; Arduini, R. M.; Quillin, M. L.; Phillips, G. N. Jr.; Olson, J. S. *J. Biol. Chem.*, **1992**, 267, 14443-14450.

[38] Cheng, X. D.; Schoenborn, B. P. *J. Mol. Biol.*, **1991**, 220, 381-399

[39] Oldfield, T. J.; Smerdon, S. J.; Dauter, Z.; Petratos, K.; Wilson, K. S.; Wilkinson, A. J. *Biochemistry*, **1992**, 31, 8732-8739.

[40] Bhaqi-Damodaran, A.; Petrik, I. D.; Marshall, N. M.; Robinson, H. Lu, Y. *A. Am. Chem. Soc*., **2014**, 136, 11882-11885.

[41] Sono, M; Smith, P. D.; Mccray, J. A.; Asakura, T. *J. Biol. Chem*., **1976**, 251, 1418-1426

[42] Shibata, T. Nagao, S.; Fukaya, M.; Tai, H.; Nagatomo, S.; Morihashi, K.; Matsuo, T.; Hirota, S. Suzuki, A.; Imai, K.; Yamamoto, Y. *J. Am. Chem. Soc*., **2010**, 132, 6091-6098.

[43] Toi, H.; Homma, M.; Suzuki, A.; Ogoshi, H. *J. Chem. Soc., Chem. Commun.*, **1985**, 1791–1792.

[44] Chang, C. K.; Ward, B.; Ebina, S. *Arch. Biochem. Biophys.*, **1984**, 231, 366-371.

[45] Neya, S.; Suzuki, M.; Hoshino, T.; Ode, H.; Imai, K.; Komatsu, T.; Ikezaki, A.; Nakamura, M.; Furutani, Y.; Kandori, H. *Biochemistry*, **2010**, 49, 5642-5650.

[46] Teale, F. W. J. *Biochim. Biophys. Acta*, **1959**, 35, 543.

[47] Shibata, T.; Matsumoto, D.; Nishimura, R.; Tai, H.; Matsuoka, A.; Nagao, S.; Matsuo, T.; Hirota, S.; Imai, K.; Neya, S.; Suzuki, A.; Yamamoto, Y. *Inorg. Chem.*, **2012**, 51, 11955-11960.

Chapter 2

Relationship between the electron density of the heme Fe atom and the vibrational frequencies of the Fe-bound carbon monoxide in myoglobin

Abstract

The vibrational frequencies of the Fe-bound carbon monoxide (CO) of myoglobin reconstituted with a series of chemically-modified heme cofactors possessing a heme Fe atom with a variety of electron densities have been analyzed. The study revealed that the stretching frequency of Fe-bound CO (ν_{CO}) increases with decreasing electron density of the heme Fe atom (ρ_{Fe}). This finding demonstrated that the ν_{CO} value can be used as a sensitive measure of the ρ_{Fe} value, and that the π back-donation of the heme Fe atom to CO is affected by the heme π-system perturbation induced through peripheral side chain modifications.

INTRODUCTION

Myoglobin (Mb), the oxygen (O_2) storage hemoprotein, has been regarded as a useful model system for understanding the structure-function relationships of metalloproteins [1-6]. O_2 binds reversibly to the ferrous heme Fe atom in Mb, and the O_2 binding properties of the protein have been shown to be obtained through subtle tuning of the intrinsic heme Fe reactivity, in addition to the heme environment furnished by nearby amino acid residues [4,5]. The importance of the heme electronic structure, particularly the electron density of the heme Fe atom (ρ_{Fe}), in the regulation of the heme Fe reactivity in the protein is now beginning to be realized [7,8]. Hence, the establishment of methodology for quantitative estimation of the ρ_{Fe} value of Mb is needed to gain a deeper understanding of the molecular mechanism responsible for the regulation of the heme Fe reactivity through the ρ_{Fe} value. It is previously used the equilibrium constant, pK_a, of the so-called "acid-alkaline transition" in metmyoglobin (metMb) to estimate the ρ_{Fe} value in the protein (Figure 2-1) [7].

MetMb possessing highly conserved distal His64 has H_2O and OH^- as coordinated external ligands under low and high pH conditions, respectively [1,9-12]. The ρ_{Fe} value is manifested in the pK_a one through its effect on the H^+ affinity of the Fe^{3+}-bound OH^-. Thus, this methodology is applicable only to Mbs capable of accommodating H_2O as an external ligand to the ferric heme Fe atom under low pH condition. Generally, in Mbs lacking distal His64, irrespective of whether they are naturally occurring mutants [13-18] or genetic ones [19], the sixth coordination site is either partially occupied by H_2O or empty. Consequently, other physicochemical parameters are needed to estimate the ρ_{Fe} values of the proteins.

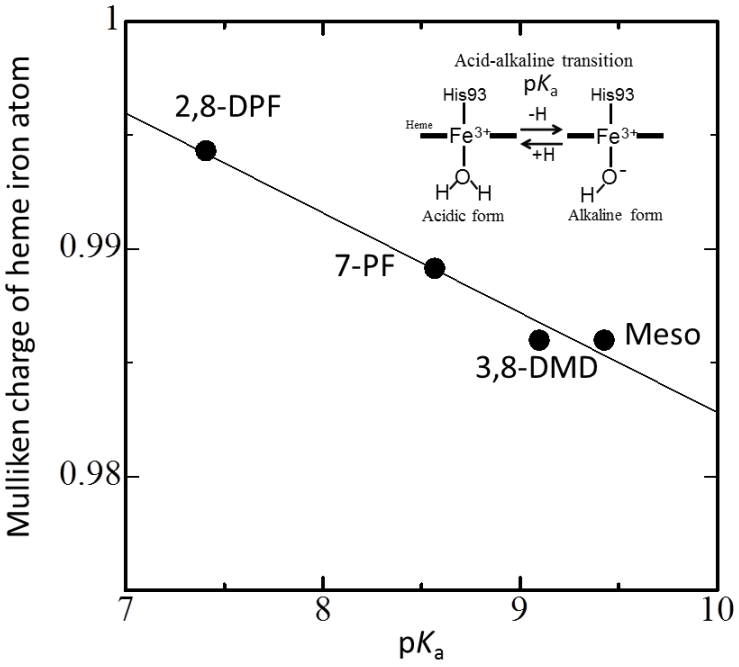

Figure 2-1. Plots of Mulliken charges of the heme iron atoms calculated for the model compounds against the equilibrium constant (pK_a) of the "acid-alkaline transition" (see inset) in metMb. The Mulliken charges for the hemes were adopted from Shibata et al.,[6] and the charge for 3,8-DMD was assumed to be equal to that for Meso. The value of 9.1 ± 0.1 has been reported for the pK_a one of Mb(3,8-DMD).[8] The plots can be represented by a straight line, supporting the validity of the use of the pK_a value as an indicator of the electron density of the heme iron atom in the protein.

In this chapter, I focused on carbon monoxide(CO) adducts of Mbs(MbCOs), because not only CO is known to be inevitably bound to the proteins, but also the proteins each possess a physiologically active ferrous heme Fe atom. I observed the vibrational frequencies of the Fe-bound CO [20-22], that is, the stretching frequency of Fe-bound CO(ν_{CO}), and the Fe-C stretching(ν_{FeC}) and Fe-C-O bending frequencies (δ_{FeCO}) in native Mb and two mutant Mbs. One is H64L mutant, which is removed the distal His64. The another mutant is L29F mutant, which stabilizes the Fe(II)-bound O_2 state due to a unique electrostatic interaction with the introduced Phe29, in addition to hydrogen bond with distal His64. Then native Mb and mutant proteins were reconstituted with mesoheme(Meso), 3,8-dimethyldeuteroporphyrinatoiron(III) (3,8-DMD) [23,24], 13,17-bis(2-carboxylatoethyl)-3,8-diethyl-2,12,18-trimethyl-7-trifluoromethylporphyrinatoiron(III) (7-PF) [25] and13,17-bis(2- carboxylatoethyl)-3,7-diethyl-12,18-trimethyl-2,8-ditrifluoromethylporphyrinatoiron(III) (2,8-DPF) [7], that are, Mb(H), H64L(H), and L29F(H), where H is Proto, Meso, 3,8-DMD, 7-PF, or 2,8-DPF. These heme cofactors differ in the numbers of CF_3, CH_3, and C_2H_5 side chains (Figure 2-2). Based on the pK_a values of the proteins, these heme cofactors could be ranked as Mb(2,8-DPF) < Mb(7-PF) < Mb(3,8-DMD) ≈Mb(Meso), in order of increasing ρ_{Fe} value (Figure 2-1). I found that the ν_{CO} value of a protein correlates well with the pK_a value in such a manner that Mb possessing a lower pK_a value exhibits a higher ν_{CO} one. The relationship between the ν_{CO} and pK_a (and hence ρ_{Fe}) values could be interpreted in terms of the resonance between the two canonical forms of the Fe-CO fragment [26]. The study not only revealed the relationship between the ν_{CO} and ρ_{Fe} values, but also demonstrated that the ν_{CO} value can be used as a sensitive measure of the ρ_{Fe} one in the protein.

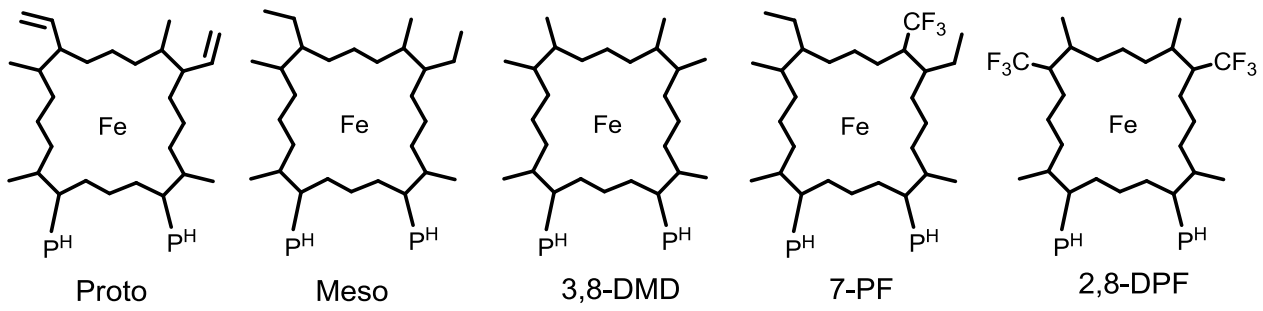

Figure 2-2. Schematic representation pf structures of the heme cofactors used in this study, i.e., proto(Proto), 3,8-dimethyldeuteroporphyrinatoiron(III)(3,8-DMD)[23,24], 13,17-bis(2-carboxylato -ethyl)-3,8-diethyl-2,12,18-trimethyl-7-trifluoromethyl-porphyri-natoiron(III)(7-PF)[25] and13,17-bis(2-carboxylatoethyl)-3,7-diethyl-12,18-trimethyl-2,8-ditrifluoromethylporphyrinatoiron(III)(2,8-DP F)[7]. Abbreviation: P^H reprents $–CH_2CH_2COOH$.

MATERIALS AND METHODS

Materials and protein samples. All reagents and chemicals were obtained from commercial sources and used as received. Sperm whale Mb was purchased as a lyophilized powder from Biozyme and used without further purification. The expression and purification of the H64L mutant (H64L(Proto)) were carried out according to the method described by Springer et al.[27]. The expression and purification of the L29F mutant protein (L29F(Proto)) were carried out according to the methods described by Carver et al.[28]. Mesoheme (Meso) was purchased from Frontier Scientific Co. 3,8-DMD [23,24], 7-PF [25], and 2,8-DPF [7] were synthesized as previously described. The apoprotein of Mb(apoMb), H64L mutant(H64L(Proto)) and L29F mutant(L29F(Proto) were prepared at 4 °C according to the procedure of Teale [29] and reconstituted Mbs and mutant proteins were prepared by slow addition of a synthetic heme cofactor to the apoMb in 50 mM potassium phosphate buffer, pH 7.0, at 4 °C. In order to prepare CO bound protein, oxidazid protein was reduced by adding $Na_2S_2O_4$ (Nakalai Chemicals Ltd.) in the presence of CO gas (Japan Air Gases), and then the protein was freed from excess reagents by passage through a Sephadex G-10 (Sigma-Aldrich Co.) column equilibrated with an appropriate buffer solution. Met-cyano forms of the Mb and mutant proteins, i.e., MbCN, H64LCN, L29FCN were prepared by adding KCN (Nakalai Chemicals Ltd.) to met-forms of the proteins obtained through oxidation of the proteins using $K_3Fe(CN)_6$ (Nakalai Chemicals Ltd.). The pH of each sample was measured with a Horiba F-22 pH meter equipped with a Horiba type 6069-10c electrode. The pH of a sample was adjusted using 0.1 M NaOH or HCl.

NMR Spectroscopy. ^1H spectra of H64LCNs and L29FCNs were recorded on a Bruker AVANCE-400 spectrometer operating at ^1H frequency of 400 MHz. Typical ^1H NMR spectra consisted of about 20k transients with a 100 kHz spectral width and 16k data points. The signal-to-noise ratio of the spectra was improved by apodization, which introduced ~10 Hz line broadening. The chemical shifts of ^1H NMR spectra are given in ppm downfield from the residual $^1H^2HO$, as an internal reference.

Resonance raman spectroscopy. Resonance raman scattering was performed with excitation at 413.1 nm with a Kr^+ laser (Spectra Physics, BeamLok 2060), dispersed with a polychromator (SPEX 1877, 1200 grooves/mm grating), and detected with a liquid nitrogen-cooled charge coupled device (CCD) detector

(CCD-1024×256-OPEN-1LS, HORIBA Jobin Yvon) [30]. A laser power of 1.6 mW was used for the measurements. CO isotopes, that is, $^{13}C^{16}O$ and $^{13}C^{18}O$, were purchased from SI Science Co., Ltd, Japan. Raman shifts were calibrated with indene as a frequency standard. The accuracy of the peak positions of well-defined Raman bands was ±1 cm^{-1}. The protein concentrations were approximately 40 μM in 100 mM potassium phosphate buffer, pH 7.4.

RESULTS

^{1}H NMR spectra of met-cyano forms of the H64L and L29F proteins. ^{1}H NMR spectra of the met-cyano forms of the H64L mutant proteins, i.e., H64L(Proto)CN, H64L(Meso)CN, H64L(3,8-DMD)CN, H64L(7-PF)CN, and H64L(2,8-DPF)CN, are shown in Figure 2-3, and those of the L29F mutant proteins, i.e., L29F(Proto)CN, L29F(Meso)CN, L29F(3,8-DMD)CN, L29F(7-PF)CN, and L29F(2,8-DPF)CN, in Figure 2-4. The paramagnetically-shifted NMR signals due to heme side chain protons and amino acid protons in close proximity to the heme in a protein have been shown to be quite sensitive to the heme electronic structure and the heme active site structure, respectively[31－33]. The shift patterns of the paramagnetically-shifted ^{1}H NMR signals of the H64L and L29F mutant proteins were similar to those of the native proteins possessing the identical heme cofactors, indicating that the heme cofactors of the mutant proteins were accommodated properly as for those in the native ones [7]. Similarity in the shifts of Ile99 $C_\delta H_3$ and $C_\gamma H$ proton signals (Figure 2-5), resolved at ~-4 and ~-10 ppm, respectively, among the mutant proteins, supported that the orientations of the heme cofactors with respect to the polypeptide chains in these mutant proteins are similar to each other. In addition, the observation of two sets of heme methyl proton signals in the spectra H64LCN(Meso), H64LCN(7-PF), and L29F(7-PF)CN, with the ratios of 9:1, 1:2.2 and 1:2 for major form (*M*):minor form (*m*), respectively, is due to the presence of well-known heme orientational isomers [34], as depicted in the inset in Figures 2-3.

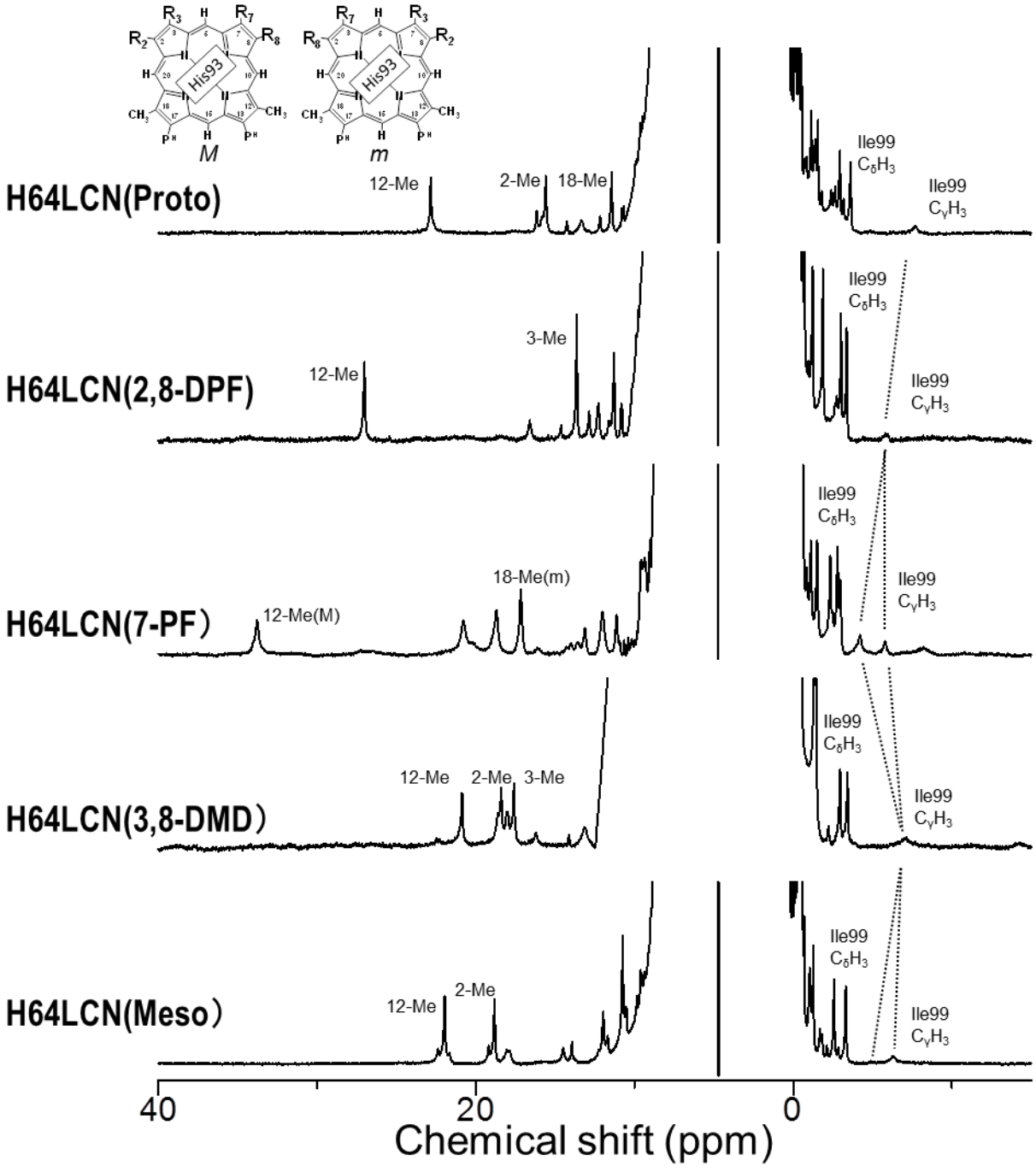

Figure 2-3. 400 MHz ^{1}H NMR spectra of met-cyano forms of the H64L mutant myoglobin and the proteins reconstituted with mesoheme at pH 6.91 (A), 7-PF at pH 7.57 (B), 2,8-DPF at pH 7.40 (C), and native Mb at pH 7.40 (D) in 90% H_2O/10% ^2H_2O at 25 ^oC. The assignments of heme methyl and Ile99 proton signals are given with the spectra, and *M* and *m* forms in the inset represent the two different orientations of the heme, relative to the protein [34]. Corresponding signals are connected by a broken line.

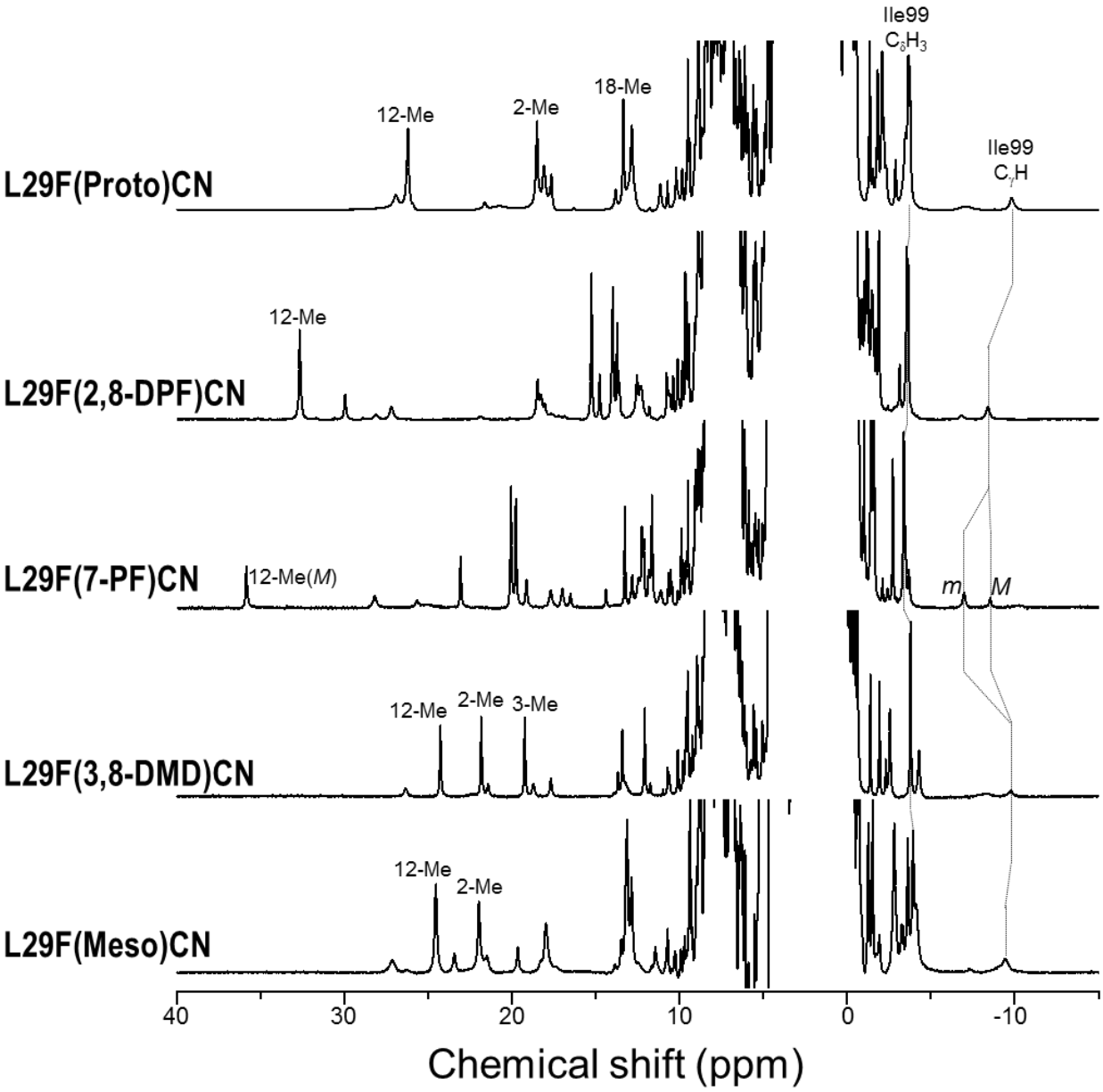

Figure 2-4. 600 MHz ^{1}H NMR spectra of L29F(Meso)CN, L29F(3,8-DMD)CN, L29F(7-PF)CN, L29F(2,8-DPF)CN, and L29F(Proto)CN at pH 7.40 in 90% H_2O/10% $^{2}H_2O$ at 25 ^{o}C. The assignments of Ile99 proton signals and the tentative ones of heme methyl proton signals are given with the spectra, and the *M* and *m* forms in the inset represent the two different orientations of 7-PF, relative to the protein[34]. Corresponding signals are connected by a broken line.

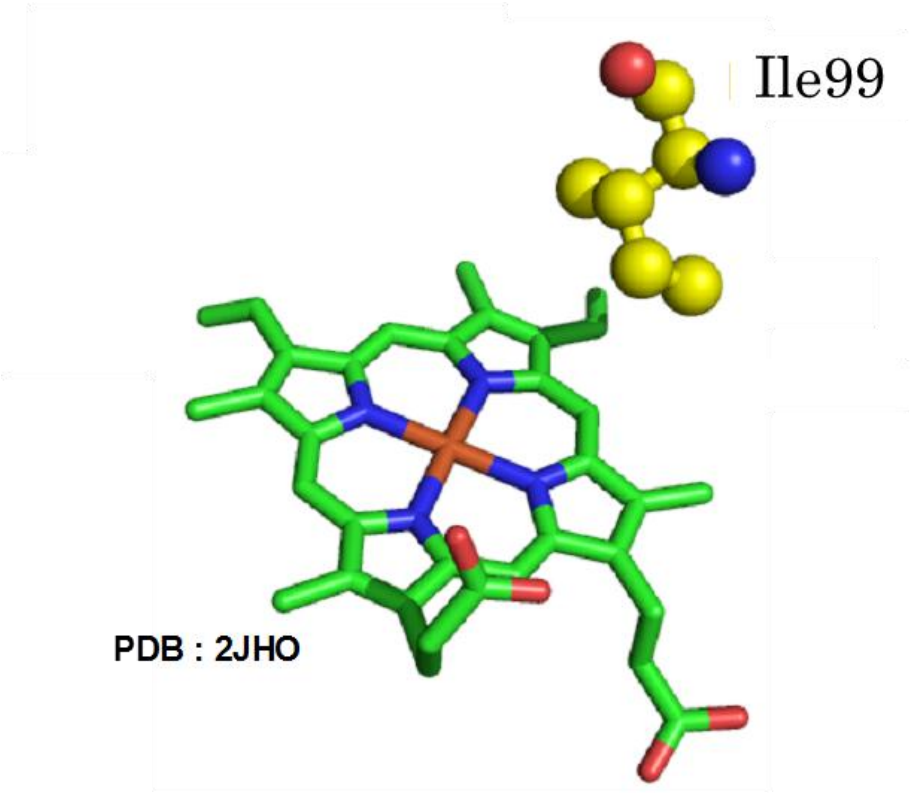

Figure 2-5. Orientation of Ile99, with respect to heme, in met-cyano form of Mb

Vibrational frequencies of Fe-bound CO of the Mb and mutant proteins. The ν_{CO}, ν_{FeC}, and δ_{FeCO} values of native MbCO proteins are summarized in Table 2-1. The ν_{CO} bonds of the proteins are shown in Figure 2-6. The ν_{CO} band of the protein contained multiple components (Figure 2-6), and the observation of the multiple ν_{CO} bands is not due to the heme orientational disorder, because of the observation of similar multiple bands in the spectra of Mbs reconstituted with C_2 symmetric hemes, that is, 3,8-DMD and 2,8-DPF. Consequently, the doublets in Figure 2-6 are due to the presence of multiple conformational states of the Fe-CO fragment [35]. Thus the increase in number of ν_{CO} bands upon the substitution of CF_3 group(s) suggested that the number of conformational states taken by the Fe-CO fragment increases with decreasing ρ_{Fe} value, possibly due to weakening of the Fe-CO bond. The positions of the individual component ν_{CO} bands of the native Mbs were determined through fitting with Voigt profiles[36], which are convolutions of Gaussian and Lorentzian functions (Figures 2-7－2-11). The high and low frequency ν_{CO} values ($\nu_{CO(H)}$ and $\nu_{CO(L)}$ values, respectively), and the weighted-average by the intensity of each band ($\nu_{CO(ave)}$) of native Mbs were determined. As shown in Figure 2-6, the ν_{CO} bands of native MbCO appeared at 1947 cm^{-1} with a shoulder at 1935 cm^{-1} (Figure 2-6), and the determined values were larger by 2-3 cm^{-1} than those previously reported, that is, a main band at 1944 cm^{-1} with a shoulder near 1933 cm^{-1}[37]. Since the ν_{CO} bands were considerably broad (Figures 2-7－2-11), uncertainty of 2-3 cm^{-1} would be associated, as a method-dependent variation, with determination of the positions of the individual component bands. The ν_{FeC} band of the native Mb also appeared as unresolved multiple peaks, possibly due to the multiple conformational states of the Fe-CO fragment, as in the case of the ν_{CO} band, and hence accurate determination of their positions was quite difficult. CO isotope substitution measurements were made to estimate the frequencies of the ν_{FeC} bands of the proteins (Figure 2-12). Finally, in contrast to the ν_{CO} and ν_{FeC} bands, the δ_{FeCO} one was observed as a single component, although the band overlapped with other unassigned porphyrin ones. Hence, the position of the δ_{FeCO} band was determined through fitting with Voigt profiles [36](Figures 2-13－2-17).

As shown in Table 2-1, the ν_{CO}, ν_{FeC}, and δ_{FeCO} values were all affected by the heme modifications. In particular, the ν_{CO} value increased dramatically with the CF_3 substitutions (Table 2-1). This finding is consistent with those of Tsubaki et al.[37], who demonstrated that the ν_{CO} value increased upon replacement of the heme vinyl group(s) with electron-withdrawing formyl one(s). Comparison of the $\nu_{CO(H)}$ values of the

proteins yielded a difference of 7 cm^{-1} for the Mb(Meso)/Mb(7-PF) system, which is half the value, 13 cm^{-1}, for the Mb(3,8-DMD)/Mb(2,8-DPF) one. Similarly, comparison of the $\nu_{CO(L)}$ values yielded a difference of 8 cm^{-1} for the Mb(Meso)/Mb(7-PF) system, which is also half the value, 15 cm^{-1}, for the Mb(3,8-DMD)/Mb(2,8-DPF) one. These results demonstrated the additive effect of the heme π-system perturbation on the ν_{CO} value, as reported for the formyl substitution system[37]. Furthermore, comparison of the ν_{FeC} bands of the proteins yielded a difference of 1 cm^{-1} for the Mb(Meso)/Mb(7-PF) system, which is half the value, 2 cm^{-1}, for the Mb(3,8-DMD)/Mb(2,8-DPF) one, which also demonstrated the additive effect of the heme π-system perturbation on the ν_{FeC} value, although the effect was rather small.

Finally, the low frequency shift of the δ_{FeCO} value with increasing number of CF_3 substitutions suggested that the orientation of the Fe-bound CO, with respect to the heme, in a protein is affected by the ρ_{Fe} value.

Table 2-1. Vibrational Frequencies of the Fe-bound CO and Fe-bound O_2 of the L29F mutant proteins, native Mbs, and the H64L mutant proteins at pH 7.40 and 25 °C.

Heme	ν_{CO}[a] (cm^{-1})					ν_{FeC}[b] (cm^{-1})			δ_{Fe-CO}[c] (cm^{-1})		
	L29F	Mb $\nu_{CO(H)}$[d]	Mb $\nu_{CO(L)}$[e]	Mb $\nu_{CO(ave)}$[f]	H64L	L29F	Mb	H64L	L29F	Mb	H64L
Meso	1928	1943	1931	1939	1965	526	515	489	581	576	575
3,8-DMD	1928	1943	1930	1940	1964	528	514	491	583	576	575
7-PF	1936	1940	1939	1945	1972	523	514	489	580	575	573
2,8-DPF	1944	1956	1945	1951	1978	518	512	483	578	574	570
Proto	1933	1947	1935	1943	1969	524	512	490	581	576	574

a: The C-O stretching frequency of the Fe-bound CO.
b: The Fe-C stretching frequency of the Fe-bound CO.
c: The Fe-C-O bending frequency of the Fe-bound CO.
d: ν_{CO} value of the high-frequency band (Figures 7－11).
e: ν_{CO} value of the low-frequency band (Figures 7－11).
f: The weighted-average ν_{CO} value.

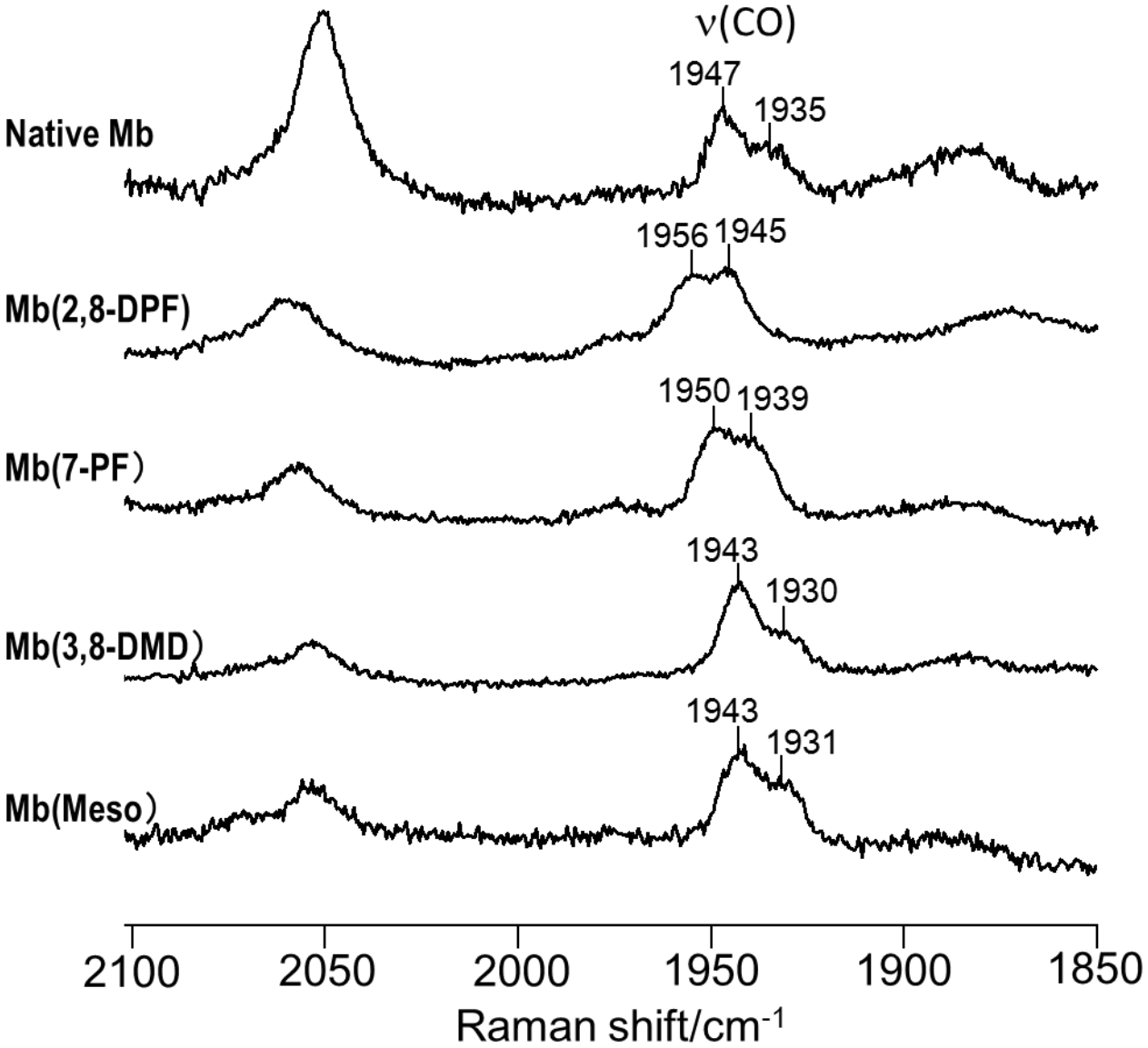

Figure 2-6. High-frequency regions of visible resonance raman spectra of MbCO(Meso), MbCO(3,8-DMD), MbCO(7-PF), MbCO(2,8-DPF), and native MbCO at pH7.40 and 25 °C. The positions of the individual component ν_{CO} bands of the proteins determined through fitting with Voigt profiles[35] (Figures 7～11) are indicated with the spectra.

	cm^{-1}	Area
Peak 0	1943	0.3362
Peak 1	1931	0.1782

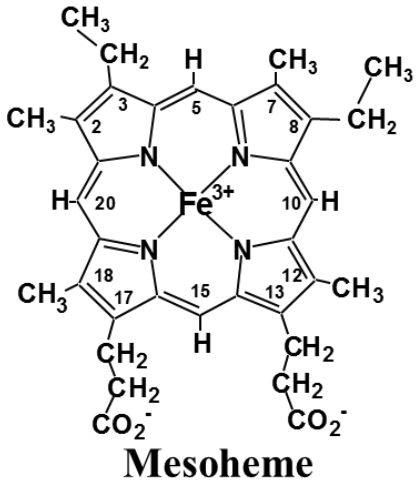

Mesoheme

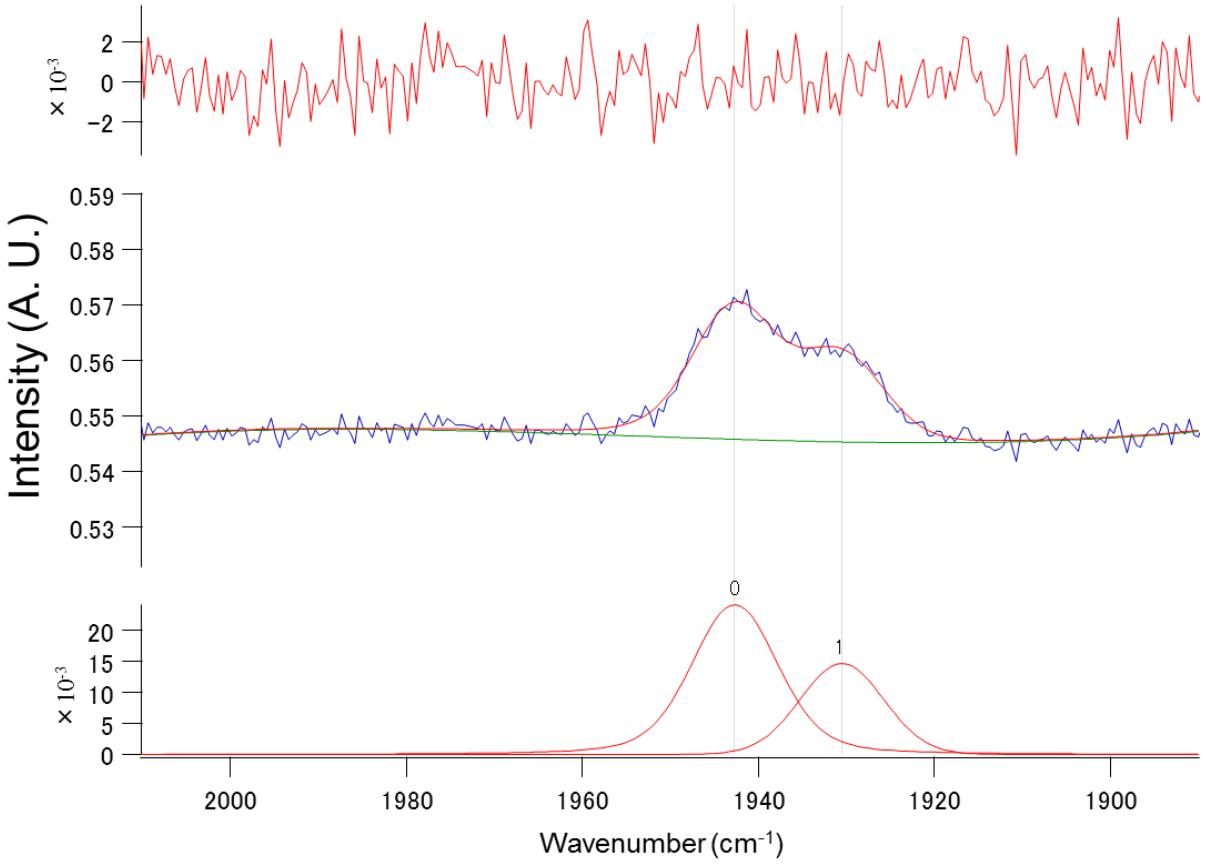

Figure 2-7. Visible resonance raman spectrum of CO form of Mb(Meso) in 100 mM potassium phosphate buffer pH 7.4 at 25 °C. Residual error (the difference between the experimental and theoretical values) (top), observed (blue) and simulated (red) ν_{CO} bands (middle), and simulated individual bands (bottom). A green line in the middle illustration indicates the baseline.

	cm^{-1}	Area
Peak 0	1943	0.4425
Peak 1	1930	0.1415

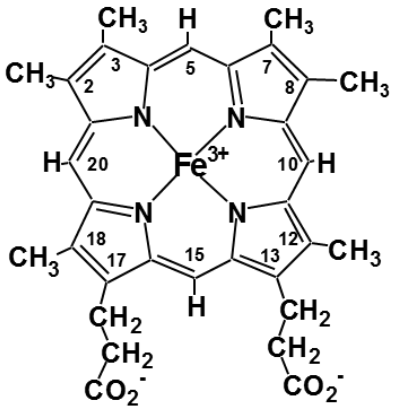

3,8-DMD

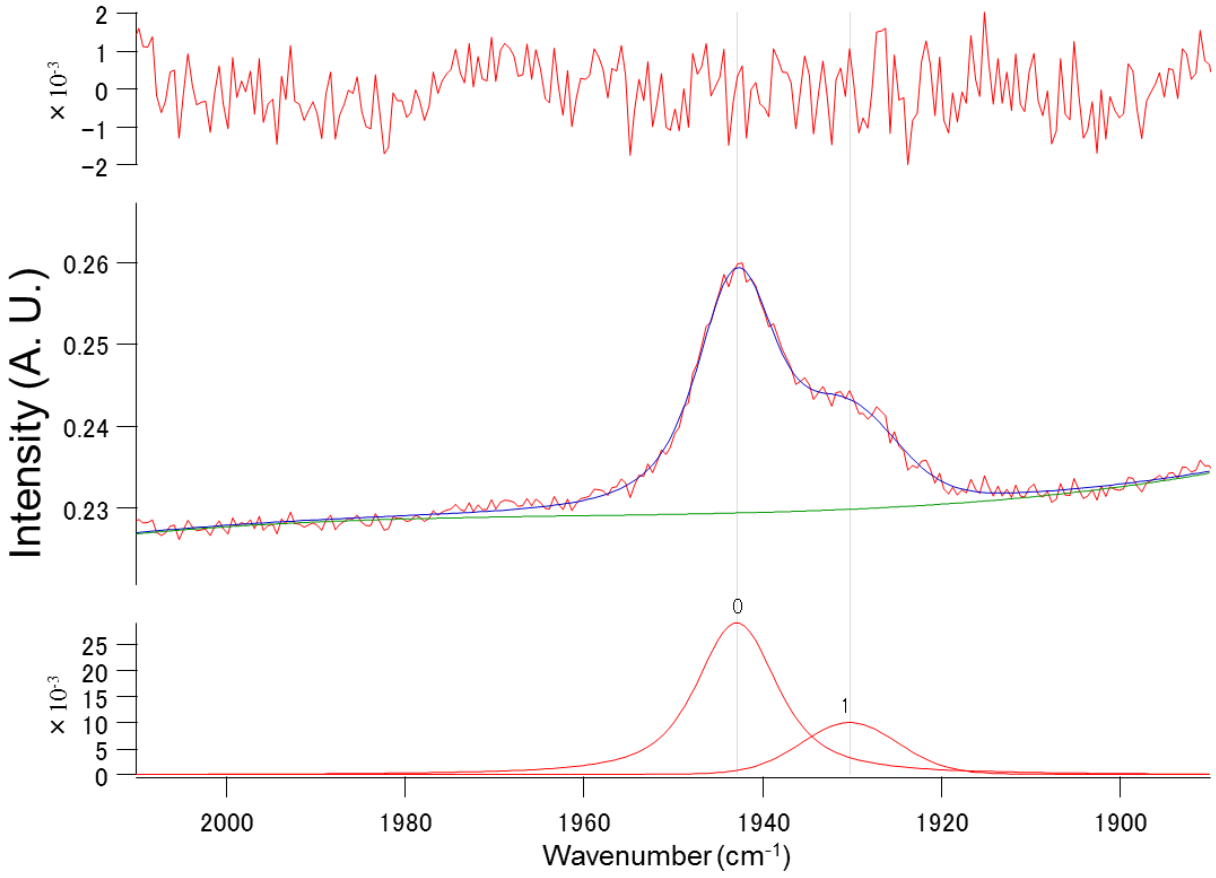

Figure 2-8. Visible resonance raman spectrum of CO form of Mb(3,8-DMD) in 100 mM potassium phosphate buffer pH 7.4 at 25 °C. Residual error (the difference between the experimental and theoretical values) (top), observed (blue) and simulated (red) ν_{CO} bands (middle), and simulated individual bands (bottom). A green line in the middle illustration indicates the baseline.

	cm^{-1}	Area
Peak 0	1950	0.2566
Peak 1	1939	0.2349

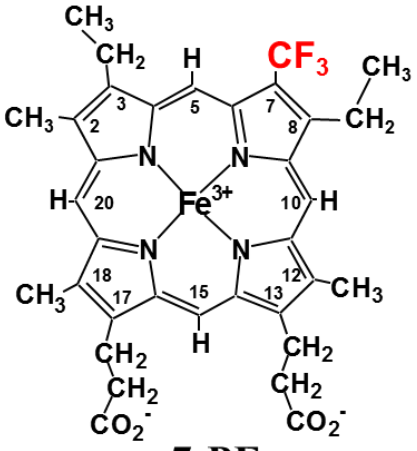

7-PF

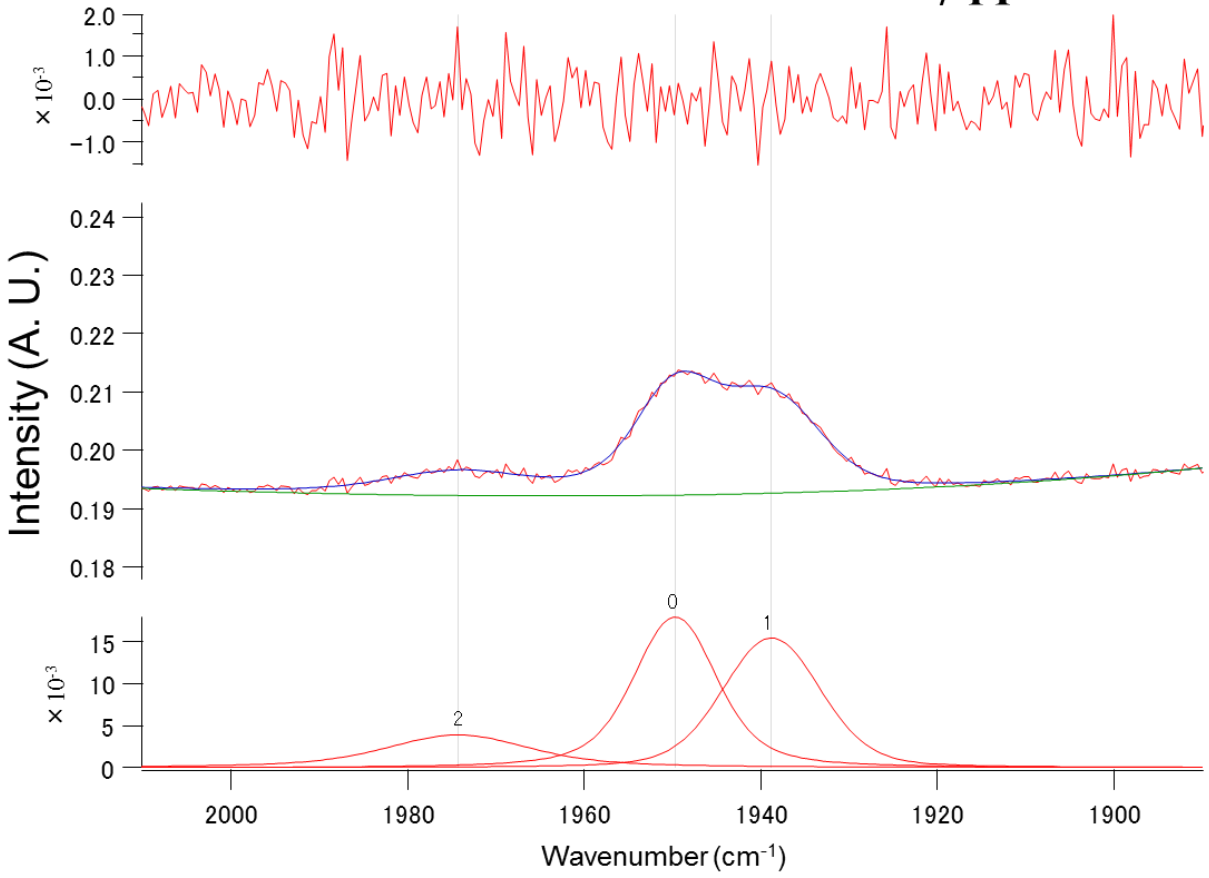

Figure 2-9. Visible resonance raman spectrum of CO form of Mb(7-PF) in 100 mM potassium phosphate buffer pH 7.4 at 25 °C. Residual error (the difference between the experimental and theoretical values) (top), observed (blue) and simulated (red) ν_{CO} bands (middle), and simulated individual bands (bottom). A green line in the middle illustration indicates the baseline.

	cm^{-1}	Height
Peak 0	1956	0.3566
Peak 1	1945	0.2848

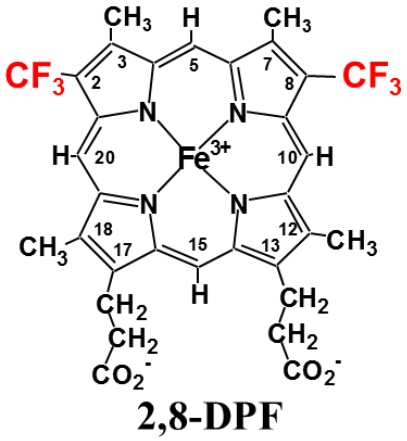

2,8-DPF

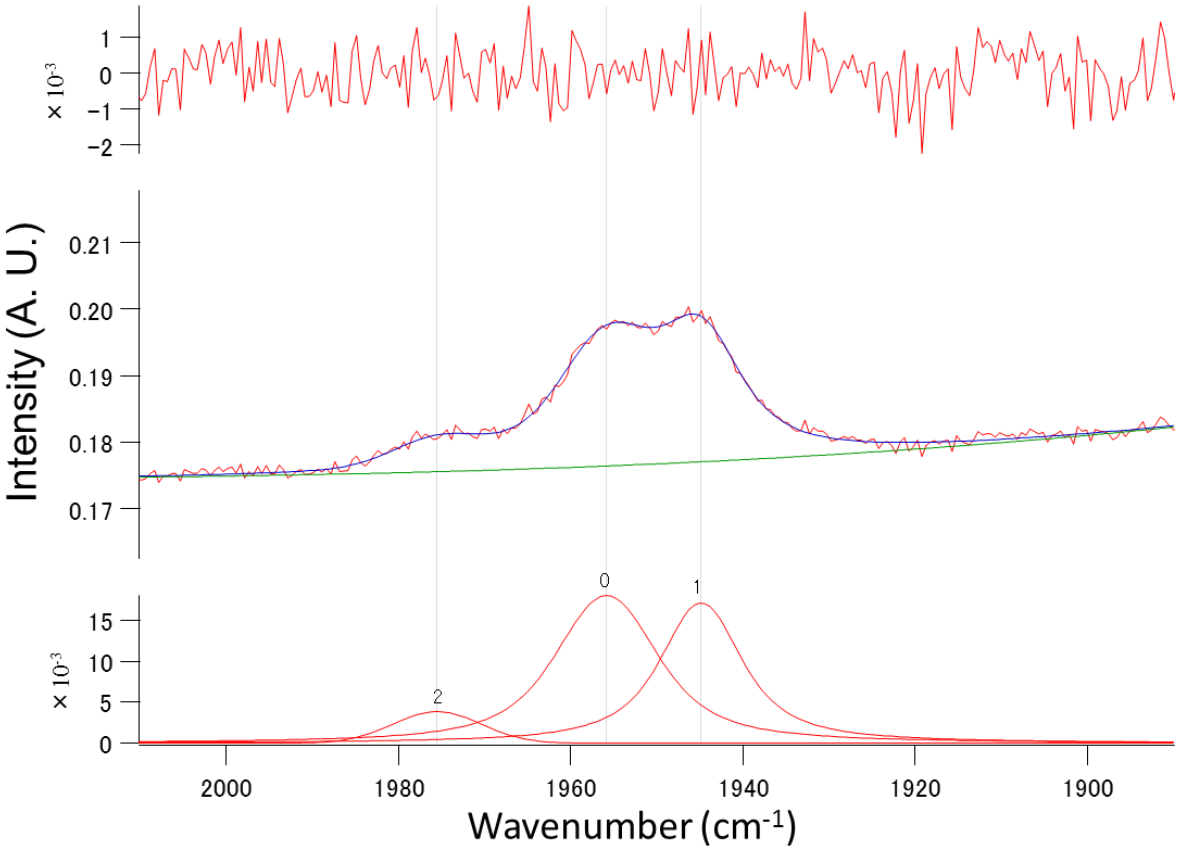

Figure 2-10. Visible resonance raman spectrum of CO form of Mb(2,8-DPF) in 100 mM potassium phosphate buffer pH 7.4 at 25 °C. Residual error (the difference between the experimental and theoretical values) (top), observed (blue) and simulated (red) ν_{CO} bands (middle), and simulated individual bands (bottom). A green line in the middle illustration indicates the baseline.

	cm^{-1}	Height
Peak 0	1947	0.1693
Peak 1	1935	0.0869

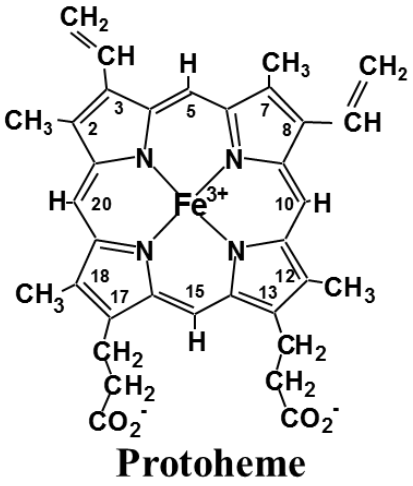

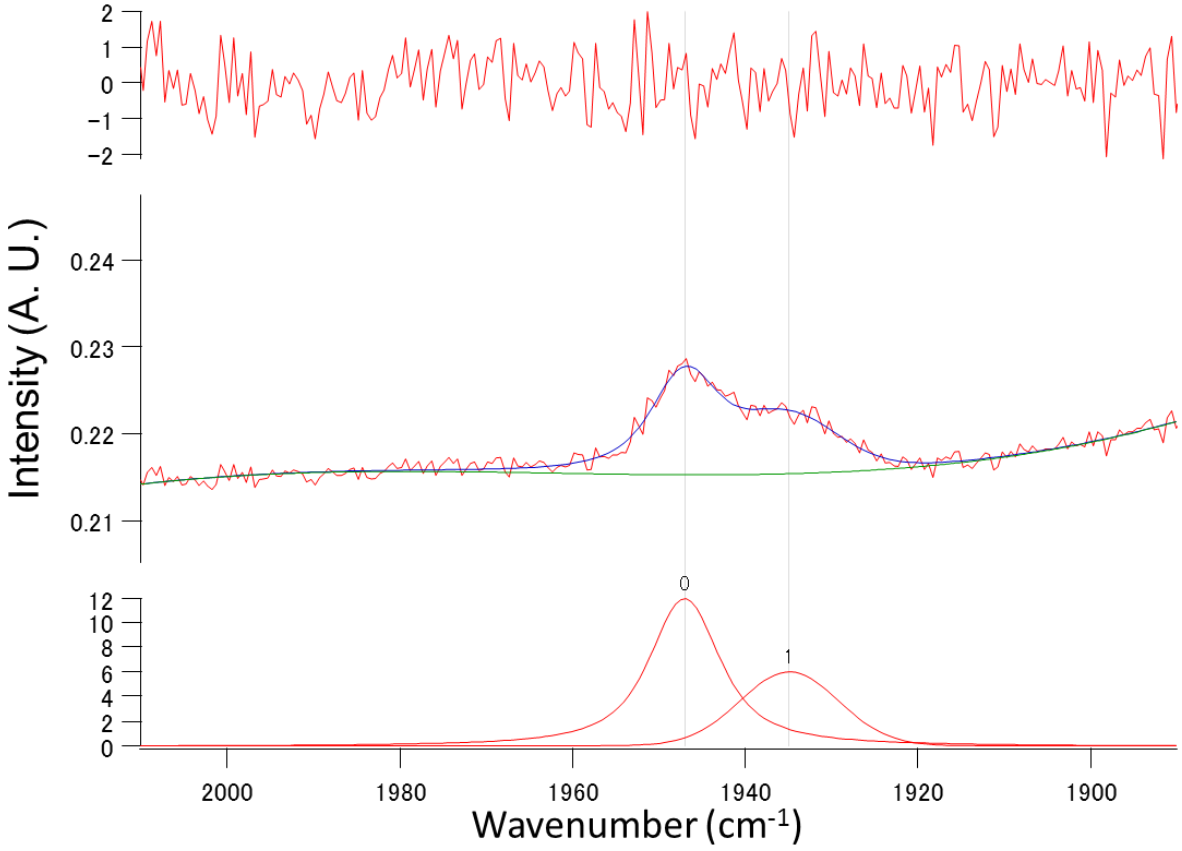

Figure 2-11. Visible resonance raman spectrum of CO form of Mb(Proto) in 100 mM potassium phosphate buffer pH 7.4 at 25 °C. Residual error (the difference between the experimental and theoretical values) (top), observed (blue) and simulated (red) ν_{CO} bands (middle), and simulated individual bands (bottom). A green line in the middle illustration indicates the baseline.

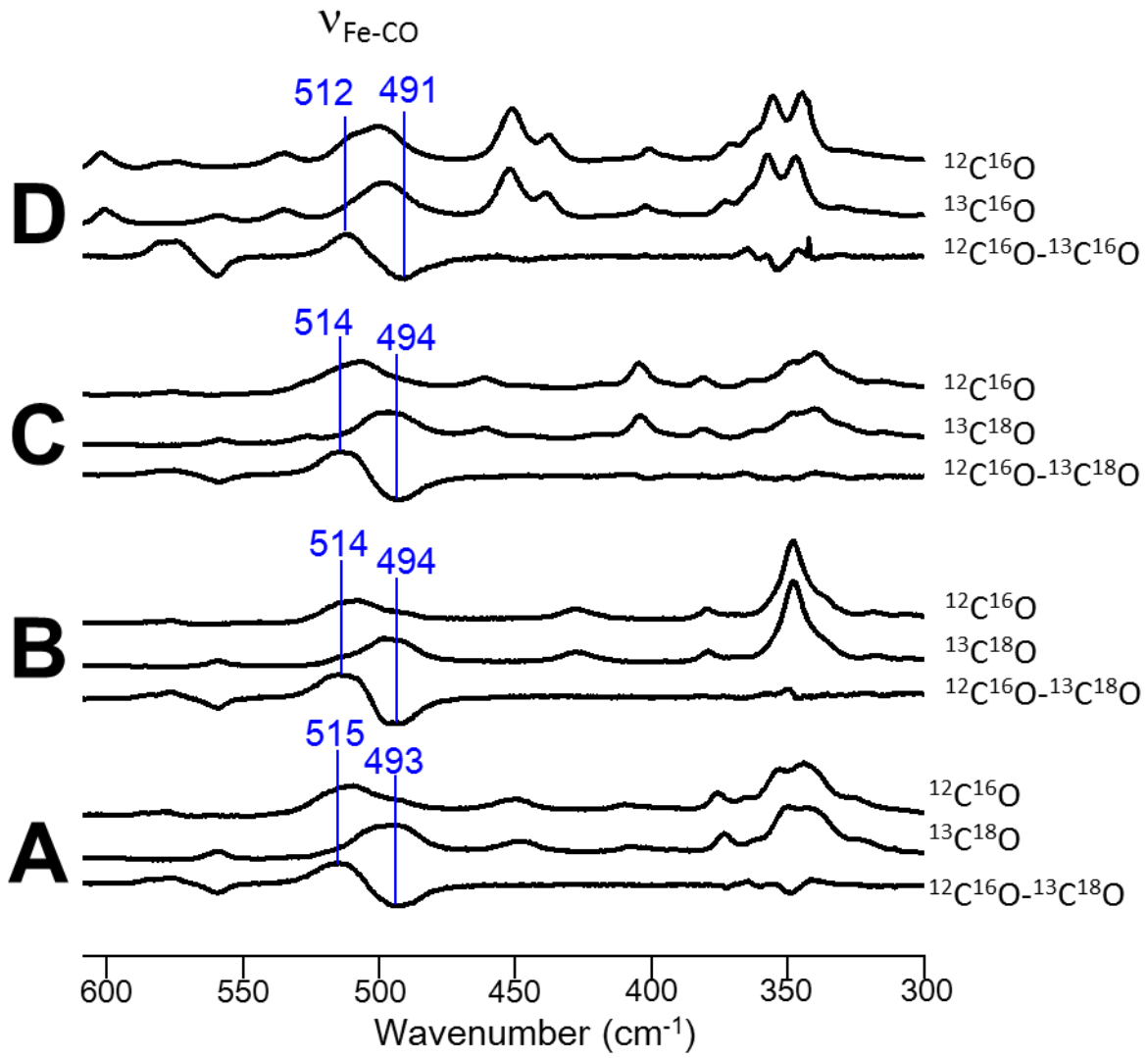

Figure 2-12. Low frequency regions of visible resonance raman spectra of CO forms of Mb(Meso) (A), Mb(3,8-DMD) (B), Mb(7-PF) (C), and Mb(2,8-DPF) (D) at 25 °C and pH7.4. In the spectra of each protein, wavenumbers of n(^{12}C-^{16}O) and n(^{13}C-^{18}O) (or n(^{13}C-^{16}O)) bands are indicated in blue numbers, and the spectrum recorded using ^{12}C-^{16}O (top) and ^{13}C-^{18}O (or ^{13}C-^{16}O) (middle) and the difference spectrum (bottom) are also shown.

	cm^{-1}	Area
Peak 0	576	10140
Peak 1	584	6322

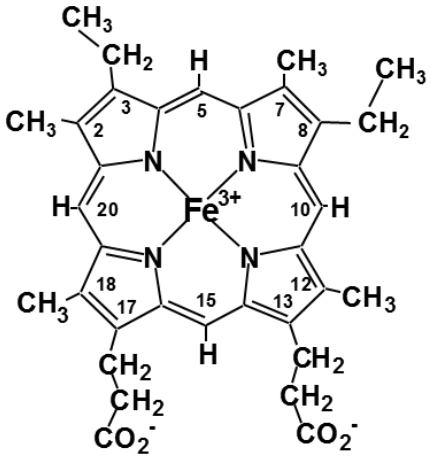

Mesoheme

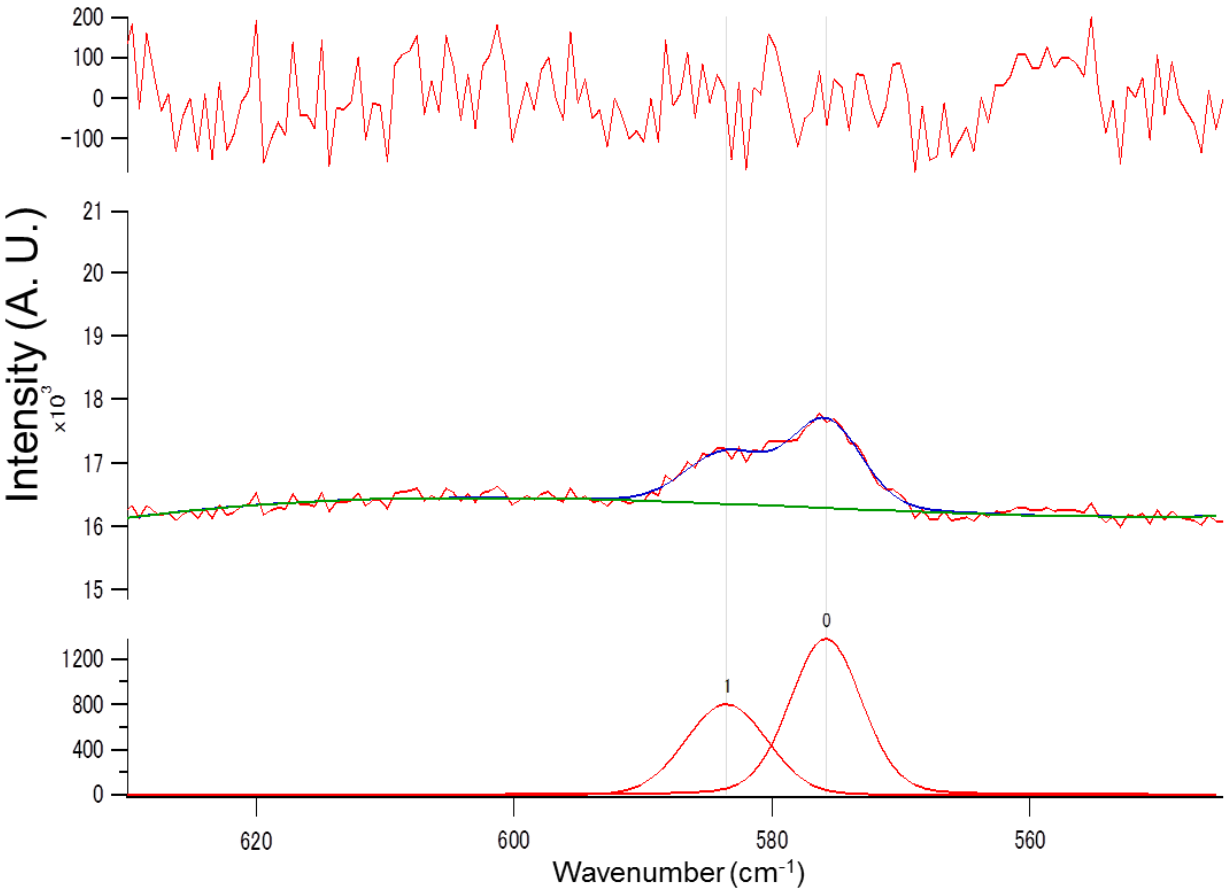

Figure 2-13. Visible resonance raman spectrum of CO form of Mb(Meso) in 100 mM potassium phosphate buffer pH 7.4 at 25 °C. Residual error (the difference between the experimental and theoretical values) (top), observed (blue) and simulated (red) d_{FeCO} bands (middle), and simulated individual bands (bottom). A green line in the middle illustration indicates the baseline.

	cm^{-1}	Area
Peak 0	576	9886
Peak 1	585	3249

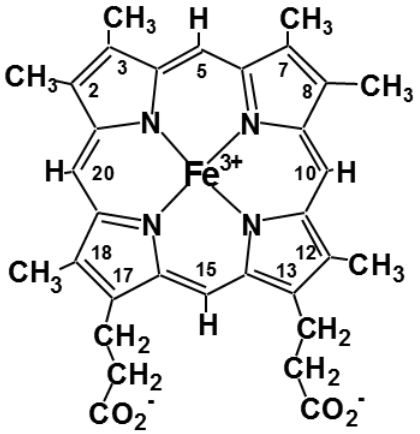

3,8-DMD

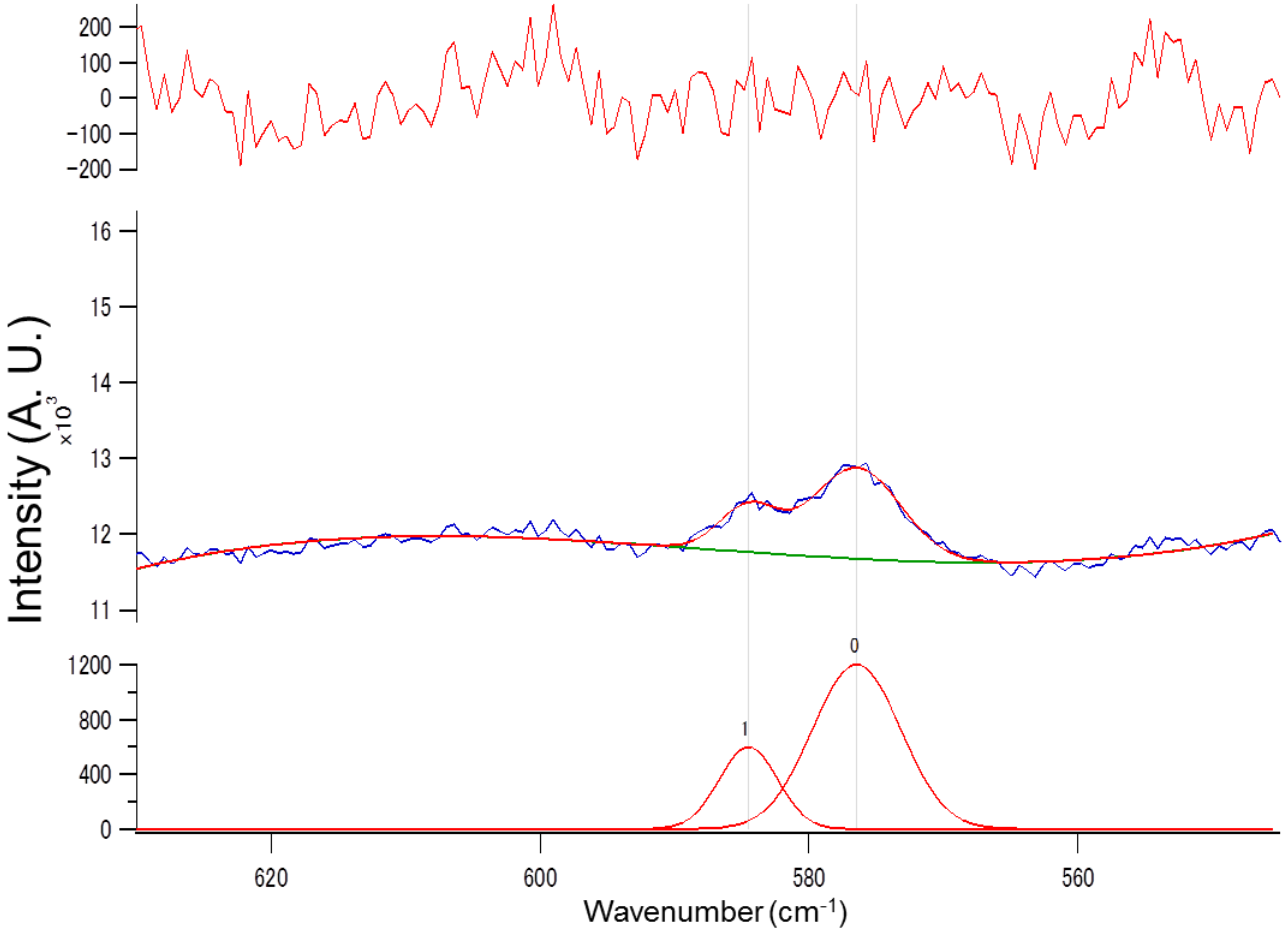

Figure 2-14. Visible resonance raman spectrum of CO form of Mb(3,8-DMD) in 100 mM potassium phosphate buffer pH 7.4 at 25 °C. Residual error (the difference between the experimental and theoretical values) (top), observed (blue) and simulated (red) d_{FeCO} bands (middle), and simulated individual bands (bottom). A green line in the middle illustration indicates the baseline.

	cm^{-1}	Area
Peak 0	575	30340
Peak 1	582	6280

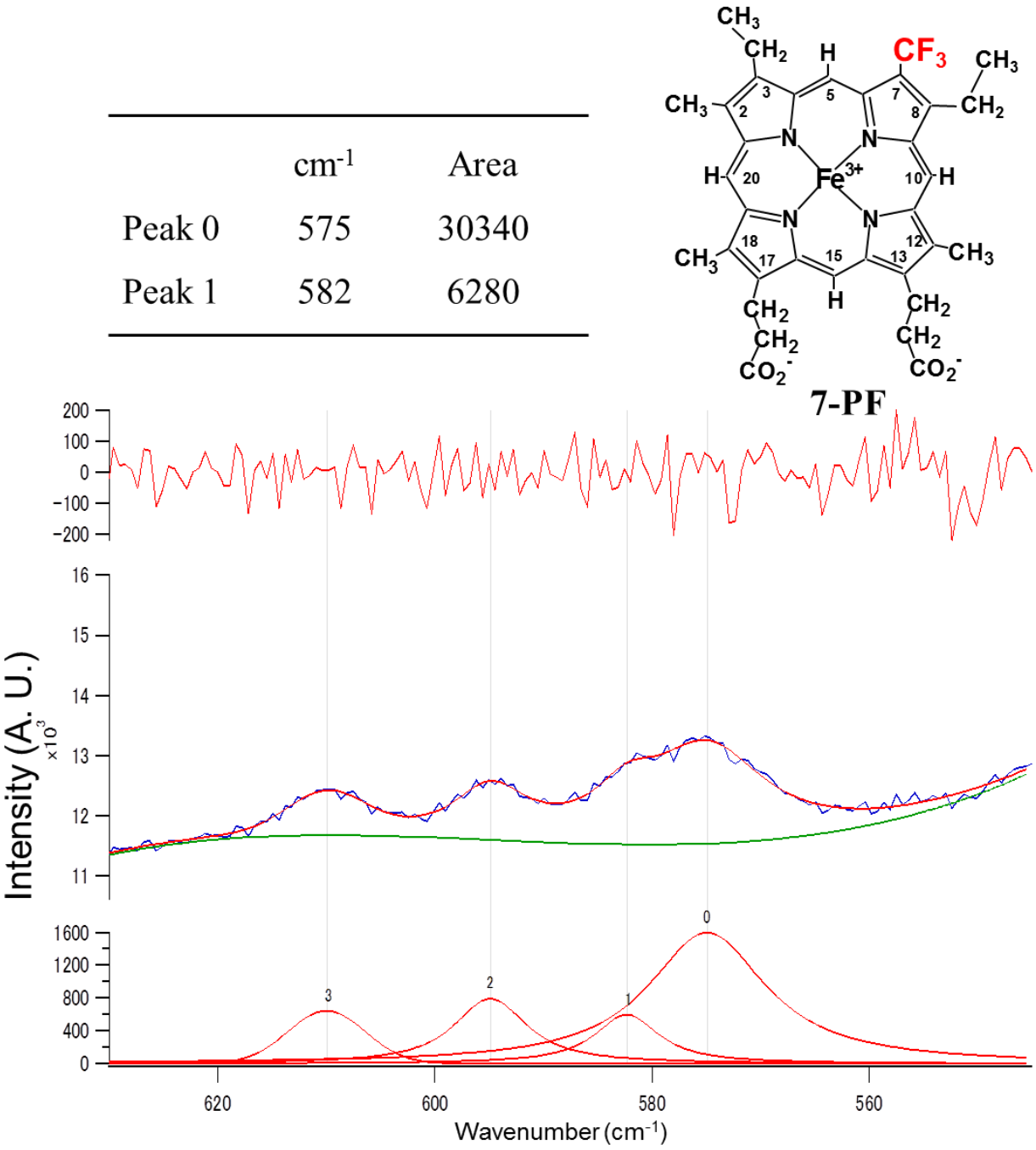

Figure 2-15. Visible resonance raman spectrum of CO form of Mb(7-PF) in 100 mM potassium phosphate buffer pH 7.4 at 25 °C. Residual error (the difference between the experimental and theoretical values) (top), observed (blue) and simulated (red) d_{FeCO} bands (middle), and simulated individual bands (bottom). A green line in the middle illustration indicates the baseline.

	cm^{-1}	Area
Peak 0	574	3.470
Peak 1	582	1.508

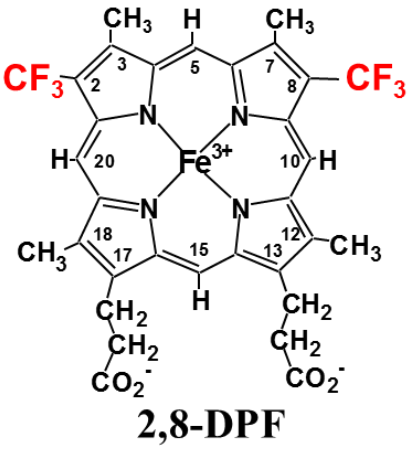

2,8-DPF

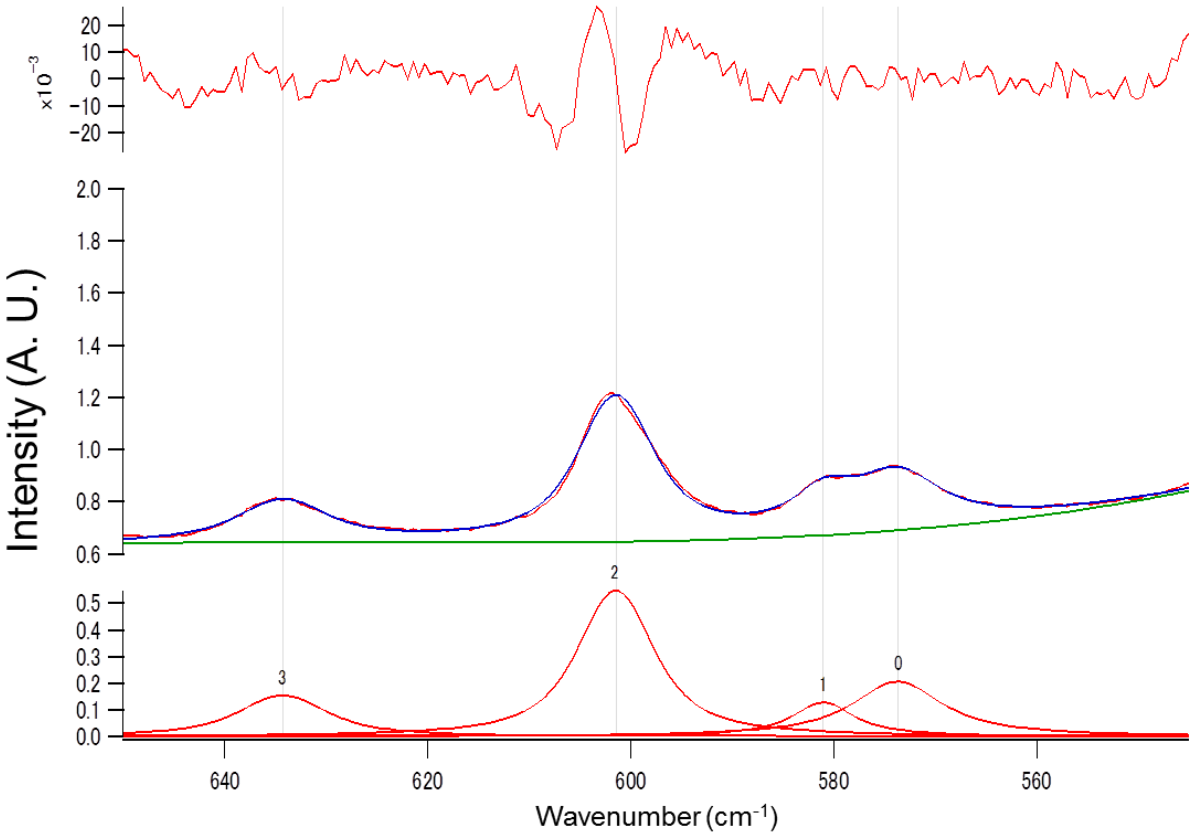

Figure 2-16. Visible resonance raman spectrum of CO form of Mb(2,8-DPF) in 100 mM potassium phosphate buffer pH 7.4 at 25 °C. Residual error (the difference between the experimental and theoretical values) (top), observed (blue) and simulated (red) d_{FeCO} bands (middle), and simulated individual bands (bottom). A green line in the middle illustration indicates the baseline.

	cm^{-1}	Area
Peak 0	576	1.489
Peak 1	584	1.842

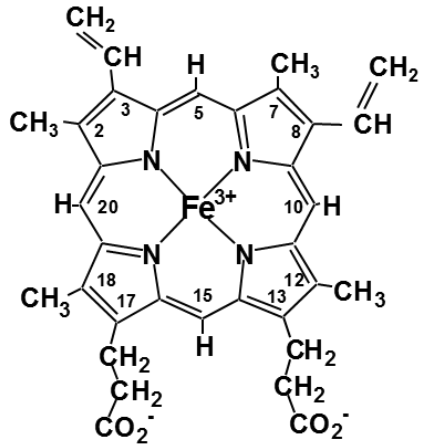

Protoheme

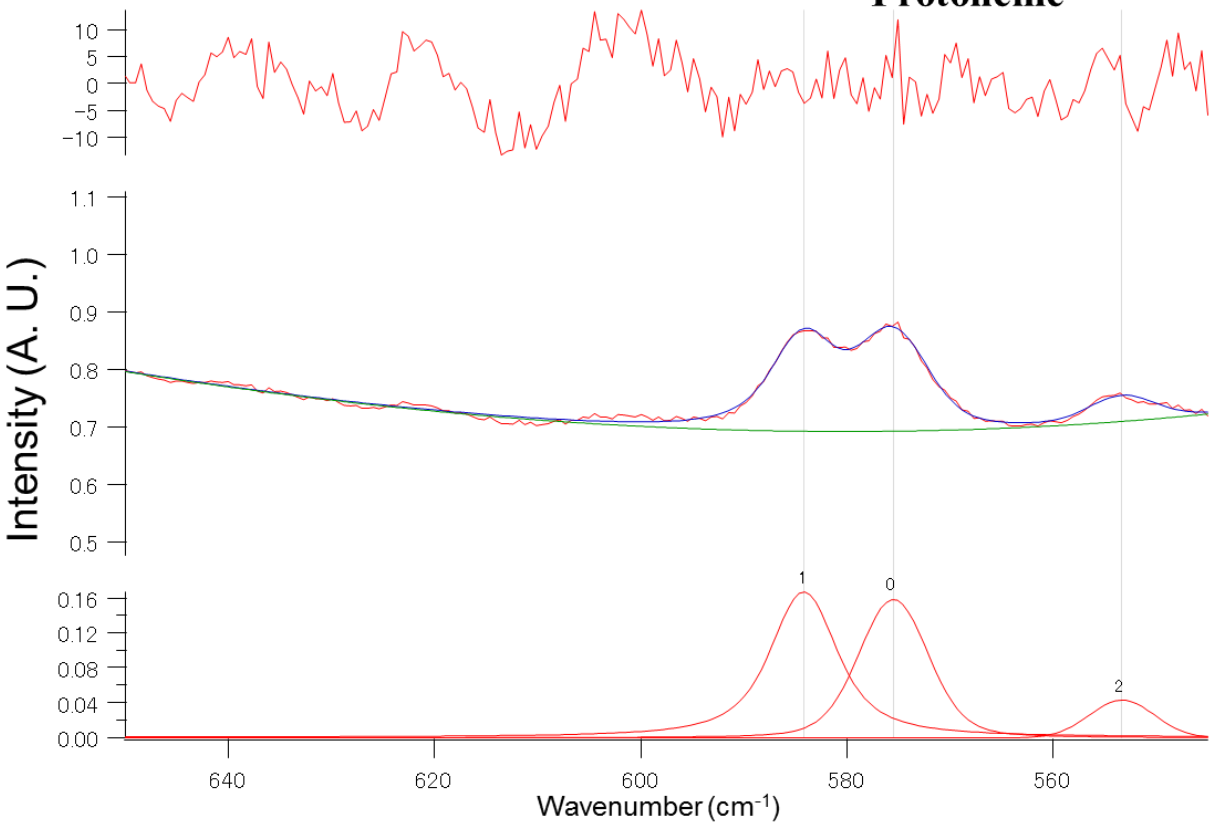

Figure 2-17. Visible resonance raman spectrum of CO form of Mb(Proto) in 100 mM potassium phosphate buffer pH 7.4 at 25 °C. Residual error (the difference between the experimental and theoretical values) (top), observed (blue) and simulated (red) d_{FeCO} bands (middle), and simulated individual bands (bottom). A green line in the middle illustration indicates the baseline.

Vibrational frequencies of Fe-bound CO of the H64L proteins. The ν_{CO}, ν_{FeC}, and δ_{FeCO} values of the H64L proteins are listed in Table 2-1. The mutant protein exhibited a single ν_{CO} band, as shown in Figure 2-18, and this is in sharp contrast to the case of the native protein exhibiting the ν_{CO} band composed of multiple components (Figure 2-6) possibly due to the presence of multiple conformational states of the Fe-CO fragment [35]. This result demonstrated the significant effect of the conformational properties of the His64 side chain on the ν_{CO} band of the protein. The ν_{FeC} and δ_{FeCO} bonds of the H64L series were observed as a single component (Figures 2-19 and 2-20). The $\nu_{CO,}$ ν_{FeC} and δ_{FeCO} values of H64LCO(Proto) were determined to be 1969, and 491 cm^{-1}, respectively, and these values were similar to the corresponding ones previously reported by Anderton et al.[38], i.e., 1966, and 489, and 573 cm^{-1} respectively.

As shown in Table 2-1, the ν_{CO} and ν_{FeC} values of H64LCO(Proto) were larger and smaller, respectively, by ~20 cm^{-1}, relative to the corresponding ones of MbCO(Proto), whereas the δ_{FeCO} one is affected only slightly by the mutation. The reciprocal relationship between the ν_{CO} and ν_{FeC} values has been reported for a variety of hemoproteins, and has been interpreted in terms of an admixture of two alternative canonical forms of the Fe-CO fragment illustrated in Scheme 2-1 [39,40]. Hence, the changes of the ν_{CO} and ν_{FeC} values due to the H64L mutation have been attributed to the effect of the removal of the electrostatic field exerted by the His64 side chain on the resonance of the Fe-CO fragment.

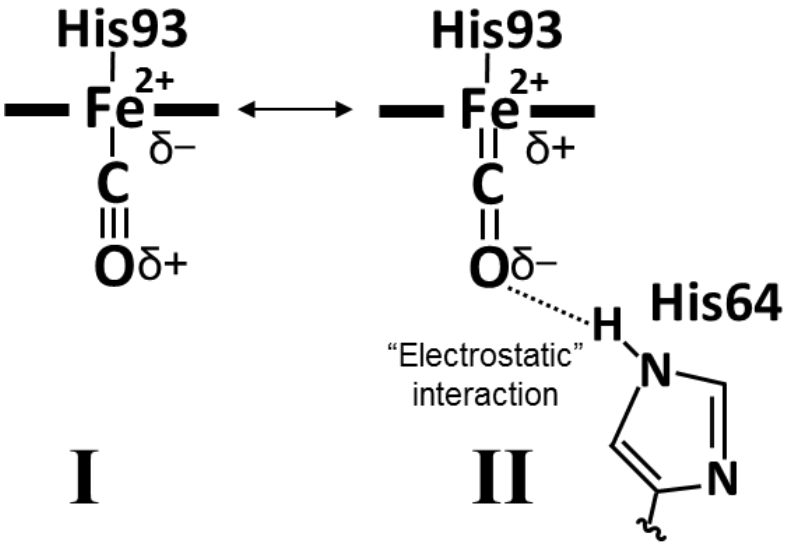

Scheme 2-1. Resonance between the two canonical forms of the Fe-CO fragment, represented by the valence bond formalism [39,40].

Comparison of the determined values among the mutant proteins revealed that the ν_{CO}, ν_{FeC}, and δ_{FeCO} values were all affected by the heme cofactor modifications. In particular, the ν_{CO} value increased dramatically with the CF_3 substitutions(Table 2-1). Comparison of the ν_{CO} values of the mutant proteins yielded a difference of 7 cm^{-1} for the H64L(Meso)/H64L(7-PF) system, which is half the value, 14 cm^{-1}, for the H64L(3,8-DMD)/H64L(2,8-DPF) one. These results demonstrated the additive effect of the heme π-system perturbation on the ν_{CO} value for the mutant protein. In addition, the ν_{CO} values of the mutant proteins were larger by 21 – 22 cm^{-1} relative to the high frequency ν_{CO} values($\nu_{CO(H)}$), i.e., the position of the highest-frequency band among the multiple ν_{CO} band components (Figure 2-6), of the native ones possessing the identical heme cofactors, indicating that the effect of the H64L mutation on the ν_{CO} value is essentially independent of the heme cofactors. On the other hand, the ν_{FeC} values of the mutant proteins were smaller by 21 – 28 cm^{-1} relative to those of the native ones possessing the identical heme cofactors. Comparison of the ν_{FeC} values of the mutant proteins yielded differences of 1 and 11 cm^{-1} for the H64L(Meso)/H64L(7-PF) and H64L(3,8-DMD)/ H64L(2,8-DPF) systems, respectively. Hence, in contrast to the case of the ν_{CO} value, an additive effect of the heme π-system perturbation was not observed for the ν_{FeC} value. Finally, as also observed for the native Mb proteins, the low frequency shift of the δ_{FeCO} value with increasing number of CF_3 substitutions suggested that the orientation of the Fe-bound CO, with respect to the heme, in the mutant protein is affected by the ρ_{Fe} value.

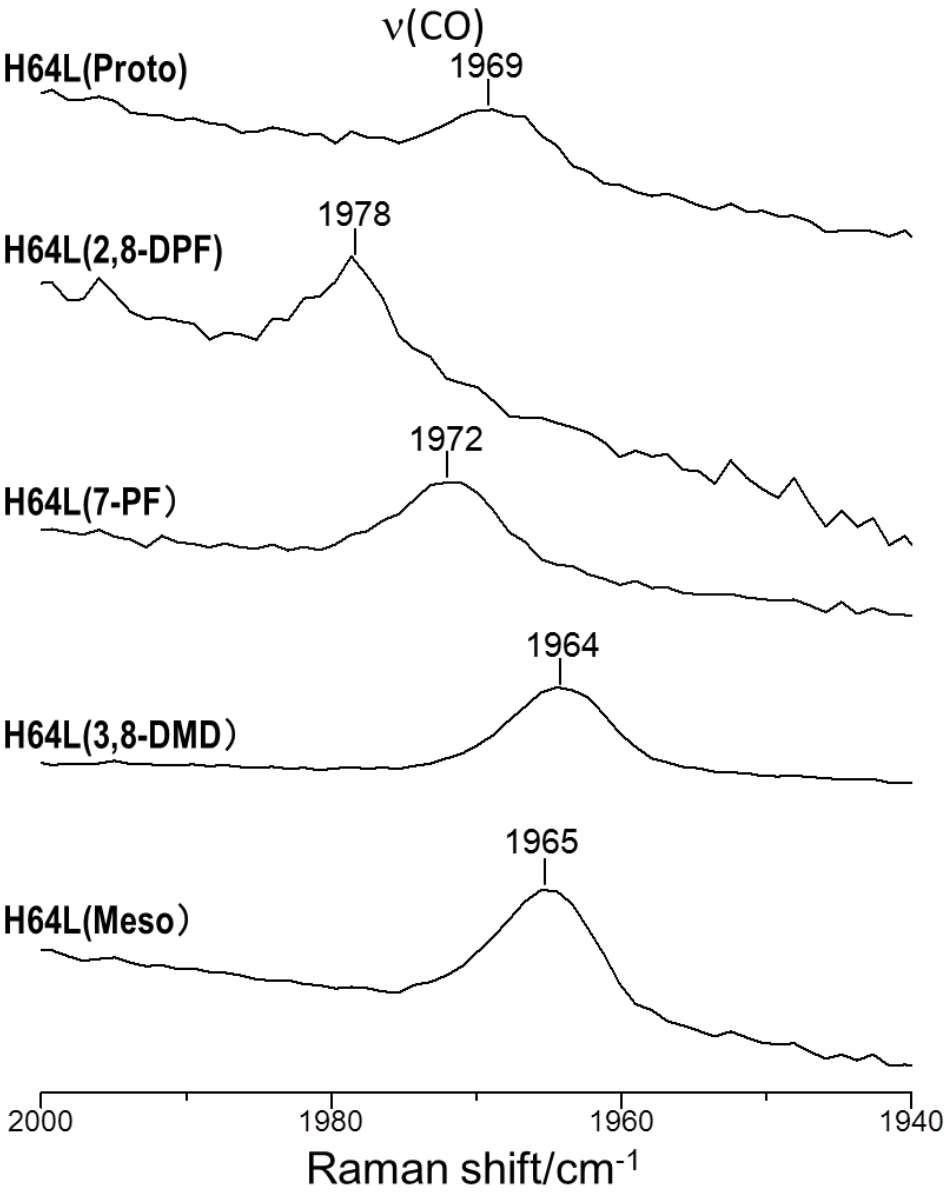

Figure 2-18. High-frequency regions of visible resonance raman spectra of H64LCO(Meso), H64LCO(3,8-DMD), H64LCO(7-PF), H64LCO(2,8-DPF), and H64LCO(Proto) at pH7.40 and 25 °C.

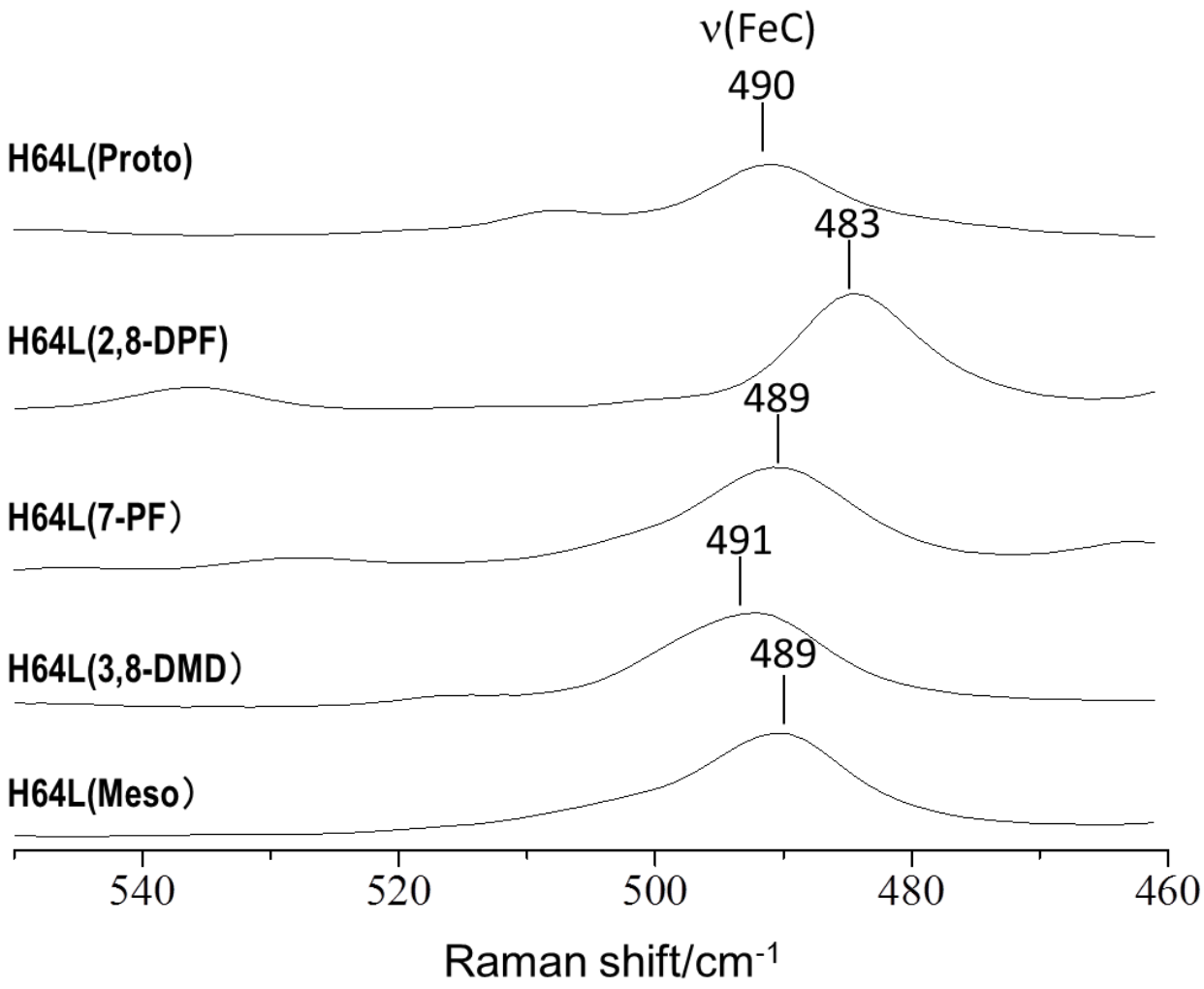

Figure 2-19. Low-frequency regions of visible resonance raman spectra of H64LCO(Meso), H64LCO(3,8-DMD), H64LCO(7-PF), H64LCO(2,8-DPF), and H64LCO(Proto) at pH7.40 and 25 °C.

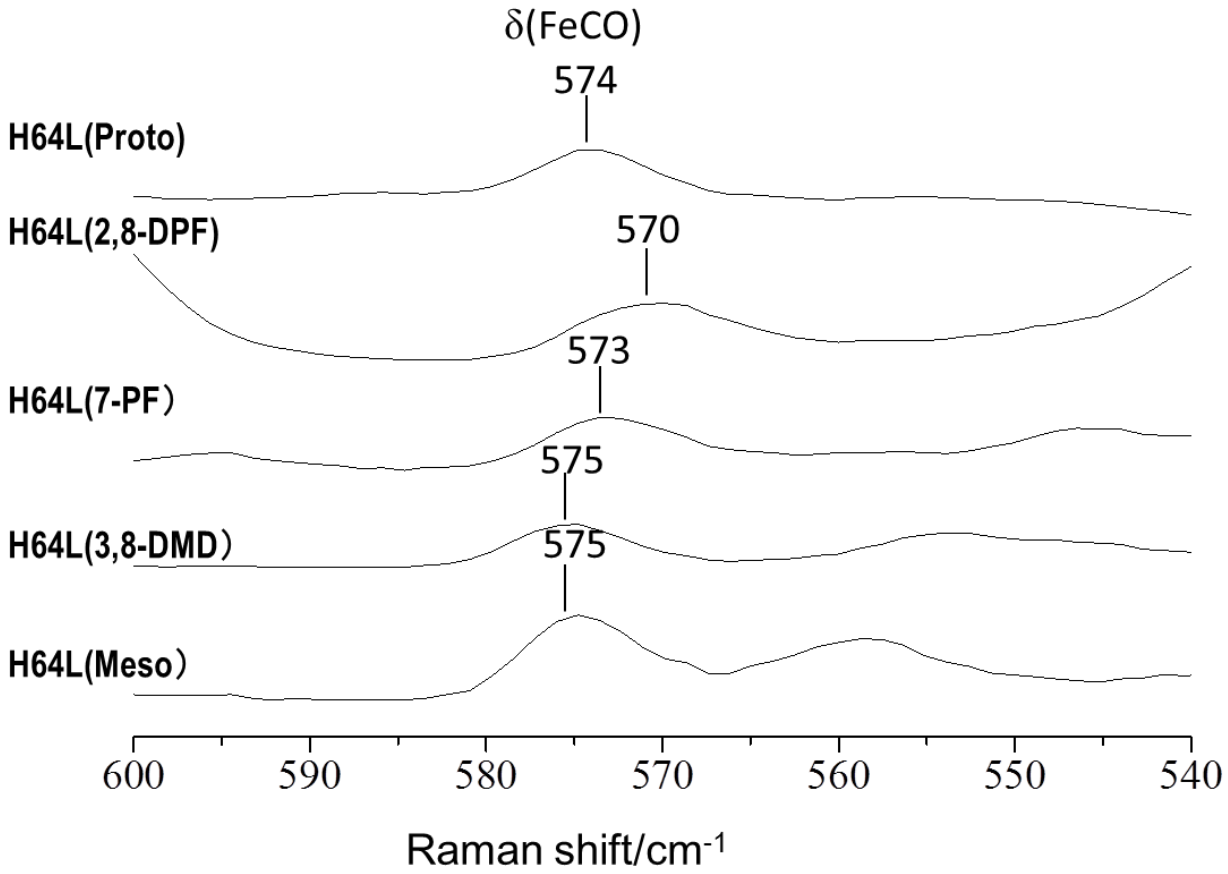

Figure 2-20. Low-frequency regions of visible resonance raman spectra of H64LCO(Meso), H64LCO(3,8-DMD), H64LCO(7-PF), H64LCO(2,8-DPF), and H64LCO(Proto) at pH7.40 and 25 °C.

Vibrational frequencies of Fe-bound CO of L29F proteins. The stretching frequency of the Fe-bound CO (ν_{CO}), together with the Fe-C stretching(ν_{FeC}) and Fe-C-O bending frequencies(δ_{FeCO}) (Figures 2-21 and 2-22), in the CO form of the L29F mutant proteins possessing various heme cofactors were determined using resonance raman spectroscopy (Table 2-1). The ν_{CO}, ν_{FeC}, and δ_{FeCO} values of L29F(Proto) were determined to be 1933, 524, and 581 cm^{-1}, respectively, these values being essentially identical to the corresponding ones previously reported by Anderton et al.[41]. The ν_{CO} values of the L29F mutant proteins were smaller by ~7-12 cm^{-1} relative to those of the native Mbs possessing identical heme cofactors, whereas these two protein systems exhibited similar ν_{CO} spans, i.e., the difference between the highest and lowest ν_{CO} values within a given protein system, and the values were 16 and 12 cm^{-1} for the L29F mutant protein and the native Mb systems, respectively. Comparison of the ν_{CO} values of the mutant proteins yielded a difference of 8 cm^{-1} for the L29F(Meso)/L29F(7-PF) system, which is half the value, 16 cm^{-1}, for the L29F(3,8-DMD)/L29F(2,8-DPF) one. These results demonstrated the additive effect of the heme π-system perturbation on the ν_{CO} value for the L29F mutant protein.

By the way, the L29F mutant proteins exhibited a single ν_{CO} band, as shown in Figure 2-21, which is in contrast to the case of the native Mbs exhibiting a ν_{CO} band composed of multiple components [35], possibly due to the presence of multiple conformational states of the Fe-CO fragment. Consequently, the Fe-CO fragment in the L29F mutant protein appeared to be forced to adapt a unique conformation through the interaction with Phe29, in addition to His64. The δ_{FeCO} values of the L29F mutant proteins were larger by ~4-7 cm^{-1}, relative to those of the native Mbs possessing identical heme cofactors, possibly reflecting such conformational constraint of the Fe-CO fragment in the mutant protein.

The ν_{FeC} values of the L29F mutant proteins were larger by ~6-14 cm^{-1} relative to those of the native Mbs possessing identical heme cofactors (Table 2-1). Furthermore, as in the cases of various hemoproteins [42], a reciprocal relationship between the ν_{CO} and ν_{FeC} values, expected from an admixture of two alternative canonical forms of the Fe-CO fragment illustrated in Scheme 2-1 [39,40], has also been observed for the L29F mutant proteins. In addition, comparison of the ν_{FeC} values of the L29F mutant proteins yielded the decrease of 3 cm^{-1} on the substitution of one CF_3 group, as demonstrated for the L29F(Meso)/L29F(7-PF) system, i.e., 526 and 532 cm^{-1} for L29F(Meso) and L29F(7-PF), respectively, and that of 10 cm^{-1} on the

substitution of two CF_3 ones, as observed for the L29F(3,8-DMD)/L29F(2,8-DPF) system, i.e., 528 and 518cm^{-1} for L29F(3,8-DMD) and L29F(2,8-DPF), respectively. Hence, in contrast to the case of the ν_{CO} value, an additive effect of the heme π-system perturbation was not observed for the ν_{FeC} value. Furthermore, the ν_{FeC} span of the L29F mutant protein system, i.e., 12 cm^{-1}, was larger than that of the native Mb one, i.e., 3 cm^{-1}.

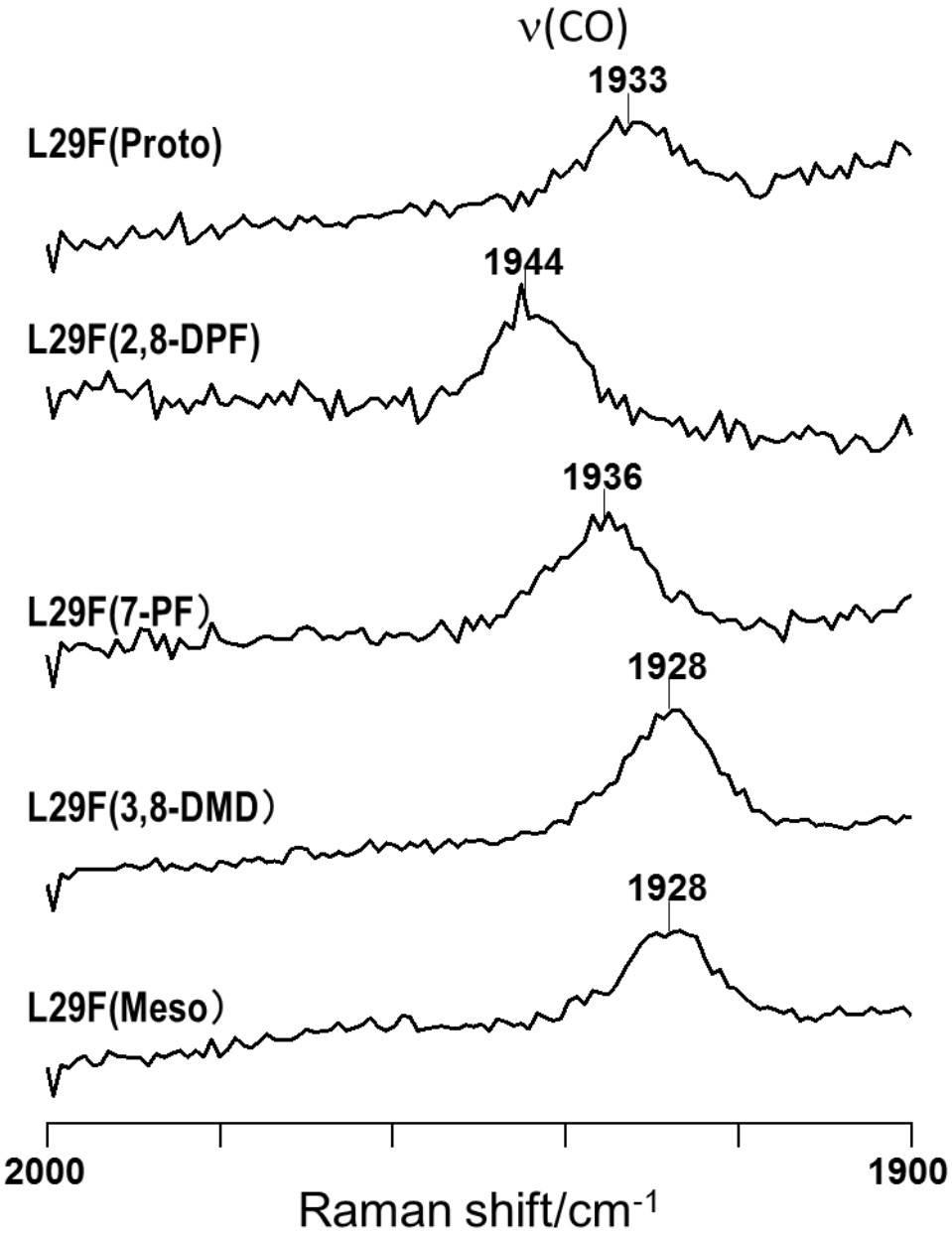

Figure 2-21. High-frequency regions of visible resonance raman spectra of CO forms of the L29F mutant proteins possessing the indicated heme cofactors, at pH7.40 and 25 °C.

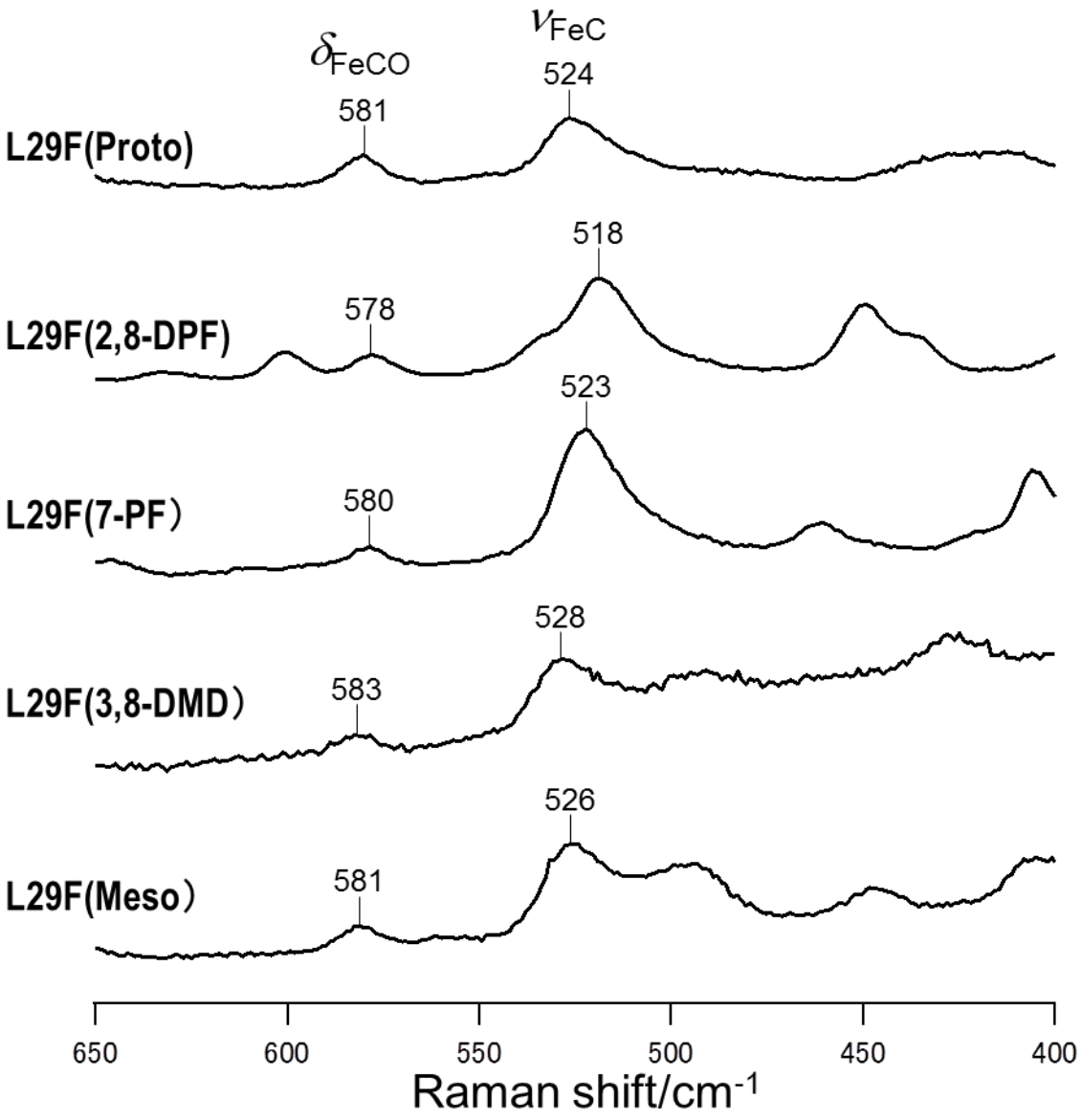

Figure 2-22. Low-frequency regions of visible resonance raman spectra of CO forms of the L29F mutant proteins possessing the indicated heme cofactors, at pH7.40 and 25 ℃.

DISCUSSION

Correlation between the vibrational frequencies and electron density of the heme Fe atom. Aadditive effects of the heme π-system perturbation on the ν_{CO} and ν_{FeC} values were observed in each of the native Mb, H64L an L29F protein systems. As shown in Figure 2-1, similar additivity was also observed between the pK_a value and the number of CF_3 substitutions, that is, the pK_a difference of 0.86 for the Mb(Meso)/Mb(7-PF) system is half the value, 1.70, for the Mb(3,8-DMD)/Mb(2,8-DPF) one. In fact, plots of the $\nu_{CO(H)}$ values of the Mbs against the pK_a ones can be described by a linear function expressed as $\nu_{CO(H)}/cm^{-1} = -6.818\times pK_a + 2007$, with a correlation coefficient (r) = -0.9716, and the relationship between the $\nu_{CO(L)}$ and pK_a values can be also represented by $\nu_{CO(L)}/cm^{-1} = -7.565\times pK_a + 2002$, with r = -0.9531 (Figure 2-23). Similarly, the $\nu_{CO(ave)}$ value exhibited a linear relationship with the pK_a value, that is, $\nu_{CO(ave)}/cm^{-1} = -6.071\times pK_a + 1996$, with r = -0.9874 (Figure 2-23). These results not only demonstrated that the ν_{CO} value is affected by the ρ_{Fe} value, as the pK_a value is, but also confirmed that the effects of the heme modifications on the ρ_{Fe} value are essentially independent of the oxidation state of the heme Fe atom.

Neya et al.[43] demonstrated, on X-ray structural determination, that the overall protein structure and side chain conformations of Mb reconstituted with porphine are essentially identical to those of the native protein. Furthermore, they also revealed that the protein structure properties of the globin fold, together with the structure of the heme active site, are inherent in its amino acid sequence, and are not largely affected by the acquired heme-protein interaction [44].

The relationship between the ν_{CO} and pK_a (and hence ρ_{Fe}) values could be interpreted in terms of the resonance between the two canonical forms of the Fe-CO fragment, represented by the valence bond formalism (Scheme 2-1) [39,40]. The larger the ρ_{Fe} value, the better the heme Fe atom can serve as a π donor to CO. The stronger the Fe-CO bond, the larger will be the bond order of the Fe-CO bond, the smaller will be the C-O bond order, and hence the weaker will be the C-O bond. Consequently, the strength of the Fe-CO and C-O bonds decrease and increase, respectively, with decreasing ρ_{Fe} value. As a result, a reciprocal relationship holds between the ν_{FeC} and ν_{CO} values, as has been demonstrated previously [42]. A similar ν_{FeC}-ν_{CO} reciprocal relationship was observed for the proteins considered in the study. This finding

indicated that the π back-donation of the heme Fe atom to CO (Fe→CO π back-donation) is affected by the in-plane electronic perturbation of the heme π-system induced through the heme modifications.

As in the case of the native Mb proteins, an additive effect of the heme π-system perturbation induced by the CF_3 substitutions on the ν_{CO} value was observed for the mutants proteins. In fact, plots of the ν_{CO} values of the H64L proteins against the $\nu_{CO(H)}$ values of the native ones can be represented by a straight line with a slope of 1 (Figure 2-24). These results supported that changes in the ρ_{Fe} value due to the CF_3 substitutions are independent of the heme environment. Hence, the differences in the vibrational frequencies among the proteins can be attributed primarily to the electronic effects exerted by the heme modifications.

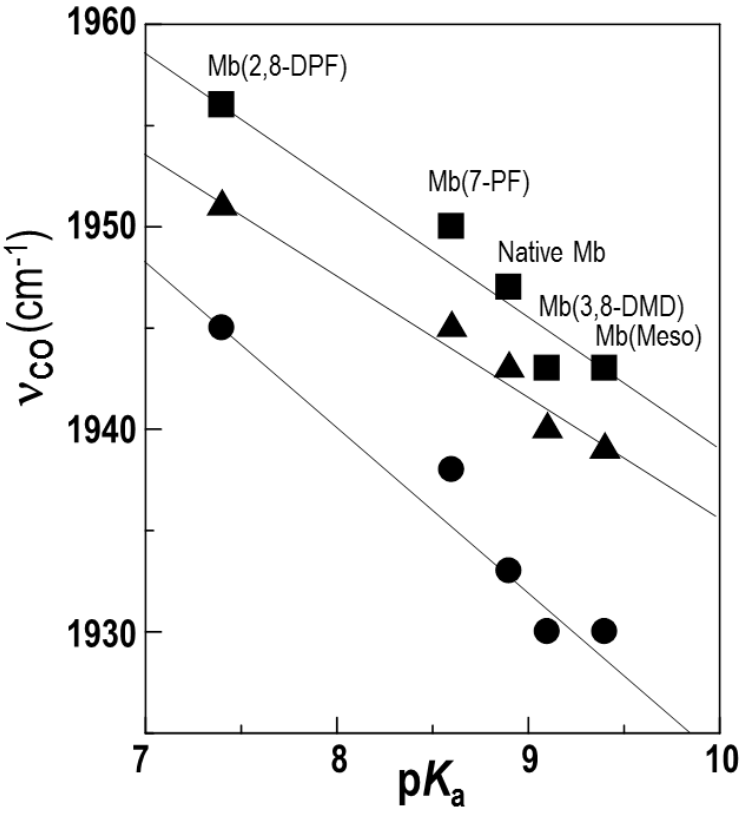

Figure 2-23. Plots of the high frequency ν_{CO} ($\nu_{CO(H)}$ (■)), low frequency ν_{CO} ($\nu_{CO(L)}$ (●)), and weighted-average ν_{CO} ($\nu_{CO(ave)}$ (▲)) values of MbCOs against the pK_a ones of the acid-alkaline transition in metMbs. The plots can be represented by straight lines.

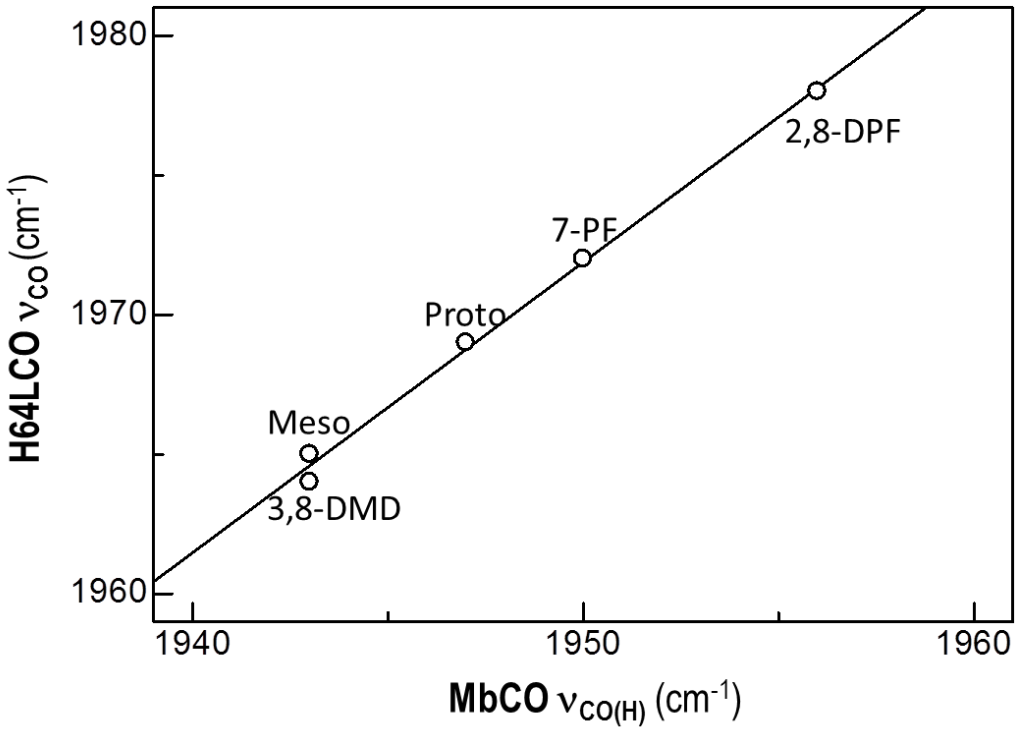

Figure 2-24. Plots of the stretching frequency of Fe-bound CO (ν_{CO}) in the H64L mutant proteins against the position of the highest-frequency band ($\nu_{CO(H)}$) among the multiple ν_{CO} band components of MbCOs (Figure 2-6).

CONCLUSION It was demonstrated that the ν_{CO} value of Mb correlates well with the pK_a value in such a manner that a protein possessing a lower pK_a value exhibits a higher ν_{CO} one. The ν_{CO}-pK_a correlation could be interpreted simply in terms of the resonance between the two canonical forms of the Fe-CO fragment, represented by the valence bond formalism. Furthermore, the linear correlation indicated not only that the effects of the heme modifications on the ρ_{Fe} value are independent of the oxidation state of the heme Fe atom and the environment of heme pocket, but also that the ν_{CO} value can be used as a sensitive measure of the ρ_{Fe} value in a protein in order to gain a deeper understanding of the molecular mechanism responsible for the electronic regulation of the heme Fe reactivity.

References

[1] Antonini, E.; Brunori, M. In *Hemoglobins and Myoglobins and their Reactions with Ligands*; North Holland Publishing: Amsterdam, **1971**.

[2] Schotte, F.; Lim, M.; Jackson, T. A.; Smirnov, A. V.; Soman, J.; Olson, J. S.; Phillips, G. N., Jr.; Wulff, M.; Anfinrud, P. A. *Science*, **2003**, 300, 1944-1947.

[3] Chu, K.; Vojtchovsky, J.; McMahon, B. H.; Sweet, R. M.; Berendzen, J.; Schlichting, I. *Nature*, **2000**, 403, 921-923.

[4] Springer, B. A.; Sligar, S. G.; Olson, J. S.; Phillips, G. N., Jr. *Chem. Rev.*, **1994**, 94, 699-714.

[5] Olson, J. S.; Phillips, G. N., Jr. *J. Biol. Inorg. Chem.*, **1997**, 2, 544-552.

[6] Capece, L.; Matri, M. A.; Crespo, A.; Doctorvich, F. Estrin, D. A.; *J. Am. Chem. Soc*., **2006**, 128, 12455-12461

[7] Shibata, T.; Nagao, S.; Fukaya, M.; Tai, H.; Nagatomo, S.; Morihashi, K.; Matsuo, T.; Hirota, S.; Suzuki, A.; Imai, K.; Yamamoto, Y. *J. Am. Chem. Soc.*, **2010**, 132, 6091-6098.

[8] Shibata, T.; Matsumoto, D.; Nishimura, R.; Tai, H.; Matsuoka, A.; Nagao, S.; Matsuo, T.; Hirota, S.; Imai, K.; Neya, S.; Suzuki, A.; Yamamoto, Y. *Inorg. Chem.*, **2012**, 51, 11955-11960.

[9] Giacometti, G. M.; Da Ros, A.; Antonini, E.; Brunori, M. *Biochemistry*, **1975**, 14, 1584-1588.

[10] Iizuka, T.; Morishima, I. *Biochim. Biophys. Acta*, **1975**, 400, 143-153.

[11] McGrath, T. M.; La Mar, G. N. *Biochim. Biophys. Acta*, **1978**, 534, 99-111.

[12] Pande. U.; La Mar, G. N.; Lecomte, J. T. L.; Ascoli, F.; Brunori, M.; Smith, K. M.; Pandey, R. K.; Parish, D. W.; Thanabal, V. *Biochemistry*, **1986**, 25, 5638-5646.

[13] Rossi-Fanelli, A.; Antonini, E. *Biokhimiia*, **1957**, 22, 336-344.

[14] Seamonds, B.; Forster, R. E.; George, P. *J. Biol. Chem.*, **1971**, 246, 5391-5397.

[15] Suzuki, T. *Biochim. Biophys. Acta*, **1987**, 914, 170-176.

[16] Yamamoto, Y.; Ossawa, A.; Inoue, Y.; Chujo, R.; Suzuki, T. *Eur. J. Biochem.*, **1990**, 192, 225-229.

[17] Yamamoto, Y.; Suzuki, T.; Hori, H. *Biochim. Biophys. Acta*, **1993**, 1203, 267-275.

[18] Koshikawa, K.; Yamamoto, Y.; Kamimura, S.; Matsuoka, A.; Shikama, K. *Biochim. Biophys. Acta*, **1998**, 1385, 89-100.

[19] Yamamoto,Y.; Kurihara, N.; Egawa, T.; Shimada, H.; Ishimura, Y. *Biochim. Biophys. Acta*, **1999**, 1433, 27-44.

[20] Makinen, M. W.; Houtchens, R. A.; Caughey, W. S. *Proc. Natl. Acad. Sci. U.S.A.*, **1979**, 76, 6042-6046.

[21] Shimada, H.; Caughey, W. S. *J. Biol. Chem.***, 1982**, 257, 11893-11900.

[22] Kerr, E. A.; Yu, N. T. In *Biological Applications of Raman Spectroscopy*; Spiro, T. G., Ed.; Wiley-Interscience: New York, 1988; Vol. 111, Chapter 2.

[23] Chang, C. K.; Ward, B.; Ebina, S. *Arch. Biochem. Biophys.*, **1984**, 231, 366-371.

[24] Neya, S.; Suzuki, M.; Hoshino, T.; Ode, H.; Imai, K.; Komatsu, T.; Ikezaki, A.; Nakamura, M.; Furutani, Y.; Kandori, H. *Biochemistry*, **2010**, 49, 5642-5650

[25] Toi, H.; Homma, M.; Suzuki, A.; Ogoshi, H. *J. Chem. Soc., Chem. Commun.*, **1985**, 1791–1792.

[26] Alben J. O.; Caughey, W. S. *Biochemistry*, **1968**, 7, 175-183.

[27] Springer, B. A.; Egeberg, K. D.; Sligar, S. G.; Rohlfs, R. J.; Mathews, A. J.; Olson, J. S. *J. Biol. Chem.*, **1989**, 264, 3057-3060.

[28] Carver, T. E.; Brantley, R. E.; Singleton, E. W.; Arduini, R. M.; Quillin, M. L.; Phillips, G. N., Jr.; Olson, J. S. *J. Biol. Chem.*, **1992**, 267, 14443-14450.

[29] Teale, F. W. J. *Biochim. Biophys. Acta*, **1959**, 35, 543.

[30] Kitanishi, K.; Kobayashi, K.; Kawamura, Y.; Ishigami, I.; Ogura, T.; Nakajima, K.; Igarashi, J.; Tanaka, A.; Shimizu, T. *Biochemistry*, **2010**, 49, 10381-10393.

[31] La Mar, G. N.; Satterlee, J. D.; de Ropp, J. S. In *The Porphyrin Handbook*, (Kadish, K., Smith, K. M., and Guilard, R., eds.), Academic Press, New York, **2000**, pp 185-298.

[32] Bertini, I.; Luchinat, C. *NMR of Paramagnetic Molecules in Biological Systems*, The Benjamin/Cummings Publishing Company, Menlo Park, California, **1986**, pp 19-46.

[33] Yamamoto, Y. *Annu. Rep. NMR Spectrosc.*, **1998**, 36, 1-77.

[34] La Mar, G. N.; Budd, D. L.; Viscio, D. B.; Smith, K. M.; Langry, L. C. *Proc. Natl. Acad. Sci. U. S. A.*, **1978**, 75, 5755-5759.

[35] Caughey, W. S.; Shimada, H.; Choc, M. G.; Tucker, M. P. *Proc. Natl. Acad. Sci. U.S.A.*, **1981**, 78, 2903-2907.

[36] Anderson C. L.; Hester, R. E.; Moore, J. N. *Biochim. Biophys. Acta*, **1997**, 1338, 107-120.

[37] Tsubaki, M.; Srivastava, R. B.; Yu, N. T. *Biochemistry*, **1982**, 21, 1132-1140.

[38] Anderton, C. L.; Hester, R. E.; Moore, J. N. *Biochim. Biophys. Acta*, **1997**, 1338, 107-120

[39] Alben J. O.; Caughey, W. S. *Biochemistry*, **1968**, 7, 175-183.

[40] Li, X.-Y.; Spiro, T. G. *J. Am. Chem. Soc.*, **1988**, 110, 6024-6033.

[41] Anderton, C. L.; Hester, R. E.; Moore, J. N. *Biochim. Biophys. Acta*, **1997**, 1338, 107-120.

[42] Li, X.-Y.; Spiro, T. G. *J. Am. Chem. Soc.*, **1988**, 110, 6024-6033.

[43] Neya, S.; Funasaki, N.; Sato, T.; Igarashi, N.; Tanaka, N. *J. Biol. Chem.***, 1993**, 268, 8935-8942.

[44] Neya, S.; Funasaki, N.; Shiro, Y.; Iizuka, T.; Imai, K. *Biochim. Biophys. Acta*, **1994**, 1208, 31-37.

Chapter 3

Electronic control of ligand-binding preference in myoglobin lacking the distal histidine residue

Abstract

The oxygen (O_2) and carbon monoxide (CO) binding properties and the autoxidation reaction rate of the H64L mutant of myoglobin reconstituted with chemically-modified heme cofactors possessing a heme Fe atom with a variety of electron densities have been investigated in order to elucidate the effect of the removal of the distal His64 on the control of the O_2 affinity, discrimination between O_2 and CO and the autoxidation reaction rate of the protein by the intrinsic heme Fe reactivity through the electron density of the heme Fe atom (ρ_{Fe}). The study revealed that, as found for the native protein, not only the O_2 affinity but also autoxidation reaction rate of the H64L mutant protein is regulated by the ρ_{Fe} value in such manner that the O_2 affinity of the proteins decreases, due to an increase in the O_2 dissociation rate constant, with a decrease in the ρ_{Fe} value. On the other hand, the CO affinity of H64L mutant was found to increase, due to a decrease in the CO dissociation rate constant, with a decrease in the ρ_{Fe} value, whereas that of the native protein was essentially independent of a change in the ρ_{Fe} value. These novel findings provided critical insights into functional roles of His64 in the protein. As a result, the regulation of the O_2/CO discrimination in the protein through the ρ_{Fe} value is affected by the distal His64. Thus, the study revealed that electronic tuning of the intrinsic heme Fe reactivity through the ρ_{Fe} value plays a vital role in the regulation of the protein function, as the heme environment furnished by the distal His64 dose.

Introduction

Myoglobin (Mb), an oxygen storage hemoprotein, is one of the most thoroughly studied proteins and has been served as a paradigm for the structure-function relationships of metalloproteins [1-9]. Dioxygen (O_2) and also carbon monoxide (CO) are reversibly bound to a ferrous heme Fe atom (Fe(II)) in Mb. During reversible O_2 binding, the Fe(II) state has to be maintained in the protein, because the ferric heme Fe atom (Fe(III)) is not able to bind to O_2 and hence is physiologically inactive. The O_2 bound Mb is easily oxidized in to Fe(III) state through a process called as "autoxidation" [10]. Additionally, Mb must favor the binding of O_2 compared to the toxic ligand CO ubiquitously produced from a variety of sources in biological systems [2]. The ability of Mb to stabilize Fe(II)-bound O_2 and discriminate against CO binding is usually evaluated on the basis of the *M* value, i.e., the ratio between the equilibrium constants for CO and O_2 binding ($K(CO)/K(O_2)$) [6]. The *M* value was reported to be ~2×10^4 for unencumbered model heme Fe(II) complexes in organic solvents [8,11], and such a strong preference of heme Fe(II) for CO binding inhibits the O_2 storage function of the protein.

The regulation of the Mb function has been shown to be achieved through the heme environment furnished by nearby amino acid residues [6-9] and electronic tuning of the intrinsic heme Fe reactivity [12-14]. The heme environmental effects on the protein function have been elucidated in some detail, and particularly it is well-known that distal His(His64) contributes significantly to increase the O_2 affinity of the protein by stabilizing Fe(II)-bound O_2 through hydrogen bonding interaction between the His64 $N_\varepsilon H$ proton and the bound O_2 (distal H-bond)(Scheme 3-1) [1,15-17]. Recently, I found that the O_2 affinity, CO/O_2 discrimination and autoxidation reaction rate (k_{ox}) of the protein are regulated by the intrinsic heme Fe reactivity through the heme electronic structure[12,13]. In order to reveal the electronic mechanism responsible for control of the Mb function, I have constructed unique system composed of Mbs reconstituted with designed artificial heme cofactors such as mesoheme(Meso), 3,8-dimethyldeuteroporphyrinatoiron(III)(3,8-DMD) [18,19], 13,17-bis(2-carboxylatoethyl)-3,8-diethyl-2,12,18-trimethyl-7-trifluoromethylporphyrinato-iron(III)(7-PF) [20], and 13,17-bis(2-carboxylatoethyl)-3,7-diethyl

-12,18-trimethyl-2,8-ditrifluoromethylporphyrinatoiron(III)(2,8-DPF) [12], i.e., Mb(Meso), Mb(3,8-DMD), Mb(7-PF), and Mb(2,8-DPF), respectively. These heme cofactors differ in the numbers of CF_3, CH_3, and C_2H_5 side chains (Figure 2-2). The substitution of strongly electron-withdrawing trifluoromethyl(CF_3) group(s), as side chain(s) of heme cofactor, enables large and stepwise alterations of the heme electronic structure, and since 7-PF and 2,8-DPF can be considered as counterparts of Meso and 3,8-DMD, respectively, the functional consequences of the substitution of one and two CF_3 groups can be elucidated from the results of comparative studies on Mb(Meso) and Mb(7-PF), and Mb(3,8-DMD) and Mb(2,8-DPF), respectively. Through studies of the reconstituted protein system [12,13], I revealed that the control of autoxidation reaction and the *M* value is achieved through the effect of a change in the ρ_{Fe} value on the O_2 binding state, which can be reasonably interpreted in terms of the effect of a change in the ρ_{Fe} value on the resonance process between the Fe^{2+}-O_2 and Fe^{3+}-O_2^--like species (Scheme 3-1) [21,22]. On the other hand, in contrast to the O_2 binding, the CO affinity of the protein was shown to be almost independent of the ρ_{Fe} value [11].

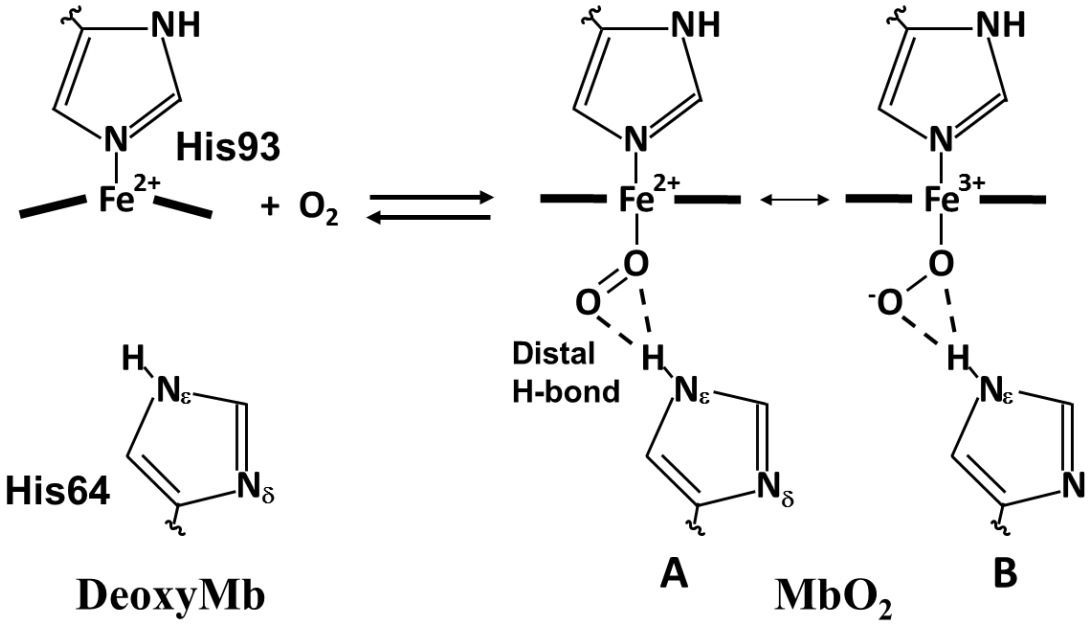

Shcme 3-1. Oxygenation of deoxy Mb.

In this chapter, I elucidated the effect of the removal of the distal His64, and hence the distal H-bond, on the control of the intrinsic heme Fe reactivity through the ρ_{Fe} value. In order to achieve my goal, I characterized the O_2 and CO binding properties and $k_{(ox)}$ of the H64L mutant (H64L(Proto)) and the mutant proteins reconstituted with Meso, 3,8-DMD, 7-PF, and 2,8-DPF, i.e., H64L(Meso), H64L(3,8-DMD), H64L(7-PF), and H64L(2,8-DPF), respectively, and then the results of the mutant proteins were compared with those of the native ones. H64L(Proto) has been investigated exhaustively as one of typical Mb mutant proteins to reveal functional and structural consequences of the removal of the distal His64 [6,23-28], and hence I could take advantage of detailed functional and structural properties reported for the mutant protein. The study demonstrated that the differences in the ρ_{Fe} values of the H64L mutant proteins are clearly reflected in the stretching frequencies of the Fe-bound CO (ν_{CO}) in CO forms of the mutant proteins [14] (see chapter 2) , and that the O_2 affinities, i.e., $K(O_2)$ values and $k_{(ox)}$ ones of the mutant proteins were found to correlate well with the ν_{CO} values. The plots of the quantity $\log(K(O_2))$ against the ν_{CO} values ($\log(K(O_2))$- ν_{CO} plots) for the mutant proteins could be represented by a straight line, and the slope of the $\log(K(O_2))$- ν_{CO} plots of the mutant proteins was identical to that of similar plots previously reported for the native ones [12]. These result demonstrated not only that the electronic control of the O_2 affinity and autoxidation reaction of Mb through the ρ_{Fe} value is not affected by the removal of the distal His64, but also that the regulations of the O_2 affinity and autoxidation reaction through the heme environment furnished by the His64 [1,6,28] and that of electronic tuning of the intrinsic heme Fe reactivity through the ρ_{Fe} value are independent to each other. In contrast to the O_2 binding, the effects of a change in the ρ_{Fe} value on the CO binding properties were found to be different between the H64L mutant and native proteins in a manner that the CO affinity of the mutant protein increased with decreasing the ρ_{Fe} value, while that of the native one was essentially independent of the ρ_{Fe} value. As a result, the M value of the H64L mutant protein was more largely affected by a given change in the ρ_{Fe} value than that of the native one.

MATERIALS AND METHODS

Materials and protein samples. All reagents and chemicals were obtained from commercial sources and used as received. Sperm whale Mb was purchased as a lyophilized powder from Biozyme and used without further purification. The expression and purification of the H64L mutant (H64L(Proto)) were carried out according to the method described by Springer et al.[6]. Mesoheme (Meso) was purchased from Frontier Scientific Co. 3,8-DMD[18,19], 7-PF[20], and 2,8-DPF[12] were synthesized as previously described. The apoproteins of H64L(Proto) and native protein (Mb(Proto)) were prepared at 4 °C according to the procedure of Teale [29], and reconstituted H64L mutant and native proteins were prepared by slow addition of a synthetic heme cofactor to the corresponding apoproteins in 50 mM potassium phosphate buffer, pH 7.0, at 4 °C [12]. In order to prepare CO and O_2 forms of the H64L mutant and native proteins, the proteins were reduced by adding $Na_2S_2O_4$ (Nakalai Chemicals Ltd.) in the presence of CO gas (Japan Air Gases) and in the air, respectively. Excess agent was removed by passage through a Sephadex G-10 (Sigma-Aldrich Co.) column equilibrated with an appropriate buffer solution. The pH of each sample was measured with a Horiba F-22 pH meter equipped with a Horiba type 6069-10c electrode. The pH of a sample was adjusted using 0.1 M NaOH or HCl.

Oxygen equilibrium curves. Oxygen equilibrium curves (OECs) of the H64L mutant proteins were measured with 30 μM protein in 100 mM phosphate buffer, pH 7.4, and 100 mM Cl^- at 20 °C, using the previously described automatic recording apparatus [30]. P_{50} values were determined through non-linear least-squares fitting of the OEC data [31].

Kinetic measurements of O_2 and CO binding. Kinetic measurements of O_2 and CO binding of the H64L mutant proteins were carried out in 100 mM phosphate buffer, pH 7.40, at 25 °C, using ligand displacement experiments described previously [32-36]. Flash photolysis using a 5 ns-pulse Nd-YAG laser (532 nm) was performed on CO forms of the H64L mutant proteins (H64LCOs) in the presence of gas mixture of O_2 and CO at a ratio of 35:65. The rate constants for O_2 association ($k_{on}(O_2)$) and the pseudo first-order rate constants for O_2 dissociation ($k_{off}(O_2)$) of H64L(Meso), H64L(3,8-DMD),

H64L(7-PF), H64L(2,8-DPF), and H64L(Proto) were determined through analysis of the time evolution of the absorbance at a wavelength optimized for each protein sample, after the photolysis, which exhibited biphasic behavior, and the fast and slow phases with time-scales of μs and ms, respectively, represent O_2 binding, i.e., $k_{on}(O_2)$, and the displacement of transiently bound O_2 by the CO present in the sample solution, i.e., $k_{off}(O_2)$, respectively. The equilibrium constants for O_2 binding ($K(O_2)$) were calculated from the kinetic data, i.e., the $k_{on}(O_2)$ and $k_{off}(O_2)$ values.

The rate constants for CO association (k_{on}(CO)) of the mutant proteins were measured through analysis of the time evolution of the absorbance at 410, 410, 410, 416, and 424 nm, respectively, after photolysis of the CO form under 1 atm of CO, i.e., the concentration of CO ([CO]) = 9.85×10^{-4} M. The k_{on}(CO) value can be determined from the observed pseudo first-order rate constant for CO association (k_{obs}(CO)) using the equation, $k_{obs}(CO) \approx k_{on}(CO)$, because the rate constant of the CO dissociation (k_{off}(CO)) is $<< k_{on}(CO) \times [CO]$. Then, the k_{off}(CO) value was determined by analysis of displacement of Fe-bound CO and the oxidation of heme Fe by $K_3Fe(CN)_6$[34-36]. Similarly to the case of the study of O_2 binding, the equilibrium constants for CO binding (K(CO)) were calculated from the kinetic data, i.e., the k_{on}(CO) and k_{off}(CO) values.

Measurement of autoxidation reaction rate. UV-vis absorption spectra were recorded for 10 μM protein samples at 25 °C using a Beckman DU 640 spectrophotometer, and 100mM potassium phosphate buffer were used to prepare sample solutions at pH 7.4. Autoxidation of reactions were characterized by only two spectral species with clear isosbestic points, and the observed time evolution could be represented well by a simple first order reaction mechanism, that is, $d[H64LO_2]/dt = - k_{ox} [H64LO_2]$, where k_{ox} is the apparent autoxidation reaction rate constant.

Resonance raman spectroscopy. Resonance raman scattering was performed with excitation at 413.1 nm with a Kr^+ laser (Spectra Physics, BeamLok 2060), dispersed with a polychromator (SPEX 1877, 1200 grooves/mm grating), and detected with a liquid nitrogen-cooled charge coupled device (CCD) detector (CCD-1024×256-OPEN-1LS, HORIBA Jobin Yvon) [37]. The protein concentrations were approximately 40 μM in 100 mM potassium phosphate buffer, pH 7.4. For the measurements of

O_2 forms of the H64L mutant proteins (H64LO_2s), the protein samples were kept cool in order to inhibit autoxidation of the proteins. Raman shifts were calibrated with indene as a frequency standard. The positions of the bands were determined through fitting with Voigt profiles, which are convolutions of Gaussian and Lorentzian functions [38], and the accuracy of the peak positions of well-defined Raman bands was ±1 cm^{-1}.

RESULTS

Effects of Heme Modifications on Functional Properties of the H64L Mutant Proteins. The $k_{on}(O_2)$, $k_{off}(O_2)$, $K(O_2)$, $k_{on}(CO)$, $k_{off}(CO)$, $K(CO)$, k_{ox} and P_{50} values, together with M ones, of the H64L mutant proteins possessing various heme cofactors are determined(Table 3-1 and Figures 3-1－3-15) The time course of CO association of H64L(7-PF) was better fitted by a sum of two exponentials, and the $k_{on}(CO)$ value close to those of the other H64L mutant proteins is indicated in Table 3-1. The P_{50} values of H64L(Meso) and H64L(3,8-DMD) could not be determined accurately due to their fast autoxidation(results not shown). The kinetic parameters of O_2 and CO binding of H64L(Proto) were similar to the corresponding ones reported by Rohlfs et al.[33]. As has been demonstrated previously [33], the $k_{on}(O_2)$ and $k_{on}(CO)$ values of H64L(Proto) were increased by factors of ~20 and ~60, respectively, by the H64L mutation, and then the $k_{off}(O_2)$ and $k_{off}(CO)$ ones by factors of ~300 and ~3, respectively, resulting in a considerable lowering of the O_2 affinity and, in contrast, a large increase in the CO one (Table 3-1). Autoxidation reaction of H64L(Proto) became fast by factors of ~20. Additionally, as has been reported previously for native Mb [13], the k_{ox} value of H64L mutant proteins decreased with the substitution of CF_3 group(s) (Table 3-1).The increases in the $k_{on}(O_2)$ and $k_{on}(CO)$ values by the mutation have been attributed, in part, to the absence of water molecules in the heme pocket [23], which have to be displaced before binding of exogenous ligands. In addition, as expected from structural consequence of the H64L mutation, the dramatic increase in the $k_{off}(O_2)$ and $k_{(ox)}$ ones by the mutation is due to the absence of the distal H-bond [1,33,39]. A large difference in the M value between Mb(Proto) and H64L(Proto), i.e., 23 ± 9 and 6900 ± 5700, respectively(Table 3-1), clearly indicated a significant contribution of the distal H-bond to the regulation of the CO/O_2 discrimination in the protein [1,6,33].

Comparison of the O_2 binding parameters among the mutant proteins possessing various heme cofactors revealed that the $k_{off}(O_2)$ value increases steadily with increasing number of CF_3 substitutions, whereas the $k_{on}(O_2)$ value is affected only slightly by the CF_3 substitutions. Consequently, the decrease in the O_2 affinity of the H64L mutant protein by the CF_3 substitutions is due solely to the increase in the $k_{off}(O_2)$ value. Hence, the effects of a change in the ρ_{Fe} value on the O_2 binding properties of the mutant protein were qualitatively similar to those of the native one [12,14]. On the

other hand, the effects of a change in the ρ_{Fe} value on the CO binding properties of the mutant protein were somewhat different from those of the native one. Although both the k_{on}(CO) and k_{off}(CO) values of the native protein were essentially independent of a change in the ρ_{Fe} value [12,14], the k_{off}(CO) value of the mutant protein was decreased by the CF_3 substitutions, whereas its k_{on}(CO) value was not largely affected, leading to an increase in the CO affinity of the mutant protein by the CF_3 substitutions. As a result, as reflected in the *M* value, the CO/O_2 discrimination of the mutant protein is enhanced remarkably with decreasing the ρ_{Fe} value(Table 3-1), i.e., the *M* value increased by a factor of ~9 on the substitution of one CF_3 group, as demonstrated for the H64L(Meso)/H64L(7-PF) system, and then by a factor of ~60 on the substitution of two CF_3 ones, as revealed through analysis of the H64L(3,8-DMD)/H64L(2,8-DPF) system.

Table 3-1. O_2 and CO binding parameters and autoxidation reaction rate for H64Ls and Mbs at pH7.4 and 25 °C.

		O_2 binding				**CO binding**				
Heme	**Protein**	$k_{on}(O_2)$ ($mM^{-1}s^{-1}$)	$k_{off}(O_2)$ (s^{-1})	$K(O_2)$ (mM^{-1})	P_{50}[c] (mmHg)	k_{on}(CO) ($mM^{-1}s^{-1}$)	k_{off}(CO) (s^{-1})	K(CO) (mM^{-1})	M (K(CO)/K(O_2))	$k_{(ox)}$ (h^{-1})
Meso	H64L	222 ± 66.6	2300 ± 970	0.097 ± 0.069	n.d[d]	28.9 ± 8.7	0.25 ± 0.075	116 ± 48.7	1200 ± 66.6	4.8 ± 0.14
	Mb[a]	8.2 ± 1.6	5.7 ± 1.1	1.5 ± 0.4	0.38	0.38 ± 0.07	0.048 ± 0.009	7.9 ± 2.4	5.5 ± 2.2	0.16 ± 0.02[b]
3,8-DMD	H64L	292 ± 87.6	1900 ± 800	0.15 ± 0.11	~10[e]	31.9 ± 9.6	0.23 ± 0.069	139 ± 58.4	930 ± 87.6	3.4 ± 0.13
	Mb[b]	12 ± 2	9.7 ± 1.9	1.3 ± 0.3	0.50	0.16 ± 0.03	0.024 ± 0.005	6.7 ± 2.0	5.1 ± 2.0	0.14 ± 0.02[b]
7-PF	H64L	212 ± 63.6	5700 ± 2400	0.037 ± 0.026	54	21.1 ± 6.3[f]	0.052 ± 0.016	580 ± 244	11000 ± 63.6	1.3 ± 0.084
	Mb[a]	12 ± 2	17 ± 3	0.5 ± 0.1	1.10	0.32 ± 0.06	0.032 ± 0.006	10 ± 3	21 ± 8	0.051 ± 0.005[b]
2,8-DPF	H64L	305 ± 91.5	31000 ± 13000	0.0098 ± 0.007	97	29.0 ± 8.7	0.053 ± 0.016	547 ± 230	56000 ± 91.5	0.9 ± 0.18
	Mb[a]	8.3 ± 1.6	110 ± 22	0.15 ± 0.03	2.80	0.69 ± 0.14	0.036 ± 0.007	19 ± 6	132 ± 53	0.033 ± 0.003[b]
Proto	H64L	228 ± 68.4	3200 ± 1300	0.071 ± 0.05	14	30.0 ± 9.0	0.061 ± 0.018	492 ± 207	6900 ± 68.4	1.9 ± 0.12
	Mb[a]	14 ± 3	12 ± 2	1.2 ± 0.3	0.58	0.51 ± 0.06	0.019 ± 0.005	27 ± 8	23 ± 9	0.083 ± 0.008[b]

a: Taken from Ref. 11. b: Taken from Ref.13. c: Determined from the oxygen equilibrium curve at pH 7.4 and 20 °C. d: Not determined due to fast autoxidation. e: Accurate determined of the value was hampered by fast autoxidation. f: The biphasic time course of CO association was fitted by the sum of two exponentials, and the value closer to those of the other H64L mutant proteins is indicated, the other one being 5.69 ± 1.7.

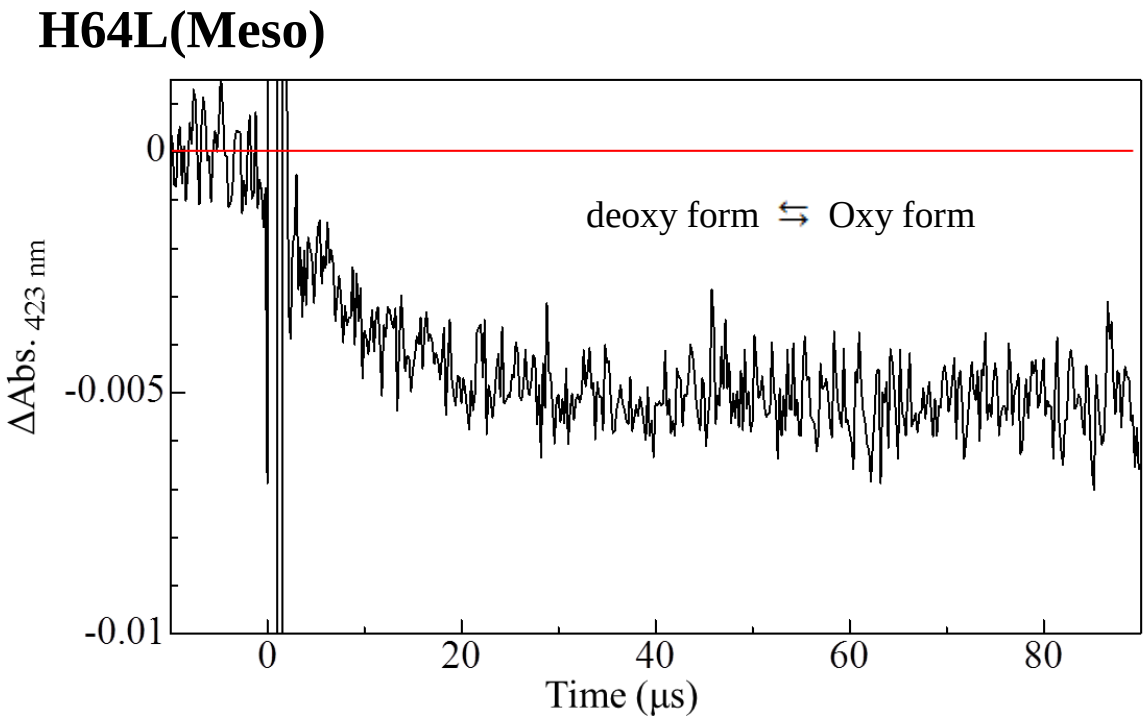

Figure 3-1. Time evolution of absorbance change at 423 nm (ΔAbs. 423 nm) after laser flash photolisis from 0 s to 100 μs of CO form of H64L(Meso) with potassium phosphate buffer, pH 7.40, and 25°C in $[O_2]$:[CO]=35:65.

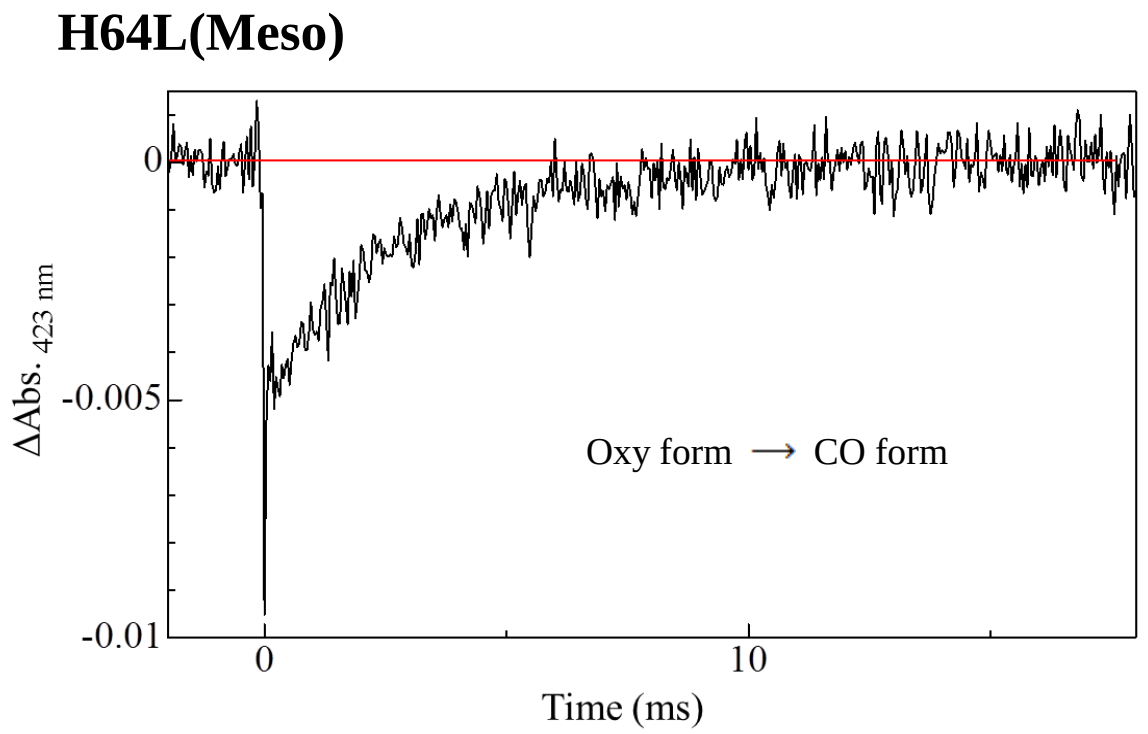

Figure 3-2. Time evolution of absorbance change at 423 nm (ΔAbs. 423 nm) after laser flash photolisis from 0 s to 20 ms of CO form of H64L(Meso) with potassium phosphate buffer, pH 7.40, and 25°C in $[O_2]$:[CO]=35:65.

H64L(3,8-DMD)

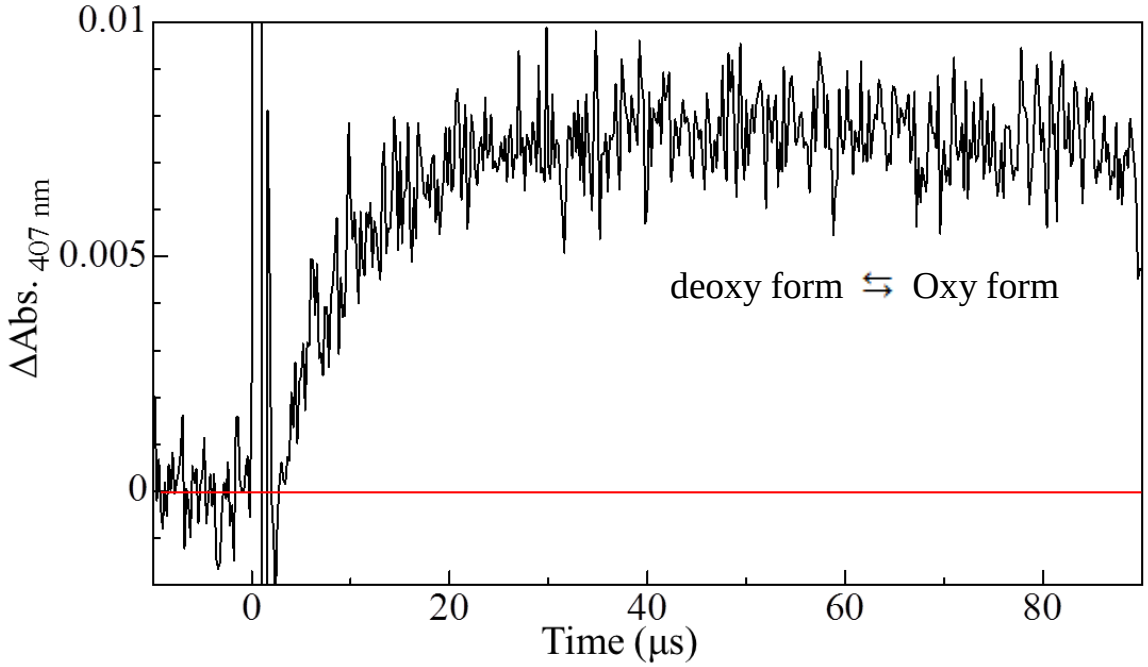

Figure 3-3. Time evolution of absorbance change at 407 nm (ΔAbs. 407 nm) after laser flash photolisis from 0 s to 100 μs of CO form of H64L(3,8-DMD) with potassium phosphate buffer, pH 7.40, and 25°C in $[O_2]$:[CO]=35:65.

H64L(3,8-DMD)

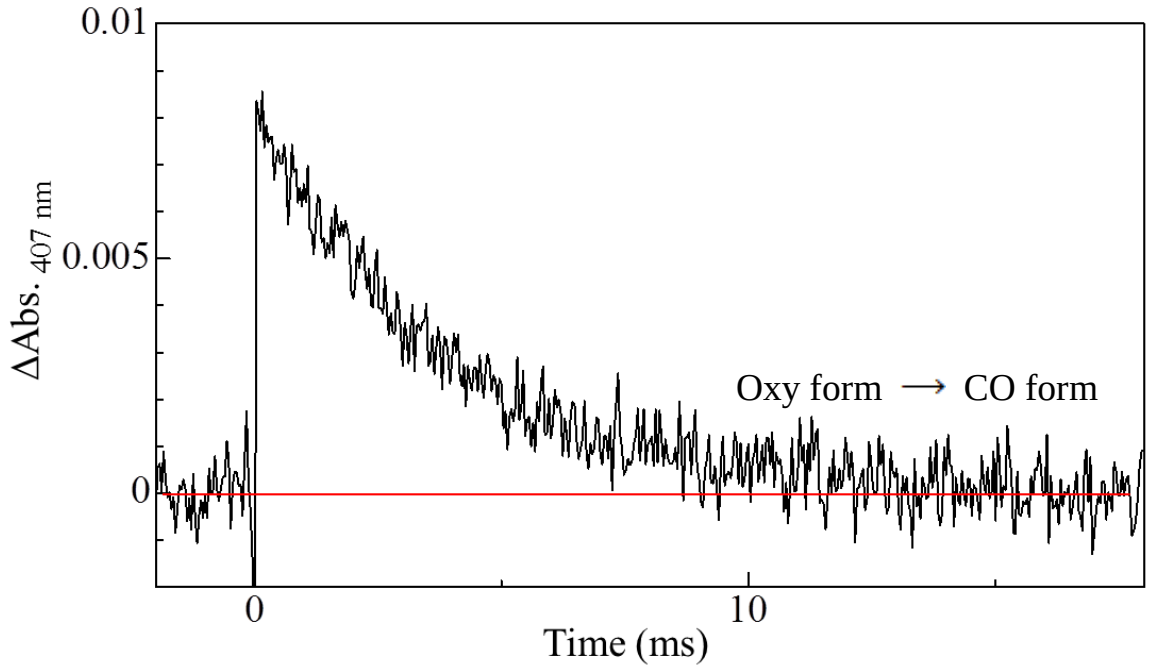

Figure 3-4. Time evolution of absorbance change at 407 nm (ΔAbs. 407 nm) after laser flash photolisis from 0 s to 20 ms of CO form of H64L(3,8-DMD) with potassium phosphate buffer, pH 7.40, and 25°C in $[O_2]$:[CO]=35:65.

H64L(7-PF)

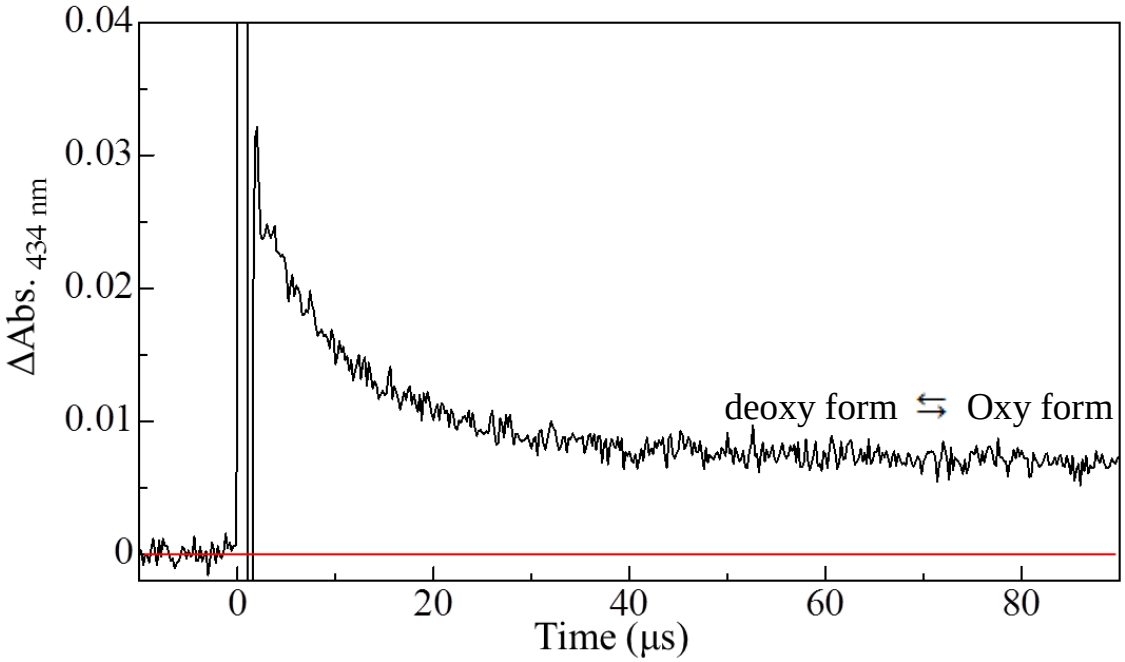

Figure 3-5 Time evolution of absorbance change at 434 nm (ΔAbs. 434 nm) after laser flash photolisis from 0 s to 100 μs of CO form of H64L(7-PF) with potassium phosphate buffer, pH 7.40, and 25°C in $[O_2]$:[CO]=35:65.

H64L(7-PF)

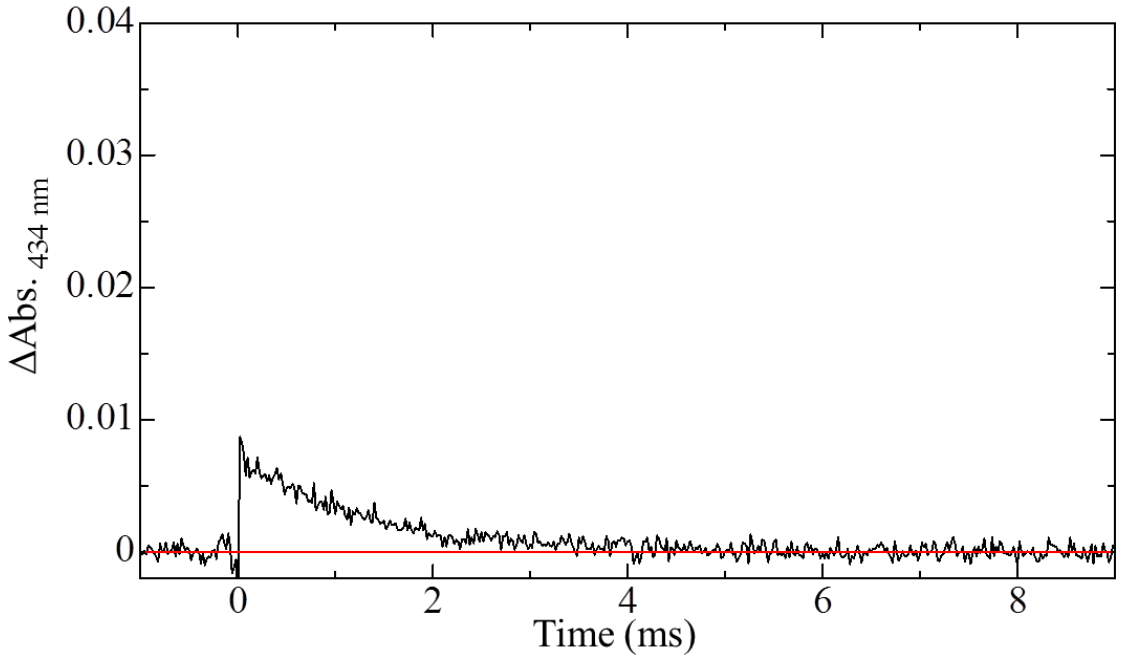

Figure 3-6. Time evolution of absorbance change at 434 nm (ΔAbs. 434 nm) after laser flash photolisis from 0 s to 10 ms of CO form of H64L(7-PF) with potassium phosphate buffer, pH 7.40, and 25°C in $[O_2]$:[CO]=35:65.

H64L(2,8-DPF)

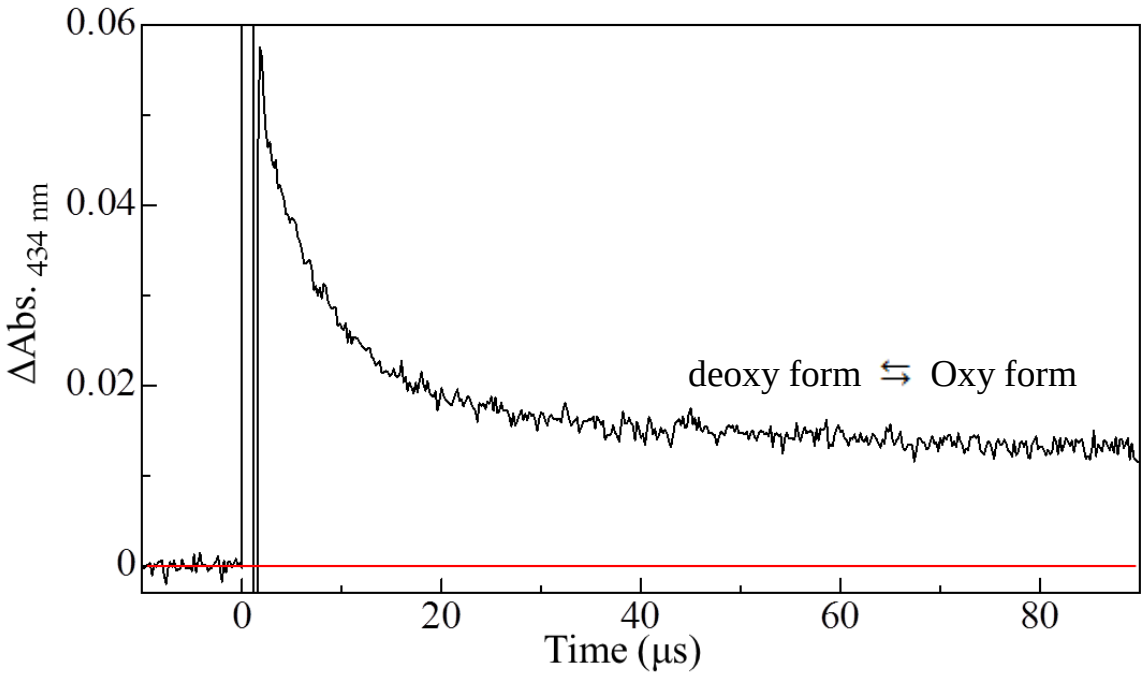

Figure 3-7. Time evolution of absorbance change at 434 nm (ΔAbs. 434 nm) after laser flash photolisis from 0 s to 100 μs of CO form of H64L(2,8-DPF) with potassium phosphate buffer, pH 7.40, and 25°C in [O_2]:[CO]=35:65.

H64L(2,8-DPF)

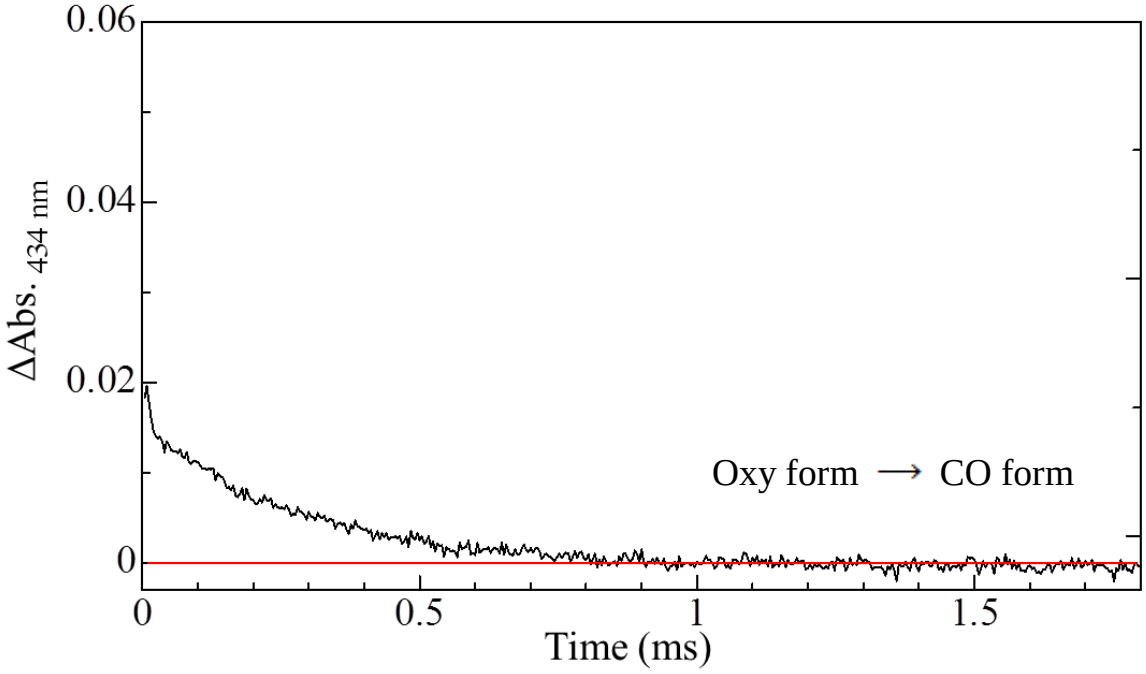

Figure 3-8. Time evolution of absorbance change at 434 nm (ΔAbs. 434 nm) after laser flash photolisis from 0 s to 2 ms of CO form of H64L(2,8-DPF) with potassium phosphate buffer, pH 7.40, and 25°C in [O_2]:[CO]=35:65.

H64L(proto)

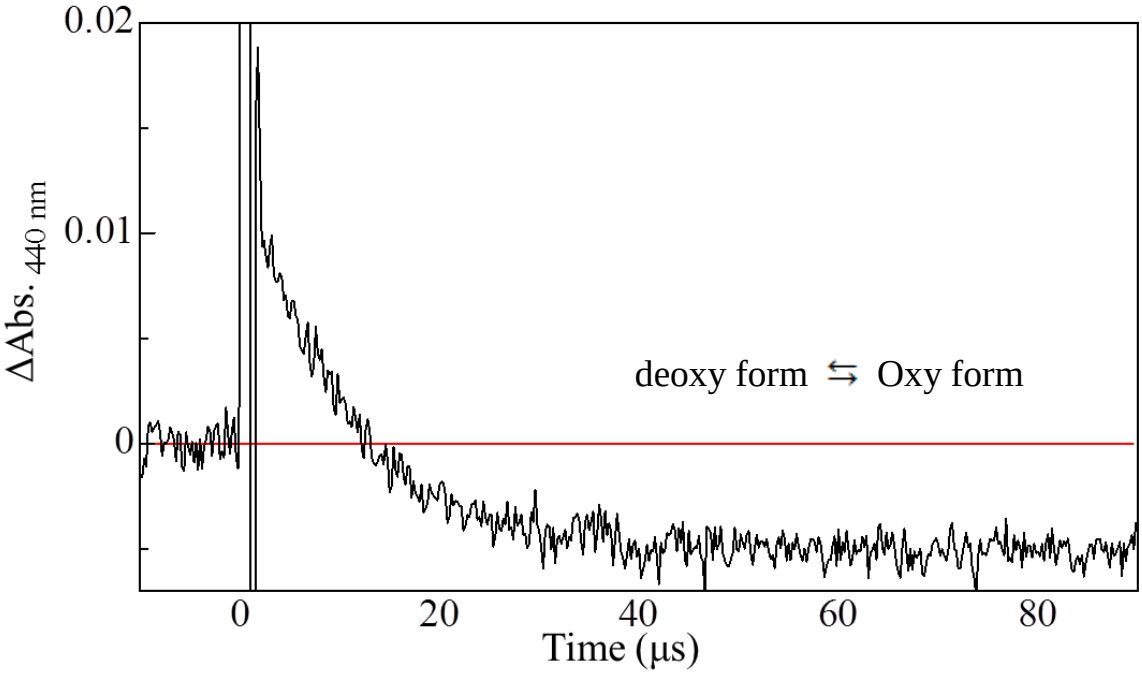

Figure 3-9. Time evolution of absorbance change at 440 nm (ΔAbs. 440 nm) after laser flash photolisis from 0 s to 100 μs of CO form of H64L(proto) with potassium phosphate buffer, pH 7.40, and 25°C in $[O_2]$:[CO]=35:65.

H64L(proto)

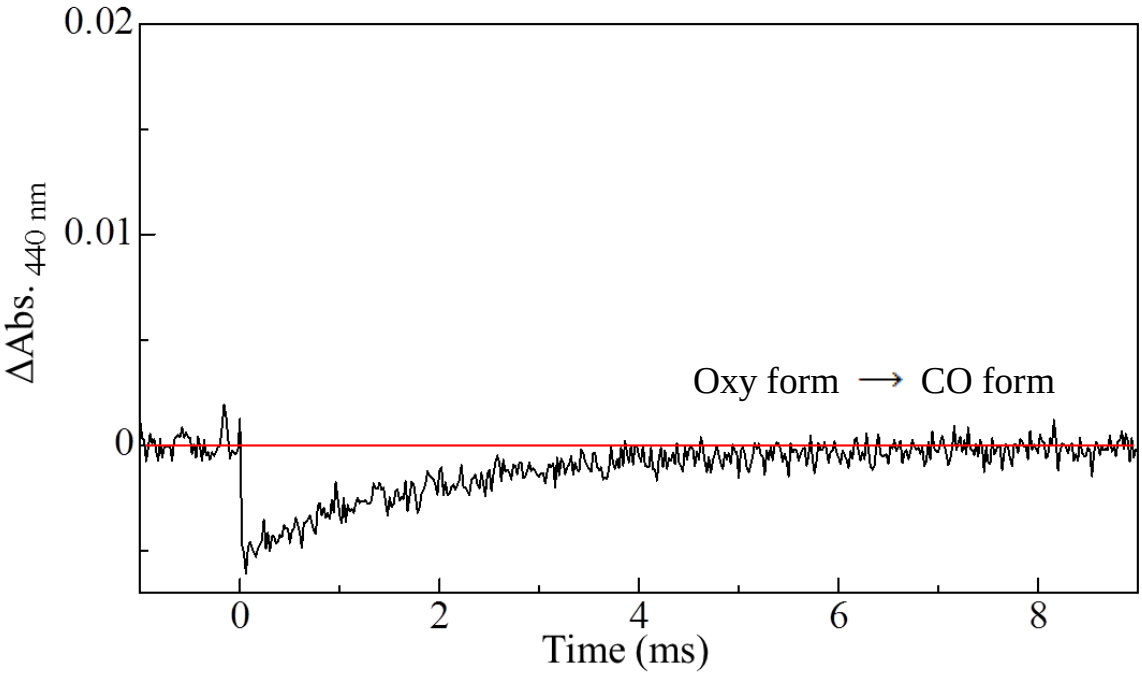

Figure 3-10. Time evolution of absorbance change at 440 nm (ΔAbs. 440 nm) after laser flash photolisis from 0 s to 10 ms of CO form of H64L(proto) with potassium phosphate buffer, pH 7.40, and 25°C in $[O_2]$:[CO]=35:65.

H64L(Meso)

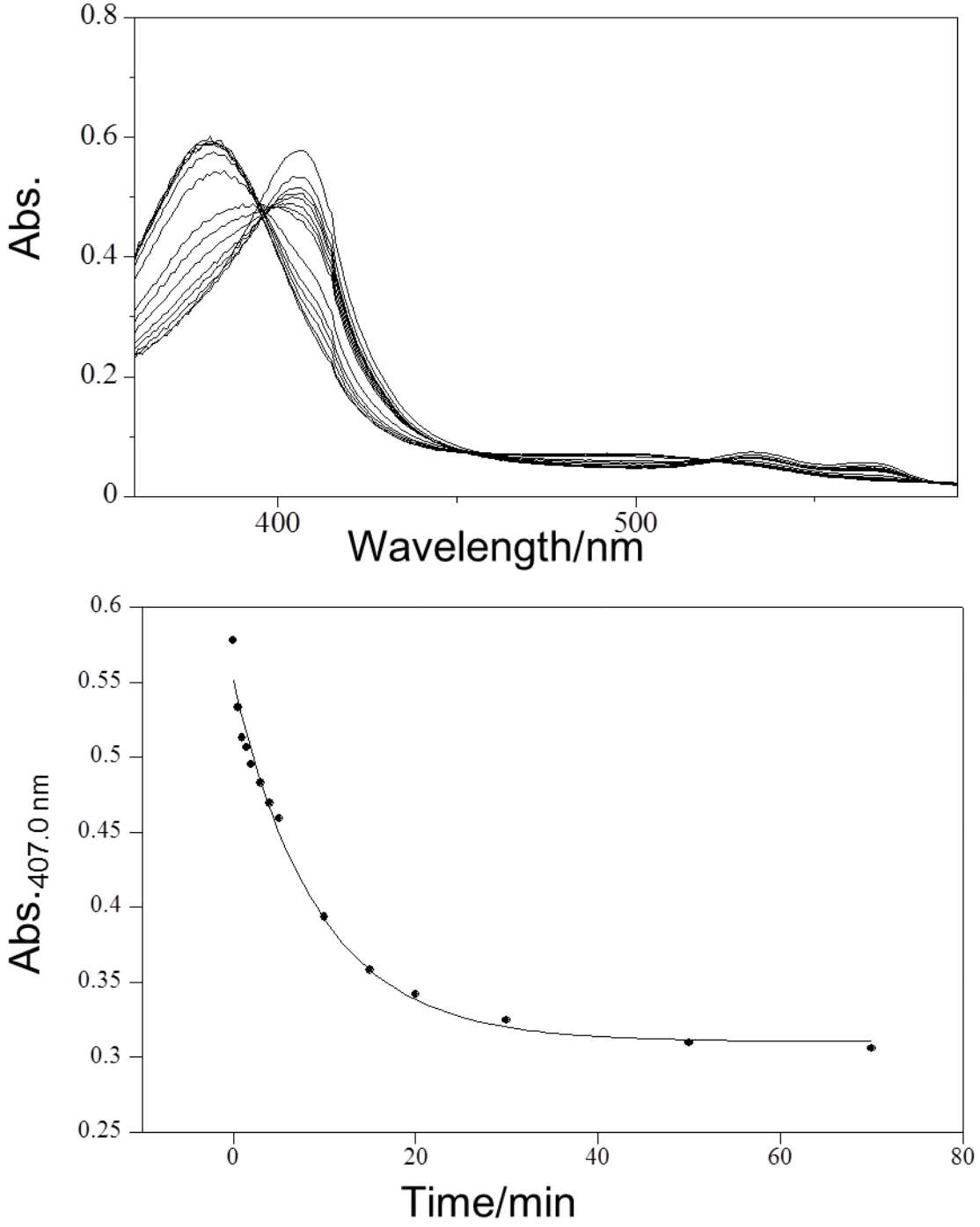

Figure 3-11. Spectral changes with time for the autodation reaction of H64L(Meso) in 100 mMpotassium buffer at pH 7.4 and 25°C. (Top)
Time evolution of absorbance at 407.0 nm. (Bottpm)

H64L(3,8-DMD)

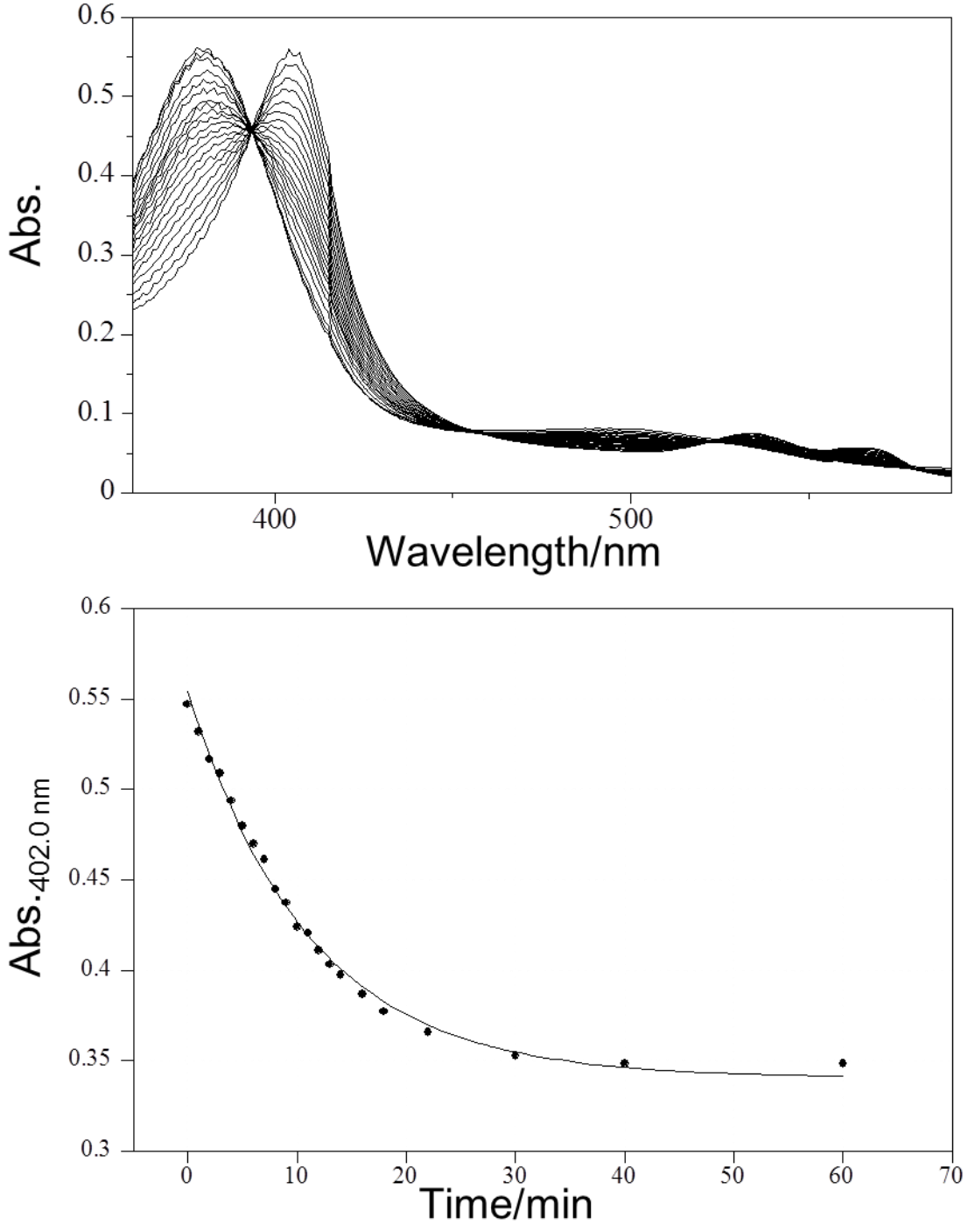

Figure 3-12. Spectral changes with time for the autodation reaction of H64L(3,8-DMD) in 100 mMpotassium buffer at pH 7.4 and 25°C. (Top)
Time evolution of absorbance at 402.0 nm. (Bottpm)

H64L(7-PF)

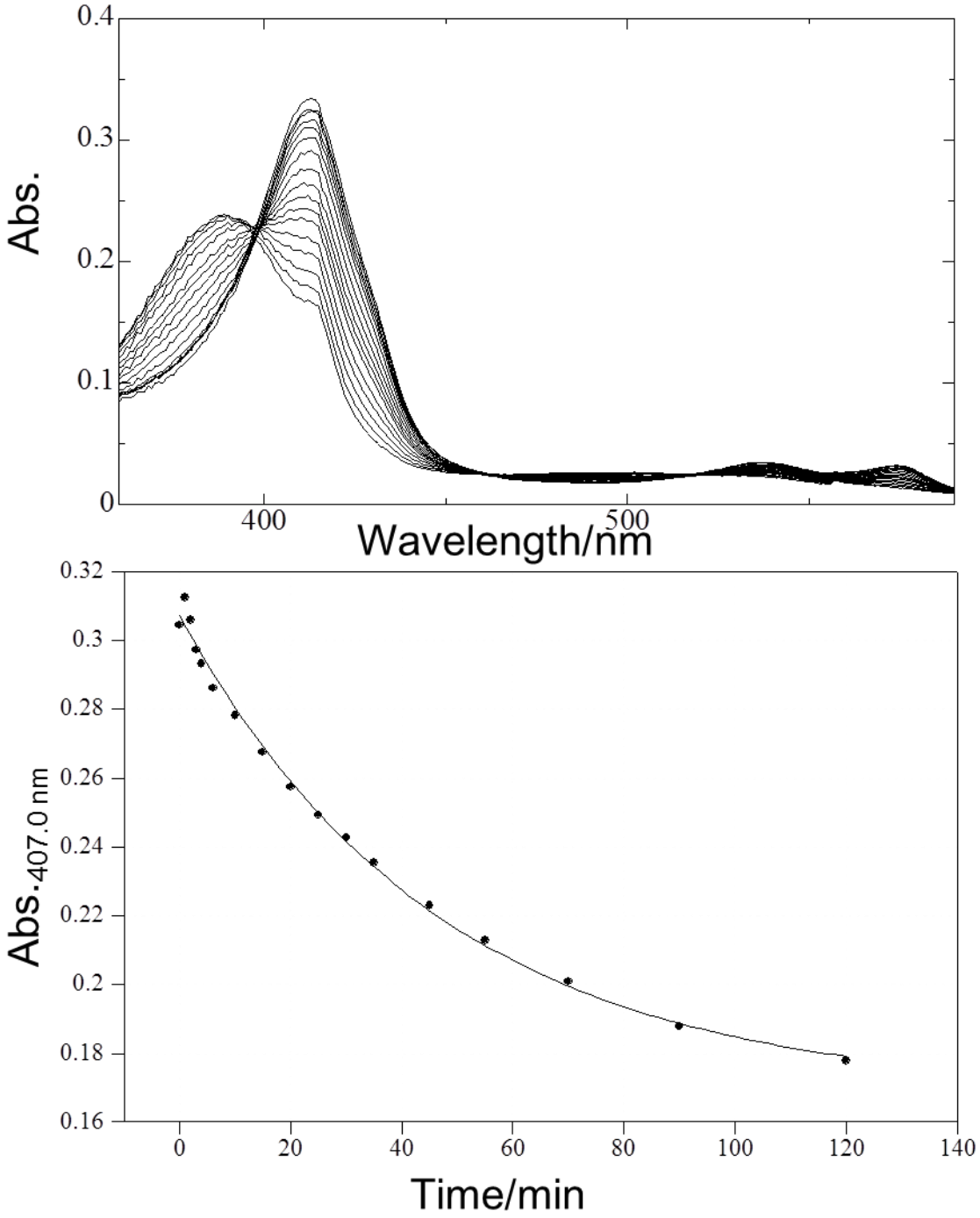

Figure 3-13. Spectral changes with time for the autodation reaction of H64L(7-PF) in 100 mMpotassium buffer at pH 7.4 and 25°C. (Top)
Time evolution of absorbance at 407.0 nm. (Bottpm)

H64L(2,8-DPF)

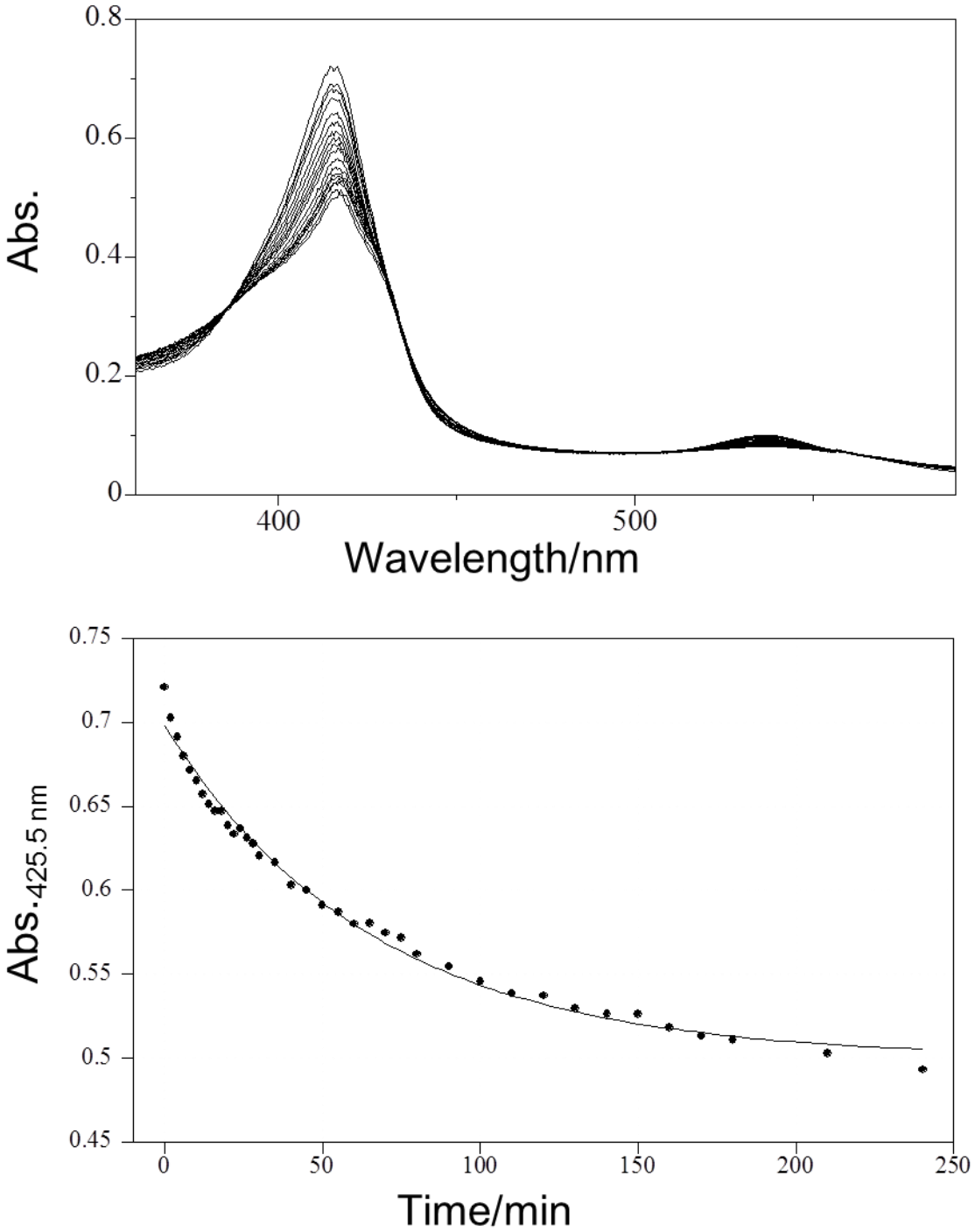

Figure 3-14. Spectral changes with time for the autodation reaction of H64L(2,8-DPF) in 100 mMpotassium buffer at pH 7.4 and 25°C. (Top)
Time evolution of absorbance at 425.5 nm. (Bottom)

H64L(proto)

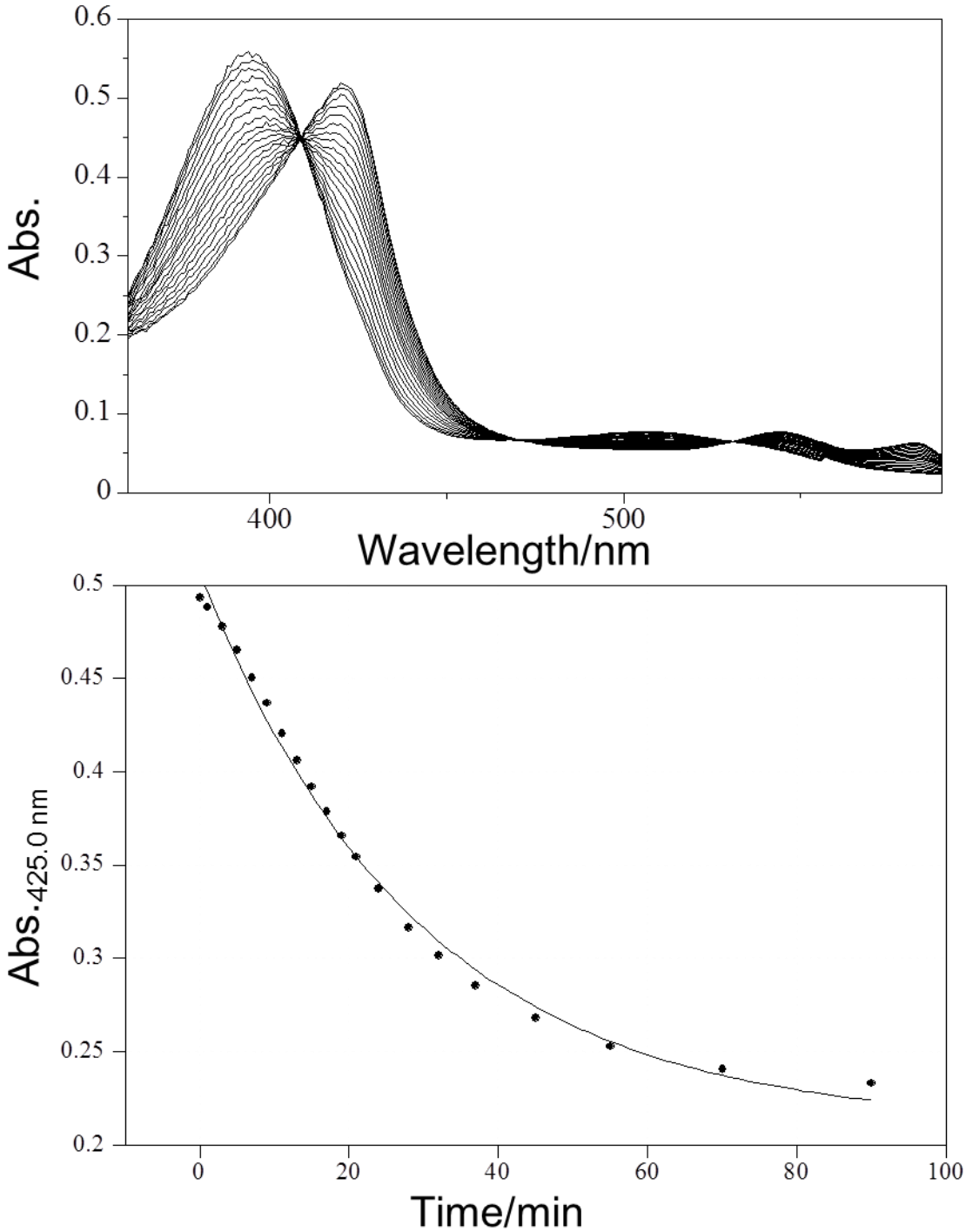

Figure 3-15. Spectral changes with time for the autodation reaction of H64L(Proto) in 100 mMpotassium buffer at pH 7.4 and 25°C. (Top)
Time evolution of absorbance at 425.0 nm. (Bottom)

Vibrational frequencies of Fe-bound O_2 of the H64L mutant and native proteins. Resonance raman spectra of O_2 forms of the mutant and native proteins(MbO_2 and $H64LO_2$, respectively) possessing various heme cofactors were observed in order to determine the vibrational frequencies of the Fe-O stretching (ν_{FeO}) of Fe-bound O_2 in the proteins (Figures 3-16 and 3-17). The ν_{FeO} bands of the proteins were observed as a single component (Figures 3-16 and 3-17), and the determined ν_{FeO} values were listed in Table 3-2. The ν_{FeO} values of 571 and 569 cm^{-1} determined for MbO_2(Proto) and $H64LO_2$(Proto), respectively, were similar to the corresponding ones previously reported by Hirota et al.[27], i.e., 571 and 570 cm^{-1} for the former and the latter, respectively. In contrast to the large mutation-dependent changes in the ν_{CO} and ν_{FeC} values (Table 3-2), the ν_{FeO} one was affected only slightly by the mutation. Comparison of the ν_{FeO} values among the mutant (or native) proteins, yielded that, although its effect is rather small, the ν_{FeO} value was decreased by the CF_3 substitutions, suggesting that the Fe^{2+}-O bond in the protein is slightly weakened by the CF_3 substitutions. Hence the weakening of the Fe^{2+}-O bond in the protein with decreasing the ρ_{Fe} value could be, in part, responsible for the decrease in the O_2 affinity of the protein by the CF_3 substitutions.

Table 3-2. Vibrational frequencies of the Fe-bound CO of H64LCOs and MbCOs and Fe-bound O_2 of $H64LO_2$s and MbO_2s at pH 7.4 and 25°C.

	ν_{CO}[a] (cm^{-1})		ν_{FeC}[b] (cm^{-1})		$\delta_{Fe\text{-}CO}$[c] (cm^{-1})		ν_{FeO}[d] (cm^{-1})	
	H64L	Mb[e]	H64L	Mb[e]	H64L	Mb[e]	H64L	Mb
Meso	1965	1943[f]	489	515	575	576	574	572
3,8-DMD	1964	1943[f]	491	514	575	576	570	571
7-PF	1972	1950[f]	489	514	573	575	568	571
2,8-DPF	1979	1956[f]	483	512	570	574	568	569
Proto	1969	1947[f]	490	512	574	576	569	571

a: The C-O stretching frequency of the Fe-bound CO. b: The Fe-C stretching frequency of the Fe-bound CO. c: The Fe-C-O bending frequency of the Fe-bound CO. d: The Fe-O stretching frequency of the Fe-bound O_2. e: Taken from Ref. 13 f: $\nu_{CO(H)}$(See Chapter 2)

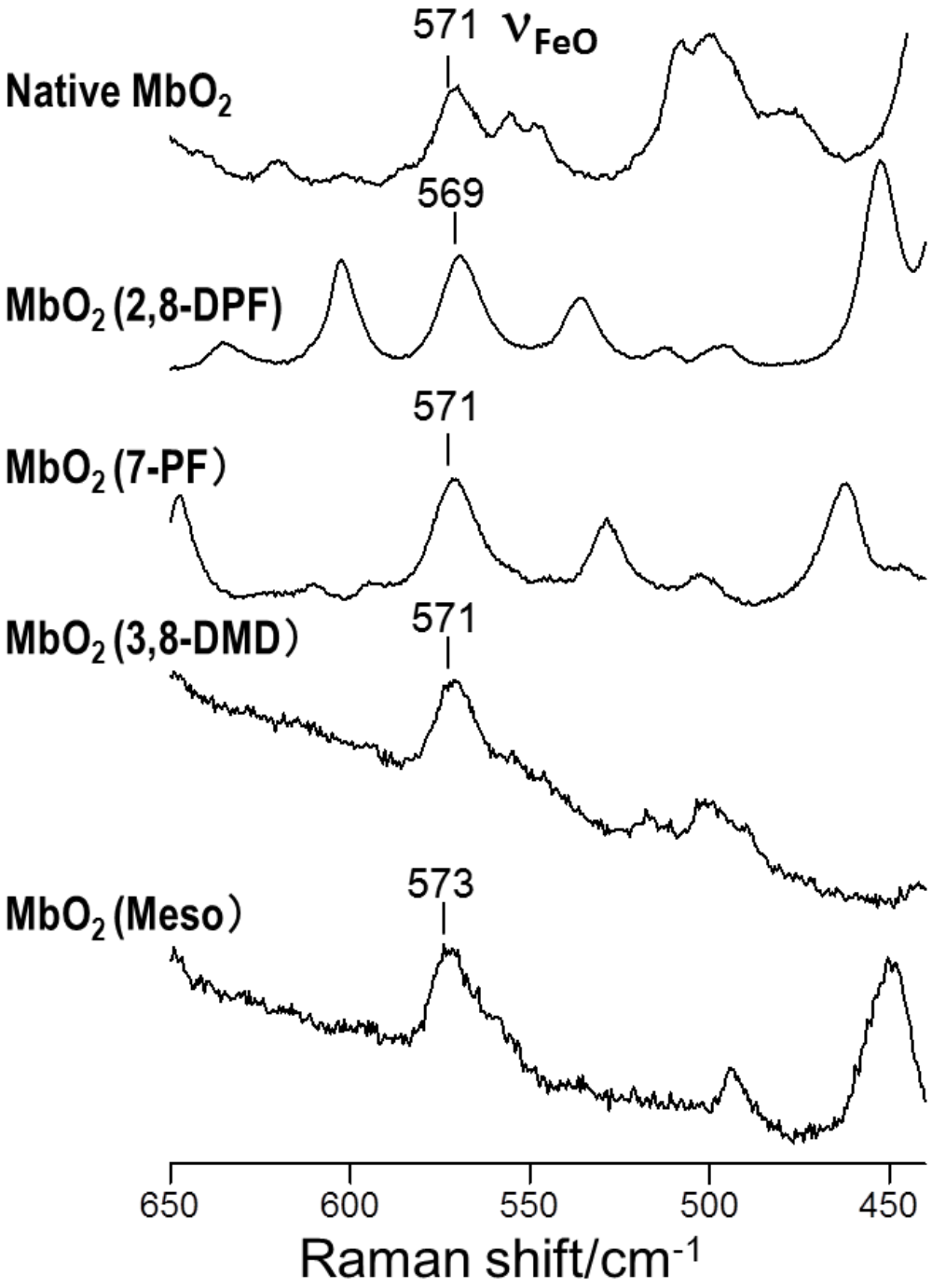

Figure 3-16. Visible resonamce raman spectra of MbO_2 s at pH 7.4 and 25°C.

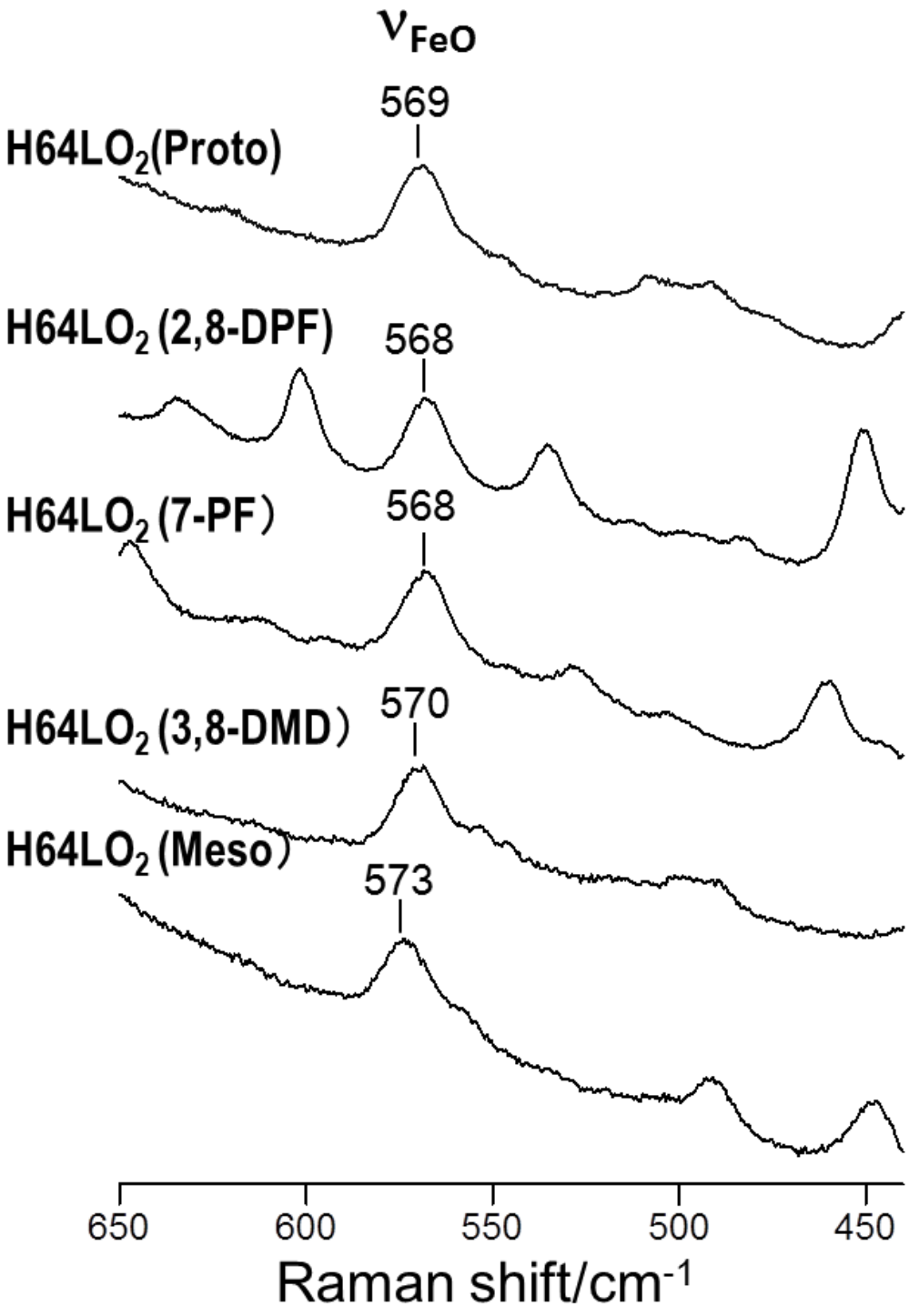

Figure 3-17. Visible resonamce raman spectra of $H64LO_2$ s at pH 7.4 and 25°C.

DISCUSSION

Effect of a change in the ρ_{Fe} value on the Fe-O bond in O_2 forms of the proteins. As shown in Table 3-2, the ρ_{FeO} value of the native protein was slightly affected by the H64L mutation. An Fe^{3+}-O_2^--like species has been expected for the Fe^{2+}-O_2 bond in O_2 form of the protein (Scheme 3-1) [21,22]. Although the resonance between the two alternative structures of the Fe-O_2 fragment is thought to be affected by the heme environment furnished by nearby amino acid residues and the heme electronic structure, the Fe-O bond order is independent of the resonance. Consequently, relatively low sensitivity of the ν_{FeO} value to replacements of amino acid residues in the heme pocket has been attributed to the fixed Fe-O bond order [27]. Comparison of the ν_{FeO} values among the mutant (or native) proteins possessing various heme cofactors demonstrated that the ν_{FeO} value decreases steadily with increasing number of CF_3 substitutions, although the differences are quite small. This result indicated that the Fe-O bond in the Fe-O_2 fragment is weakened by the CF_3 substitutions, possibly owing to the hindrance of the formation of the Fe^{3+}-O_2^--like species through obstruction of Fe-O bond polarization by decreasing the ρ_{Fe} value due to the CF_3 substitutions. This result also supported the idea proposed by Pauling [21], that the Fe-O bond strength is affected by electronic nature of the bond.

Electronic control of CO affinity of the H64L mutant protein. The k_{off}(CO) values of the mutant proteins exhibited CF_3 substitution-dependent changes such that the values of H64LCO(7-PF) and H64LCO(2,8-DPF) were ~1/4 to ~1/5 of those of the corresponding counterparts, i.e., H64LCO(Meso) and H64LCO(3,8-DMD), respectively, although their k_{on}(CO) values were similar with each other (Table 3-1). The results of the mutant proteins were different from those of the native ones demonstrating that not only the k_{on}(CO) value, but also the k_{off}(CO) one was essentially independent of the heme cofactor modifications. The heme cofactor dependent changes of the k_{off}(CO) value of the mutant protein could be interpreted in terms of the stabilities of the canonical structures of the Fe-CO fragment associated with electrostatic interaction between partial charges of the Fe-bound CO and nearby amino acid side chains (Scheme 2-1) [40,41]. The distal His64 provides positive electrostatic potential near O atom of the Fe-bound CO and, due to the electrostatic interaction between the His64 and Fe-bound CO, Structure II in Scheme 2-1 prevails structure I [25]. Therefore, the increase in the

k_{off}(CO) value by the H64L mutation could be, to some extent, attributed to a decrease in the contribution of Structure II to the stabilization of the Fe-CO bond due to the lack of positive electrostatic potential to stabilize the partial negative charge of the Fe-bound ligand. On the other hand, the decrease in the ρ_{Fe} value by the CF_3 substitution is expected to stabilize Structure I in Scheme 2-1, contributing to enhancement of the stability of the Fe-CO bond. In contrast, since the ρ_{Fe} values of H64L(Meso) and H64L(3,8-DMD) are larger than those of the other mutant proteins, the stability of Structure I in these two proteins is lower, and hence they exhibited larger k_{off}(CO) values(Table 3-1). Thus, the present results suggested that the k_{off}(CO) value of the mutant protein is determined by not only electronic environment nearby the Fe-bound ligand, but also the heme electronic structure. This interpretation was supported by the plots of the quantity log(K(CO)) against the ν_{CO} values for the mutant proteins (Figure 3-18), which could be represented by a straight line with a slope of ~0.05 ($1/cm^{-1}$). The large deviation of the plot for H64L(2,8-DPF) from the straight line could be due to its altered Fe-CO conformation as reflected in its δ_{FeCO} value.

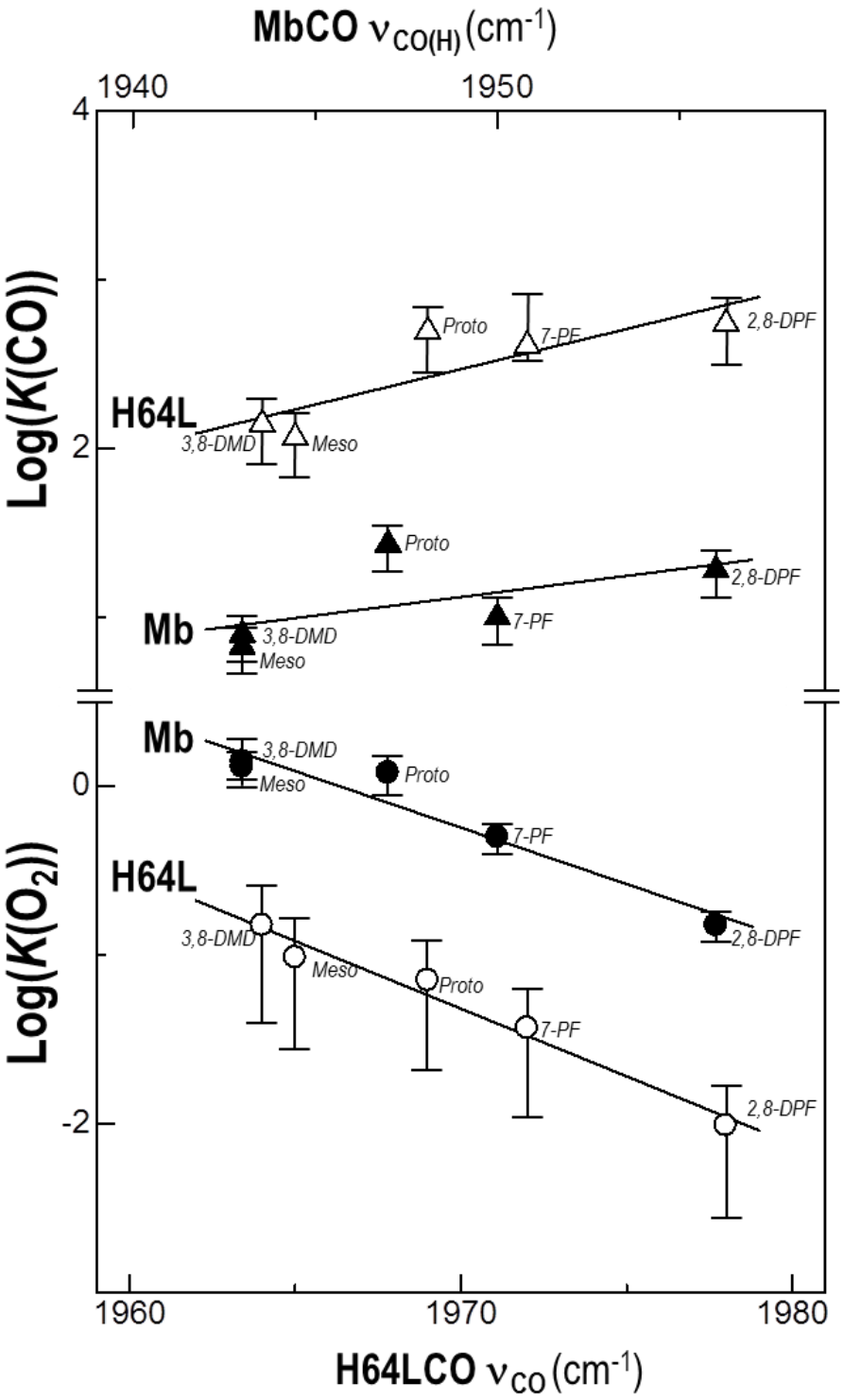

Figure 3-18. Plots of the quantity log(K(O_2)) and log(K(CO)) against the ν_{CO} and$\nu_{CO(H)}$ values for the H64L mutant and native proteins, respectively, log(K(O_2))-ν_{CO}(○), log(K(CO))-ν_{CO}(△), log(K(O_2))- $\nu_{CO(H)}$ (●), and log(K(CO))- $\nu_{CO(H)}$(▲) plots. The lower and upper horizontal axes represent the ν_{CO} and $\nu_{CO(H)}$ values for the H64L mutant and native proteins, respectively, and are graduated in such a way that the mean ν_{CO} and $\nu_{CO(H)}$ values are at the center of the axes. The best fitting straight lines were drawn for the each set of the plots. The log(K(O_2))-ν_{CO}, log(K(O_2))-$\nu_{CO(H)}$, and log(K(CO))- $\nu_{CO(H)}$ plots could be represented by straight lines with slopes of ~0.05, ~-0.08, and ~-0.08 (1/cm^{-1}), respectively. Although the log(K(CO))- $\nu_{CO(H)}$ plots also appeared to be represented by a straight line, the linear relationship between the log(K(CO)) and $\nu_{CO(H)}$ values of the protein could not be supported by the log(k_{on}(CO))- $\nu_{CO(H)}$ and log(k_{on}(CO))- $\nu_{CO(H)}$ plots.

Electronic control of O_2 affinity and autoxidation rate of the H64L mutant protein. I have shown that the O_2 affinity and autoxidation reaction of the native protein are regulated by the ρ_{Fe} value through the resonance process between the Fe^{2+}-O_2 and Fe^{3+}-O_2^--like species (Scheme 3-1) [12,14,21,22]. The O_2 binding parameters and $k_{(ox)}$ values in Table 3-1 demonstrated that the O_2 affinity and autoxidation reaction of the H64L mutant protein is also controlled in a similar manner. In order to characterize the relationship between the O_2 affinity and the ρ_{Fe} value in the mutant and native proteins, the log($K(O_2)$)-ν_{CO} plots for the two different protein systems were compared to each other in Figures 3-18－3-20. The plots of the mutant and native proteins could be represented by straight lines with slopes of ~ -0.08 (1/cm^{-1}) (Figure 3-18), suggesting that the effect of a change in the ρ_{Fe} value on the O_2 affinity is essentially independent of the removal of the distal His64, and hence the distal H-bond. Furthermore, the Mb(3,8-DMD)/Mb(2,8-DPF) and H64L(3,8-DMD)/H64L(2,8-DPF) systems exhibited the decrease in the $K(O_2)$ value by factors of ~9 and ~15, respectively, on the substation of two CF_3 groups. On the other hands, comparision between the mutant and native protein possessing identical heme cofactors indicated that the $K(O_2)$ value was decreased by a factor of ~9 to ~17 by the H64L mutation. Consequently, the decrease in the O_2 affinity of the protein through a decrease in the ρ_{Fe} value induced by the substation of two CF_3 groups was found to be almost comparable to that due to the removal of the distal His64. Additionally, the $k_{(ox)}$ value of H64L mutan decreased with decreasingρ_{Fe} value, as previously reported [13]. Thus, in addition to the heme environment furnished by the His64 [1,6], the electronic tuning of the intrinsic heme Fe reactivity through the ρ_{Fe} value was found to be a major determinant for control of the O_2 affinity and autoxidation reaction of the protein.

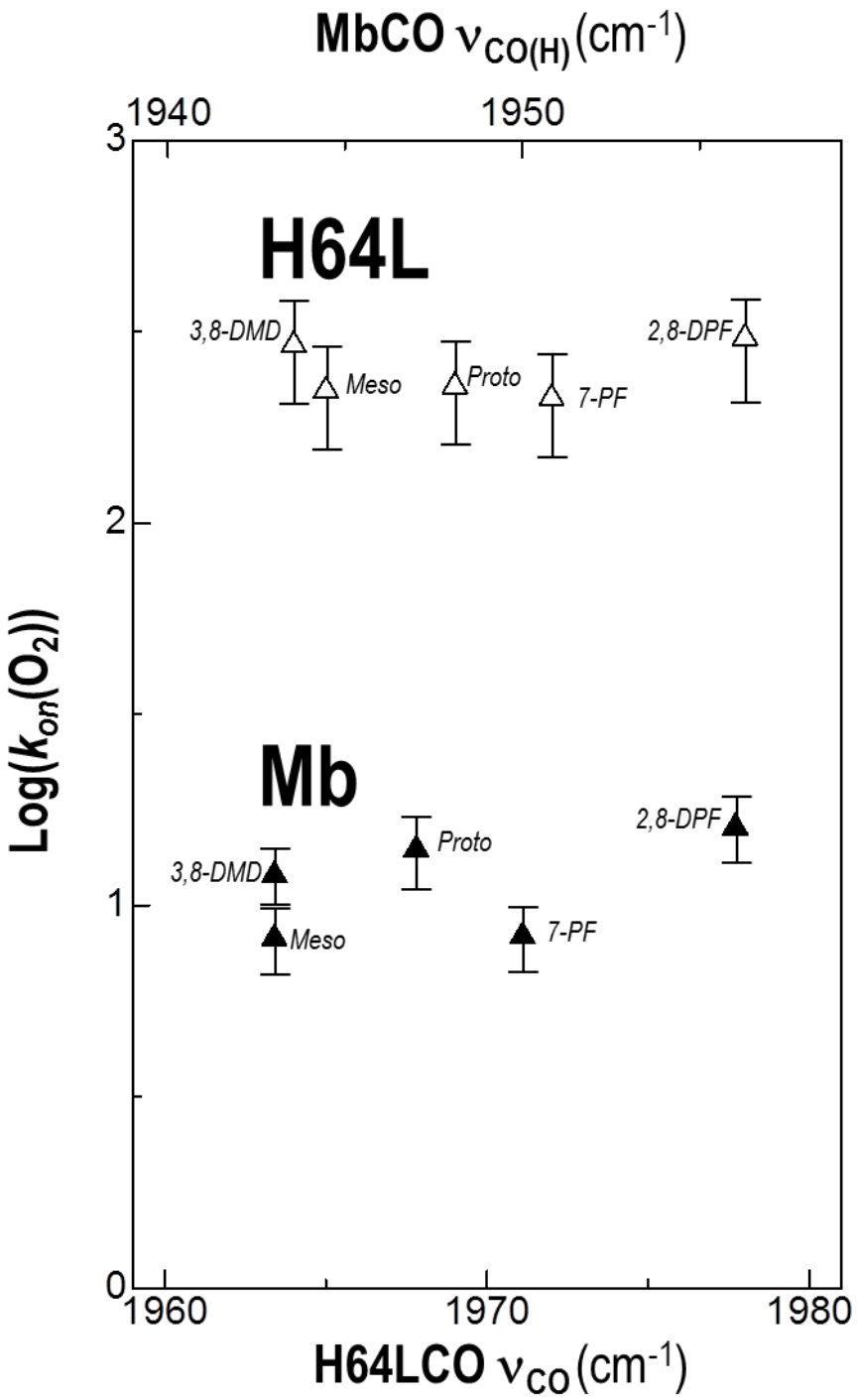

Figure 3-19. Plots of the quantity of $\log(k_{on}(O_2))$ against the ν_{CO} and $\nu_{CO(H)}$ for the H64L mutant and native proteins, respectively, $\log(k_{on}(O_2))$- ν_{CO} (△) and $\log(k_{on}(O_2))$- $\nu_{CO(H)}$ (▲) plots. The lower and upper horizontal axes represent theν_{CO} and $\nu_{CO(H)}$ values for the H64L mutant and native proteins, respectively, and are graduated in such a way that the mean ν_{CO} and $\nu_{CO(H)}$ values are at the center of the axes.

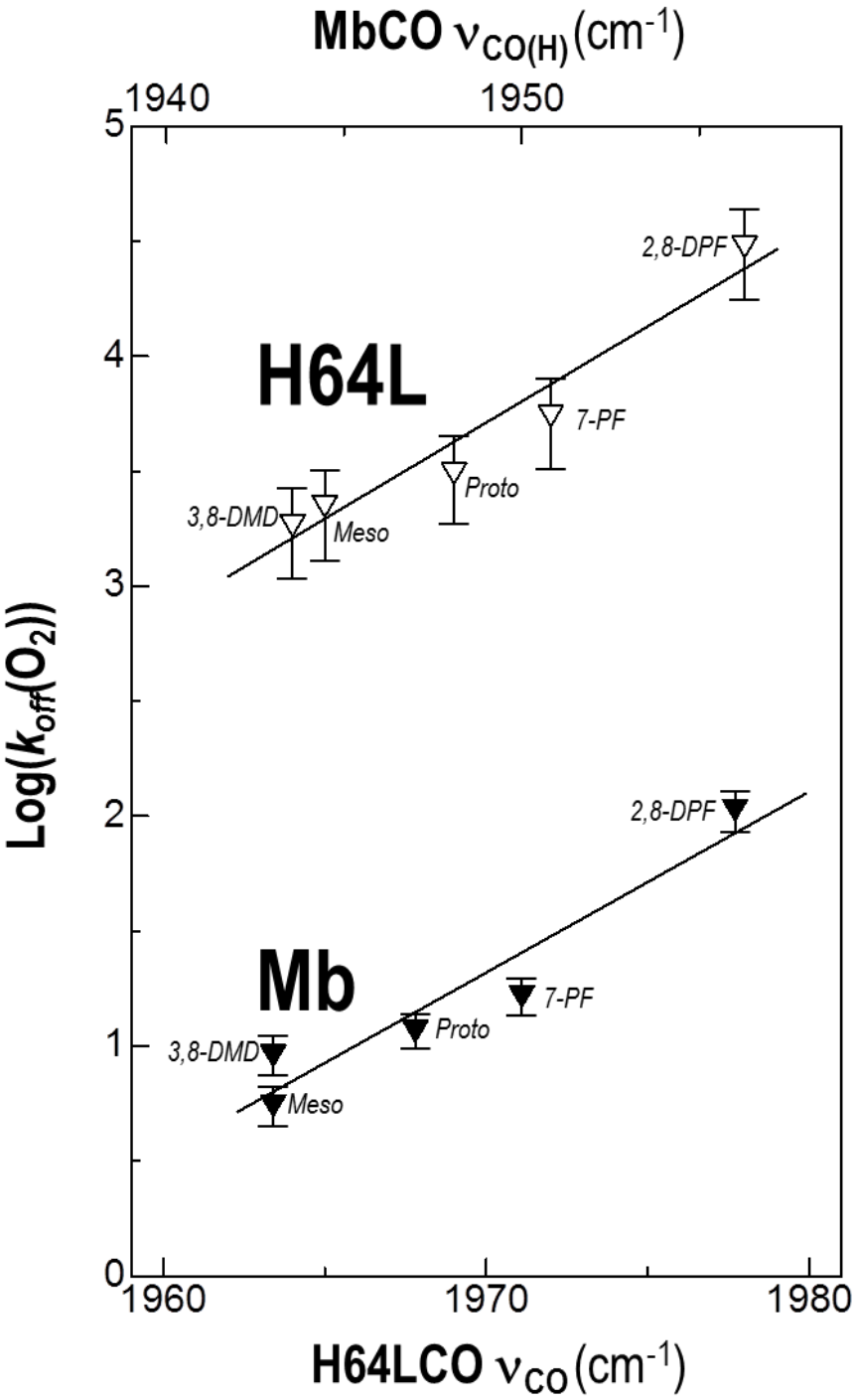

Figure 3-20. Plots of the quantity of log(k_{off}(O_2)) against the ν_{CO} and $\nu_{CO(H)}$ for the H64L mutant and native proteins, respectively, log(k_{off}(O_2))- ν_{CO} (▽) and log(k_{off}(O_2))- $\nu_{CO(H)}$ (▼) plots. The lower and upper horizontal axes represent the ν_{CO} and $\nu_{CO(H)}$ values for the H64L mutant and native proteins, respectively, and are graduated in such a way that the mean ν_{CO} and $\nu_{CO(H)}$ values are at the center of the axes. The best fitting straight lines were drawn for the each set of the plots.

Electronic control of O_2/CO discrimination in the H64L mutant protein. The *M* value of the H64L mutant protein was increased by factors of ~9 and ~60 by the substitution of one and two CF_3 groups, respectively, as revealed through analysis of the H64L(Meso)/H64L(7-PF) and H64L(3,8-DMD)/H64L(2,8-DPF) systems, respectively, whereas that of the native protein was increased by factors of only ~4 and ~25 by the substitution of one and two CF_3 groups, respectively[14]. These results demonstrated that the distal His64 drastically diminishes the effect of a change in the ρ_{Fe} value on the *M* one. The $k_{off}(O_2)$ and $k_{off}(CO)$ values of the mutant protein were increased and decreased, respectively, with a decrease in the ρ_{Fe} value, whereas both the $k_{on}(O_2)$ and $k_{on}(CO)$ ones were almost independent of the ρ_{Fe} value (Figures 3-19－3-22). Hence the remarkably large increase in the *M* values of the mutant protein induced by a decrease in the ρ_{Fe} value is due to the opposite ρ_{Fe} dependency of the O_2 and CO affinities, i.e., the former and latter decreases and increased with a decrease in the ρ_{Fe} value, respectively. Thus both the heme environment furnished by His64 and the electronic tuning of the intrinsic heme Fe reactivity through the ρ_{Fe} value contribute significantly to regulate the protein function.

Understanding the mechanisms for the O_2/CO discrimination in Mb is a problem of immense fundamental and practical importance. Respiratory proteins have to exhibit considerably small *M* values in order to perform their biological activities in the presence of low levels of CO. The *M* value of Mb(Proto), i.e., ~20 (Table 1), is ~1/1000 of those of simple heme Fe(II) model complexes, i.e., $\sim 2\times10^4$ [8,10], and the dramatic reduction of the *M* value in the protein has been interpreted in terms of the heme environment furnished by nearby amino acid residues, particularly the distal His64. The ~1000-fold decrease in the *M* value of the protein has been accounted for by a ~100-fold increase in the O_2 affinity by stabilizing Fe(II)-bound O_2 through the distal H-bond, together with ~10-fold decrease in the CO affinity possibly due to unfavorable steric interaction of Fe-bound CO with His64 and other distal residues [2]. The present study demonstrated that, even in the absence of His64, the *M* value of the protein can be regulated solely through the ρ_{Fe} value. This finding provided novel insights into mechanisms for the O_2/CO discrimination in the protein.

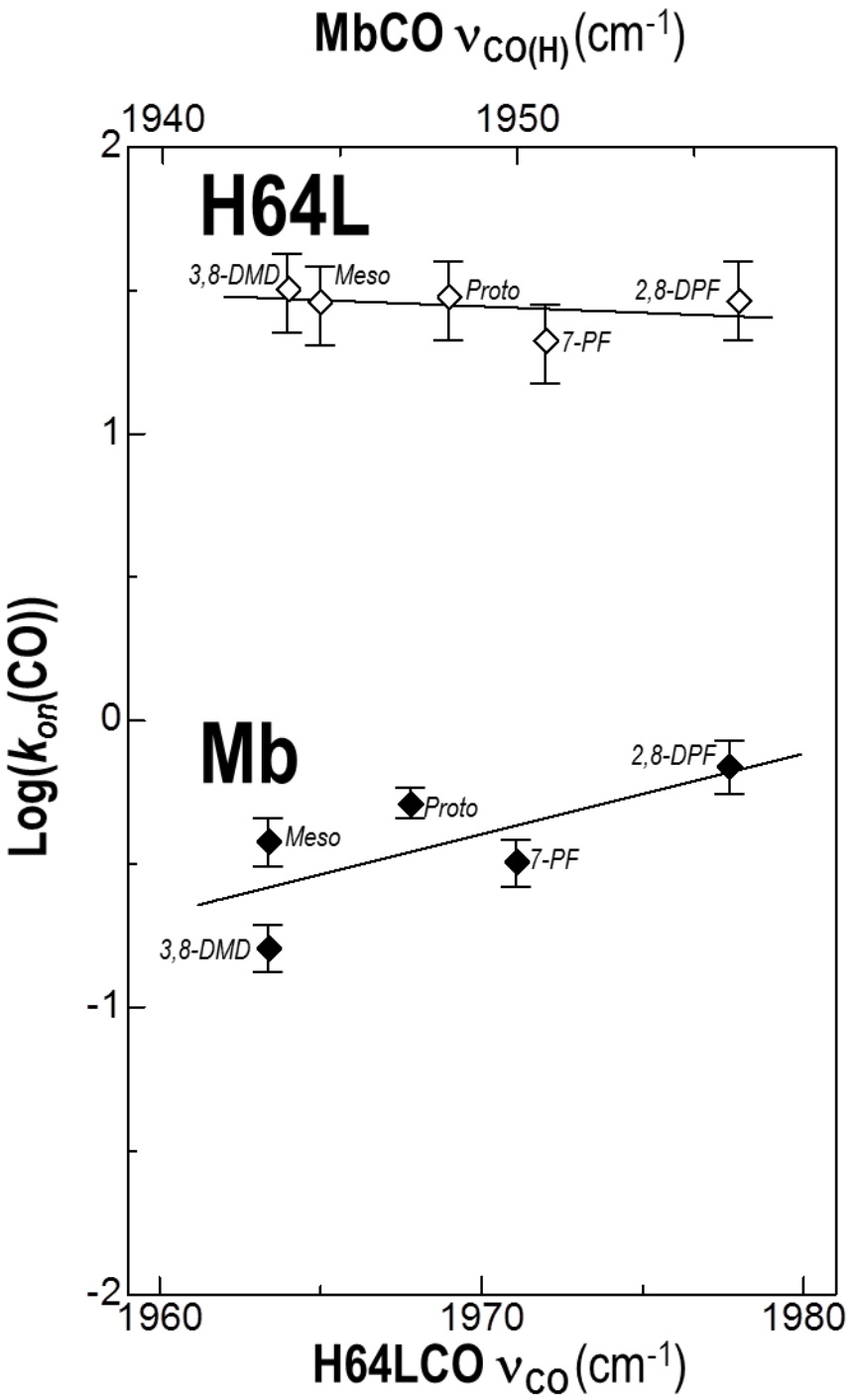

Figure 3-21. Plots of the quantity of log(k_{on}(CO)) against the ν_{CO} and $\nu_{CO(H)}$ for the H64L mutant and native proteins, respectively, log(k_{on}(CO))- ν_{CO} (◇) and log(k_{on}(CO))- $\nu_{CO(H)}$ (◆) plots. The lower and upper horizontal axes represent the ν_{CO} and $\nu_{CO(H)}$ values for the H64L mutant and native proteins, respectively, and are graduated in such a way that the mean ν_{CO} and $\nu_{CO(H)}$ values are at the center of the axes. The best fitting straight lines were drawn for the each set of the plots. Obviously, it is not appropriate to fit the log(k_{on}(CO))- $\nu_{CO(H)}$ plots as a straight line.

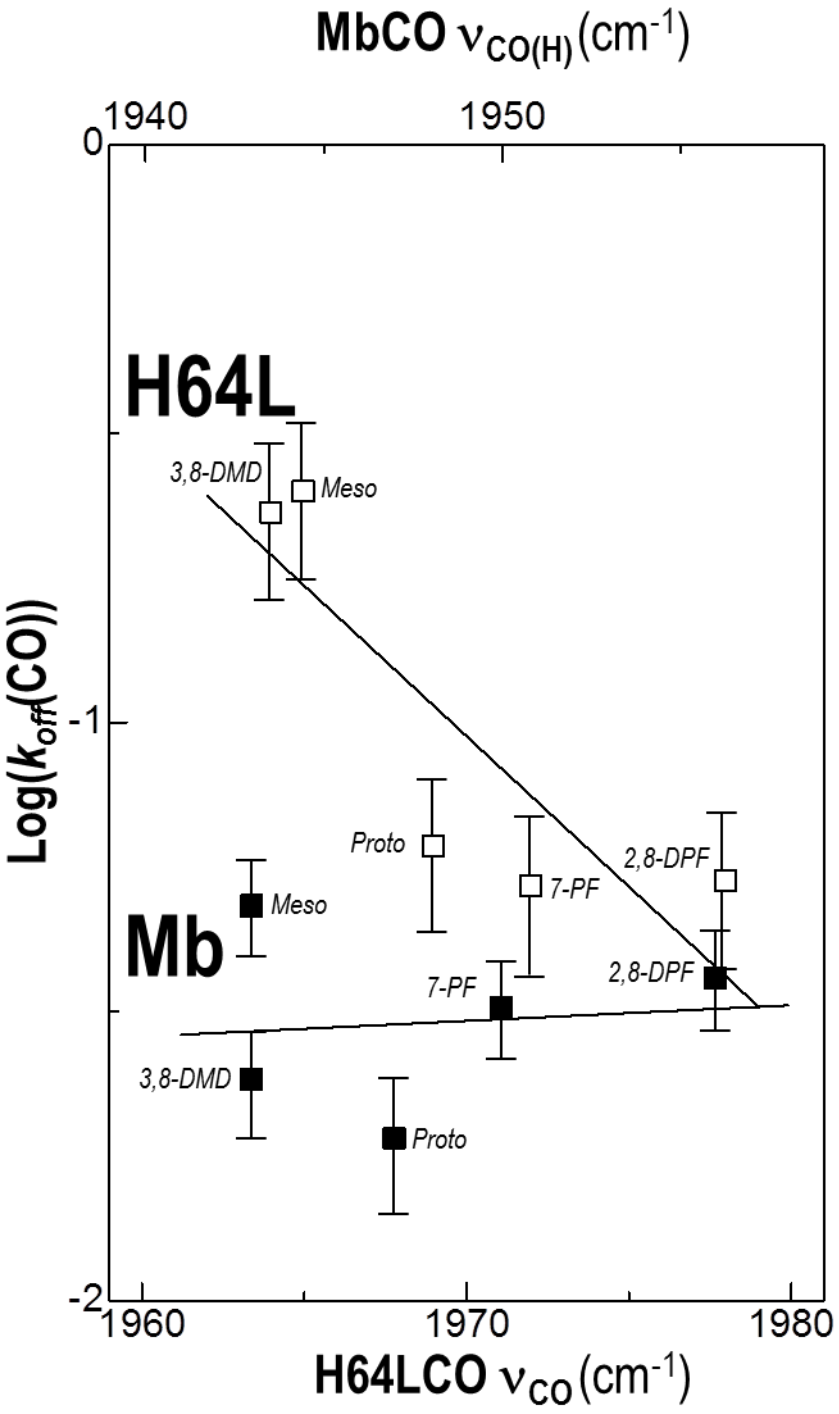

Figure 3-22. Plots of the quantity of log(k_{off}(CO)) against the ν_{CO} and $\nu_{CO(H)}$ for the H64L mutant and native proteins, respectively, log(k_{off}(CO))- ν_{CO} (□) and log(k_{off}(CO))- $\nu_{CO(H)}$ (■) plots. The lower and upper horizontal axes represent the n_{CO} and $n_{CO(H)}$ values for the H64L mutant and native proteins, respectively, and are graduated in such a way that the mean ν_{CO} and $\nu_{CO(H)}$ values are at the center of the axes. The best fitting straight lines were drawn for the each set of the plots.

CONCLUSION

As in the case of the native protein, the O_2 affinity and autoxidation reaction rate of the H64L mutant protein was found to be regulated by the ρ_{Fe} value. The O_2 affinity of the protein decreases, due to an increase in the $k_{off}(O_2)$ value, with a decrease in the ρ_{Fe} value. The autoxidation reaction rate of the protein decreases with a decrease in the ρ_{Fe} value. On the other hand, we found that the CO affinity of the H64L mutant protein increases, due to a decrease in the $k_{off}(CO)$ value, with a decrease in the ρ_{Fe} value, whereas the CO affinity of the native one was essentially independent of a change in the ρ_{Fe} value. As a result, the regulation of the O_2/CO discrimination in Mb through the heme electronic structure is largely affected by the distal His64. These results not only demonstrated that the O_2 and CO affinities of Mb lacking the distal His64 can be controlled solely by the ρ_{Fe} value, but also revealed a novel relationship between the regulations of the Mb function through the heme environment furnished by the distal His64, and electronic tuning of the intrinsic heme Fe reactivity through the ρ_{Fe} value. These findings provided crucial insights into the structure-function relationships in the protein.

References

(1) Olson, J. S.; Mathews, A. J.; Rohlfs, R. J.; Springer, B. A.; Egeberg, K. D.; Sligar, S. G.; Tame, J.; Renaud, J.-P.; Nagai, K. *Nature*, **1988**, 336, 265-266.

(2) Kachalova, G. S.; Popov, A. N.; Bartunik, H. D. *Science*, **1999**, 284, 473-476.

(3) Chu, K.; Vojtchovsky, J.; McMahon, B. H.; Sweet, R. M.; Berendzen, J.; Schlichting, I. *Nature*, **2000**, 403, 921-923.

(4) Schotte, F.; Lim, M.; Jackson, T. A.; Smirnov, A. V.; Soman, J.; Olson, J. S.; Phillips, G. N., Jr.; Wulff, M.; Anfinrud, P. A. *Science*, **2003**, 300, 1944-1947.

(5) Antonini, E.; Brunori, M. *Hemoglobins and Myoglobins and their Reactions with Ligands*; North Holland Publishing: Amsterdam, **1971**.

(6) Springer, B. A.; Egeberg, K. D.; Sligar, S. G.; Rohlfs, R. J.; Mathews, A. J.; Olson, J. S. *J. Biol. Chem.*, **1989**, 264, 3057-3060.

(7) Springer, B. A.; Sligar, S. G.; Olson, J. S.; Phillips, G. N., Jr. *Chem. Rev.*, **1994**, 94, 699-714.

(8) Olson, J. S.; Phillips, G. N., Jr. *J. Biol. Inorg. Chem.*, **1997**, 2, 544-552.

(9) Capece, L.; Marti, M. A.; Crespo, A.; Doctorvich, F.; Estrin, D. A. *J. Am. Chem. Soc.*, **2006**, 128, 12455-12461.

(10) Geoge, P.; Strantmann, C. J. *Biochem. J.*, **1954**, 57, 568-573

(11) Olson, J. S.; McKinnie, R. E.; Mims, M.P.; White, D. K. *J. Am. Chem. Soc.*, 1983, 105, 1522-1527.

(12) Shibata, T.; Nagao, S.; Fukaya, M.; Tai, H.; Nagatomo, S.; Morihashi, K.; Matsuo, T.; Hirota, S.; Suzuki, A.; Imai, K.; Yamamoto, Y. *J. Am. Chem. Soc.*, **2010**, 132, 6091-6098.

(13) Shibata, T.; Matsumoto, D.; Nishimura, R.; Tai, H.; Matsuoka, A.; Nagao, S.; Matsuo, T.; Hirota, S.; Imai, K.; Neya, S.; Suzuki, A.; Yamamoto, Y. *Inorg. Chem.*, **2012**, 51, 11955-11960.

(14) Nishimura, R.; Shibata, T.; Tai, H.; Ishigami, I.; Ogura, T.; Nagao, S.; Matsuo, T.; Hirota, S.; Imai, K.; Neya, S.; Suzuki, A.; Yamamoto, Y. *Inorg. Chem.*, **2013**, 52, 3349-3355.

(15) Phillips, S. E. V.; Schoenborn, B. P. *Nature*, **1981**, 292, 81-82.

(16) Kitagawa, T.; Ondrias, M. R.; Rousseau, D. L.; Ikeda-Saito, M.; Yonetani, T. *Nature*, **1982**, 298, 869-871.

(17) Lukin, J. A.; Simplaceanu, V.; Zou, M.; Ho, N. T.; Ho, C. *Proc. Natl. Acad. Sci. U.S.A.*, **2000**, 97, 10354-10358.

(18) Chang, C. K.; Ward, B.; Ebina, S. *Arch. Biochem. Biophys.*, **1984**, 231, 366-371.

(19) Neya, S.; Suzuki, M.; Hoshino, T.; Ode, H.; Imai, K.; Komatsu, T.; Ikezaki, A.; Nakamura, M.; Furutani, Y.; Kandori, H. *Biochemistry*, **2010**, 49, 5642-5650.

(20) Toi, H.; Homma, M.; Suzuki, A.; Ogoshi, H. *J. Chem. Soc., Chem. Commun.*, **1985**, 1791–1792.

(21) Pauling, L. *Nature*, **1964**, 203, 182-183.

(22) Maxwell, J. C.; Volpe, J. A.; Barlow, C. H.; Caughey, W. S. *Biochem. Biophys. Res. Commun.*, **1974**, 58, 166-171.

(23) Quillin, M. L.; Arduini, R. M.; Olson, J. S.; Phillips, G. N., Jr. *J. Mol. Biol.*, **1993**, 234, 140-155.

(24) Sakan, Y.; Ogura, T. ; Kitagawa, T. ; Fraunfelter, F. A. ; Mattera, R. ; Ikeda-Saito, M. *Biochemistry*, **1993**, 32, 5815-5824.

(25) Li, T.; Quillin, M. L.; Phillips, G. N., Jr.; Olson, J. S. *Biochemistry*, **1994**, 33, 1433-1446.

(26) Anderton, C. L.; Hester, R. E.; Moore, J. N. *Biochim. Biophys. Acta*, **1997**, 1338, 107-120.

(27) Hirota, S.; Li, T.; Phillips, G. N., Jr.; Olson, J. S.; Mukai, M.; Kitagawa, T. *J. Am. Chem. Soc.*, **1996**, 118, 7845-7846.

(28) Birukou, I.; Schweers, R. L.; Olson, J. S. *J. Biol. Chem.*, **2010**, 285, 8840-8854.

(29) Teale, F. W. J. *Biochim. Biophys. Acta*, **1959**, 35, 543.

(30) Imai, K. *Methods Enzymol*., **1981**, 76, 438-449.

(31) Imai, K. *Methods Enzymol*., **1981**, 76, 470-486.

(32) Olson, J. S. *Method. Enzymol.*, **1981**, 76, 631-651.

(33) Rohlfs, R. J.; Mathews, A. J.; Carver, T. E.; Olson, J. S.; Springer, B. A.; Egeberg, K. D.; Sliger, S. G. *J. Biol. Chem.*, **1990**, 265, 3168-3176.

(34) Hayashi, T.; Dejima, H.; Matsuo, T.; Sato, H.; Murata, D.; Hisaeda, Y. *J. Am. Chem. Soc.*, **2002**, 124, 11226-11227.

(35) Matsuo, T.; Dejima, H.; Hirota, S.; Murata, D.; Sato, H.; Ikegami, T.; Hori, H.; Hisaeda, Y.; Hayashi, T. *J. Am. Chem. Soc.*, **2004**, 126, 16007-16017.

(36) Matsuo, T.; Ikegami, T.; Sato, H.; Hisaeda, Y.; Hayashi, T. *J. Inorg. Biochem*., **2006**, 100, 1265-1271.

(37) Kitanishi, K.; Kobayashi, K.; Kawamura, Y.; Ishigami, I.; Ogura, T.; Nakajima, K.; Igarashi, J.; Tanaka, A.; Shimizu, T. *Biochemistry*, **2010**, 49, 10381-10393.

(38) Reilly, J. T.; Walsh, J. M.; Greenfield, M. L.; Donohue, M. D. *Spectrochim. Acta*, **1992**, 48A, 1459-1479.

(39) Suzuki, T.; Watanabe, Y.; Nagasawa, M., Matsuoka, A. Shikama, K. *Eur. J. Biochem*., **2000**, 267, 6166-6174.

(40) Alben J. O.; Caughey, W. S. *Biochemistry*, **1968**, 7, 175-183.

(41) Li, X.-Y.; Spiro, T. G. *J. Am. Chem. Soc.*, **1988**, 110, 6024-6033.

Chapter 4

Control of O_2 vs CO binding preference of myoglobin

Abstract

The L29F mutant of myoglobin (Mb), where the Leu29 residue was replaced by phenylalanine(Phe), was shown to exhibit remarkably high affinity to oxygen (O_2), possibly due to stabilization of the heme Fe atom-bound O_2 in the mutant protein through a proposed unique electrostatic interaction with the introduced Phe29, in addition to well-known hydrogen bonding with His64 [Carver, T. E.; Brantley, R. E.; Singleton, E. W.; Arduini,R. M.; Quillin, M. L.; Phillips, G. N., Jr.; Olson, J. S. J. Biol.Chem., 1992, 267, 14443−14450]. I analyzed the O_2 and carbon monoxide (CO) binding properties of the L29F mutant protein reconstituted with chemically modified heme cofactors possessing a heme Fe atom with various electron densities, to determine the effect of a change in the electron density of the heme Fe atom (ρ_{Fe}) on the O_2 versus CO discrimination. This study demonstrated that the preferential binding of O_2 over CO by the protein was achieved through increasing ρ_{Fe}, and the ordinary ligand-binding preference, that is, the preferential binding of CO over O_2, by the protein was achieved through decreasing ρ_{Fe}. Thus, the O_2 and CO binding preferences of the L29F mutant protein could be controlled through electronic modulation of intrinsic heme Fe reactivity through a change in ρ_{Fe}. The present study highlighted the significance of the tuning of the intrinsic heme Fe reactivity through the heme electronic structure in functional regulation of Mb.

INTRODUCTION

Myoglobin (Mb) is a hemoprotein found in muscle cells, where it is responsible for the storage of dioxygen (O_2) in energy metabolism [1]. In addition to O_2, carbon monoxide (CO) is also reversibly bound to a ferrous heme Fe atom (Fe(II)) in Mb. As an O_2 storage protein, Mb must discriminate O_2 against the toxic ligand CO ubiquitously produced from a variety of sources in biological systems [2]. The ligand binding affinity of unencumbered model heme Fe(II) complexes is ~2×10^4 times higher for CO than for O_2, but this ratio is considerably reduced in the proteins [3,4]. Ever since the three-dimensional structure of Mb was determined as the first protein crystal structure [5], the elucidation of the mechanism responsible for the discrimination between O_2 and CO has attracted many researchers' interest [1-4,6,7]. Distal histidine residue (His64) has been shown to play a central role in the control of O_2 versus CO binding in Mb [1-4,6,7]. His64 forms a hydrogen bond with Fe(II)-bound ligand to stabilize its bound state[8-15], and the hydrogen bond is formed more favorably with Fe(II)-bound O_2 than with Fe(II)-bound CO[16,17]. I found that the O_2 affinity of Mb is largely affected by electron density of the heme Fe atom (ρ_{Fe}), whereas the CO one is almost independent of the ρ_{Fe} value.[18,19] Thus, even in the absence of His64, the O_2 versus CO discrimination of the protein can be controlled by electronic tuning of the intrinsic heme Fe reactivity through the ρ_{Fe} value.

In this study, I attempted to control the O_2 versus CO ligand binding preference in the L29F mutant protein, where Leu29 residue is replaced by Phe, through altering the ρ_{Fe} value. The L29F mutant protein exhibits the O_2 affinity almost as high as the CO one [20,21]. The X-ray crystallographic study of the L29F mutant revealed that, in addition to the above-mentioned hydrogen bonding with His64, the coordination of O_2 to Fe(II) in the mutant is also stabilized by a favorable electrostatic interaction of the polar Fe(II)-bound O_2 with the multipole of the phenyl ring of the introduced Phe29 [20]. Due to the aids of both His64 and Phe29, the rate constant for O_2 dissociation ($k_{off}(O_2)$) of the L29F mutant was decreased by a factor of ~1/8 compared with that of the native Mb[20]. In addition, the rate constant for O_2 association ($k_{on}(O_2)$) of the mutant protein was larger by a factor of ~2 than that of the native Mb, whereas the rate constants for CO association and dissociation (k_{on}(CO) and k_{off}(CO), respectively) of the mutant protein were similar to those of the native one [20].

The strategy is based on the previous findings that the $k_{off}(O_2)$ value increases (decreases) with

decreasing (increasing) the ρ_{Fe} one, whereas the other kinetic values, i.e., the $k_{on}(O_2)$, $k_{on}(CO)$, and $k_{off}(CO)$ ones, were essentially independent of the ρ_{Fe} one [18,19]. The relationship between the ρ_{Fe} and $k_{off}(O_2)$ values could be interpreted in terms of the effect of a change in the ρ_{Fe} value on the resonance process between the Fe^{2+}-O_2 and Fe^{3+}-O_2^--like species (Scheme 3-1) [8,22], and, for example, a decrease in the ρ_{Fe} value stabilizes the Fe^{2+}-O_2 species over the Fe^{3+}-O_2^--like one, resulting in an increase in the $k_{off}(O_2)$ one. In order to largely alter the ρ_{Fe}, I substituted strongly electron-withdrawing trifluoromethyl(CF_3) group(s), as side chain(s) of heme cofactor, to prepare 13,17-bis(2-carboxylatoethyl)-3,8-diethyl-2,12,18-trimethyl-7-trifluoromethylporphyrinatoiron(III) (7-PF) [23] and 13,17-bis(2-carboxylatoethyl)-3,7-diethyl-12,18-trimethyl-2,8-ditrifluoromethylporphyrinato -iron(III)(2,8-DPF) [18] (Figure 2-2). In addition, mesoheme(Meso) and 3,8-dimethyldeuteroporphyrinato -iron(III)(3,8-DMD) [24,25] were used as counterparts of 7-PF and 2,8-DPF, respectively. Apoprotein of the L29F mutant protein was reconstituted with Meso, 3,8-DMD, 7-PF, and 2,8-DPF to yield the mutant proteins possessing the corresponding heme cofactors, i.e., L29F(Meso), L29F(3,8-DMD), L29F(7-PF), and L29F(2,8-DPF), respectively. Pairwise comparison between L29F(Meso) and L29F(7-PF), and between L29F(3,8-DMD) and L29F(2,8-DPF) provides the structural and functional consequences of the substitution of one and two CF_3 groups, respectively. As expected from the previous findings, the preferential binding of O_2 over CO was observed in L29F(Meso) and L29F(3,8-DMD), whereas L29F(7-PF) and L29F(2,8-DPF) exhibited the ordinary ligand binding preference. Thus the O_2 versus CO ligand binding preference in the L29F mutant protein could be controlled through a change in the ρ_{Fe} value. These findings confirmed the significant effect of a change in the heme electronic structure on Mb function.

MATERIALS AND METHODS

Materials and protein samples. All reagents and chemicals were obtained from commercial sources and used as received. The expression and purification of the L29F mutant protein (L29F(Proto)) were carried out according to the methods described by Carver et al.[20] Mesoheme (Meso) was purchased from Frontier Scientific Co. 2,8-DPF [18], 7-PF[23], and 3,8-DMD[24,25] were synthesized as previously described. The apoprotein of the L29F mutant protein was prepared at 4 °C according to the procedure of Teale [26], and reconstituted L29F mutant proteins were prepared by slow addition of a synthetic heme cofactor to the apoprotein in 50 mM potassium phosphate buffer, pH 7.0, at 4 °C [18]. In order to prepare the CO and O_2 forms of the L29F mutant proteins, the proteins were reduced by adding $Na_2S_2O_4$ (Nakalai Chemicals Ltd.) in the presence of CO gas (Japan Air Gases) and in the air, respectively. Excess agent was removed by passage through a Sephadex G-10 (Sigma-Aldrich Co.) column equilibrated with an appropriate buffer solution. The pH of each sample was measured with a Horiba F-22 pH meter equipped with a Horiba type 6069-10c electrode. The pH of a sample was adjusted using 0.1 M NaOH or HCl.

Kinetic measurements of O_2 and CO binding. Kinetic measurements of the proteins were carried out in 100 mM phosphate buffer, pH 7.40, at 20 °C using the procedure reported previously [1,27-29]. The O_2 associations for L29F(Proto), L29F(Meso), L29F(3,8-DMD), L29F(7-PF), and L29F(2,8-DPF) were characterized through analysis of the time evolution of the absorbance at 404, 410, 400, 397,410 nm, respectively, after photolysis of their oxy forms, in the presence of various O_2 concentrations ($[O_2]$), using a 5 ns-pulse Nd-YAG laser (532 nm, Continuum Surelite Ⅱ). The probe light (Xe-lamp) was passed through a monochrometer before a sample with adjusting a suitable wavelength in each experiment. The fitting of the time evolution of the absorbance to the first-order rate equation yielded a pseudo first-order rate constant for O_2 association ($k_{obs}(O_2)$), which can be expressed in terms of $k_{on}(O_2)$ and $k_{off}(O_2)$ as $k_{obs}(O_2) = k_{on}(O_2) \times [O_2] + k_{off}(O_2)$. Since $k_{off}(O_2) \ll k_{on}(O_2) \times [O2]$, $k_{on}(O_2)$ can be determined from the pseudo-first-order rate constant for O_2 association($k_{obs}(O_2)$) through the equation $k_{obs}(O_2) = k_{on}(O_2) \times [O_2]$, where $[O_2] = 2.52\times10^{-4}$ M. Pseudo-first-order rate constants for O_2 dissociation ($k_{off}(O_2)$) for L29F(Proto), L29F(Meso), L29F(3,8-DMD), L29F(7-PF), and

L29F(2,8-DPF) were also measured through the analysis of the time evolution of the absorbance at 570, 565, 567, 564, and 560 nm, respectively, after rapidly mixing their oxy forms with excess sodium dithionite using a stopped-flow apparatus.

The CO associations for L29F(Proto), L29F(Meso), L29F(3,8-DMD), L29F(7-PF), and L29F(2,8-DPF) were similarly measured through analysis of the time evolution of the absorbance at 420, 410, 410, 409, and 415 nm, respectively, after the photolysis of their CO forms under 1 atm of CO, i.e., $[CO] = 9.85 \times 10^{-4}$ M. Since $k_{off}(CO) << k_{on}(CO) \times [CO]$, the $k_{on}(CO)$ value can be determined from the pseudo first-order rate constant for CO association ($k_{obs}(CO)$) through the equation, $k_{obs}(CO) = k_{on}(CO) \times [CO]$.

The CO dissociation for the mutant proteins was characterized utilizing the following reactions which consist of the displacement of Fe-bound CO and the oxidation of heme iron by $K_3Fe(CN)_6$ [27,29],

$$Mb_{Fe(II)}(CO) \underset{k_{on}(CO)}{\overset{k_{off}(CO)}{\rightleftharpoons}} Mb_{Fe(II)} + CO \xrightarrow{k_{ox}} Mb_{Fe(III)}(H_2O)$$

where $Mb_{Fe(II)}$ and $Mb_{Fe(III)}(H_2O)$ represent the deoxy and met-aquo forms of the protein, respectively, and k_{ox} the rate constant for the oxidation of the heme iron. Under the experimental conditions of high [CO] and $[K_3Fe(CN)_6]$, where a steady-state assumption can be made for $[Mb_{Fe(II)}]$, a pseudo first-order rate constant for the oxidation of the proteins ($k_{obs}(ox)$) can be expressed in terms of a pseudo first-order rate constant for CO dissociation (k_{off} (CO)), $[K_3Fe(CN)_6]$, and a constant, c, as $k_{obs}(ox) = k_{off}(CO) \times [K_3Fe(CN)_6] / (c + [K_3Fe(CN)_6])$. The saturated value in plots of the $k_{obs}(ox)$ values against $[K_3Fe(CN)_6]$ affords the k_{off} (CO) value. The $k_{obs}(ox)$ values for L29F(Proto), L29F(Meso), L29F(3,8-DMD), L29F(7-PF), and L29F(2,8-DPF) in various $[K_3Fe(CN)_6]$ were determined through analysis of the time evolution of the absorbance at 530, 519, 520, 523, and 525 nm, respectively. The probe light (Xe-lamp) was passed through a monochrometer before a sample with adjusting a suitable wavelength in each experiment. Prior to kinetic measurements, it was confirmed in preliminary experiments using a photo diode array detector that the reaction of a ligand-bound Mb with $K_3Fe(CN)_6$ really yielded the corresponding met-aquo form without accumulation of any intermediates.

Resonance raman spectroscopy. Resonance raman scattering was performed with excitation at 413.1 nm with a Kr^+ laser (Spectra Physics, BeamLok 2060), dispersed with a polychromator (SPEX 1877, 1200 grooves/mm grating), and detected with a liquid nitrogen-cooled charge coupled device (CCD) detector (CCD-1024×256-OPEN-1LS; HORIBA Jobin Yvon) [30]. The protein concentrations were approximately 40 μM in 100 mM potassium phosphate buffer, pH 7.4. Raman shifts were calibrated with indene as a frequency standard. The positions of the bands were determined through fitting with Voigt profiles, which are convolutions of Gaussian and Lorentzian functions [31], and the accuracy of the peak positions of well-defined Raman bands was ±1 cm^{-1}.

RESULTS

Effects of heme cofactor modifications on functional properties of the L29F mutant protein. The kinetic parameters of mutant proteins were determined (Table 4-1 and Figures 4-1－4-4). The kinetic parameters obtained for L29F(Proto) agreed well with those reported previously[20], except the $k_{off}(CO)$ value which was larger by a factor of ~3 compared with the previous one. L29F(Meso) and L29F(3,8-DMD) exhibited the $k_{off}(O_2)$ values smaller by a factor of ~1/2 relative to that of L29F(Proto), that is, 0.78 ± 0.2 s^{-1} and 0.8 ± 0.2 s^{-1} for L29F(Meso) and L29F(3,8-DMD), respectively, whereas the other kinetic values, i.e., the $k_{on}(O_2)$, $k_{on}(CO)$, and $k_{off}(CO)$ ones, of L29F(Meso) and L29F(3,8-DMD) were similar to the corresponding ones of L29F(Proto). As a result, the O_2 affinities, i.e., the $K(O_2)$ values, of L29F(Meso) and L29F(3,8-DMD) were increased by a factor of ~2, relative to that of L29F(Proto), that is 27 ± 8 μM^{-1} and 31 ± 9μM^{-1} for L29F(Meso) and L29F(3,8-DMD), respectively, and hence the O_2 affinities of these mutant proteins were higher than the CO ones of the corresponding proteins (Table 4-1). Thus, the preferential binding of O_2 over CO in the mutant protein could be achieved through a change in the ρ_{Fe} value. On the other hand, the O_2 affinities of L29F(7-PF) and L29F(2,8-DPF) were considerably lower than that of L29F(Proto) due to the dramatic increases in the $k_{off}(O_2)$ value upon CF_3 substitution(s) (Table 4-1). The O_2 affinity of the mutant protein was lowered by a factor of ~1/5 on the substitution of one CF_3 group, as demonstrated for the L29F(Meso)/L29F(7-PF) system, that is, the $K(O_2)$ values of L29F(Meso) and L29F(7-PF) were 27 ± 8 μM^{-1} and 5.8 ± 2 μM^{-1}, respectively, and then by a factor of ~1/18 on the substitution of two CF_3

ones, as revealed on analysis of the L29F(3,8-DMD)/L29F(2,8-DPF) system, i.e., the $K(O_2)$ values of L29F(3,8-DMD) and L29F(2,8-DPF) were 31 ± 9 μM^{-1} and 1.7 ± 0.5 μM^{-1}, respectively. In contrast to the O_2 binding, the CO affinity of the mutant protein was essentially independent of the CF_3 substitutions.

Table 4-1. O_2 and CO Binding Parameters for the L29F mutant proteins, native Mbs, and the H64L mutant proteins at pH 7.40 and 25 °C

Heme	Protein	O_2 binding			CO binding			M[b]
		$k_{on}(O_2)$ ($\mu M^{-1}s^{-1}$)	$k_{off}(O_2)$ (s^{-1})	$K(O_2)$ (μM^{-1})	$k_{on}(CO)$ ($\mu M^{-1}s^{-1}$)	$k_{off}(CO)$ (s^{-1})	$K(CO)$ (μM^{-1})	
Meso	L29F	21 ± 4.2	0.78 ± 0.16	27 ± 7.6	0.19 ± 0.038	0.013 ± 0.0026	15 ± 4.2	0.56 ± 0.22
	Mb[b]	8.2 ± 1.6	5.7 ± 1.1	1.5 ± 0.4	0.38 ± 0.07	0.048 ± 0.009	7.9 ± 2.4	5.5 ± 2.2
	H64L[c]	222 ± 67	2300 ± 970	0.097 ± 0.069	29 ± 8.7	0.25 ± 0.075	116 ± 48.7	1200 ± 990
3,8-DMD	L29F	25 ± 5.0	0.80 ± 0.16	31 ± 8.7	0.21 ± 0.042	0.012 ± 0.0024	18 ± 5.0	0.58 ± 0.23
	Mb[d]	12 ± 3	9.7 ± 3	1.3 ± 0.3	0.16 ± 0.07	0.024 ± 0.007	6.7 ± 1.7	5.1 ± 2.1
	H64L[c]	292 ± 88	1900 ± 800	0.15 ± 0.11	32 ± 9.6	0.23 ± 0.069	139 ± 58.4	930 ± 770
7-PF	L29F	22 ± 4.4	3.8 ± 0.76	5.8 ± 1.6	0.38 ± 0.076	0.014 ± 0.0028[e]	27 ± 7.6	4.7 ± 1.9
	Mb[b]	8.3 ± 1.6	17 ± 3	0.5 ± 0.1	0.32 ± 0.06	0.032 ± 0.006	10 ± 3	21 ± 8
	H64L[c]	212 ± 64	5700 ± 2400	0.037 ± 0.026	21 ± 6.3	0.052 ± 0.016[f]	580 ± 244	11000 ± 9100
2,8-DPF	L29F	31 ± 6.2	18 ± 3.6	1.7 ± 0.48	0.33 ± 0.066	0.017 ± 0.0034	19 ± 6.3	11 ± 4.4
	Mb[b]	16 ± 3	110 ± 22	0.15 ± 0.03	0.69 ± 0.13	0.036 ± 0.007	19 ± 6	132 ± 53
	H64L[c]	305 ± 92	31000 ± 13000	0.0098 ± 0.007	29 ± 8.7	0.053 ± 0.016	547 ± 230	56000 ± 46000
Proto	L29F	26 ± 5.2	1.5 ± 0.30	17 ± 4.8	0.23 ± 0.046	0.016 ± 0.0032	14 ± 5.3	0.82 ± 0.33
	Mb[b]	14 ± 3	12 ± 2	1.2 ± 0.3	0.51 ± 0.06	0.019 ± 0.005	27 ± 8	23 ± 9
	H64L[c]	228 ± 68	3200 ± 1300	0.071 ± 0.05	30 ± 9.0	0.061 ± 0.018	492 ± 207	6900 ± 5700

a: M represents the quantity $K(CO)/K(O_2)$.
b: Taken from ref. 18.
c: Taken from ref. 41.
d: Taken from ref. 19.
e: Calculated from a weight average of fitted parameters because the time course was biphasic, and sum of two exponentials provided better fits to the data.
f: Biphasic time evolution of CO association was fitted by a sum of two exponentials, and the value closer to those of the other H64L mutant proteins is indicated, and the other one was 5.69 ± 1.7.

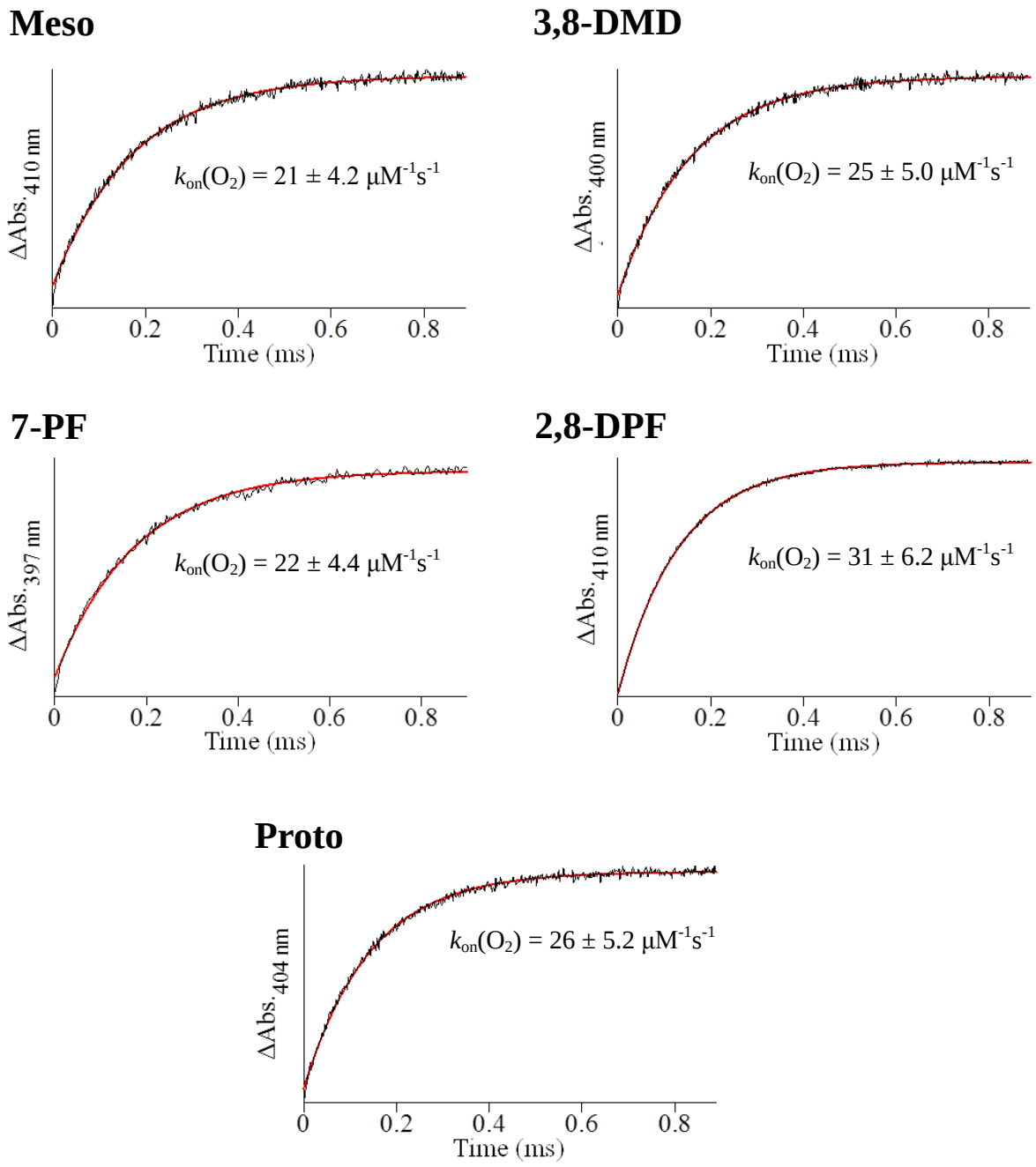

Figure 4-1. Time evolution of absorbance change (*ΔAbs.*), at the indicated wavelength (nm), after photolysis of O_2 forms of the L29F mutant proteins possessing the indicated heme cofactors, in 100 mM potassium phosphate buffer, pH 7.40, at 25°C. The $k_{on}(O_2)$ value was determined through fitting the time evolution with the assumption of first-order kinetics, indicated in red.

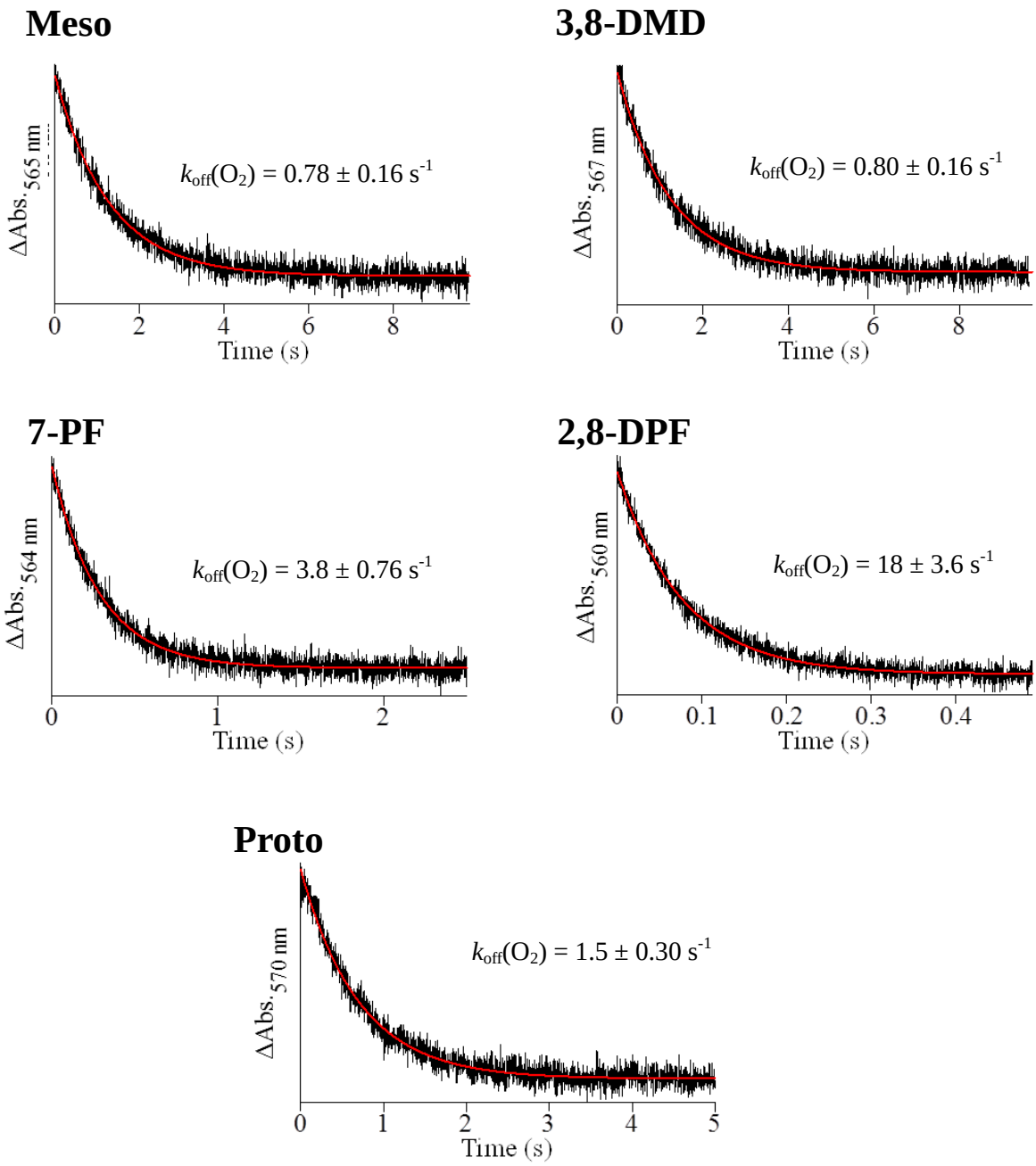

Figure 4-2. Time evolution of absorbance change (*ΔAbs.*), at the indicated wavelength (nm), after mixing O_2 forms of the L29F mutant proteins possessing the indicated heme cofactors, in 100 mM potassium phosphate buffer, pH 7.40, and 5 mM sodium dithionite at 25 °C. The $k_{off}(O_2)$ value was determined through fitting with the assumption of first-order kinetics, indicated in red.

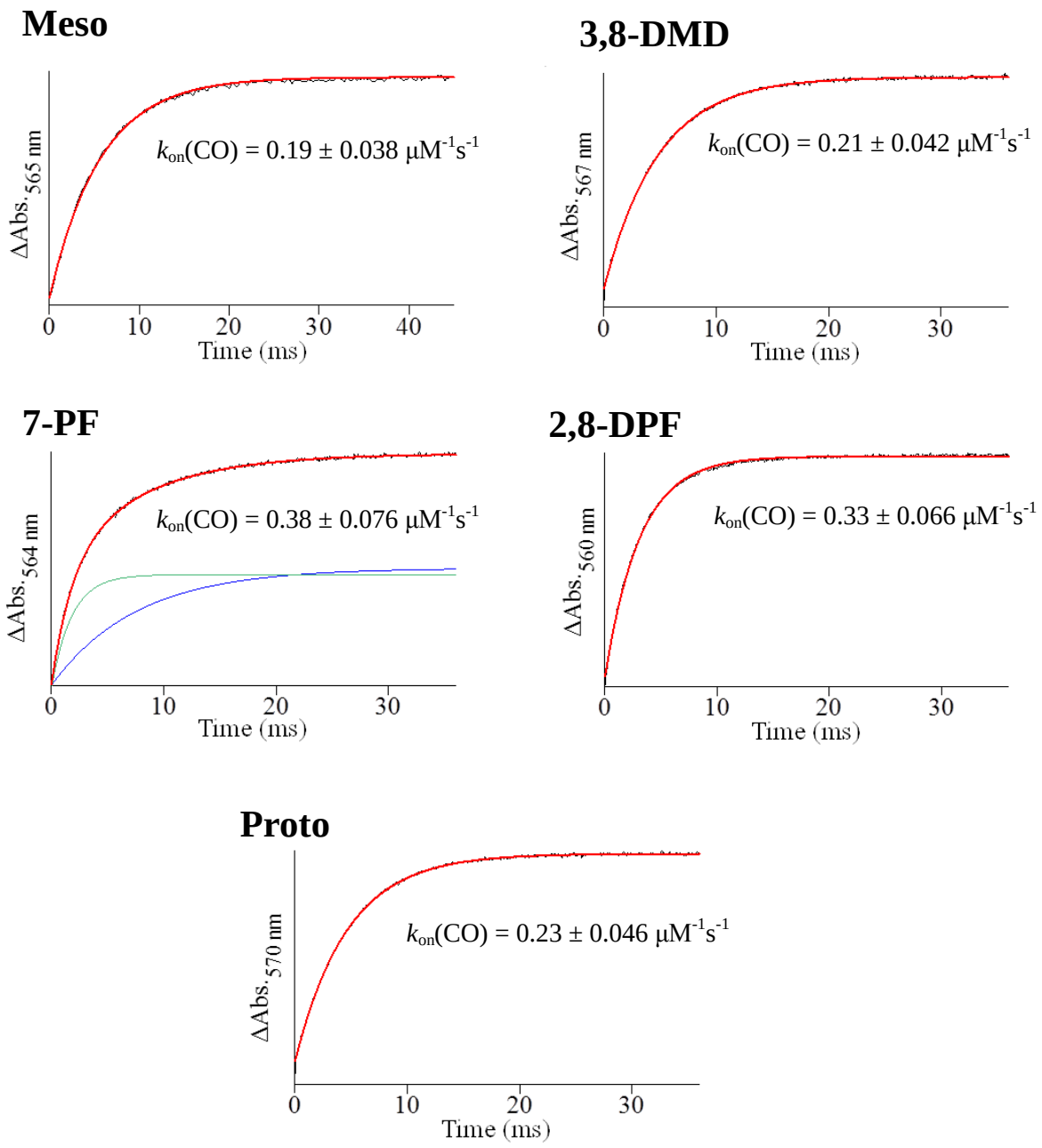

Figure 4-3. Time evolution of absorbance change (*ΔAbs.*), at the indicated wavelength (nm), after photolysis of O_2 forms of the L29F mutant proteins possessing the indicated heme cofactors, in 100 mM potassium phosphate buffer, pH 7.40, at 25 ^{o}C. The k_{on}(CO) value was determined through fitting the time evolution with the assumption of first-order kinetics, indicated in red. In the case of the L29F mutant protein possessing 7-PF, biphasic time evolution was fitted by a sum of two exponentials.

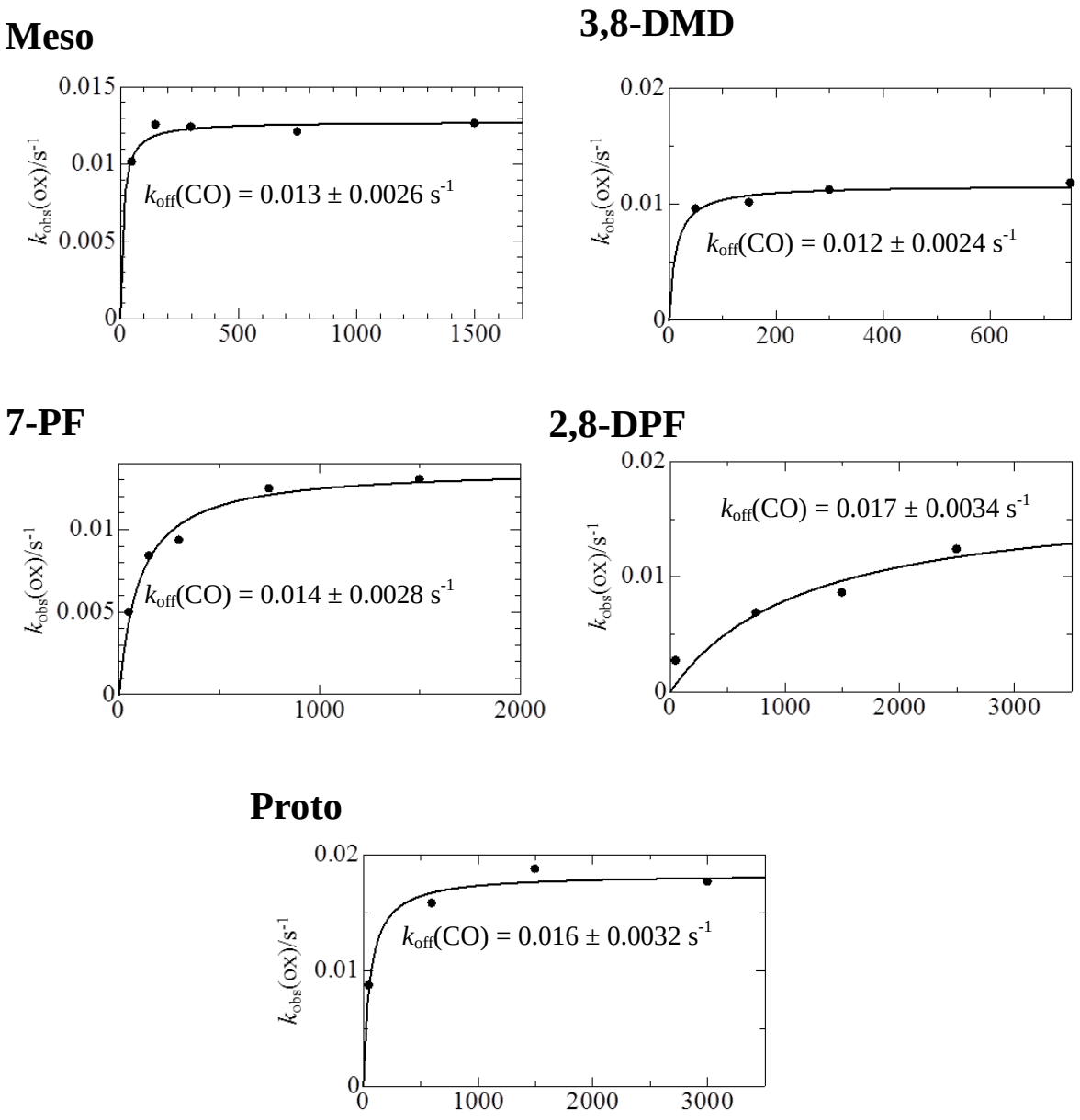

Figure 4-4. . Plots of pseudo first-order rate constant for the oxidation of the proteins (k_{obs}(ox)) against [$K_3Fe(CN)_6$] for CO forms of the L29F mutant proteins possessing the indicated heme cofactors in 100 mM potassium phosphate buffer, pH 7.40, at 25 ^{o}C. The k_{off}(CO) was determined through the fitting.

Vibrational Frequencies of Fe-bound O_2 of the L29F Mutant Protein. Resonance Raman spectra of the O_2 forms of the L29F mutant proteins possessing various heme cofactors were obtained in order to determine the vibrational frequencies of the Fe-O stretching (ν_{FeO}) of Fe-bound O_2 in the proteins (Figures 4-5－4-10 and Table 4-2). The ν_{FeO} value of 569 cm^{-1} determined for L29F(Proto) was essentially identical to that previously reported by Hirota et al.[32], i.e., 568 cm^{-1}. The ν_{FeO} values of the native protein were decreased by 1-3 cm^{-1} relative to those of the L29F mutant proteins possessing identical heme cofactors.

Table 4-2. Vibrational frequencies of the Fe-bound CO and Fe-bound O_2 of the L29F mutant proteins, native Mbs and the H64L mutant proteins at pH 7.4 and 25°C.

Heme	ν_{CO}[a] (cm^{-1})			ν_{FeC}[b] (cm^{-1})			$\delta_{Fe\text{-}CO}$[c] (cm^{-1})			ν_{FeO}[d] (cm^{-1})		
	L29F	Mb[e]	H64L[f]	L29F	Mb[e]	H64L[f]	L29F	Mb[e]	H64L[f]	L29F	Mb[e]	H64L[f]
Meso	1928	1939[g]	1965	526	515	489	581	576	575	570	573	573
3,8-DMD	1928	1940[g]	1964	528	514	491	583	576	575	569	571	570
7-PF	1936	1945[g]	1972	523	514	489	580	575	573	568	571	568
2,8-DPF	1944	1951[g]	1978	518	512	483	578	574	570	568	569	568
Proto	1933	1943[g]	1969	524	512	490	581	576	574	569	571	569

a: The C-O stretching frequency of the Fe-bound CO. b: The Fe-C stretching frequency of the Fe-bound CO. c: The Fe-C-O bending frequency of the Fe-bound CO. d: The Fe-O stretching frequency of the Fe-bound O_2. e: Taken from Ref. 19. e: Taken from Ref. 33. g: $\nu_{CO(H)}$(See Chapter 2)

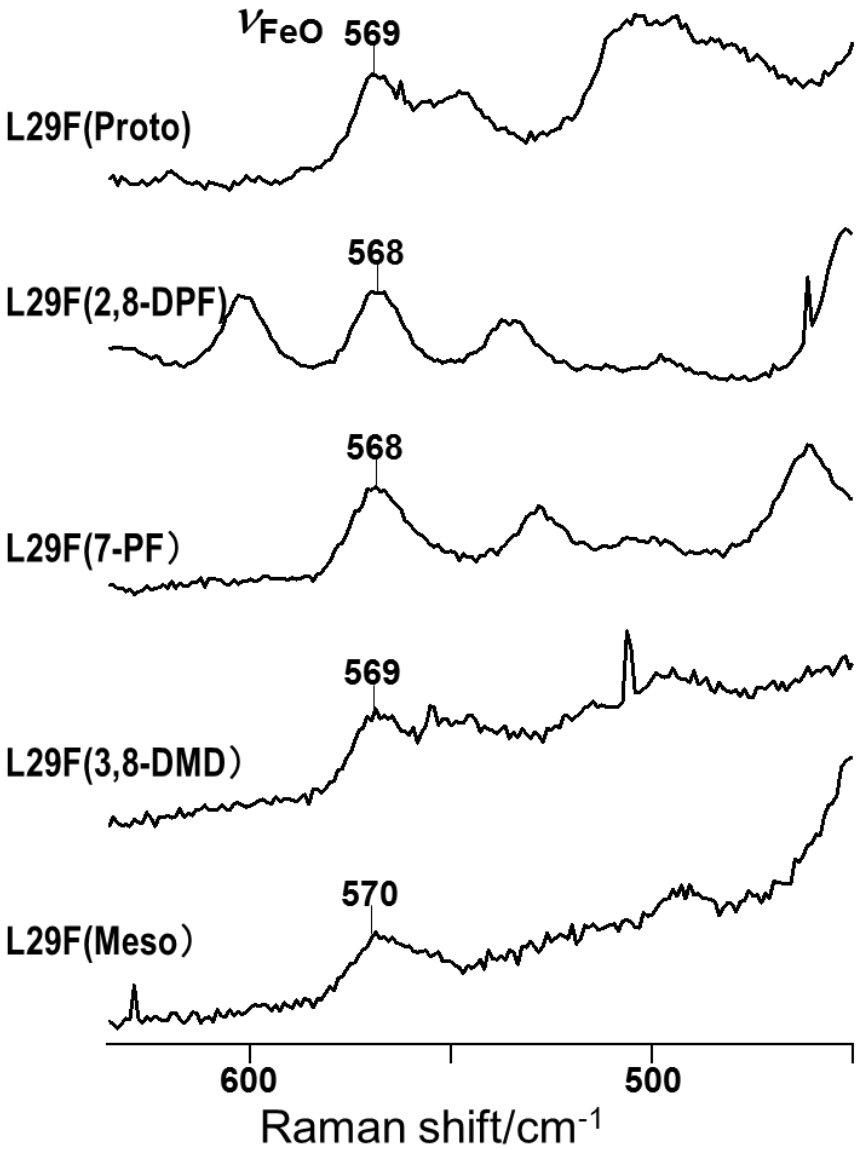

Figure 4-5. Visible resonance Raman spectra of O_2 form of the L29F mutant proteins possessing the indicated heme cofactors, at pH 7.40 and 25 °C. The positions of the bonds were determined through fitting with Voigt profiles(Figures 4-6－4-10)[31].

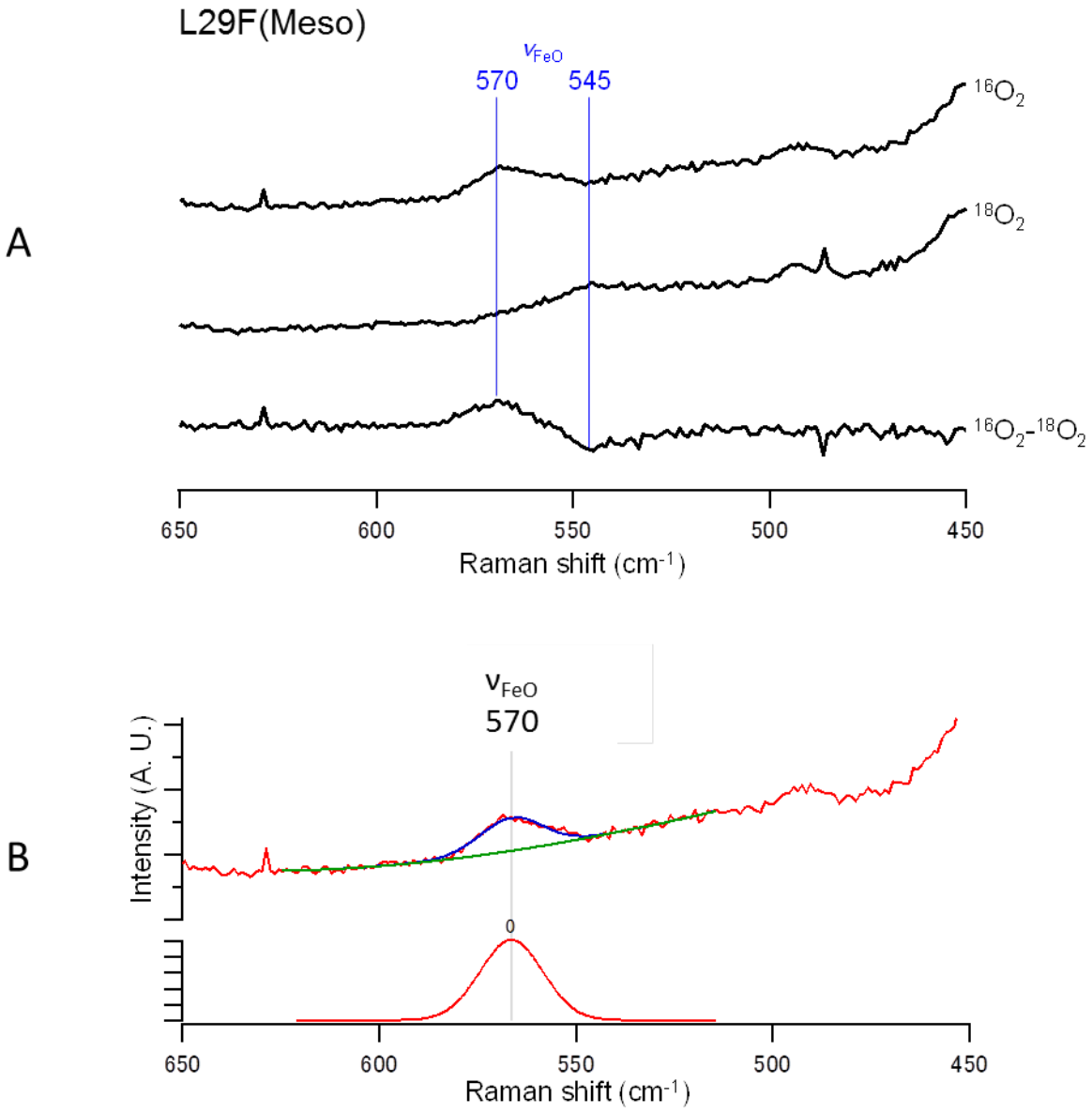

Figure 4-6. Visible resonance Raman spectra of O_2 form of L29F(Meso) at pH 7.40 and 25 °C.
A: In the spectra, the wavenumbers of $\nu_{FeO}(^{16}O_2)$ and $\nu_{FeO}(^{18}O_2)$ bands are indicated in red. The spectra recorded using $^{16}O_2$ (top) and $^{18}O_2$ (middle), and the difference spectrum (bottom) being shown.
B: Fitting of visible resonance Raman spectrum of O_2 form of L29F(Meso) in 100 mM potassium phosphate buffer, pH 7.40, at 25 °C. Observed (blue) and simulated bands (red) ν_{FeO} band (top), and simulated individual band one (bottom). The green line in the top illustration indicates the baseline. The wavenumber of the ν_{FeO} band determined through fitting with Voigt profiles[31] is indicated with the spectra.

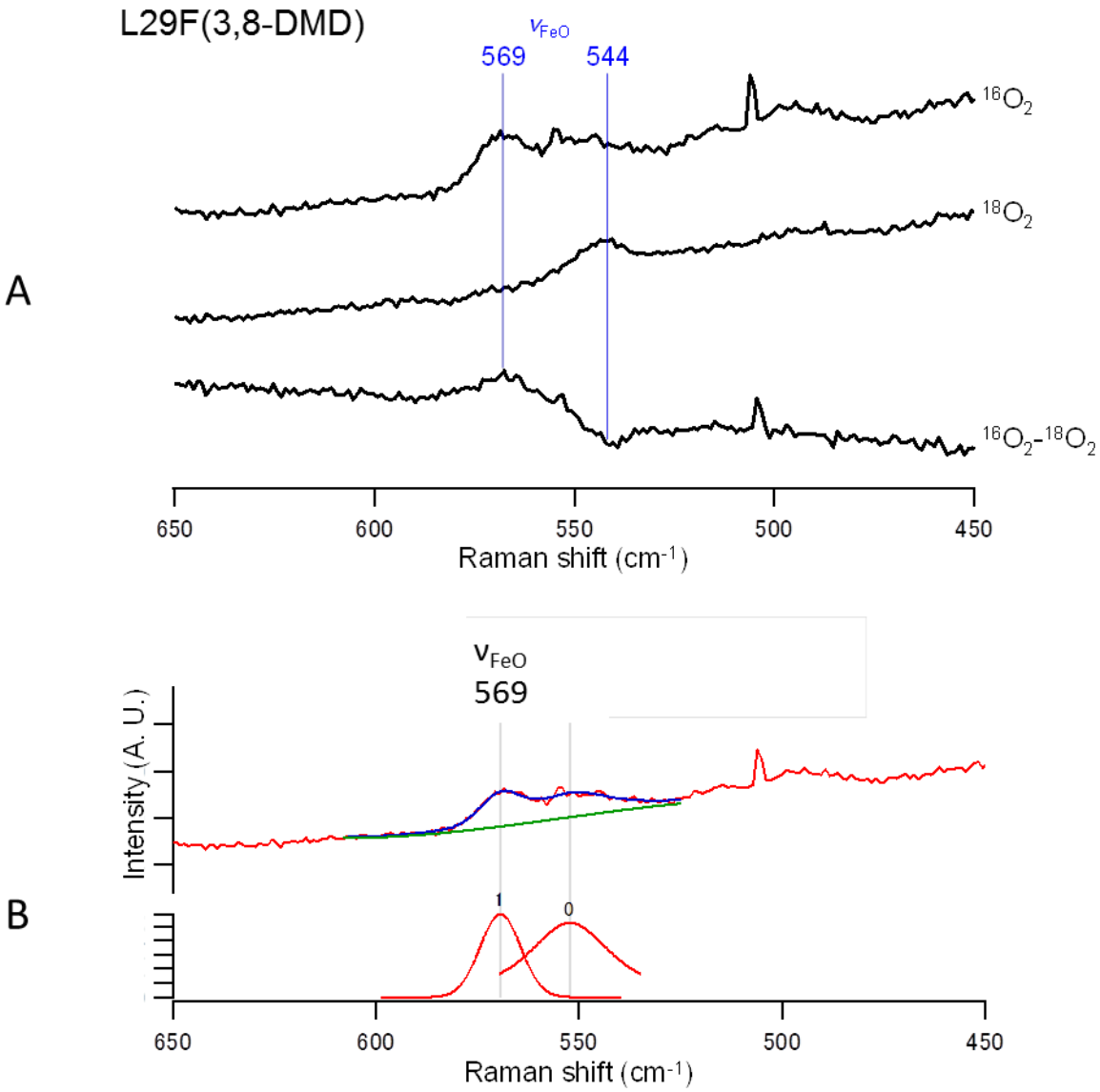

Figure 4-7. Visible resonance Raman spectra of O_2 form of L29F(3,8-DMD) at pH 7.40 and 25 °C. A: In the spectra, the wavenumbers of $\nu_{FeO}(^{16}O_2)$ and $\nu_{FeO}(^{18}O_2)$ bands are indicated in red. The spectra recorded using $^{16}O_2$ (top) and $^{18}O_2$ (middle), and the difference spectrum (bottom) being shown.
B: Fitting of visible resonance Raman spectrum of O_2 form of L29F(3,8-DMD) in 100 mM potassium phosphate buffer, pH 7.40, at 25 °C. Observed (blue) and simulated bands (red) ν_{FeO} band (top), and simulated individual band one (bottom). The green line in the top illustration indicates the baseline. The wavenumber of the ν_{FeO} band determined through fitting with Voigt profiles[31] is indicated with the spectra.

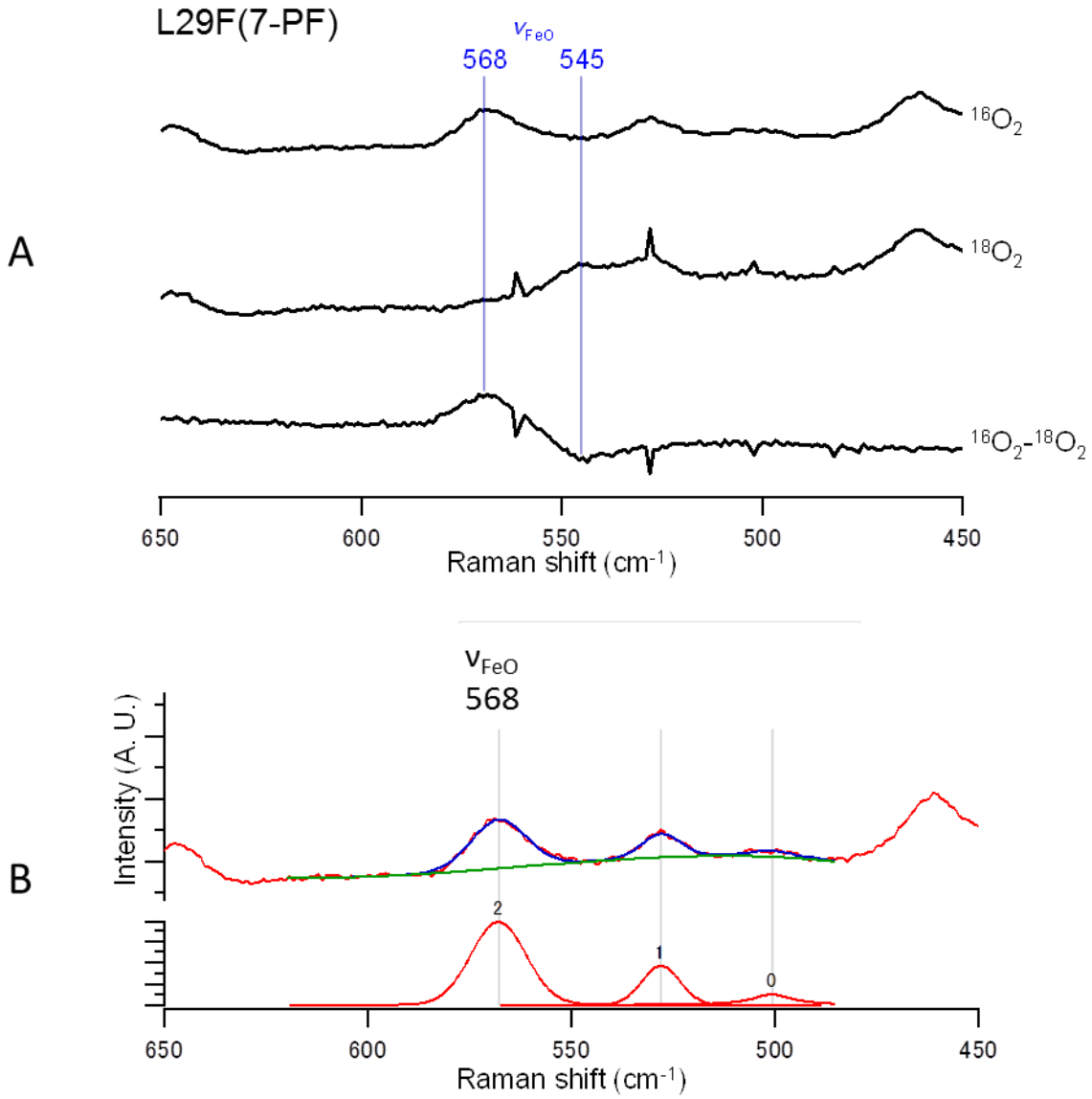

Figure 4-8. Visible resonance Raman spectra of O_2 form of L29F(7-PF) at pH 7.40 and 25 °C.
A: In the spectra, the wavenumbers of $\nu_{FeO}(^{16}O_2)$ and $\nu_{FeO}(^{18}O_2)$ bands are indicated in red. The spectra recorded using $^{16}O_2$ (top) and $^{18}O_2$ (middle), and the difference spectrum (bottom) being shown.
B: Fitting of visible resonance Raman spectrum of O_2 form of L29F(7-PF) in 100 mM potassium phosphate buffer, pH 7.40, at 25 °C. Observed (blue) and simulated bands (red) ν_{FeO} band (top), and simulated individual band one (bottom). The green line in the top illustration indicates the baseline. The wavenumber of the ν_{FeO} band determined through fitting with Voigt profiles[31] is indicated with the spectra.

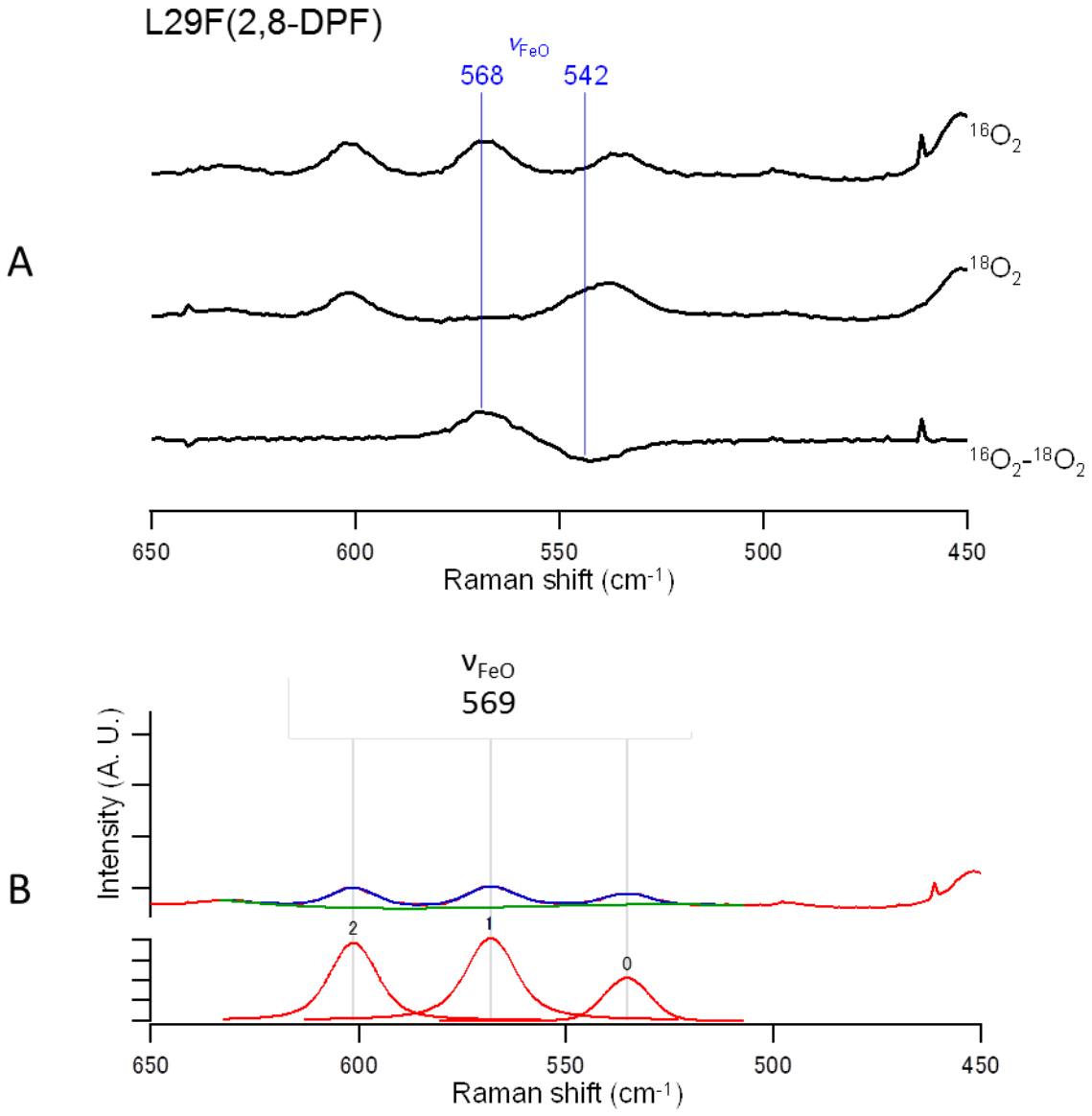

Figure 4-9. Visible resonance Raman spectra of O_2 form of L29F(2,8-DPF) at pH 7.40 and 25 °C.
A: In the spectra, the wavenumbers of $\nu_{FeO}(^{16}O_2)$ and $\nu_{FeO}(^{18}O_2)$ bands are indicated in red. The spectra recorded using $^{16}O_2$ (top) and $^{18}O_2$ (middle), and the difference spectrum (bottom) being shown.
B: Fitting of visible resonance Raman spectrum of O_2 form of L29F(2,8-DPF) in 100 mM potassium phosphate buffer, pH 7.40, at 25 °C. Observed (blue) and simulated bands (red) ν_{FeO} band (top), and simulated individual band one (bottom). The green line in the top illustration indicates the baseline. The wavenumber of the ν_{FeO} band determined through fitting with Voigt profiles[31] is indicated with the spectra.

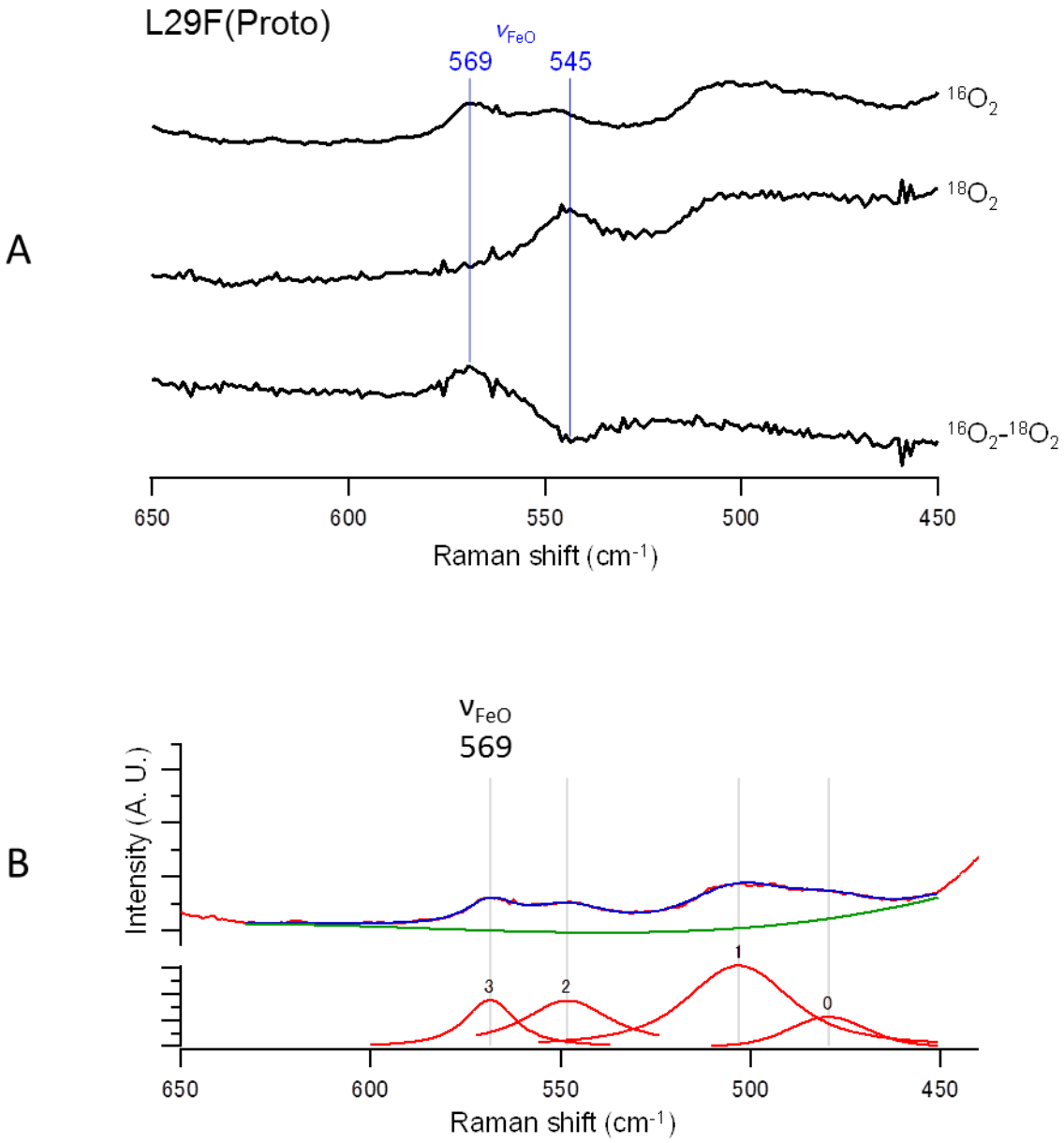

Figure 4-10. Visible resonance Raman spectra of O_2 form of L29F(Proto) at pH 7.40 and 25 °C.
A: In the spectra, the wavenumbers of $\nu_{FeO}(^{16}O_2)$ and $\nu_{FeO}(^{18}O_2)$ bands are indicated in red. The spectra recorded using $^{16}O_2$ (top) and $^{18}O_2$ (middle), and the difference spectrum (bottom) being shown.
B: Fitting of visible resonance Raman spectrum of O_2 form of L29F(Proto) in 100 mM potassium phosphate buffer, pH 7.40, at 25 °C. Observed (blue) and simulated bands (red) ν_{FeO} band (top), and simulated individual band one (bottom). The green line in the top illustration indicates the baseline. The wavenumber of the ν_{FeO} band determined through fitting with Voigt profiles[31] is indicated with the spectra.

DISCUSSION

Effects of Heme Cofactor Modifications on the Vibrational Frequencies of Fe-bound O_2 of the L29F Mutant Protein. As shown in Table 4-2, the ν_{FeO} values of the native Mbs were decreased by 1-3 cm^{-1} relative to those of the L29F mutant proteins possessing identical heme cofactors. Similarly to the case of the Fe-CO fragment in the CO form of a protein, the Fe-O_2 fragment in the O_2 form of a protein exists as an admixture of two alternative canonical forms, i.e., the Fe^{2+}-O_2 and Fe^{3+}-O_2^--like species (Scheme 3-1) [8,22]. Hence, although the resonance between the two forms is affected by the heme environment furnished by nearby amino acid residues, the Fe-O bond order is independent of the resonance [32], leading to the low sensitivity of the ν_{FeO} value to replacement of amino acid residues in the heme pocket.

The mutant proteins were ranked as L29F(2,8-DPF) ~ L29F(7-PF) < L29F(3,8-DMD) ~ L29F(Proto) < L29F(Meso), in order of increasing the ν_{FeO} value, although the differences are small. The weakening of the Fe-O bond in the protein, as manifested in the ν_{FeO} one, however, cannot fully account for the large increase in the $k_{off}(O_2)$ value of the mutant protein with decreasing the ν_{Fe} one, as have been reported previously for the native Mbs and the H64L mutant proteins.

Effects of Heme Cofactor Modifications on O_2 versus CO Discrimination of the L29F Mutant Protein. **I** have shown that the O_2 affinity of the protein decreases (increases), due to an increase (a decrease) in the $k_{off}(O_2)$ value, with a decrease (an increase) in the ρ_{Fe} value [18,19]. Plots of the quantities $\log(k_{on}(O_2))$, $\log(k_{off}(O_2))$, and $\log(K(O_2))$ against the ρ_{CO} values (see chapter 2) ($\log(k_{on}(O_2))$- ν_{CO}, $\log(k_{off}(O_2))$- ν_{CO}, and $\log(K(O_2))$- ν_{CO} plots, respectively) for the L29F mutant protein system confirmed that the O_2 affinity of the mutant protein is regulated through the ρ_{Fe} value in a similar manner (Figure 4-11). The $\log(k_{off}(O_2))$- ν_{CO} plots for the L29F mutant proteins could be represented by a straight line with a slope of +0.09 ($1/cm^{-1}$), and the obtained slope was similar to those of the plots for the native Mbs and the H64L mutant proteins previously reported, i.e., +0.01 ($1/cm^{-1}$) for the two protein systems, demonstrating that the regulation of the $k_{off}(O_2)$ value through the ρ_{Fe} one is independent of the heme environment furnished by nearby amino acid residues.

Comparison of the $K(O_2)$ values of the three protein systems yielded that the $K(O_2)$ value of the native protein was increased by a factor of ~11-24 by the introduction of Phe29, through the L29F mutation, and, conversely, was decreased by a factor of ~1/17-1/9 by the removal of His64, through the H64L one. Consequently, Phe29 in the L29F mutant protein was found to play a role as important as His64 in the native protein in order to enhance the O_2 affinity of the protein. Furthermore, the O_2 affinity of the L29F mutant protein is lowered by factors of ~1/5 and ~1/18 on the substitution of one and two CF_3 groups, respectively. Similarly, the O_2 affinity of the native Mb was lowered by factors of ~1/3 and ~1/9 on the substitution of one and two CF_3 group, respectively, and that of the H64L mutant protein by factors of ~1/3 and ~1/15 on the substitution of one and two CF_3 group, respectively [33]. These results confirmed that the control of the O_2 affinity of the protein through the ρ_{Fe} value is independent of that through the heme environment furnished by nearby amino acid residues.

In contrast to the O_2 binding, similar plots for the CO binding, i.e., $\log(k_{on}(CO))$- ν_{CO}, $\log(k_{off}(CO))$-ν_{CO}, and $\log(K(CO))$- ν_{CO} plots, for the L29F mutant protein system indicated that the CO binding properties of the L29F mutant protein system were not largely affected by the ν_{Fe} value (Figure 4-11). The ability of Mb to stabilize Fe(II)-bound O_2 and to discriminate against CO binding is usually evaluated on the basis of the *M* value, i.e., the ratio between the equilibrium constants for CO and O_2 binding ($K(CO)/K(O_2)$)[6]. The *M* value was increased by a factor of ~5 on the substitution of one CF_3 group, as demonstrated for the L29F(Meso)/L29F(7-PF) system, and then by a factor of ~11 on the substitution of two CF_3 ones, as observed for the L29F(3,8-DMD)/L29F(2,8-DPF) one. Plots of the quantity log*M* against the ν_{CO} values (log*M*-ν_{CO} plots) for the L29F mutant protein system could be represented by a straight line with a slope of +0.08 ($1/cm^{-1}$). The log*M*-ν_{CO} plots for the native Mb and the H64L mutant protein systems could be represented by straight lines with similar slopes. These results are inevitable, because, among the kinetic parameters for O_2 and CO binding, only the $k_{off}(O_2)$ value is affected by a change in the ρ_{Fe} value, which is sensitively reflected in ν_{CO} [33], in addition to the heme environment furnished by nearby amino acid residues, as described above. Furthermore, the log*M*-ν_{CO} plots in Figure 4-12 demonstrated that the *M* value of the protein could be regulated over a range of $\sim 10^5$ through combined use of the amino acid replacements, through protein engineering, and the chemical modification of heme cofactor.

The three different protein systems could be ranked as L29F < native Mb < H64L, in order of increasing *M* value. L29F(Proto), Mb(Proto), and H64L(Proto) [33] exhibited the *M* values of 0.83 ± 2, 23 ± 9, and 6900 ± 5700, respectively, (Table 4-1) and hence the *M* value of Mb(Proto) was increased by a factor of ~300 due to the removal of His64 through the H64L mutation, and then conversely was decreased by a factor of ~1/30 due to the introduction of Phe29 through the L29F mutation, indicating that not only His64, but also Phe29 contributes significantly to the preferential binding of O_2 over CO of the protein. Comparison of the *M* values of the L29F mutant proteins indicated that the substitution of one and two CF_3 groups increased the value by factors of ~8 and ~20, respectively. The effects of the substitution of CF_3 group(s) on the *M* value of the L29F mutant protein were almost comparable to those of the native protein, i.e., the *M* value of the native protein was increased by factors of ~4 and ~25 on the substitution of one and two CF_3 groups, respectively, again confirming that the electronic tuning of the intrinsic heme Fe reactivity through the ρ_{Fe} value and the heme environment furnished by nearby amino acid residues contribute independently to control Mb function.

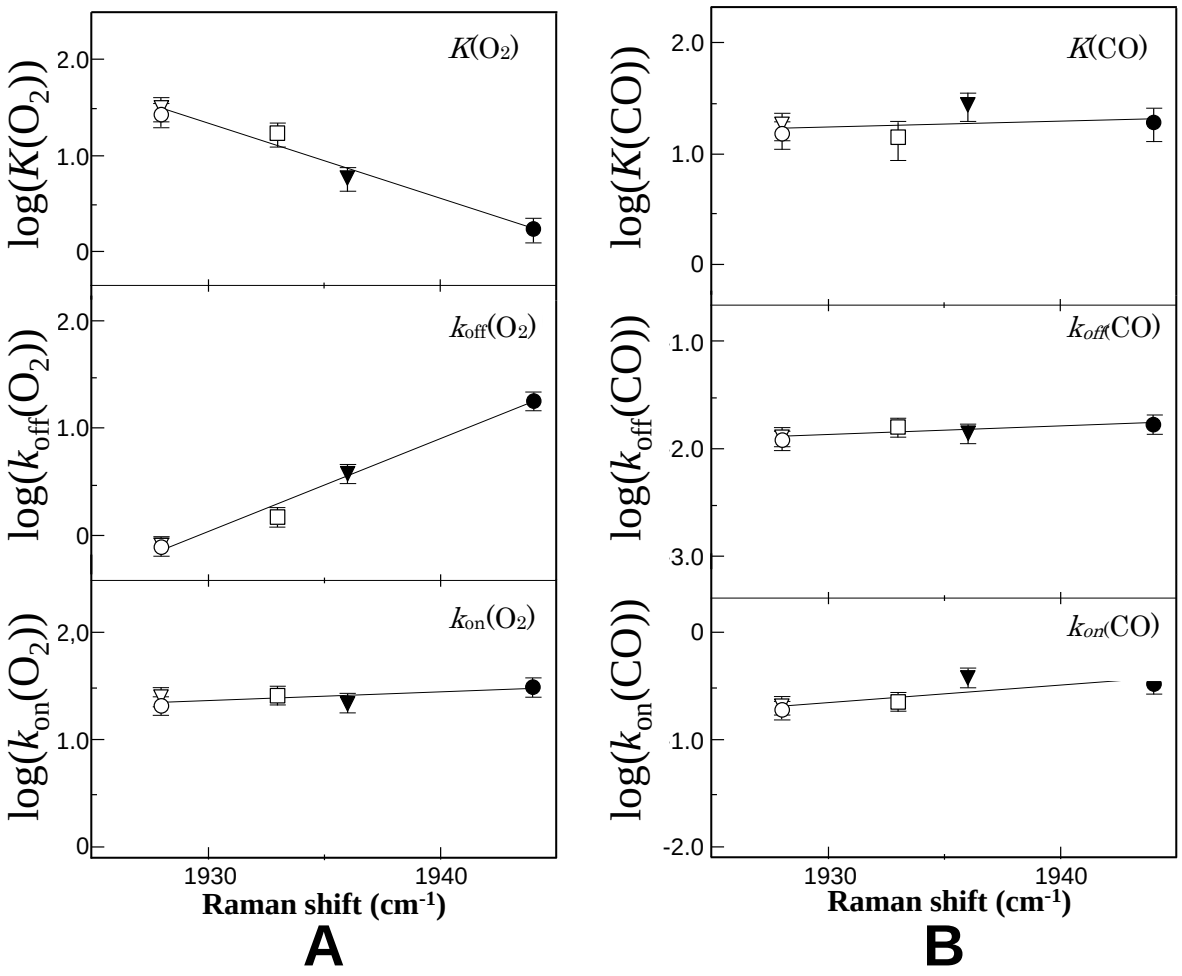

Figure 4-11. Plots of the quantities log($k_{on}(O_2)$), log($k_{off}(O_2)$), and log($K(O_2)$) against the ν_{CO} values for the L29F mutant proteins possessing Meso (▽), 3,8-DMD (○), 7-PF (▼), 2,8-DPF (●), and Proto(□) (A), and similar plots for the quantities log(k_{on}(CO)), log(k_{off}(CO)), and log(K(CO)) (B).

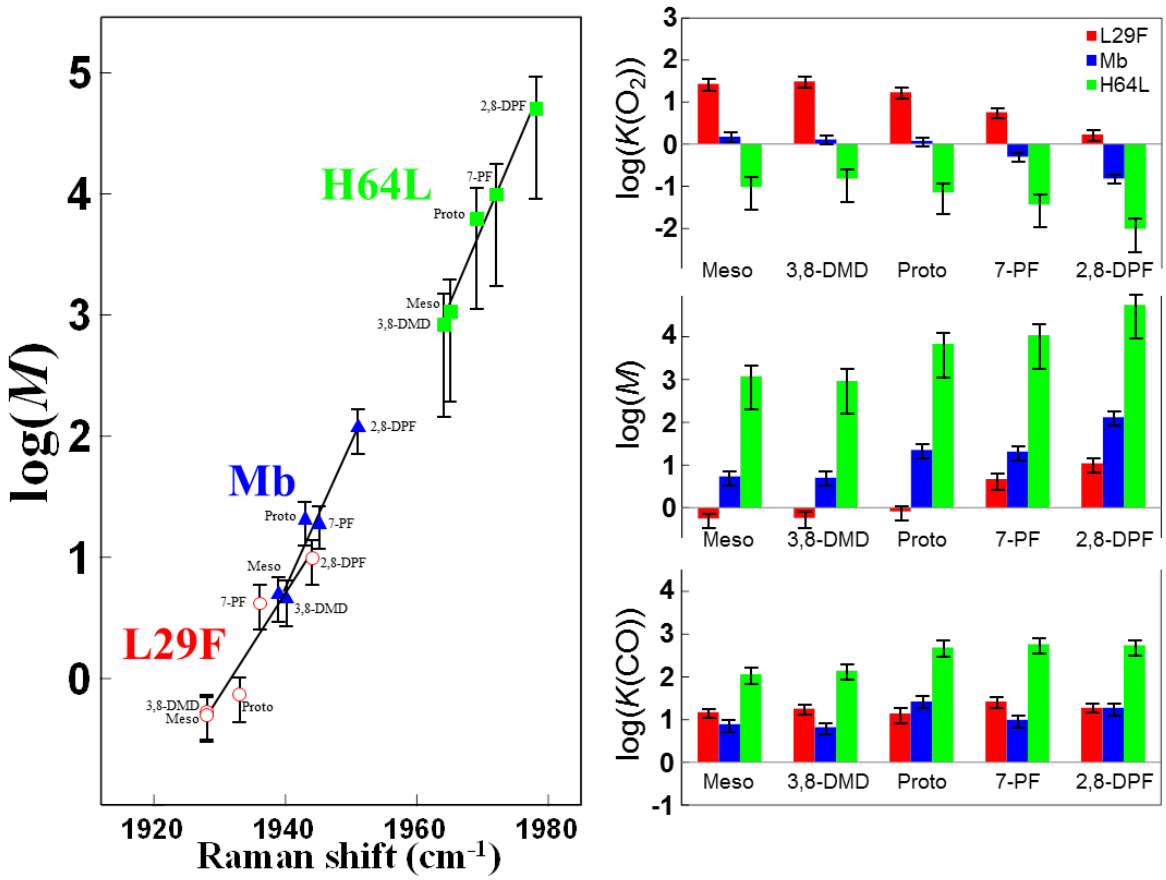

Figure 4-12. Plots of the quantities log(*M*) against the ν_{CO} values for the L29F mutant proteins (○), Mb (▲), and the H64L mutant ones (■).(left) Since the native Mb exhibited a ν_{CO} band composed of multiple components, the weighted-average by the intensity of each band was used as the ν_{CO} value for the plots. Bar graphs illustrate the effects of modifications of the heme cofactors no the quantities log(*K*(CO))(lower), log(*M*)(middle) and log($K(O_2)$)(upper) for the L29F mutant proteins(red), native Mbs(blue) and H64Lmutant proteins(green)(right)

CONCLUSION

The O_2 versus CO ligand binding preference of the L29F mutant protein of Mb has been shown to be regulated through a change in the electron density of the heme Fe atom. The study confirmed that the effects of a change in the electron density of the heme Fe atom and the heme environment furnished by nearby amino acid residues on the functional properties of the protein are independent to each other, and the ratio between the equilibrium constants for CO and O_2 binding in the protein can be regulated over a range of $\sim 10^5$ through combined use of the chemical modification of heme cofactor and the amino acid replacements. These findings provide useful insights for designing functional properties of O_2 binding hemoprotein.

References

(1) Antonini, E.; Brunori, M. *Hemoglobins and Myoglobins and their Reactions with Ligands*; North Holland Publishing: Amsterdam, **1971**.

(2) Kachalova, G. S.; Popov, A. N.; Bartunik, H. D. *Science*, **1999**, 284, 473-476.

(3) Olson, J. S.; Phillips, G. N., Jr. *J. Biol. Inorg. Chem.*, **1997**, 2, 544-552.

(4) Olson, J. S.; McKinnie, R. E.; Mims, M.P.; White, D. K. *J. Am. Chem. Soc.*, **1983**, 105, 1522-1527.

(5) Kendrew, J. C.; Bodo, G.; Dintzis, H. M.; Parrish, R. G.; Wyckoff, H.; Phillips, D. C. *Nature*, **1958**, 181, 662-666.

(6) Springer, B. A.; Egeberg, K. D.; Sligar, S. G.; Rohlfs, R. J.; Mathews, A. J.; Olson, J. S. *J. Biol. Chem.*, **1989**, 264, 3057-3060.

(7) Springer, B. A.; Sligar, S. G.; Olson, J. S.; Phillips, G. N., Jr. *Chem. Rev.*, **1994**, 94, 699-714.

(8) Pauling, L. *Nature*, **1964**, 203, 182-183.

(9) Moffat, K.; Deatherage, J. R.; Seyberg, D. W. *Science*, **1979**, 206, 1035−1042.

(10) Phillips, S. E. V. *J. Mol. Biol.*, **1980**, 142, 531-554.

(11) Shaanan, B. *J. Mol. Biol.*, **1983**, 171, 31-59.

(12) Mims, M. P.; Porras, H. G.; Olson, J. S.; Noble, R. W.; Peterson, J. A. *J. Biol. Chem.*, **1983**, **258**, 14219-14232.

(13) Nagai, K.; Luisi, B.; Shih, D.; Miyazaki, G.; Imai, K.; Poyart, C.; De Young, A.; Kwiatkowsky, L.; Noble, R. W.; Lin, S.-H; Yu, N.-T. *Nature*, **1987**, 329, 858-860.

(14) Perutz, M. F. In *Molecular Basis of Blood Diseases* (Stammatoyanopoulos, G., Nienhaus, A. W., Leder, P., and Majerus, P. W., eds.), Saunders, Philadelphia, **1987**, pp 127-178.

(15) Rohlfs, R. J.; Mathews, A. J.; Carver, T. E.; Olson, J. S.; Springer, B. A.; Egeberg, K. D.; Sliger, S. G. *J. Biol. Chem.*, **1990**, 265, 3168-3176.

(16) Phillips, S. E. V.; Schoenborn, B. P. *Nature*, **1981**, 292, 81-82.

(17) Hanson, J. C.; Schoenborn, B. E. J. Mol. Biol., **1981**, 153, 117-146

(18) Shibata, T.; Nagao, S.; Fukaya, M.; Tai, H.; Nagatomo, S.; Morihashi, K.; Matsuo, T.; Hirota, S.; Suzuki, A.; Imai, K.; Yamamoto, Y. *J. Am. Chem. Soc.*, **2010**, 132, 6091-6098.

(19) Nishimura, R.; Shibata, T.; Tai, H.; Ishigami, I.; Ogura, T.; Nagao, S.; Matsuo, T.; Hirota, S.; Imai, K.; Neya, S.; Suzuki, A.; Yamamoto, Y. *Inorg. Chem.*, **2013**, 52, 3349-3355.

(20) Carver, T. E.; Brantley, R. E.; Singleton, E. W.; Arduini, R. M.; Quillin, M. L.; Phillips, G. N., Jr.; Olson, J. S. *J. Biol. Chem.*, **1992**, 267, 14443-14450.

(21) Gibson, Q. H.; Regan, R.; Elber, R.; Olson, J. S.; Carver, T. E. *J. Biol. Chem.*, **1992**, 267, 22022-22034.

(22) Maxwell, J. C.; Volpe, J. A.; Barlow, C. H.; Caughey, W. S. *Biochem. Biophys. Res. Commun.*, **1974**, 58, 166-171.

(23) Toi, H.; Homma, M.; Suzuki, A.; Ogoshi, H. *J. Chem. Soc., Chem. Commun.*, **1985**, 1791–1792.

(24) Chang, C. K.; Ward, B.; Ebina, S. *Arch. Biochem. Biophys.*, **1984**, 231, 366-371.

(25) Neya, S.; Suzuki, M.; Hoshino, T.; Ode, H.; Imai, K.; Komatsu, T.; Ikezaki, A.; Nakamura, M.; Furutani, Y.; Kandori, H. *Biochemistry*, **2010**, 49, 5642-5650.

(26) Teale, F. W. J. *Biochim. Biophys. Acta*, **1959**, 35, 543.

(27) Matsuo, T.; Dejima, H.; Hirota, S.; Murata, D.; Sato, H.; Ikegami, T.; Hori, H.; Hisaeda, Y.; Hayashi, T. *J. Am. Chem. Soc.*, **2004**, 126, 16007-16017.

(28) Olson, J. S. *Method. Enzymol.*, **1981**, 76, 631-651.

(29) Matsuo, T.; Ikegami, T.; Sato, H.; Hisaeda, Y.; Hayashi, T. *J. Inorg. Biochem.*, **2006**, 100, 1265-1271.

(30) Kitanishi, K.; Kobayashi, K.; Kawamura, Y.; Ishigami, I.; Ogura, T.; Nakajima, K.; Igarashi, J.; Tanaka, A.; Shimizu, T. *Biochemistry*, **2010**, 49, 10381-10393.

(31) Reilly, J. T.; Walsh, J. M.; Greenfield, M. L.; Donohue, M. D. *Spectrochim. Acta*, **1992**, 48A, 1459-1479.

(32) Hirota, S.; Li, T.; Phillips, G. N., Jr.; Olson, J. S.; Mukai, M.; Kitagawa, T. *J. Am. Chem. Soc.*, **1996**, 118, 7845-7846.

(33) Nishimura, R.; Shibata, T.; Ishigami, I.; Ogura, T.; Tai, H.; Nagao, S.; Matsuo, T.; Hirota, S.; Shoji, O.; Watanabe, Y.; Imai, K.; Neya, S.; Suzuki, A.; Yamamoto, Y. *Inorg. Chem.*, **2014**, 53, 1092-1099.

Chapter 5

Effect of the electron density of the heme Fe atom on the Fe-histidine coordination bond in deoxy myoglobin

Abstract

The stretching frequency of the coordination bond between the heme Fe atom and proximal histidine (His93) N_ε atom ($\nu_{Fe\text{-}His}$), and the NMR shift of the His93 $N_\delta H$ proton (His93$N_\delta H$ shift) of the deoxy form of a hemoprotein have been used to determine the electronic nature of the His93 imidazole highly relevant to regulation of heme Fe reactivity. The analysis of the $\nu_{Fe\text{-}His}$ values and His93$N_\delta H$ shifts of the deoxy forms of myoglobins reconstituted with artificial heme cofactors possessing strongly electron-withdrawing trifluoromethyl (CF_3) group(s) as peripheral side chain(s) revealed that the bond between the heme Fe and His93 becomes stronger with increasing number of CF_3 substitutions due to an increase in acidity of the His93 $N_\delta H$ hydrogen bonded to the carbonyl O atom of Leu89. Thus, the study demonstrated that the electronic nature of the His93 imidazole in deoxy Mb is affected by electronic perturbation induced by chemical modification of the heme cofactor.

INTRODUCTION

Myoglobin (Mb), an oxygen (O_2) storage hemoprotein, is probably at present the best, albeit incompletely, understood metalloprotein in terms of its structure-function relationship[1-7]. In the heme active site of Mb[3,4], the proximal histidine (His93) imidazole is coordinated to a heme Fe atom as axial ligand, with its $N_\delta H$ hydrogen bonded to the carbonyl O atom of Leu89 (His93-Leu89 H-bond) (Figure 5-1), and O_2 binds reversibly to the ferrous Fe atom on the side of the heme cofactor opposite to His93. The O_2 binding properties of the protein have been shown to be regulated through both the heme environment furnished by nearby amino acid residues and the intrinsic heme Fe reactivity[6-9]. I am interested in characterizing the electronic regulation of the intrinsic heme Fe reactivity through the heme electronic structure, particularly the electron density of the heme Fe atom (ρ_{Fe}). In order to achieve this, I established a unique Mb system composed of proteins reconstituted with a series of chemically modified heme cofactors. I introduced trifluoromethyl (CF_3) group(s) into a heme cofactor as peripheral side chain(s), in order to greatly and systematically alter the ρ_{Fe} value, and such CF_3 substitutions were suitable for minimizing the steric structural change of the protein associated with alteration of the heme electronic structure due to modification of the heme cofactor[8-11]. I have prepared proteins reconstituted with mesoheme(Meso), 3,8-dimethyldeuteroporphyrinato -iron(III)(3,8-DMD) [12,13], 13,17-bis(2-carboxylatoethyl)-3,8-diethyl-2,12,18-trimethyl-7-trifluoromethyl -porphyrinatoiron(III)(7-PF) [14], and 13,17-bis(2- carboxylatoethyl)-3,7-diethyl-12,18-trimethyl-2,8 -ditrifluoromethylporphyrinatoiron(III)(2,8-DPF) [8], that is, Mb(Meso), Mb(3,8-DMD), Mb(7-PF), and Mb(2,8-DPF), respectively. These heme cofactors differ in the numbers of CF_3, CH_3, and C_2H_5 side chains, and the reconstituted proteins could be ranked as Mb(2,8-DPF) < Mb(7-PF) < Mb(3,8-DMD) ≈ Mb(Meso), in order of increasing ρ_{Fe} value (Figure 2-2) [8,9]. In addition, since 7-PF and 2,8-DPF can be considered as counterparts of Meso and 3,8-DMD, respectively, the effects of the substitution of one and two CF_3 groups on the structural and functional properties of the protein could be inferred from the results of comparative studies on Mb(Meso)/Mb(7-PF), and Mb(3,8-DMD)/Mb(2,8-DPF), respectively. Through the studies on these proteins, I revealed that the ρ_{Fe} value plays critical roles in the regulation of various functions of the protein, such as, O_2 affinity,

discrimination between O_2 and carbon monoxide (CO), and autoxidation, that is, spontaneous oxidation of the ferrous Fe state of the oxygenated protein into the ferric Fe one[8-11].

In this chapter, I characterized the effects of the CF_3 substitutions on the heme active site structure in the deoxy form of Mb (deoxy Mb) in order to obtain a deeper understanding of the mechanism underlying the electronic regulation of the intrinsic heme Fe reactivity. Among the physiologically active forms of the protein, deoxy Mb has been the least understood in terms of the molecular properties of its heme active site, despite its physiological importance [15-20]. I investigated the coordination bond between the heme Fe atom and His93N_ε atom (Fe-His bond) in the deoxy Mbs on the basis of the stretching frequency of the Fe-His bond ($\nu_{Fe\text{-}His}$) determined by resonance Raman spectroscopy, and the shift of the NMR signal due to the His93N_δH proton (His93N_δH shifts). In the protein, a decrease in the ρ_{Fe} value is likely to lead to enhancement of the electron donation of His93 N_ε to the heme Fe atom (His93→Fe donation), which in turn results in an increase in acidity of His93 N_δH, and hence reinforcement of the His93-Leu89 H-bond. Thus, the present study demonstrated that the electronic nature of the His93 imidazole in deoxy Mb is affected by electronic perturbation induced by chemical modification of the heme cofactor, and that a protein with a stronger Fe-His bond exhibits a lower O_2 affinity.

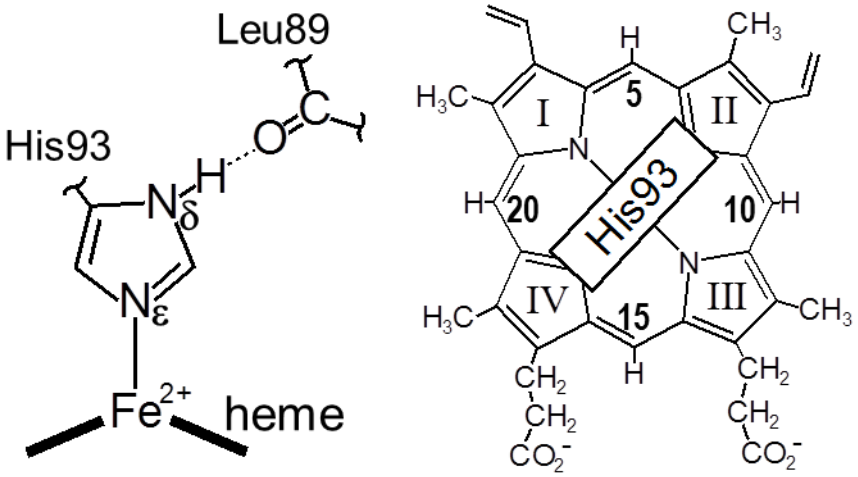

Figure 5-1. Coordination structure of the heme Fe atom in deoxy Mb with hydrogen bonding between the N_δH hydrogen of His93 and the carbonyl oxygen of Leu89.

MATERIALS AND METHODS

Materials and protein samples. All reagents and chemicals were obtained from commercial sources and used as received. Sperm whale Mb was purchased as a lyophilized powder from Biozyme and used without further purification. Mesoheme (Meso) was purchased from Frontier Scientific Co. 3,8-DMD [12,13], 7-PF [14], and 2,8-DPF [8] were synthesized as previously described. The apoprotein of Mb (apoMb) was prepared at 4 °C according to the procedure of Teale [21], and reconstituted Mbs were prepared as described previously [8,10]. Deoxy Mb was prepared from metmyoglobin (metMb), which had been evacuated and flushed with N_2 gas several times, by adding $Na_2S_2O_4$ (Nacalai Chemicals Ltd.). To prepare CO adduct of the protein (MbCO), metMb was reduced by adding $Na_2S_2O_4$ in the presence of CO gas (Japan Air Gases), and then the protein was freed from excess reagents by passage through a Sephadex G-10 (Sigma-Aldrich Co.) column equilibrated with an appropriate buffer solution. The ^2H_2O content of the samples was ~10%. The pH of a sample was adjusted using 0.1 M NaOH or HCl. The pH of each sample was measured with a Horiba F-22 pH meter equipped with a Horiba type 6069-10c electrode.

Resonance raman spectroscopy. Resonance raman scattering was performed with excitation at 413.1 nm with a Kr^+ laser (Spectra Physics, BeamLok 2060), dispersed with a polychromator (SPEX 1877 or Ritsu Oyo Kogaku MC-100DG, both equipped with 1200 grooves/mm grating), and detected with a liquid nitrogen-cooled CCD detector (CCD-1024×256-OPEN-1LS, HORIBA Jobin Yvon or LN/CCD-1100-PB/VISAR/1, Roper Scientific) [22]. A laser power of 5 mW was used for the measurements. Raman shifts were calibrated with indene and tetrachloromethane as frequency standards. The accuracy of the peak positions of well-defined Raman bands was ±1 cm^{-1}. The protein concentration was approximately 40 μM in 100 mM potassium phosphate buffer, pH 7.4.

^{1}H and ^{19}F NMR spectroscopies. ^{1}H and ^{19}F NMR spectra were recorded on a Bruker AVANCE-400 spectrometer operating at the ^{1}H frequency of 400 MHz and a Bruker AVANCE-500 spectrometer operating at the ^{19}F frequency of 471 MHz, respectively. Typical ^{1}H and ^{19}F NMR spectra consisted of about 20k transients with a spectral width of 100 kHz and 16k data points. The

signal-to-noise ratio of the spectra was improved by apodization, which introduced 100 Hz line broadening. The chemical shifts of ^{1}H and ^{19}F NMR spectra are given in ppm downfield from the residual $^{1}H^{2}HO$, as an internal reference, and trifluoroacetic acid as an external reference, respectively.

RESULTS

Stretching frequencies of the Fe-His bonds in deoxy Mbs. I first determined the $\nu_{Fe\text{-}His}$ values of native deoxy Mb, deoxy Mb(Meso), deoxy Mb(3,8-DMD), deoxy Mb(7-PF), and deoxy Mb(2,8-DPF). These proteins exhibited a well-resolved $\nu_{Fe\text{-}His}$ band at ca. 220 cm^{-1} (Figure 5-2). The $\nu_{Fe\text{-}His}$ bands of deoxy Mb(3,8-DMD), deoxy Mb(7-PF), and deoxy Mb(2,8-DPF) have been unambiguously assigned through the replacement of ^{56}Fe by ^{54}Fe, which resulted in the bands shifting by ca. +2 cm^{-1} (Figures 5-3－5-5). The positions of the $\nu_{Fe\text{-}His}$ bands of the proteins were determined through fitting with Voigt profiles, which are convolutions of Gaussian and Lorentzian functions (Figures 5-6－5-10) [23], and the determined values are summarized in Table 5-1. The $\nu_{Fe\text{-}His}$ value of 221 cm^{-1} determined for native deoxy Mb was essentially identical to the reported value, that is, 220 cm^{-1} [25]. The $\nu_{Fe\text{-}His}$ values of deoxy Mb(Meso), deoxy Mb(3,8-DMD), deoxy Mb(7-PF), and deoxy Mb(2,8-DPF) were determined for 221, 219, 223, and 223 cm^{-1}, respectively (Table 5-1). Thus, $\nu_{Fe\text{-}His}$ differences ($\Delta\nu_{Fe\text{-}His}$) of 2 and 4 cm^{-1} were observed for the Mb(Meso)/Mb(7-PF) and Mb(3,8-DMD)/Mb(2,8-DPF) systems, respectively (Table 5-2), indicating that the Fe-His bond becomes stronger with increasing number of CF_3 substitutions. Thus the $\nu_{Fe\text{-}His}$ values of the proteins were affected by the heme modifications.

Fujii et al.[26] have demonstrated from detailed ESR studies of oxochromium(V) porphyrin complexes possessing various peripheral substituents that the introduction of electron-withdrawing group into the porphyrin strengthens the coordination bond between Cr(V) and axial ligand. The effect of a change in the ρ_{Fe} value on the strength of the Fe-His bond demonstrated in this study is completely consistent with the finding of Fujii et al.[26].

Table 5-1. $\nu_{Fe\text{-}His}$ values and His93N_δH ^{1}H NMR shifts of deoxy Mbs at pH 7.40 and 25℃, and O_2 and CO binding paramerters for Mbs at pH7.4 and 20°C

Mb	$\nu_{Fe\text{-}His}$[a] (cm^{-1})	His93N_δH[b] (ppm)	O_2 binding	CO binding
			$k_{on}(O_2)$ ($\mu M^{-1}s^{-1}$)/ $k_{off}(O_2)$ (s^{-1})	$k_{on}(CO)$ ($\mu M^{-1}s^{-1}$)/$k_{off}(CO)$ (s^{-1})
Mb(Meso)	217	80.5	8.2 ± 1.6[d] / 5.7 ± 1.1[d]	0.38 ± 0.07[d]/0.048 ± 0.009[d]
Mb(3,8-DMD)	216	78.6	12 ± 3[e] / 9.4 ± 3[e]	0.16 ± 0.07[e]/0.024 ± 0.007[e]
Mb(7-PF)	221	76.6(77.9)[c]	8.3 ± 1.6[d] / 17 ± 3[d]	0.32 ± 0.06[d]/0.032 ± 0.006[d]
Mb(2,8-DPF)	222	73.7	16 ± 3[d] /110 ± 22[d]	0.69 ± 0.13[d]/0.036 ± 0.007[d]
Native Mb	218	77.3	14 ± 3[f] / 12 ± 2[f]	0.51 ± 0.06[f]/0.019 ± 0.005[f]

a) The stretching frequency of the Fe-His bond in deoxy Mb. b) The chemical shift of His93N_δH in deoxy Mb. c) The chemical shifts of minor form of heme orientational disorder. d) Taken from Ref. 8. e) Taken from Ref. 9. f) Taken from Ref. 24

Table 5-2. Effect of CF_3 substitutions on $\nu_{Fe\text{-}His}$ and His93N_δH ^{1}H NMR shifts of deoxy Mbs at pH 7.40 and 25°C

	$\Delta\nu_{Fe\text{-}His}$[a] ($cm^{-1}$)	ΔHis93N_δH[b] (ppm)
Mb(Meso)/Mb(7-PF)	4	-3.9
Mb(3,8-DMD)/Mb(2,8-DPF)	6	-4.9

a) $\Delta\nu_{Fe\text{-}His}$ = $\nu_{Fe\text{-}His}$ of i – $\nu_{Fe\text{-}His}$ of j, where i and j are deoxy Mb(7-PF) and deoxy Mb(Meso), respectively, for the Mb(Meso)/Mb(7-PF) system, and deoxy Mb(2,8-DPF) and deoxy Mb(3,8-DMD), respectively, for the Mb(3,8-DMD)/Mb(2,8-DPF) one.
b) ΔHis93N_δH = His93N_δH of i – His93N_δH of j, where i and j are deoxy Mb(7-PF) and deoxy Mb(Meso), respectively, for the Mb(Meso)/Mb(7-PF) system, and deoxy Mb(2,8-DPF) and deoxy Mb(3,8-DMD), respectively, for the Mb(3,8-DMD)/Mb(2,8-DPF) one.

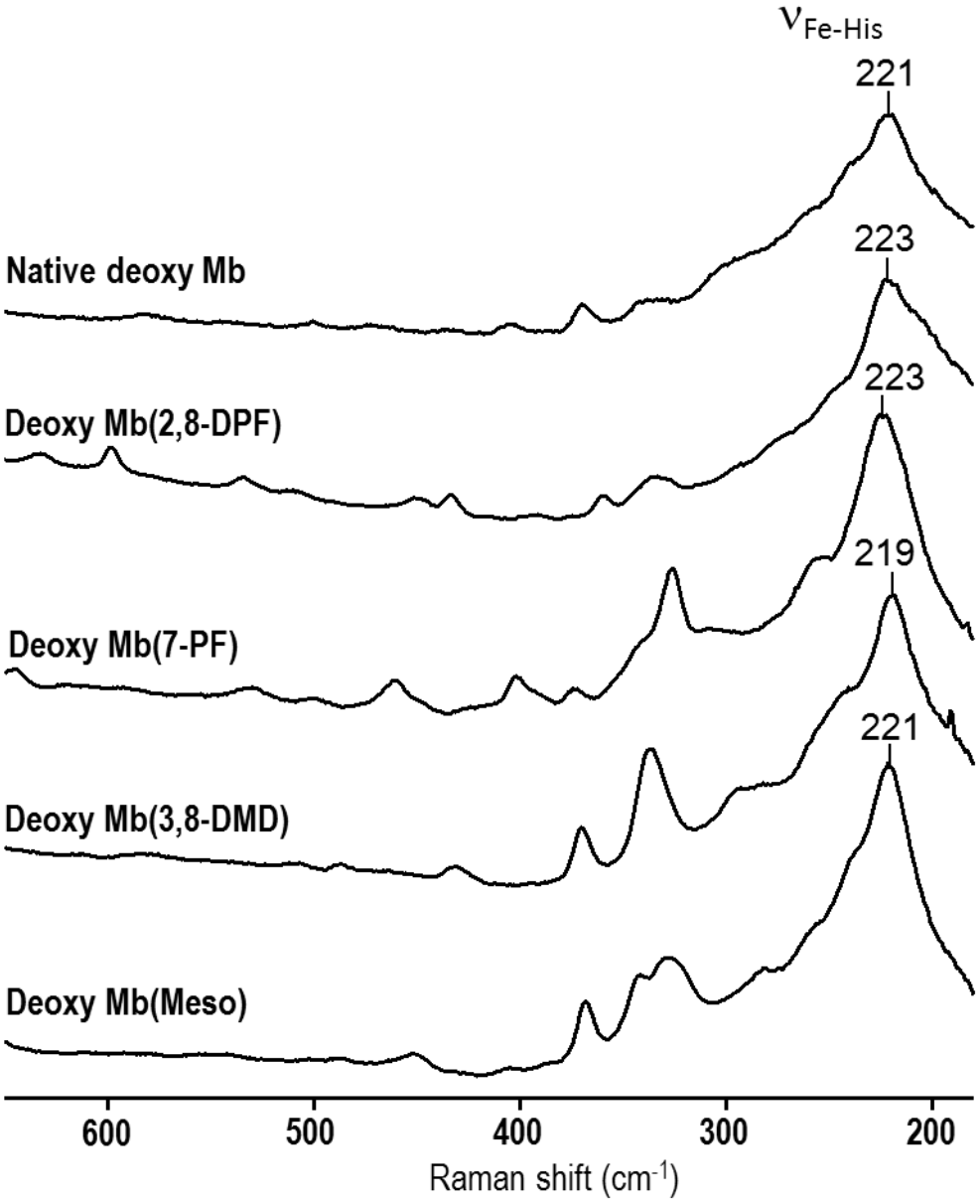

Figure 5-2. Visible resonance Raman spectra of deoxy Mb(Meso), deoxy Mb(3,8-DMD), deoxy Mb(7-PF), deoxy Mb(2,8-DPF), and native deoxy Mb at pH7.40 and 25°C.

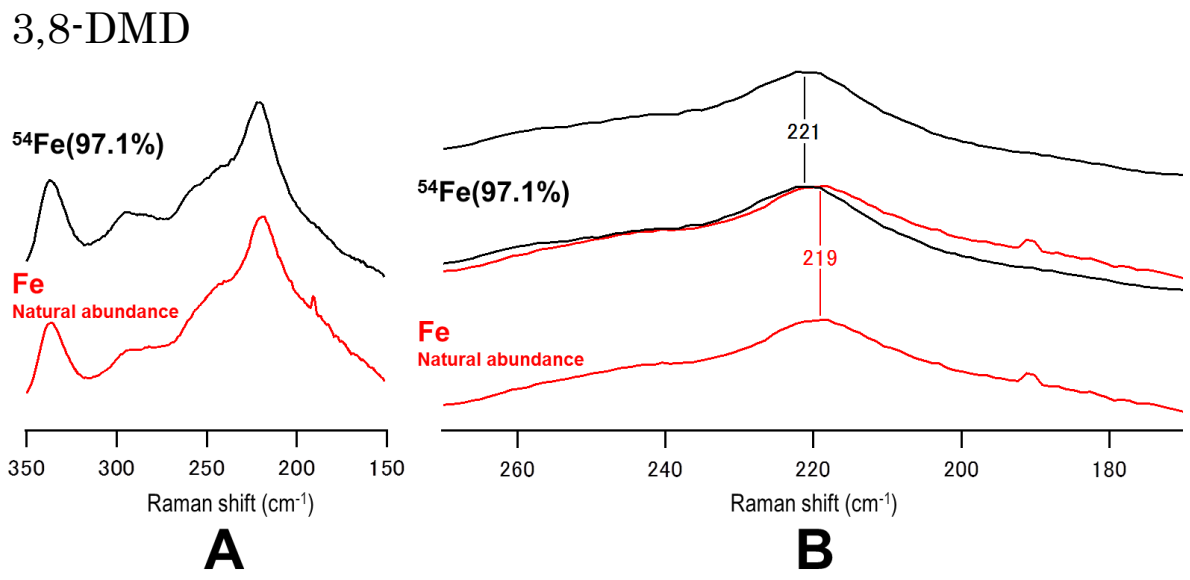

Figure 5-3. Visible resonance Raman spectra of deoxy Mb(3,8-DMD) at pH7.40 and 25°C.
A: The spectra of the protein possessing natural abundance Fe (red) and ^{54}Fe-labelled 3,8-DMD (black).
B: The expanded spectra, 170-270 cm^{-1}, of natural abundance Fe 3,8-DMD (bottom), and ^{54}Fe-labelled one (top), and an overlay of the two spectra (middle).

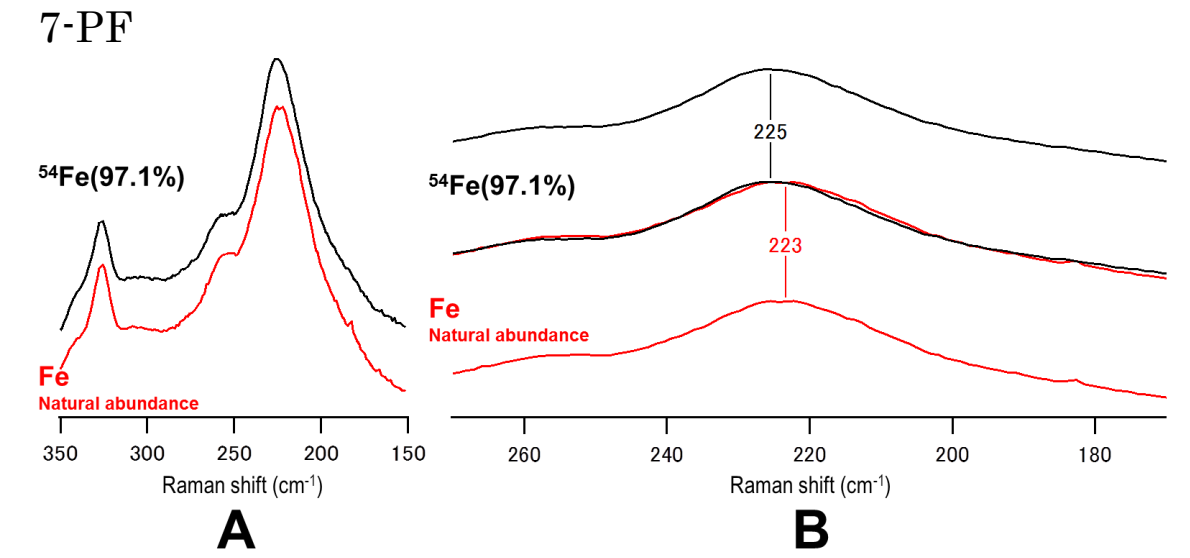

Figure 5-4. Visible resonance Raman spectra of deoxy Mb(7-PF) at pH7.40 and 25 °C.
A: The spectra of the protein possessing natural abundance Fe (red) and ^{54}Fe-labelled 7-PF (black).
B: The expanded spectra, 170-270 cm^{-1}, of natural abundance Fe 7-PF (bottom), and ^{54}Fe-labelled one (top), and an overlay of the two spectra (middle).

2,8-DPF

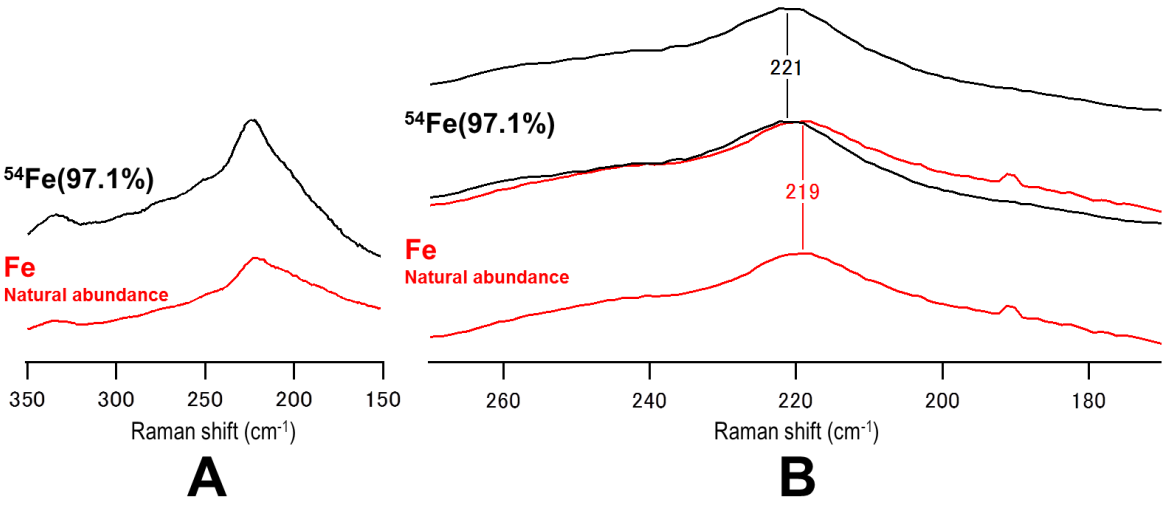

Figure 5-5. High frequency regions of visible resonance Raman spectra of deoxy Mb(2,8-DPF) at pH7.40 and 25 °C.
A: The spectra of the protein possessing natural abundance Fe (red) and ^{54}Fe-labelled 2,8-DPF (black).
B: The expanded spectra, 170-270 cm^{-1}, of natural abundance Fe 2,8-DPF (bottom), and ^{54}Fe-labelled one (top), and an overlay of the two spectra (middle).

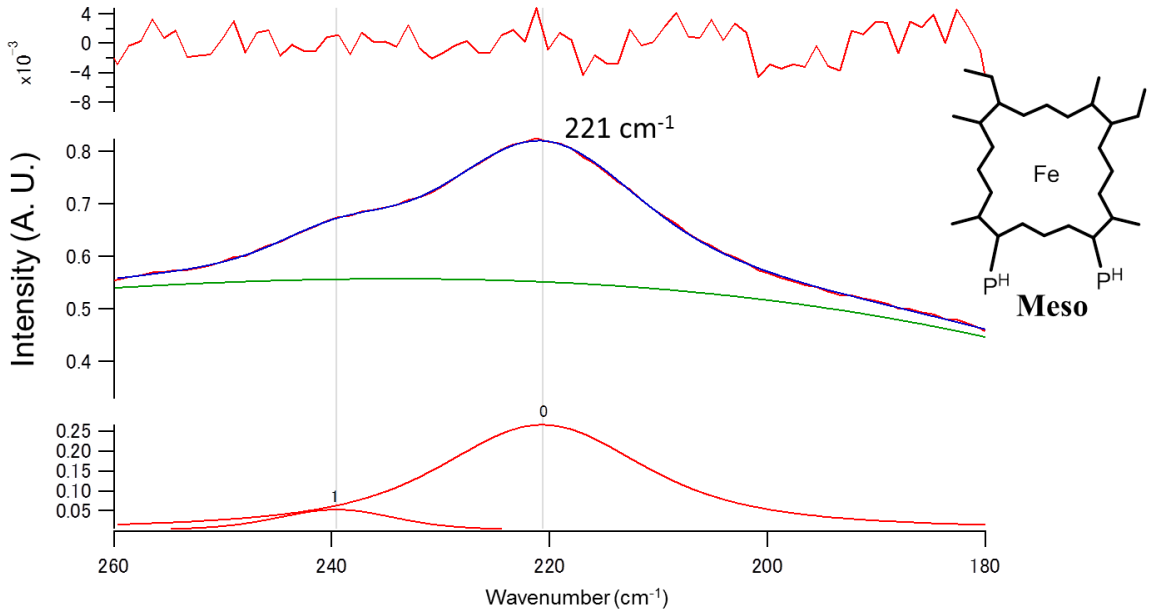

Figure 5-6. Visible resonance Raman spectrum of the deoxy form of Mb(Meso) in 100 mM potassium phosphate buffer, pH 7.4, at 25°C. Residual error (the difference between the experimental and theoretical values) (top), observed (blue) and simulated (red) Fe-N(His93) stretching frequency ($\nu_{Fe\text{-}His}$) bands (middle), and simulated individual bands (bottom). The green line in the middle illustration is the baseline. The wavenumber of 221 cm^{-1} was determined for the $\nu_{Fe\text{-}His}$ value (Peak 0). The origin of Peak 1 is unknown.

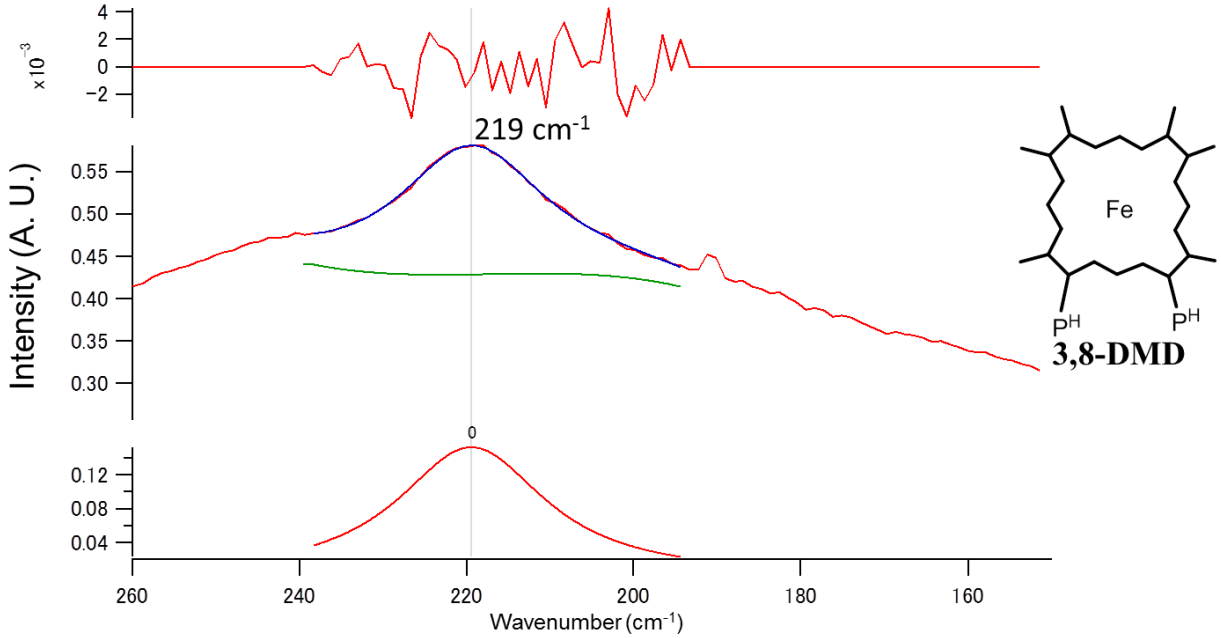

Figure 5-7. Visible resonance Raman spectrum of the deoxy form of Mb(3,8-DMD) in 100 mM potassium phosphate buffer, pH 7.4, at 25°C. Residual error (the difference between the experimental and theoretical values) (top), observed (red) and simulated (blue) Fe-N(His93) stretching frequency ($\nu_{Fe\text{-}His}$) bands (middle), and simulated individual bands (bottom). The green line in the middle illustration is the baseline. The wavenumber of 219 cm^{-1} was determined for the $\nu_{Fe\text{-}His}$ value.

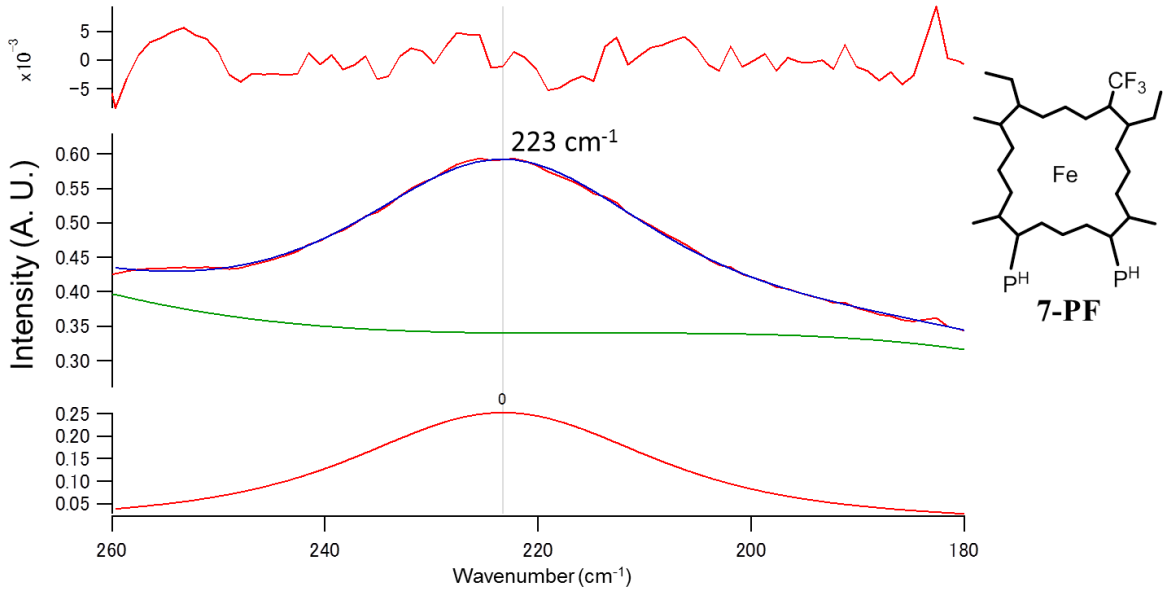

Figure 5-8. Visible resonance Raman spectrum of the deoxy form of Mb(7-PF) in 100 mM potassium phosphate buffer, pH 7.4, at 25°C. Residual error (the difference between the experimental and theoretical values) (top), observed (red) and simulated (blue) Fe-N(His93) stretching frequency ($\nu_{Fe\text{-}His}$) bands (middle), and simulated individual bands (bottom). The green line in the middle illustration is the baseline. The wavenumber of 223 cm^{-1} was determined for the $\nu_{Fe\text{-}His}$ value (Peak 0).

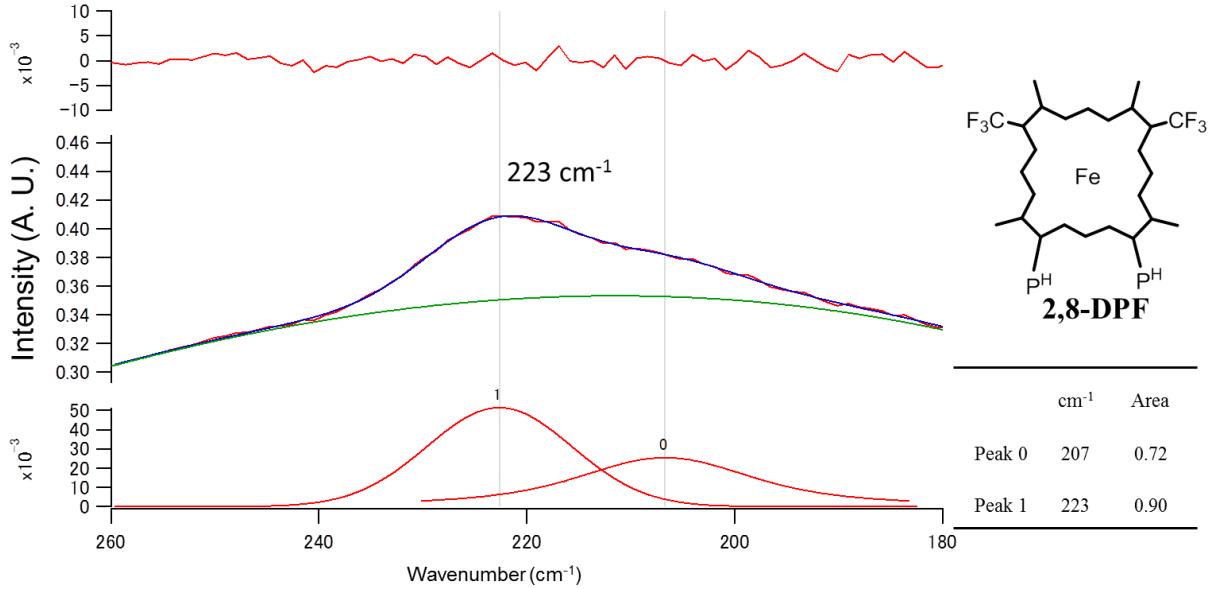

Figure 5-9. Visible resonance Raman spectrum of the deoxy form of Mb(2,8-DPF) in 100 mM potassium phosphate buffer, pH 7.4, at 25°C. Residual error (the difference between the experimental and theoretical values) (top), observed (red) and simulated (blue) Fe-N(His93) stretching frequency ($\nu_{Fe\text{-}His}$) bands (middle), and simulated individual bands (bottom). The green line in the middle illustration is the baseline. Since the $\nu_{Fe\text{-}His}$ value was expected to be about 220 cm^{-1}, we attributed peak 1 to the $\nu_{Fe\text{-}His}$ band. The wavenumber of 223 cm^{-1} was determined for the $\nu_{Fe\text{-}His}$ value (Peak 1). The origin of Peak 0 is unknown.

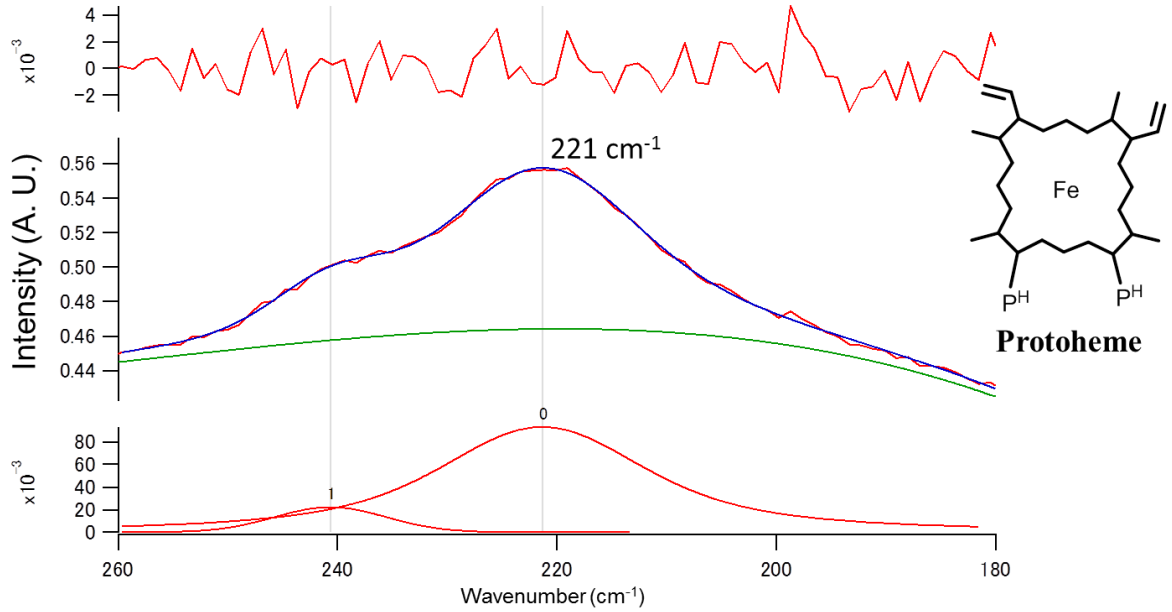

Figure 5-10. Visible resonance Raman spectrum of the deoxy form of native Mb in 100 mM potassium phosphate buffer, pH 7.4, at 25°C. Residual error (the difference between the experimental and theoretical values) (top), observed (blue) and simulated (red) Fe-N(His93) stretching frequency ($\nu_{Fe\text{-}His}$) bands (middle), and simulated individual bands (bottom). The green line in the middle illustration is the baseline. The wavenumber of 221 cm^{-1} was determined for the $\nu_{Fe\text{-}His}$ value.

NMR signal of the His93 $N_{\delta}H$ proton in deoxy Mbs. I next observed the NMR signal of the labile His93$N_{\delta}H$ proton in deoxy forms of the proteins, resolved in the far downfield-shifted region at ~80 ppm (Figure 5-11). The appearance of two His93$N_{\delta}H$ proton signals in the spectrum of deoxy Mb(7-PF) is due to the well-documented heme orientational disorder [28], that is, the presence of isomers possessing two heme orientations differing by 180° rotation about the 5,15-*meso* axis, that is, *M* and *m* forms (see inset of Figure 4) [27,29]. It has been shown that the *m* isomer is dominant over the *M* one in Mb(7-PF) [27], while the *M* one dominates in Mb(Meso) [30], and proteins possessing C_2 symmetric heme cofactors, that is, 3,8-DMD and 2,8-DPF, do not exhibit the heme orientational disorder. These proteins can be ranked as Mb(2,8-DPF) < Mb(7-PF) < Mb(3,8-DMD) < Mb(Meso), in order of increasing His93$N_{\delta}H$ shift (Table 5-1). The order of the His93$N_{\delta}H$ shift is essentially identical to that of the ρ_{Fe} value, that is, Mb(2,8-DPF) < Mb(7-PF) < Mb(3,8-DMD) ≈ Mb(Meso)[8,9], indicating a close relationship between the Fe-His bond in deoxy Mb and the ρ_{Fe} value. A His93$N_{\delta}H$ shift difference (ΔHis93$N_{\delta}H$) of -3.9 ppm was observed for the *M* form of the Mb(Meso)/Mb(7-PF) system, and that of -4.9 ppm for the Mb(3,8-DMD)/Mb(2,8-DPF) one (Table 5-2).

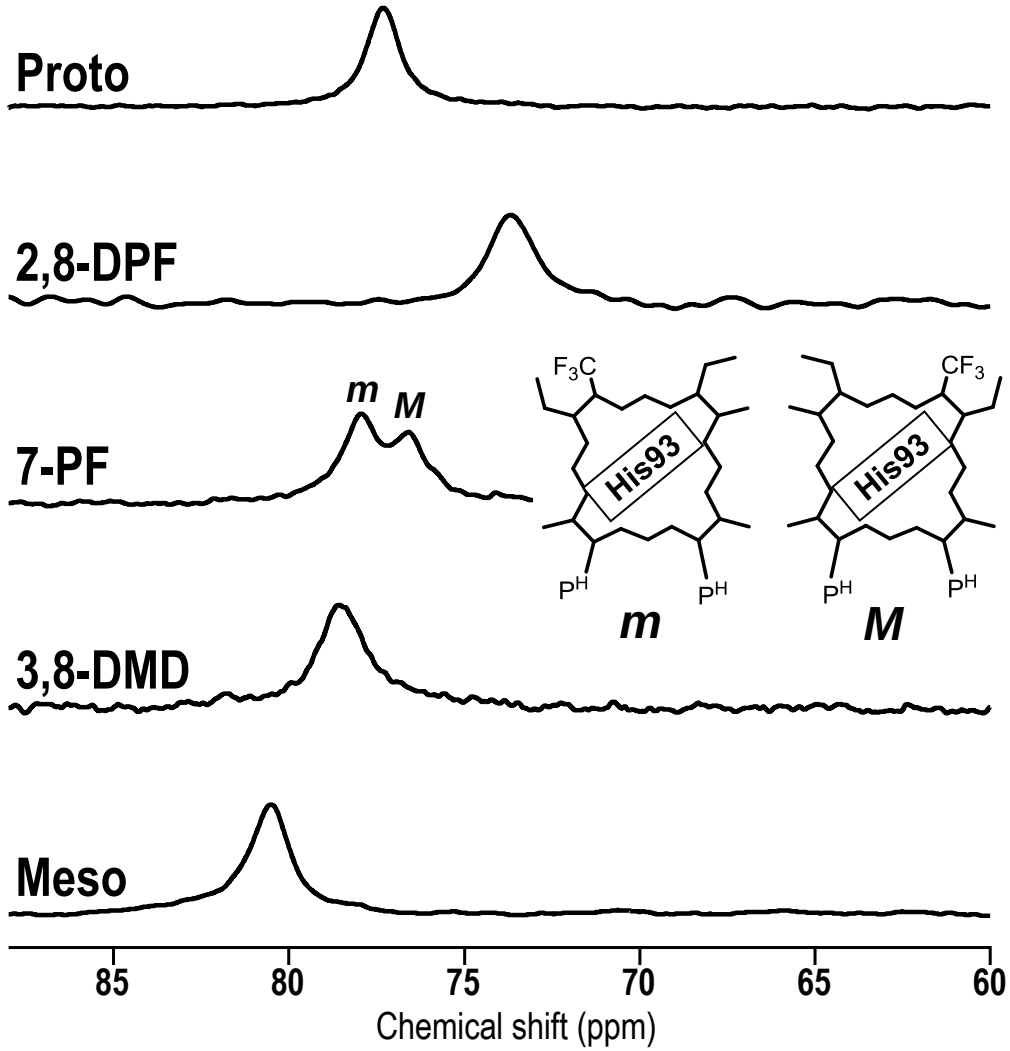

Figure 5-11. NMR signals of the His93N_{δ}H protons of the deoxy proteins at pH 7.4 and 25 °C, from bottom to top, deoxy Mb(Meso), deoxy Mb(3,8-DMD), deoxy Mb(7-PF), deoxy Mb(2,8-DPF), and native deoxy Mb, respectively. Two different orientations of 7-PF relative to His93, *m* and *M* forms are shown in inset. The two signals at 76.6 and 77.9 ppm in the spectrum of deoxy Mb(7-PF) have been assigned to the *M* and *m* forms, respectively[27].

^{19}F NMR spectrum of deoxy Mb(2,8-DPF). Finally, the ^{19}F NMR spectrum of deoxy Mb(2,8-DPF) is compared with that of deoxy Mb(7-PF) in Figure 5-12, the spectra of CO adducts of the proteins, that is, Mb(2,8-DPF)CO and Mb(7-PF)CO, being also shown for comparison. Two well-separated signals were observed in each one of the spectra in Figure 5-12, and their shifts are summarized in Table 5-3. The appearance of two signals in the spectra of Mb(2,8-DPF)CO and deoxy Mb(2,8-DPF) is due to removal of the chemical equivalence of the two CF_3 groups of the heme cofactor, through asymmetric heme-protein interaction, in the heme active site, as has been reported for other C_2 symmetric heme cofactors [31,32]. On the other hand, as described above, the appearance of the two signals in the spectrum of Mb(7-PF) has been shown to be due to the heme orientational disorder (see inset of Figure 5-11) [27].

Despite the difference in the origin of the signal splitting between deoxy Mb(2,8-DPF) and deoxy Mb(7-PF), the ^{19}F NMR spectra of the two proteins shared common features such as a relatively small paramagnetic shift (δ_{para}) for the high-spin ferrous heme complex in the $S = 2$ state, that is, δ_{para} values of 5.39 – 31.23 ppm were estimated with consideration of the CO adducts of the corresponding proteins as diamagnetic references, and relatively great signal splitting, that is, 21.08 and 24.06 ppm for deoxy Mb(2,8-DPF) and deoxy Mb(7-PF), respectively (Table 5-3). These spectral features were consistent with the significant contribution of a π spin delocalization mechanism in the high-spin d^6 system due to the *d*-electron configuration derived from the ^5E ground state (see below) [27].

Table 5-3. Analysis of ^{19}F NMR shifts (ppm) of deoxy Mb(7-PF) and deoxy Mb(2,8-DPF) at pH 6.5 and 25°C

	Deoxy Mb(7-PF)		Deoxy Mb(2,8-DPF)	
	7-CF_3(*m*)	7-CF_3(*M*)	2-CF_3	8-CF_3
δ_{obs}[a]	60.26[f]	36.20[f]	60.41	39.33
δ_{dia}[b]	29.03[f]	30.81[f]	29.21	29.68
δ_{para}[c]	31.23	5.39	31.20	9.65
δ_{pc}[d]	~-2	~2	~-2	~2
δ_{c}[e]	~33	~3	~33	~8

a) The observed shift. b) The diamagnetic shifts observed for MbCO(7-PF) and MbCO(2,8-DPF). c) The paramagnetic shifts calculated using the equation $\delta_{obs} = \delta_{dia} + \delta_{para}$. d) The paramagnetic pseudo-contact shift. The shifts were obtained from Ref. 19. e) The paramagnetic contact shift. f) Taken from Ref. 28.

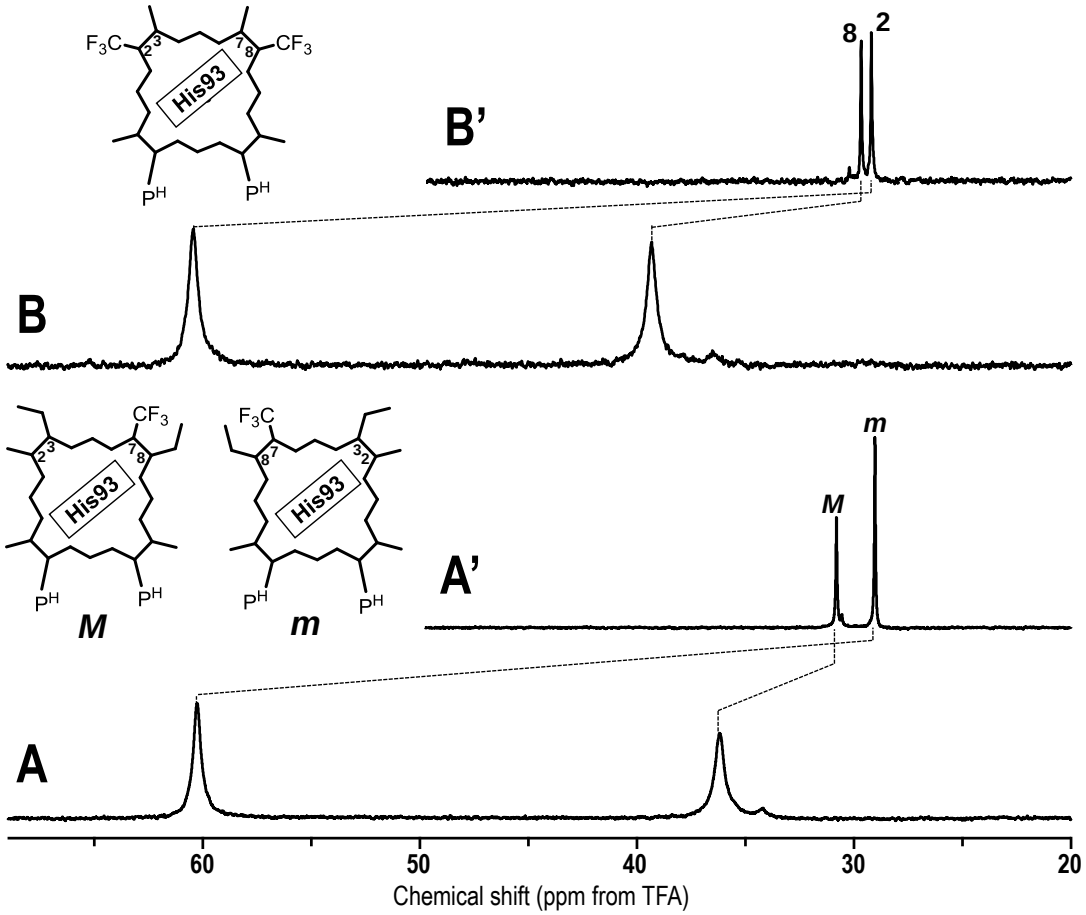

Figure 5-12. ^{19}F NMR spectra of (A) deoxy Mb(7-PF), (A´) MbCO(7-PF), (B) deoxy Mb(2,8-DPF), and MbCO(2,8-DPF) at 25℃ in 90% H_2O/10% ^2H_2O at pH 6.5. The orientations of 7-PF and 2,8-DPF relative to His93 are illustrated in the inset. Signal assignments are indicated in the spectra. The signal assingments for deoxy Mb(2,8-DPF) and MbCO(2,8-DPF) are tentative.

DISCUSSION

Ground state *d*-Electron configuration of the heme Fe atom in deoxy Mb and effect of a change in the ρ_{Fe} value on the Fe-His bond. The ground state *d*-electron configuration of the heme Fe atom in deoxy Mb remains to be elucidated [16,19,33-35]. A theoretical model based on the crystal field calculations [33], as well as on molecular orbital calculations [34], has been proposed to determine the electronic structure of the high-spin ferrous heme complex in the $S = 2$ state. According to the proposed model, among 210 possible states of the d^6 configuration for the ferrous heme complex, the low-lying electronic terms are $^5B_2$, ^5E, ^3E, and ^1A, with $^5B_2$ or one of the ^5E components as the ground state. Investigations of the Mössbauer effect of deoxy Mb and deoxy Hb demonstrated that the ground state is one of the components of the ^5E term split by rhombic distortions [35]. Since the *d*-orbital splittings derived from the ^5E, $(d_{xz})^2(d_{yz})(d_{xy})(d_{z^2})(d_{x^2-y^2})$ or $(d_{yz})^2(d_{xz})(d_{xy})(d_{z^2})(d_{x^2-y^2})$, and $^5B_2$, $(d_{xy})^2(d_{xz})(d_{yz})(d_{z^2})(d_{x^2-y^2})$, states for the high-spin d^6 system with $S = 2$ are close in energy [16,33-35], the contributions of these electronic states to the electronic and magnetic nature of deoxy Mb have been shown to complicate data interpretation. In the ^5E state, the degeneracy of the energy levels for the two configurations is removed by the interaction between the heme Fe d_π-orbital and His93 N_ε *p*-orbital and, depending upon the relative energy of the d_{xz} and d_{yz} orbitals, π spin delocalization occurs into either pyrroles I, III or II, IV (Figure 5-1) [16]. On the other hand, the non-degenerate $^5B_2$ state delocalizes twice as much spin density to the porphyrin π-system and the delocalization occurs equally to all pyrroles because there are π electron spins in both the d_{xz} and d_{yz} orbitals. The ^{19}F NMR signals of deoxy Mb(2,8-DPF) exhibited relatively large signal splitting and relatively small δ_{para} values for the high-spin d^6 system with $S = 2$ (Table 5-3), and these spectral features were consistent with the π spin delocalization mechanism expected from the ^5E ground stat [27]. With the *d*-electron configuration derived from the ^5E ground state, the σ and π donations of *p* electrons of the His93 N_ε atom into the singly occupied the d_{z^2} and d_π orbitals of the heme Fe atom, respectively (Fe←His σ and π donation, respectively), contribute to the formation of the Fe-His bond, and hence the strengthening of the Fe-His bond with decreasing ρ_{Fe} value through the CF_3 substitution(s), as manifested in the $\Delta\nu_{Fe\text{-}His}$ values of 4 and 6 cm^{-1} observed for the Mb(Meso)/Mb(7-PF) and Mb(3,8-DMD)/Mb(2,8-DPF)

systems, respectively (Table 5-2), could be due to enhancement of both the Fe←His σ and π donations.

Relationship between the resonance raman $\nu_{Fe\text{-}His}$ value and the His93 $N_\delta H$ ^1H NMR shift. A change in the Fe-His bond strength was clearly manifested in the His93N_δH shift (Table 5-2). Comparison of the $\Delta\nu_{Fe\text{-}His}$ and ΔHis93N_δH values of the Mb(Meso)/Mb(7-PF) and Mb(3,8-DMD)/Mb(2,8-DPF) systems (Table 5-2) indicated that the His93N_δH shift decreases with increasing Fe-His bond strength. The His93N_δH shift is expressed as the sum of the diamagnetic shift (δ_{dia}) and δ_{para}, and then δ_{para} is expressed as the sum of the paramagnetic contact (δ_c) and pseudo-contact shifts (δ_{pc}). The δ_c and δ_{pc} values reflect the unpaired electron density delocalized into the 1*s* orbital of the N_δH hydrogen, and the spatial relationship between the N_δH proton and the unpaired electron localized at the heme Fe atom, respectively [36]. Since the shift of the His93 N_δH proton signal of native MbCO, that is, 9.38 ppm [37], could be used as an appropriate δ_{dia} value, and the δ_{pc} value has been determined to be 3.10 ppm [19], values of ~61.2 - ~68.1 ppm were estimated for the δ_c values of the proteins. These results clearly indicated that the δ_c value dominates the His93N_δH shift. The unpaired electrons of the heme Fe atom of deoxy Mb can be delocalized into the His93 imidazole through the Fe-His σ and π bonds (σ- and π-delocalization, respectively) [19,36,38]. The delocalization of the positive spin of the unpaired electron through the σ- and π-delocalization results in the net spin density of the opposite sign, that is, negative, and the positive spin on the His93N_ε atom, respectively, and the spin on the His93N_ε atom further delocalizes, through the π system of the imidazole ring, into the N_δ atom, and then finally into the 1*s* orbital of the His93N_δH hydrogen, through σ spin polarization. As a result, the positive spin is delocalized into the 1*s* orbital of the His93 N_δH hydrogen through the σ-delocalization, whereas the negative spin is delocalized through the π-delocalization. Thus, the δ_c value for the His93N_δH shift is determined as the difference between the σ- and π-delocalization, and hence the large positive δ_c values indicated that the σ-delocalization dominates over the π-delocalization, as pointed out previously [19].

The strength of the Fe-His bond is affected by steric and electronic factors [39]. La Mar and de Ropp [39] demonstrated, in a study involving horse radish ferrous peroxidase, where the proximal His $N_\delta H$ proton shift is greatly affected by the hydrogen bond between the $N_\delta H$ proton and a protein acceptor residue through its effect on the delocalization of the unpaired electron along the N_δ-H bond, and that simultaneous consideration of changes of the $\nu_{Fe\text{-}His}$ value and the axial His $N_\delta H$ proton shift enables differentiation of the steric and electronic influences on the Fe-His bond. In the case of deoxy Mb, the delocalization of the unpaired electron from the N_δ atom to the 1*s* orbital of the $N_\delta H$ hydrogen decreases with increasing strength of the His93-Leu89 H-bond because the interaction between the $N_\delta H$ hydrogen and the unpaired electron density on the His93 imidazole ring is hampered by enhancement of polarization of the charge in the N_δ-H bond. Furthermore, a change in the strength of the His93-Leu89 H-bond also influences the Fe-His bond strength in such a manner that the Fe-His bond becomes stronger with increasing His93-Leu89 H-bond strength because of enhancement of the Fe←His σ donation. Consequently, the strengthening of the Fe-His bond through an increase in the His93-Leu89 H-bond strength results in an increase in the $\nu_{Fe\text{-}His}$ value and, inversely, a decrease in the His93$N_\delta H$ shift [39]. Thus, combined analysis of the $\nu_{Fe\text{-}His}$ values and the His93$N_\delta H$ shifts of the proteins clearly demonstrated that the His93-Leu89 H-bond is strengthened with increasing number of CF_3 substitutions.

In the case of deoxy Mb(7-PF), the His93$N_\delta H$ shift of the *m* isomer was larger by 1.3 ppm relative to that of the *M* one (Figure 5-11 and Table 5-1). In the absence of detailed knowledge about their δ_{dia} and δ_{pc} values as well as the relative contributions of the σ- and π-delocalization to their δ_c ones, it is not possible at present to interpret the His93$N_\delta H$ shifts of the *m* and *M* forms of the protein in terms of the Fe-His bond. By the way, assuming a linear relationship between the ΔHis93$N_\delta H$ and $\Delta\nu_{Fe\text{-}His}$ values of the proteins, the ΔHis93$N_\delta H$ value of 1.3 ppm is accounted for by the $\Delta\nu_{Fe\text{-}His}$ value of ~1 cm^{-1}, and the line width of the $\nu_{Fe\text{-}His}$ band was large enough to make detection of the individual bands exhibiting such slight separation difficult under the present Raman measurement conditions.

Functional consequences of a change in the Fe-His bond strength through the ρ_{Fe} value. The nature of the axial Fe-His bond is thought to play a crucial role in functional control of hemoprotein [2,39,40]. The study demonstrated that the Fe-His bond is affected by an electronic interaction among the heme π-system, heme Fe atom, and Fe-bound imidazole hydrogen bonded to a protein acceptor residue. Hence, this finding confirmed the proposal that the strength of the Fe-His bond can be modulated indirectly by the hydrogen bond between Fe-bound imidazole and a protein acceptor residue [39-46]. Since the strengthening of the Fe-His bond upon CF_3 substitutions is due to enhancement of the Fe←His donation, an increase in Lewis acidity of the heme Fe atom with decreasing ρ_{Fe} value is expected to increase the O_2 and CO association rate constants ($k_{on}(O_2)$ and k_{on}(CO), respectively). In contrast to this expectation, the $k_{on}(O_2)$ and k_{on}(CO) values were not largely affected by the CF_3 substitutions(Table 5-1). These results supported that the rate-determining step for O_2 and CO binding of the protein is ligand entry from the solvent [47]. In contrast, the O_2 dissociation rate constant ($k_{off}(O_2)$) was largely affected by a change in the ρ_{Fe} value, whereas the CO dissociation one (k_{off}(CO)) was essentially independent of the ρ_{Fe} value. Thus the electronic control of not only the O_2 affinity, but also the O_2/CO discrimination of the protein is primarily achieved through the effect of a change in the ρ_{Fe} value on the $k_{off}(O_2)$ one, as described previously [8,9].

Matsukawa et al.[40] investigated the relationship between the $\nu_{Fe\text{-}His}$ value and the Adair constant accounts for the average affinity of tetrameric hemoglobin (Hb) as to binding of the first O_2, usually abbreviated as K_1, of various naturally occurring mutant deoxy Hbs possessing a variety of O_2 affinities. They found that the K_1 value decreases, and hence the O_2 affinity of the protein increases with increasing $\nu_{Fe\text{-}His}$ value, and the relationship between the O_2 affinity and the $\nu_{Fe\text{-}His}$ value of the proteins has been explained in terms of the effect of the strain imposed on the Fe-His bond by the protein moiety on the heme Fe reactivity. In contrast, I found that Mb with a stronger Fe-His bond exhibits a lower O_2 affinity(Table 5-1), and that the heme Fe reactivity in the protein is regulated through an electronic interaction among the heme π-system, heme Fe atom, and Fe-bound imidazole.

CONCLUSION

The ρ_{Fe} value affected the electronic nature of His93 imidazole in beoxy Mb. A decrease in Lewis acidity of the His93 $N_{\delta}H$ hydrogen bonded to the carbonyl O atom of Leu89 with decreasing the ρ_{Fe} value enhanced the coordination bond between the heme Fe atom and His93. These findings demonstrated the importance of the ρ_{Fe} value in control of the function of the protein.

References

[1] Antonini, E.; Brunori, M. *Hemoglobins and Myoglobins and their Reactions with Ligands*, North Holland Publishing, Amsterdam, **1971**.

[2] Perutz, M. F. *Br. Med. Bull.*, **1976**, 32, 195-208.

[3] Takano, T. *J. Mol. Biol.*, **1977**, 110, 569-584.

[4] Takano, T. *J. Mol. Biol.*, **1977**, 110, 537-568.

[5] Schotte, F.; Lim, M.; Jackson, T. A.; Smirnov, A. V.; Soman, J.; Olson, J. S.; Phillips, G. N., Jr.; Wulff, M.; Anfinrud, P. A. *Science*, **2003**, 300, 1944-1947.

[6] Springer, B. A.; Sligar, S. G.; Olson, J. S.; Phillips, G. N., Jr. *Chem. Rev.*, **1994**, 94, 699-714.

[7] Olson, J. S.; Phillips, G. N., Jr. *J. Biol. Inorg. Chem.*, **1997**, 2, 544-552.

[8] Shibata, T.; Nagao, S.; Fukaya, M.; Tai, H.; Nagatomo, S.; Morihashi, K.; Matsuo, T.; Hirota, S.; Suzuki, A.; Imai, K.; Yamamoto, Y. *J. Am. Chem. Soc.*, **2010**, 132, 6091-6098.

[9] Nishimura, R.; Shibata, T.; Tai, H.; Ishigami, I.; Ogura, T.; Nagao, S.; Matsuo, T.; Hirota, S.; Imai, K.; Neya, S.; Suzuki, A.; Yamamoto, Y. *Inorg. Chem.*, **2013**, 52, 3349-3355.

[10] Shibata, T.; Matsumoto, D.; Nishimura, R.; Tai, H.; Matsuoka, A.; Nagao, S.; Matsuo, T.; Hirota, S.; Imai, K.; Neya, S.; Suzuki, A.; Yamamoto, Y. *Inorg. Chem.*, **2012**, 51, 11955-11960.

[11] Nishimura, R.; Matsumoto, D.; Shibata, T.; Yanagisawa, S.; Ogura, T.; Tai, H.; Matsuo, T.; Hirota, S.; Neya, S.; Suzuki, A.; Yamamoto, Y. *Inorg. Chem.* **2014**, 53, 9156-9165.

[12] Chang, C. K.; Ward, B.; Ebina, S. *Arch. Biochem. Biophys.*, **1984**, 231, 366-371.

[13] Neya, S.; Suzuki, M.; Hoshino, T.; Ode, H.; Imai, K.; Komatsu, T.; Ikezaki, A.; Nakamura, M.; Furutani, Y.; Kandori, H. *Biochemistry*, **2010**, 49, 5642-5650.

[14] Toi, H.; Homma, M.; Suzuki, A.; Ogoshi, H. *J. Chem. Soc., Chem. Commun.*, **1985**, 1791–1792.

[15] Yamamoto, Y.; Iwafune, K.; Chûjô, R.; Inoue, Y.; Imai, K.; Suzuki, T. *J. Biochem.*, **1992**, 112, 414-420.

[16] La Mar, G. N.; Davis, N. L.; Johnson, R. D.; Smith, W. S.; Hauksson, J. B.; Budd, D. L.; Dalichow, F.; Langry, K. C.; Morris, I. K.; Smith, K. M. *J. Am. Chem. Soc.*, **1993**, 115, 3869-3876.

[17] Busse, S. C.; Jue, T. *Biochemistry*, **1994**, 33, 10934-10943.

[18] La Mar, G. N.; Dalichow, F.; Zhao, X.; Dou, Y.; Ikeda-Saito, M.; Chiu, M. L.; Sligar, S. G. *J. Biol. Chem.*, **1994**, 269, 29629-29635.

[19] Bougault, C. M.; Dou, Y.; Ikeda-Saito, M.; Langry, K. C.; Smith, K. M.; La Mar, G. N. *J. Am. Chem. Soc.*, **1998**, 120, 2113-2123.

[20] Ma, D.; Musto, R.; Smith, K. M.; La Mar, G. N. *J. Am. Chem. Soc.*, **2003**, 125, 8494-8504.

[21] Teale, F. W. J. *Biochim. Biophys. Acta*, **1959**, 35, 543.

[22] Kitanishi, K.; Kobayashi, K.; Kawamura, Y.; Ishigami, I.; Ogura, T.; Nakajima, K.; Igarashi, J.; Tanaka, A.; Shimizu, T. *Biochemistry*, **2010**, 49, 10381-10393.

[23] Anderson C. L.; Hester, R. E.; Moore, J. N. *Biochim. Biophys. Acta*, **1997**, 1338, 107-120.

[24] Rohlfs, A.J.; Mathews, A. J.; Carver, T. E.; Olson, J. S.; Springer, B. A.; Egeberg, K. D.; Slinger, S. G. *J. Biol. Chem*. **1990**, 265, 3168-3176.

[25] Kitagawa, T.; Nagai, K.; Tsubaki, M. *FEBS Lett.*, **1979**, 104, 376-378.

[26] Fujii, H.; Yoshimura, T.; Kamada, H. *Inorg. Chem.*, **1997**, *36*, 1122-1127.

[27] La Mar, G. N.; Budd, D. L.; Viscio, D. B.; Smith, K. M.; Langry, K. C. *Proc. Natl. Acad. Sci. U.S.A.*, **1979**, 75, 5755-5759.

[28] Yamamoto, Y.; Nagao, S.; Hirai, Y.; Inose, T.; Terui, N.; Mita, H.; Suzuki, A. *J. Biol. Inorg. Chem.*, **2004**, 9, 152-160.

[29] Nagao, S.; Hirai, Y.; Suzuki, A.; Yamamoto, Y. *J. Am. Chem. Soc.*, **2005**, 127, 4146-4147.

[30] Hirai, Y.; Yamamoto, Y.; Suzuki, A. *Bull. Chem. Soc. Jpn.*, **2000**, 73, 2309-2316.

[31] Yamamoto, Y.; Hirai, Y.; Suzuki, A. *J. Biol. Inorg. Chem.*, **2000**, 5, 455-462.

[32] Hirai, Y.; Nagao, S.; Mita, H.; Suzuki, A.; Yamamoto, Y. *Bull. Chem. Soc. Jpn.*, **2004**, 77, 1485-1486.

[33] Eicher, H.; Trautwein, A. *J. Chem. Phys.* **1969**, 50, 2540-2551.

[34] Trautwein, A.; Zimmermann, R.; Harris, F. E. *Theor. Chim. Acta*, **1975**, 37, 89-104

[35] Eicher, H.; Bade, D.; Parak, F. *J. Chem. Phys.* **1976**, 64, 1446-1455.

[36] Bertini, I.; Luchinat, C. *NMR of Paramagnetic Molecules in Biological Systems*, The Benjamin/Cummings Publishing Company, Menlo Park, CA, **1986**, pp.19-46.

[37] Thériault, Y.; Pochapsky, T. C.; Dalvit, C.; Chiu, M. L.; Sligar, S. G.; Wright, P. *J. Biomol. NMR*, **1994**, 4, 491-504.

[38] La Mar, G. N. In *NMR of Paramagnetic Molecules, Principles and Applications*, G. N. La Mar, W. D. Horrocks, Jr., R. H. Holm, Eds., Academic Press, New York, **1973**, pp 85-126.

[39] La Mar, G. N.; de Ropp, J. S. *J. Am. Chem. Soc.*, **1982**, 104, 5203.-5206.

[40] Matsukawa, S.; Mawatari, K.; Yoneyama, Y.; Kitagawa, T. *J. Am. Chem. Soc.*, **1985**, 107, 1108-1113.

[41] Stein, P.; Mitchell, M.; Spiro, T. G. *J. Am. Chem. Soc.*, **1980**, 102, 7795-7798.

[42] Teraoka, J.; Kitagawa, T. *Biochem. Biophys. Res. Commmun.*, **1980**, *93*, 694-700.

[43] Teraoka, J.; Kitagawa, T. *J. Biol. Chem.* **1981**, 256, 3969-3977.

[44] Peisach, J. *Ann. N. Y. Acad. Sci.*, **1975**, *244*, 187-203.

[45] Swarts, J. C.; Stanford, M. A.; Moy, J. N.; Hoffman, B. M.; Valentine, J. S. *J. Am. Chem. Soc.*, **1979**, *101*, 3396-3398.

[46] Valentine, J. S.; Sheridan, R. P.; Allen, L. C.; Kahn, P. *Proc. Natl. Acad. Sci. USA*, **1979**, *76*, 1009-1013.

[47] Nienhaus, K.; Deng, P.; Olson, J. S.; Warren, J. J.; Nienhaus, G. U. *J. Biol. Chem.*, **2003**, *278*, 42532-42544.

Chapter 6

Conclusions

1. The stretching frequency of Fe-bound CO(ν_{CO}) reflects the heme environment furnished nearby amino acid residues and heme electronic structure through the resonance between the two canonical forms of the Fe-CO fragment, represented by the valence bond formalism. Additionally, the effect of the heme modification on the electron density of the heme Fe atom(ρ_{Fe}) is independent of the heme environment.

2. Function of myoglobin(Mb) is controlled through the effect of a change in the ρ_{Fe} value, which can be interpreted in term of the resonance process between the Fe^{2+}-O_2 and Fe^{3+}-O_2^--like species. A decrease in the ρ_{Fe} value inhibits electron transfer from heme Fe atom to bound O_2, resulting in a shift of the resonance toward the Fe^{2+}-O_2 species. Since O_2 dissociation from the heme Fe atom is thought to occur only at the Fe^{2+}-O_2 species, and autoxidation reaction is thought to occur only at the Fe^{3+}-O_2^--like species. Shift of the resonance toward the Fe^{2+}-O_2 species with decreasing the ρ_{Fe} value should cause an increase in the O_2 dissociation rate and an decrease in autoxidation reaction rate, and vice versa. On the other hand, CO affinity is affected by both the heme environment furnished nearby amino acid residues and electronic tuning of the intrinsic heme Fe reactivity through the ρ_{Fe} value. Using the chemical modification of heme cofactors and the replacement of amin acid residues in heme pocket, the ratio between the equilibrium constants for CO and O_2 binding in the protein can be regulated over a range of $\sim 10^5$.

3. The bond between the heme Fe and His93 becomes stronger with increasing number of CF_3 substitutions due to an increase in acidity of the His93 $N_\delta H$ hydrogen bonded to the carbonyl O atom of Leu89 in deoxy Mb. The heme Fe reactivity in the protein is regulated through an electronic interaction among the heme π-system, heme Fe atom, and Fe-bound imidazole.

List of publication

1. Shibata, T.; Matsumoto, D.; Nishimura, R.; Tai, H.; Matsuoka, A.; Nagao, S.; Matsuo, T.; Hirota, S.; Imai, K.; Neya, S.; Suzuki, A.; Yamamoto, Y. *Inorg. Chem.***2012**, 51, 11955-11960.
2. Nishimura, R.; Shibata, T.; Tai, H.; Ishigami, I.; Ogura, T.; Nagao, S.; Matsuo, T.; Hirota, S.; Imai, K.; Neya, S.; Suzuki, A.; Yamamoto, Y. *Inorg. Chem.* **2013**, 52, 3349-3355.
3. Nishimura, R.; Shibata, T.; Ishigami, I.; Ogura, T.; Tai, H.; Nagao, S.; Matsuo, T.; Hirota, S.; Shoji, O.; Watanabe, Y.; Imai, K.; Neya, S.; Suzuki, A.; Yamamoto, Y. *Inorg. Chem.*, **2014**, 53, 1091-1099.
4. Nishimura, R.; Matsumoto, D.; Shibata, T.; Yanagisawa, S.; Ogura, T.; Tai, H.; Matsuo, T.; Hirota, S.; Neya, S.; Suzuki, A.; Yamamoto, Y. Electronic Control of Ligand-Binding Preference of a Myoglobin Mutant., *Inorg. Chem.* **2014**, 53, 9156-9165.
5. Nishimura, R.; Shibata, T.; Tai, H.; Ishigami, I.; Yanagisawa, S.; Ogura, T.; Neya, S.; Suzuki, A.; Yamamoto, Y. *Bull. Chem. Soc. Jpn.* **2014**, 87, 905 - 911.
6. Saito, K.; Tai, H.; Fukaya, M.; Shibata, T.; Nishimura, R.; Neya, S.; Yamamoto, Y. *J. Biol. Inorg. Chem.*, **2011**, 17, 437-445.

謝辞

本学化学系 教授 山本泰彦 先生には、本研究を進めるにあたり、熱心なご指導と、的確なご助言をいただきました。さらに、研究の意義、面白さや楽しさを教えていただきました。また、学会や、他大学への測定、海外短期留学など、研究者として成長するための様々な支援していただき、心より感謝し、深く御礼申しあげます。先生を超える化学者になることが最大の恩返しだと思っています。今後の私の行方を温かく見守っていただけたら幸いです。

国立長岡工業高等専門学校物質工学科 教授 鈴木秋弘 先生には、本研究を遂行するにあたり欠かすことのできないフッ素化ヘムを合成、提供して戴きました。深く感謝し御礼申し上げます。

奈良先端技術大学院大学物質創成科学研究科教授 廣田俊 先生、准教授 松尾貴史 先生には、反応速度測定において、大変お世話になりました。深く感謝し御礼申し上げます。また、研究室の方々にも大変良くしてもらい、とても感謝しております。

兵庫県立大学大学院生命理学研究科 教授 小倉尚志 先生、柳沢幸子 先生には、共鳴ラマンスペクトルの測定において、大変お世話になりました。深く感謝し御礼申し上げます。また、研究室の方々にも大変良くしてもらい、とても感謝しております。

千葉大学大学院薬学研究院 教授 根矢三郎 先生には、本研究を遂行するにあたり欠かすことのできないヘムを合成、提供して戴きました。深く感謝し御礼申し上げます。

名古屋大学 教授 渡邊芳人 先生、助教授 荘司長三 先生、RiceUniversity Prof. J. S. Olson には、本研究を遂行するにあたり欠かすことのできない変異体の遺伝子が導入された大腸菌やプラスミドを提供して戴きました。深く感謝し御礼申し上げます。

本学数理物質系化学域 特任助教 柴田友和 先生には、研究生活で暖かいご助言とご指導をしていただき、楽しい研究生活を送ることができました。心より感謝し、御礼申しあげます。

本学数理物質科学研究科博士前期課程 1 年 木下真志くん、盛高佑貴くん、研究生 許力揚くん、本学化学類 4 年 片平裕弥くん、金井佑生くん、高谷駿介くんには研究室の運営などで大変お世話になりました。これからの活躍に期待しています。

最終学年度には皆様に大変なご迷惑とご心配をおかけしてしまい申し訳ありませんでした。主治医の筑波記念病院 小林 先生、福岡大学大学病院 向坂 先生の懸命な治療と皆様からの病気への理解、温かい支援のおかげで日常生活を送れるまで回復いたしました。ほんとうにありがとうございました。

最後に、勉学に励む上で恵まれた環境を与えてくれた筑波大学、そして筑波大学への進学から九年間、多くのサポートや激励をくれた父、母、妹、祖母、支えてくれた全ての人に感謝いたします。本当にありがとうございました。

2015 年 2 月